SMIP99

SMIP99 SEMINAR ON UTILIZATION OF STRONG-MOTION DATA

San Francisco, California
September 15, 1999

PROCEEDINGS

Sponsored by

California Strong Motion Instrumentation Program
Division of Mines and Geology
California Department of Conservation

Supported in Part by

California Seismic Safety Commission
Federal Emergency Management Agency

DEPARTMENT OF CONSERVATION
Division of Mines and Geology

The California Strong Motion Instrumentation Program (CSMIP) is a program within the Division of Mines and Geology of the California Department of Conservation and is advised by the Strong Motion Instrumentation Advisory Committee (SMIAC), a committee of the California Seismic Safety Commission. Current program funding is provided by an assessment on construction costs for building permits issued by cities and counties in California, with additional funding from the California Department of Transportation, the Office of Statewide Health Planning and Development, and the California Department of Water Resources.

In January 1997, a joint project, TriNet, between CDMG, Caltech and USGS was funded by the Federal Emergency Management Agency (FEMA) through the California Office of Emergency Services (OES). The goals of the project are to record and rapidly communicate ground shaking information in southern California, and to analyze the data for the improvement of seismic codes and standards.

DISCLAIMER

SMIP99

SMIP99 SEMINAR ON
UTILIZATION OF STRONG-MOTION DATA

San Francisco, California
September 15, 1999

PROCEEDINGS

Edited by

Moh Huang

Sponsored by

California Strong Motion Instrumentation Program
Division of Mines and Geology
California Department of Conservation

Supported in Part by

California Seismic Safety Commission
Federal Emergency Management Agency

PREFACE

The California Strong Motion Instrumentation Program (CSMIP) in the Division of Mines and Geology of the California Department of Conservation promotes and facilitates the improvement of seismic codes and design practices through the Data Interpretation Project. The objective of this project is to increase the understanding of earthquake strong ground shaking and its effects on structures through interpretation and analysis studies of CSMIP and other applicable strong-motion data. The ultimate goal is to accelerate the process by which lessons learned from earthquake data are incorporated into seismic code provisions and seismic design practices.

Since the establishment of CSMIP in the early 1970s, over 750 stations, including 510 ground-response stations, 160 buildings, 20 dams and 60 bridges, have been installed. Significant strong-motion records have been obtained from many of these stations. One of the most important sets of strong-motion records is from the 1994 Northridge earthquake. During this earthquake strong-motion records were obtained from 116 ground-response stations and 77 extensively-instrumented structures. In addition to these records, CSMIP in cooperation with the City of Los Angeles and other agencies, collected and archived accelerograms recorded at over 300 high-rise buildings during the Northridge earthquake. These buildings were instrumented by the building owners as required by the City's Building Code. The strong-motion records from the Northridge earthquake have been and will be the subject of CSMIP data interpretation projects.

The SMIP99 Seminar is the eleventh in a series of annual events designed to transfer recent interpretation findings on strong-motion data to practicing seismic design professionals and earth scientists. The purpose of the Seminar is to increase the utilization of strong-motion data in improving seismic design and practices. In this seminar, investigators of the CSMIP-funded data interpretation projects and invited experts will present the results from their studies on site response studies, vertical ground motion, steel frame buildings, concrete frame buildings, and soil-structure interactions. In addition, there will be presentations on the Consortium of Organizations for Strong-Motion Observation Systems (COSMOS), including mission and objectives of COSMOS, discussion of a common format for data distribution, development of "user-friendly" interfaces , and a virtual strong-motion data center for data dissemination through the Internet. Peter Yanev of EQE International will present a luncheon address on the Turkey Earthquake of 17 August 1999 that claimed more than 15,000 lives.

The papers in this Proceedings volume presented by the investigators of the CSMIP-funded data interpretation projects represent interim results. Following this seminar the investigators will be preparing final reports with their final conclusions. These reports will be more detailed and will update the results presented here. CSMIP will make these reports available after the completion of the studies.

Anthony F. Shakal
CSMIP Program Manager

Moh J. Huang
Data Interpretation Project Manager

TABLE OF CONTENTS

SMIP99 SEMINAR ON UTILIZATION OF STRONG-MOTION DATA

Park Plaza Hotel, San Francisco Airport, California
September 15, 1999

PROGRAM

8:00 - 9:00 **Registration**

9:00 - 9:10 **Welcoming Remarks**
Bruce Bolt, UC Berkeley, Chair, Strong Motion Instrumentation Advisory Committee (SMIAC)
James Davis, State Geologist, Division of Mines and Geology

9:10 - 9:20 **Introductory Remarks**
Anthony Shakal and *Moh Huang*, DMG/Strong Motion Instrumentation Program

SESSION I GROUND MOTION
Moderator: *Bruce Bolt*, UC Berkeley
Chair, SMIAC Ground Response Subcommittee

9:20 - 9:45 **Site Response Study of Weak and Strong Ground Motion Including Nonlinearity**
F. Su, Y. Zeng, *John Anderson*, University of Nevada, Reno, and V. Graizer, DMG/SMIP

9:45 - 10:10 **Vertical Ground Motion: Characteristics, Relationship with Horizontal Components, and Building Code Implications**
Yousef Bozorgnia, Exponent Failure Analysis Associates, K. Campbell, EQE International, and M. Niazi, Berkeley Geophysical Consultants

10:10 - 10:30 **Questions and Answers for Session I**

10:30 - 10:50 Break

SESSION II BUILDING RESPONSE
Moderator: *Chris Poland*, Degenkolb Engineers
Chair, SMIAC Buildings Subcommittee

10:50 - 11:15 **Seismic Performance of Four Instrumented Steel Moment Resistsing Frame Buildings During the 1994 Northridge Earthquake**
Farzad Naeim, R. Lobo, K. Skliros and M. Sgambelluri, John A. Martin & Associates

11:15 - 1140 **Evaluation of Soil-Structure Interaction Effects from Strong-Motion Recordings**
Jonathan Stewart, UCLA, Los Angeles

11:40 - 12:05 **Evaluation of Response of a Tall Concrete Frame Building to Multiple Earthquakes**
Gary Hart, M. Skokan, A. Dumortier, UCLA, Los Angeles, and S. Huang, Hart Consultant Group, Los Angeles

12:05 - 12:25 **Questions and Answers for Session II**

12:25 - 1:55 **Luncheon**
Introduction *James Davis*, State Geologist, Division of Mines and Geology
Topic: **Overview of the Turkey Earthquake of August 17, 1999**
Speaker: *Peter Yanev*, Chairman, EQE International

SPECIAL SESSION: CONSORTIUM OF ORGANIZATIONS FOR STRONG-MOTION OBSERVATION SYSTEMS (COSMOS)

2:00 - 2:20 **The Consortium of Organizations for Strong-Motion Observation Systems (COSMOS) - Mission and Objectives**
Bruce Bolt, President

2:20 – 2:40 **Toward a Common Format for Strong-Motion Data**
Anthony Shakal, DMG/SMIP and Roger Borcherdt, U.S. Geological Survey

2:40 – 3:00 **On the Development of "User-Friendly" Interfaces for the Use of Strong-Motion Data on the Internet**
Roger Borcherdt, U.S. Geological Survey and Anthony Shakal, DMG/SMIP

3:00 - 3:40 **A Virtual Strong-Motion Data Center for Data Dissemination through the Internet**
Ralph Archuleta, A. Tumarkin, *Grant Lindley*, UC Santa Barbara; Roger Borcherdt, National Strong Motion Program of USGS; and Anthony Shakal, Strong Motion Instrumentation Program of DMG

3:40 - 4:00 **Questions and Answers for Special Session**

4:00 **Closing Remarks**

♦ ♦

5:30 – 7:30 **COSMOS Reception at UC Berkeley Faculty Club**

September 16

8:30 – 3:30 **COSMOS Annual Meeting at Pacific Earthquake Engineering Research Center, Richmond**

SITE RESPONSE STUDY OF WEAK AND STRONG GROUND MOTION INCLUDING NONLINEARITY

Feng Su, Yuehua Zeng, John G. Anderson

Seismological Laboratory, University of Nevada-Reno,Reno, Nevada

Vladimir Graizer

California Division of Mines and Geology
Strong Motion Instrumentation Program, Sacramento, California

ABSTRACT

Site response from both weak and strong ground motion recorded at co-located sites were estimated and compared. We find weak and strong motion site responses differ significantly at stations where peak acceleration is above 0.3g, peak velocity is above 20 cm/sec, or shear strain is above 0.06% during the mainshock. The nonlinearity is present across the entire frequency band that we analyzed, from 0.5-14 Hz, and it occurred on sediment sites as well as on soft rock sites. We than compared these observations with a standard engineering model of nonlinear soil response. The model works well for the frequency range from 1.5 to 10 Hz. It diverged from data in frequencies below 1.5 Hz and above 10 Hz, but it is premature to assign much significance to this divergence because the engineering model we used was generic rather than site specific. Finally, we estimated the spectral attenuation parameter Kappa (κ) and compare it between weak and strong motion data at co-located sites. Our result suggests that some of the variability in measurements of κ comes from variability at the source. Kappa may be reduced from weak motion values at sites where nonlinearity is strong, but the source variability has the effect of reducing our confidence in that conclusion.

.

INTRODUCTION

The recent development of modern seismic instrumentation provides high quality ground motion records from strong motions as well as small earthquakes. This paper aimed to analyze ground response records corresponding to different levels of shaking. Our objectives are (1) to study site response from weak and strong motion including possible nonlinear effects; (2) to examine what we observed from data against a commonly used engineering model for nonlinearity; (3) to evaluate if nonlinear effects modify the spectral attenuation parameter Kappa and if weak motion estimates of kappa are reliable for strong motion.

The Northridge, California earthquake (M_L=6.7) occurred on Jan. 17, 1994. It was followed by hundreds of aftershocks. The mainshock and many of these aftershocks were recorded by the strong motion network stations operated by the California Strong Motion Instrumentation Program (CSMIP). These high quality data provide a unique data set to study weak and strong motion at the same sites. In this study, we have collected seismograms from CSMIP and the SCEC data base at stations with both mainshock and aftershock seismograms.

COMPARISON OF WEAK AND STRONG MOTION SITE RESPONSE AT CO-LOCATED SITES

Site response refers to the highly variable effect of near surface geological structures on the Fourier spectral amplitude of ground motion. In this section of the paper, we summarize the results of Su et al. (1998). They first computed the synthetic Green's function, *G(f,r),* in a regional layered elastic model using an improved reflectivity method of Luco and Apsel (1983). The small event source is treated as a point source with a Brune (1970, 1971) time function. Then the Fourier spectrum of the synthetic Green's function, M(f,r), is

$$M(f,r)=G(f,r)\ \frac{M_0}{\rho\beta^2}\ \frac{(2\pi f)^n}{1+(f/f_0)^2}e^{-\pi\Delta\kappa_s f} \qquad (1)$$

In Equation (1) M_0 is the seismic moment, f_0 is the corner frequency, ρ and β are the material density and S-wave velocity at the source, n is equal to 2 for acceleration seismograms, and $\Delta\kappa_s$ is related to the spectral decay parameter. The Green's function, G(f,r), is computed using a velocity model that includes attenuation along the travel path and in the near surface. The parameter $\Delta\kappa_s$ is an adjustment for the difference between attenuation in the layered crustal model and the site-specific attenuation which may differ. This paper uses a convention that the spectral decay parameter κ is simply measured from the slope of the raw high-frequency acceleration spectrum, as it was defined by Anderson and Hough (1984), and that systematic residuals from a model (as used here or by Anderson, 1991, or Schneider et al, 1993, for example) should be designated as $\Delta\kappa$.

Parameters in Equation (1) that must be adjusted are the seismic moment M_0, the corner frequency f_0, and the attenuation parameter $\Delta\kappa_s$. They are determined for the individual seismograms using the method described by Anderson and Humphrey (1991). That method minimizes the misfit between the spectrum and model by linearizing the fitting for moment and $\Delta\kappa_s$, and systematically testing all plausible values of f_0. The final estimates of seismic moment, $\overline{M}_0$, and corner frequency, $\bar{f}_0$ for each event are obtained by log averaging over the initial estimated M_0 and f_0 from all the stations. Then, we define the reference synthetic spectrum M'(f,r) as

$$M'(f,r)=G(f,r)\ \frac{\overline{M}_0}{\rho\beta^2}\ \frac{(2\pi f)^n}{1+(f/\bar{f}_0)^2}e^{-\pi\overline{\Delta\kappa_s} f} \qquad (2)$$

where $\overline{\Delta\kappa_s}$ is averaged over $\Delta\kappa_s$ from all stations.

The estimate of the site response function from each event is defined as the residual between the logarithms of the observed spectrum, S(f), and the reference synthetic spectrum, M'(f,r). That is,

$$r_s(f)=\log\ [S(f)/M'(f,r)\ ] \qquad (3)$$

Since M'(f,r) is the model prediction using the optimal source derived from the observations at several stations, the residual $r_S(f)$ represents the difference in the responses of wave propagation to a particular site compared to wave propagation through the average regional structure. The estimates from several aftershocks are averaged to obtain the final estimates for weak motion site response at each station.

The strong-motion site response was estimated by the spectral ratio of the observed strong ground motion to the synthetic seismogram calculated using the composite source model in the same layered crustal sturcture, and with the same correction for $\Delta\kappa_s$, as that used in the weak motion estimation.

Using the above methods, Su et al (1998) estimated weak and strong motion site response functions from the Northridge mainshock and its aftershocks. Figure 1 shows the location of the weak and strong motion stations and events we used in site response estimation. Information about these weak and strong motion stations is also listed in Table 1. Figures 2a and 2b compare strong motion with weak motion site response functions for the horizontal and vertical components, respectively. Both strong and weak motion site amplification were normalized to a rock station LA00 before taking the ratio to further eliminate any source bias in the strong motion site response estimation. This normalization implies an assumption that the nonlinear site response at station LA00, if there is any, is negligible. LA00 is situated on a Mesozoic rock site south of the fault and away from the rupture direction. Thus, we considered it the best choice for a station that is unlikely to be strongly affected by either details of the rupture model or nonlinear site response. In the end, this means that the Greens' functions *G(f,r)* have been used to make a more sophisticated adjustment for geometrical spreading than simpler assumptions such as (1/r) that have been used in some other studies of site response for widely distributed stations.

Figure 2b shows that for the vertical component, the weak and strong motion site responses generally agree. In contrast, for the horizontal components (Figure 2a), the weak motion site responses are almost never smaller than the strong motion responses, and often the weak motion response is greater. The difference between weak and strong motion site response is most significant at stations TAG, JFPP and NWHP.

To quantify the difference between weak and strong motion site response, we define the average strong to weak motion ratio, *ASW Ratio*, as

$$ASW\ \ Ratio = \exp\left\{\frac{1}{N_f}\sum_{i=1}^{N_f}\ln\left(\frac{r_S(f_i)}{r_W(f_i)}\right)\right\} \qquad (4)$$

where $r_s(f_i)$ is the strong motion site response function and $r_w(f_i)$ is the weak motion site response function, after normalization to response at station LA00. Only the horizontal component of the site response function is considered. N_f is the total number of the frequency points used in the average. The frequencies are equally spaced on a logarithmic scale over the frequency band from about 0.5 Hz to about 14 Hz.. Here we used the ASW Ratio instead of the AWS Ratio, the

inverse of the ratio in Equation (4) used by Su et al. (1998), to consistent with what the engineer used discussed later.

The solid circles in Figures 3a, b and c give *ASW Ratio* as a function of the peak ground acceleration (PGA), peak ground velocity (PGV), and shear strain (e_{max}) observed at each station during the main shock, respectively. The values of PGA and PGV are obtained from the seismograms of the mainshock. For a general solution to the wave equation in a homogeneous medium, the strain is equal to the ratio of particle velocity to medium velocity. Thus, we estimate e_{max} as $e_{max}=(PGV/v_s)$ where v_s is the average shear velocity in the upper 30 meters at the site. The v_s is estimated from the generalized geology at each site according to Park and Elrick (1998). To be specific, we uses v_s equal to 332 m/s, 397 m/s, and 569 m/s for Quaternary, Tertiary, and Mesozoic sites, respectively.

If site responses from strong and weak motion are about the same, the *ASW Ratio* will be close to unity. In Figure 3, at stations with relatively low amplitudes of ground motions, the *ASW Ratio* is near unity, indicating that the strong and weak motion site response functions agree with each other within the uncertainty. However, the *ASW Ratio* decreases as the recorded peak motions increase, indicating there is a deamplification effect in strong motion compared to weak motion. When the recorded peak acceleration is greater than about 0.3g, peak velocity is greater than about 20 cm/sec, or shear strain is greater than about 0.06%, this strong motion deamplification effect becomes significant. There could be some nonlinearity in the stress-strain relationship at smaller amplitudes, but the effects of nonlinearity are emerging from the other uncertainties and becoming significant for ground motions above the threshholds identified here.

Figure 3 shows direct evidence of nonlinearity at the sites with the higher levels of ground motions. It demonstrates a relationship between nonlinear site response and peak ground acceleration, peak ground velocity, and shear strain. The nonlinearity is not only present in sediment sites but also on soft rock sites like TAG and LA01(see Table 1 for their site condition and *ASW Ratio*). This is not surprising in the context of laboratory studies which find nonlinearity of rock samples (Johnson and McCall, 1994, Johnson and Rasolofosaon, 1996).

Figure 3 suggests a threshold in peak acceleration, peak velocity, and peak strain that can be used in several ways. Whenever an observation exceeds the threshold, nonlinear site response should be anticipated. Whenever linear calculations predict ground motions that exceed the threshold, reevaluation using nonlinear methods is necessary. Finally, these results can be used to test the commonly used nonlinear models. That is, when these calculations are performed, a linear calculation can also be carried out, and the ratio would be expected to consistent with Figure 3. This is discussed in next section.

To investigate this nonlinear site response in the frequency domain, we examined the ratios of strong to weak motion site amplification as a function of frequency and averaged the ratios over the stations. This average, obviously, has no particular meaning since it depends on the distribution of stations. It takes on meaning when, for a group of strongly shaken stations, it has an average that differs from unity. Figure 4 shows the averaged ratio (thick line) over 15 sediment stations we studied. Its 95% confidence zone is indicated by the green shades. On average, the ratio is equal to 0.6, meaning the average site deamplification during earthquake

strong motion is about 0.6 times those of weak motions. This deamplification is significant and it occurred across the entire frequency band we studied, implying nonlinearity is present at all these frequencies.

COMPARISON OF THE OBSERVATIONS WITH AN ENGINEERING MODEL PREDICTION

A typical approach to simulating nonlinear soil response is to estimate the effects of nonlinear wave propagation through a stack of sediments. For this, following Ni et al (1997), we chose a time-domain wave propagation model of Lee and Finn (1978). In this model, the entire seismogram is treated as a vertically-propagating shear wave that excites the stack of sediments from the bottom. The calculations can be performed either assuming linear elastic response of the sediment or assuming the sediments follow a non-linear stress-strain relationship that obeys the Masing rule (1926). The shape of the nonlinear stress-strain relationship is controlled by a "modulus reduction curve" that gives the average secant shear modulus as a function of the strain. A model of modulus reduction curves, which includes the effects of both confining pressure (depth) and rigidity, has been presented in EPRI(1993), and is used as the input for our calculations.

A common site model was used for all sites. It has a mean shear wave velocity of 370 m/s for the upper 30 meters (Park and Elrick, 1998) with a water table at 3 meters below the surface. The total thickness of the soil column is 100 meters. Test runs suggest that the simulation result become less dependent on the depth of the sediments when the thickness of the soil column is greater than 60 meters.

We then generated over 1000 synthetic accelerograms for a dense distribution of stations surrounding the Northridge area. These were generated using the composite source model (Zeng et al, 1994). Assuming the linear response of the soil column represents the weak motion site amplification and its nonlinear response represents the strong motion site amplification, we computed the same *ASW Ratio* from each station and plotted them on Figure 5. The general trends of *ASW Ratio* as a function of peak acceleration (figure 5a) are similar between model and observation, although the model falls off a little less rapidly than the data, especially for the peak velocity (figure 5b) and strain (figure 5c). The synthetics also show less scatter than the data.

To compare nonlinear response in the frequency domain between the model and the data, we used site specific synthetic predictions as input to generate synthetic accelerograms under both linear and nonlinear approaches at the 15 sediment sites. Following a similar procedure as used for the data, we calculated the ratio of strong (nonlinear) to weak (linear) motion site response for each site, and then averaged it over the 15 sites included in Figure 4. In Figure 6 the synthetic average is plotted with the data for comparison. The results show that the model matches well with the data in the frequency range from about 1.5 to 10 Hz. However, they diverge at frequencies below 1.5 Hz and above 10 Hz. At frequencies above 10 Hz, the model shows a rapid increase in amplitude ratio, up to a factor of two for nonlinear response in comparison with linear response at about 14 Hz. This is a model artifact due to the nonlinear stress-strain relation, which produces a sudden change in shear modulus as the shear strain reverses. At frequencies below 1.5 Hz, the amplitude ratio from data is significantly different

from unity, although it shows a trend of convergence to unity. In contrast, the synthetic ratio is essentially equal to unity. The departure of the synthetics from the data below 1.5 Hz is the cause of a less rapid fall off in the synthetics for the *ASW Ratio* versus ground motion parameters (Figure 5), especially for peak velocity or strain, since the ground velocity pulses are dominated by lower frequency waves than that of the ground acceleration.

In order to check if the low amplitude ratio measured from data for frequencies 0.5 to 1.5 Hz is real, we carefully examined the data to be certain that signals are significantly above noise levels. In addition, our site response functions were normalized to the rock station LA00 so the source effect from mainshock and aftershocks is minimized. Our result of the observed nonlinearity presented at all frequencies studied is also consistent with the result by Field et al (1997) who referenced their site amplifications to the average of several rock sites. A recent work by Cultrera et al. (1998) on the site responses at the Jensen Filtration Plant shows that the weak motion records of aftershocks within two minutes of the mainshock exhibit a nonlinear deamplification comparable to that of the mainshock, suggesting that the nonlinear shear modulus reduction that occurred during strong shaking may not recover back as quickly as the current engineering model predicts. Thus the longer period and relatively lower amplitude motion will experience the same nonlinear deamplification as that of the high frequency waves. As a consequence, the observed ground motion suffers further amplitude reduction than the model prediction.

It is premature to assign much significance to the disagreement of the model with the observations at low and high frequencies. One hypothesis is that there is a problem with the way that the nonlinearity is modeled. A nonlinear reduction in low frequencies could result from a delay in recovery of the shear modulus reduction after strong shaking. However, we used a generic soil model which we applied to all of the stations. Detailed models at each of the stations would undoubtedly differ even if the average velocity for the station is the same. For instance, one way that the detailed models would likely differ is by having alternating layers of higher and lower velocities; in this case nonlinearity in the low velocity layers could have a stronger effect on the low frequency waves than what is predicted by a model in which these layers are absent. It will be important to test the difference between the linear and nonlinear response with the specific site characteristics that are being developed in the ROSRINE project in future investigation.

SYNTHETIC SEISMOGRAMS INCORPORATING NONLINEARITY

Eventually, it is our hope that the models for generating synthetic seismograms might be so good that they can replace regression analysis. The results of the above sections strongly suggest that it is necessary to incorporate nonlinearity into these models in a systematic way when computing ground motions at short distances.

We undertook to test how well our synthetic seismogram model performed for the Northridge case. The model was tested previously by Anderson and Yu (1996) in a blind prediction and the resulting ground motion prediction is consistent statistically to the observation. Zeng and Anderson (1996) demonstrated that a specific realization of the composite source is capable of matching waveforms at low frequencies. For this study, we

carried out an experiment closer to that of Anderson and Yu (1996). Our parameters were not generated using a blind test as they did, but rather picked to be consistent with the source parameters used by Zeng and Anderson. We used a different regional velocity model and a different Q model that has subsequently been demonstrated to be more appropriate. Synthetics were passed through the generic nonlinear soil model as described above.

Our initial set of accelerograms showed a higher amount of directivity at high frequencies than we considered to be realistic. Motivated by the fact that we do not observe any distinct radiation pattern and wave polarization at high frequency, we therefore introduced an effective high frequency source radiation term. This source radiation consists of energy contributions from an angular cross section centered at the direction from the source to receiver in order to simulate high frequency wave reflection and scattering at the fault zone. The total source radiation then equals

$$b*\textit{effective-source-radiation} + (1- b)*\textit{double-couple-source-radiation} \qquad (5)$$

where b is a continuos function of frequency. It equals 1 above a high frequency threshold and tapers to 0 at low frequency since this reflection and scattering at the source zone has less an effect at lower frequencies.

This modification to the composite source model was validated with the Northridge strong motion observations. Figure 7 gives examples of the nature of the observed ground motions and the model predictions. Figure 8 compares the results of this improved method and that of a regression prediction (Abrahamson and Silva, 1997) to the observed PGA and to SA at a period of 3 second. Our synthetics as modified by Equation (5) predict the trends of the observed ground motion parameters better than the regression. The figures also show the standard errors of prediction from the improved composite source model and from the Abrahamson and Silva's regression. For comparison, without the modification in Equation (5), the standard errors in prediction PGA increased from 0.455 to 0.554, and for predicting SA at a period of 3 second increased from 0.65 to 0.66. Since the modification is to simulate near source scattering effect at high frequency, the improvement high frequency simulation is expected. The scatter in the data is caused in part by the local site and basin response effects which are not modeled in the current context of high frequency simulation.

COMPARISON OF THE SPECTRAL ATTENUATION PARAMETER KAPPA MEASURED FROM WEAK AND STRONG MOTION RECORDS

The parameter kappa (κ) was defined by Anderson and Hough (1984) to describe the shape of the high frequency spectrum of accelerograms. The study was actually motivated in part by an earlier paper by Hanks (1982) recognizing that the acceleration spectrum falls off rapidly at high frequencies. Anderson and Hough observed that the high-frequency acceleration spectrum falls off approximately exponentially with frequency, i.e. $A(f) \sim \exp(-\pi\kappa f)$. Based on observations at a single station, they found that κ increased with distance from the earthquake, but that the intercept of that trend varied from one station to another. Based on this observation they proposed that the most reasonable explanation for the systematic behavior of the parameter kappa was that the parameter was caused by attenuation. They suggested that the

attenuation had a strong contribution from site conditions, but that it also had a contribution from regional wave propagation. Anderson (1991) attempted to generalize the model, describing the observations of κ in southern California from Anderson and Hough (1984), Hough et al (1988), and Hough and Anderson (1988) with the model:

$$\kappa = \kappa_0 + \tilde{\kappa}(r) \qquad (6)$$

where the term κ_0 was conceived of as predominantly a site term and $\tilde{\kappa}(r)$ characterized the distance dependence. The relationship between κ and the seismological measure of energy loss, Q, is not straightforward. The normalization of κ is the same as the normalization of t^*, which is directly related to Q ($t^*=r/(Qv_s)$), but as pointed out first by Anderson and Hough (1984) and Anderson (1986), κ will only equal t^* if Q is independent of frequency. Many observations exist suggesting a frequency dependence of Q. This difficulty, however, does not seem to severely limit the usefulness of κ to characterize the acceleration spectrum at high frequencies, since κ is defined as an observational parameter.

Anderson (1986) pointed out the implications of this model for small earthquakes: if the small earthquake spectrum is affected the same way as the strong motion spectrum, distinguishing between the effects of the source and the attenuation would become difficult for smaller events as the corner frequency moves into the high frequency band where κ is measured. To overcome this difficulty Anderson and Humphrey (1991) proposed a method to measure κ relative to a Brune (1970) model for the spectrum of small events. This method was applied by Humphrey and Anderson (1992) and Su et al (1996) with apparent success. Schneider et al (1993) point out the usefulness of the parameter κ for predicting strong motions from future events, so it is important to be able to estimate κ for the site without waiting for a strong earthquake to occur. However, considering differences in the earthquake sources and particularly the potential importance of nonlinear site response, it is important to check how well measurements of κ from small events predict κ at the same site during large events. In this study, we use some of the excellent CSMIP data to make this comparison.

This comparison is particularly timely due to some studies on κ in southern Nevada. Estimates of κ by Biasi and Smith (1997) from extremely small earthquakes, still assuming a Brune spectral shape with a stress drop similar to the stress drop of larger events, gave values of κ that were larger than those obtained by Su et al (1996). Furthermore, both of these studies showed a larger amount of scatter in estimates of κ that one would expect for a parameter dominated by wave propagation.

We examine κ from two data sets in southern California. First, we examine κ from weak and strong motions for the data set used by Su et al (1998). Secondly, we examine it from a subset of the strong motion records of Northridge aftershocks recorded on CSMIP instruments. For both data sets, we assumed that the distance-dependent term can be linearized over the short distance range used in this data as $\tilde{\kappa}(r) = ar$. Then, we have

$$\kappa = \kappa_0 + ar \qquad (7)$$

where a is related to the Earth's velocity and Q structure and r is the hypocentral distance. Conceptually, a would equal $1/(QsVs)$ if Q_S were independent of frequency.

In the study of the aftershock data used in Su et al (1998), we measured κ in the frequency band of 5 to 20 Hz. The analysis procedure was somewhat different from the approach described by Equations 1-4, instead following the approach used by Su et al (1996) for small events in southern Nevada. Once the basic measurement of κ was obtained from each seismogram, we used a least-squares method to determine the constants a and an average value of κ_0 for each station from weak motion data. In this case, we obtained a=0.00136 *s/km.* For strong motion data, we measured the slope of the accelerograms directly (as in Anderson and Hough, 1984), and adjusted the slope for distance using the same constant a. In addition to the data used by Su et al (1998), we used CSMIP aftershock data from two closely spaced stations at Tarzana, that is, the station at Cedar Hills Nursery (NUR) and Clubhouse (CLU). The two stations are about 150 meters apart. Figure 9 shows the locations of the Tarzana stations and the events we used. In this case also, κ was measured directly from the S-wave spectrum of the accelerogram. Figure 10 shows these spectra and the spectral fits that produce the individual κ measurements.

If the estimates of κ_0 are to be usefully compared between weak and strong motion records, then it is critical that the distance correction must be reliable. For that reason, before presenting the data, we test the distance correction for the second set of data. For an individual observation, we calculate κ_0^i with the equation:

$$\kappa_0^i = \kappa - ar \qquad (8)$$

Obviously, if the model behind Equation (7) holds, then κ_0^i should be the same for every observation, and that constant would be recognized as the site term κ_0. The distance correction in Equation 8 can be considered if the individual estimates of κ_0^i are independent of distance.

For this purpose, Figure 11a shows the individual estimates of κ and of κ_0^i versus distance for the value of a for the station NUR and Figure 11b for the the station CLU. The raw measurements of κ show a rather strong distance dependence. After correction, κ_0^i is not correlated with distance, indicating that a is reasonable. This value of a is larger than the value estimated by Anderson and Hough (1984) for the same region. The difference is that in this case, the distances are smaller, and the path is therefore expected to be much shallower. The smaller value of a is expected from a depth dependence to Q.

Figure 12 shows κ_0^i estimated from 21 main shock accelerograms (solid circle) used by Su et al (1998) and the station average for weak motion (open circle) at the same stations. These are plotted against the observed PGA during the mainshock. This figure indicates that κ_0^i from weak and strong motion data are not simply the same. For peak accelerations in the range where nonlinearity is present, i.e. above 0.3g (Fig. 3), most of the values of κ_0^i from the weak motions are greater than the corresponding value for the strong motion record. A reduction in kappa for strong motion records is in the same direction as the predictions of Yu et al (1993) and Ni et al (1997), although those papers may predict a greater difference than what is observed.

Figure 13a compares unadjusted estimates of κ at the adjacent Tarzana stations, NUR and CLU, and Figure 13b compares the estimates of κ_0^i between the two stations. The unadjusted estimates of κ are strongly correlated, but this is to be expected since the differences in hypocentral distances are significant for different aftershocks. The residuals after adjusting for distance, the various estimates of κ_0^i, have a smaller range, but the residuals are still correlated.

It seems most likely that the correlation is related to the earthquake source in some generalized way. The residuals are not related to the source depth as we have checked. However, Several other source parameters might be hypothesized to have an impact. One is the source spectral shape, which may have some variation in the high-frequency rolloff A second possibility is that there is some dependence of κ on the radiation pattern at the source. The take-off angles to the two Tarzana stations are probably nearly identical for each event, but are expected to be sampling different sections of the radiation pattern for different events. Another possibility is that the residual is associated with some local anomaly in attenuation or scattering in the vicinity of the source. With the data used in this study, it is not possible to distinguish among these possibilities.

The significance of this result is that the spectral decay parameter is affected by more physical phenomena than that presented in Equations (6) and (7). Figure 12 suggests that nonlinear site response might cause κ to be decreased. Figure 13 suggests that the source of moderate-sized earthquakes affects the spectral decay at high frequencies. Equations (6) and (7) may need to be modified by the addition of a source term. Both Figures 12 and 13 indicate that some caution is needed in extrapolating from values of κ_0 estimated from small earthquakes to the value expected in large events.

CONCLUSION

In summary, nonlinearity appears to have decreased the average amplitudes of ground motions at sites that experienced the strongest shaking in the Northridge earthquake across the entire frequency band from 0.5-14 Hz. The data indicate that the nonlinearity was present when the peak acceleration exceeded 0.3g, the peak velocity exceeded 20 cm/sec, or the peak strain exceeded 0.06%. A comparison of these observations with a standard engineering model of nonlinear soil response indicates that the model works well for the frequency range from 1.5 to 10 Hz. However, the model diverged from data in frequencies below 1.5 Hz and above 10 Hz. At frequencies below 1.5 Hz, the data show continuous nonlinear deamplification in contrast to the model prediction. At frequencies above 10 Hz, the model generated additional high frequency energy which is actually an artifact of the nonlinear stress-strain relationship used. Nevertheless, the average model improves predictions of synthetic seismograms to the point where they are comparable to predictions of regression equations. Our result suggests that some of the variability in measurements of the spectral attenuation parameter κ comes from variability at the source, in contrast to the models in which κ is controlled entirely by path and site effects. Our results also suggest that κ measurements may be affected by nonlinear site response.

REFERENCES

Anderson, J. G. (1986). Implication of attenuation for studies of the earthquake source, Earthquake Source Mechanics, Geophysical Monograph 37, (Maurice Ewing Series 6), American Geophysical Union, Washington, D.C. 311-318.

Anderson, J.G. (1991). A preliminary descriptive model for the distance dependence of the spectral decay parameter in southern California, Bulletin of the Seismological Society of America 81, 2186-2193.

Anderson, J. G. and S. Hough (1984). A Model for the shape of the Fourier amplitude spectrum of acceleration at high frequencies: Bull. Seism. Soc. Am. 74, 1969-1994.

Anderson, J. G. and J. R. Humphrey, Jr. (1991). A least-squares method for objective determination of earthquake source parameters, Seismological Research Letters, 62, 201-209.

Anderson, J. G. and G. Yu, Predictability of strong motions from the Northridge, California, Earthquake. Bull. Seism. Soc. Am. 86, S100 (1996).

Biasi, G. P. and K. D. Smith (1997). Project report: site effects for seismic monitoring stations in the vicinity of Yucca Mountain, Nevada, WBS#1.2.3.2.8.4.1, Task #SPT38BM4.

Brune, J. N., Tectonic stress and the spectra of seismic shear waves from earthquakes from earthquakes, J. Geophys. Res. 75, 4997 (1970).

Brune, J. N., Correction, J. Geophys. Res. 76, 5002 (1971).

Cultrera, G., D. M. Boore, W. B. Joyner and C. M. Dietel, Nonlinear soil response in the vicinity of the Van Norman Complex following the 1994 Northridge, California, earthquake, Submitted to Bull. Seism. Soc. Am. (1998).

EPRI, Guidelines for determining design basic ground motions. Volume 1: Method and guidelines for estimating earthquake ground motion in Eastern North America, report, EPRI TR-102293, Nov. (1993).

Lee, K. W. and W. D. L. Finn (1978). DESRA-2: dynamic effective stress response analysis of soil deposit with energy transmitting boundary including assessment of liquefaction potential, *Soil Mechanics Series*, University of British Columbia, Vancouver, Canada.

Field, E. H., P. A. Johnson, I. A. Beresnev and Y. Zeng, Nonlinear sediment amplification during the 1994 Northridge earthquake, Nature, 599 (1997).

Frankel, A., High-frequency spectral falloff for earthquakes, fractal dimension of complex rupture, b-value, and the scaling of strength on faults, J. Geophys. Res., 96, 6291 (1991).

Gao, S., H. Liu, P. M. Davis, and L. Knopoff, Localized amplification of seismic waves and correlation with damage due to the Northridge earthquake: evidence for focusing in Santa Monica, Bull. Seism. Soc. Am. 86, S209 (1996).

Hanks, T. C. (1982) fmax, Bull. Seism. Soc. Am 72, 1867-1880.

Hough, S.E. and J. G. Anderson (1988). High-frequency spectra observed at Anza, California: implications for Q structure, Bull. Seism. Soc. Am. 78, 692-707.

Hough, S. E., J. G. Anderson, J. Brune, F. Vernon III, J. Berger, J. Fletcher, L. Haar, T. Hanks and L. Baker (1988). Attenuation near Anza, California, Bull. Seism. Soc. Am. 78, 672-691.

Humphrey, J. R. Jr. and J. G. Anderson (1992). Shear wave attenuation and site response in Guerrero, Mexico, Bulletin of the Seismological Society of America 82, 1622-1645.

Johnson, P. A. and K. R. McCall, Observation and implications of nonlinear elastic wave response in rock, Geophy. Res. Let., 21, 165 (1994).

Johnson, P. A. and R. N. J. Rasolofosaon, Manifestation of nonlinear elasticity in rock: convincing evidence over large frequency and strain intervals from laboratory studies, Nonlinear Processes in Geophysics, 3, 77 (1996).

Lee, K. W. and D. L. Finn, DESRA-2: Dynamic effective stress response analysis of soil deposit with energy transmitting boundary including assessment of liquefaction potential, Soil Mechanics Series, University of British Columbia, Vancouver, Canada (1978)

Masing, G., Eigenspannungen und Verfestigung beim Messing, proceedings, 2nd International congress of Applied Mechanics, Zurich (1976).

Ni, S.-D., R. V. Siddharthan and J. G. Anderson (1997). Characteristics of nonlinear response of deep saturated soil deposits, Bull. Seism. Soc. Am. 87, 342-355.

Park, S. and S. Elrick, Predictions of shear-wave velocities in southern California using surface geology, Bull. Seism. Soc. Am. 88, 677 (1998)

SCEC phase III report. (1998).

Schneider, J. F., Silva, W. J., and C. Stark (1993). Ground motion model for the 1989 M 6.9 Loma Prieta earthquake including effects of source, path, and site, Earthquake Spectra 9, 251-___.

Su, F., J. G. Anderson, J. N. Brune, Y. Zeng (1996). A comparison of direct S-wave and coda wave site amplification determined from aftershocks of the Little Skull Mountain earthquake, Bull. Seism. Soc. Am. 86, 1006-1018.

Su, F., J. G. Anderson and Y. Zeng, Study of weak and strong ground motion including nonlinearity from the Northridge, California, Earthquake sequence, Bull. Seism. Soc. Am, in press (1998)

Su, F., Y. Zeng, and J. G. Anderson, Simulation of the Loma Prieta earthquake strong ground motion using a composite source model, EOS, 75, 448 (1994).

Yu, G., J. G. Anderson, R. Siddharthan (1993). On the characteristics of nonlinear soil response, Bull. Seism. Soc. Am., 83, 218-244

Yu, G., K. N. Khattri, J. G. Anderson, J. N. Brune and Y. Zeng (1995). Strong ground motion from the Uttarkashi, Himalaya, India earthquake: comparison of observations with synthetics using the composite source model, Bull. Seism. Soc. Am. **85**, 31-50.

Zeng, Y., J. G. Anderson and F. Su, Subevent rake and random scattering effects in realistic strong ground motion simulation, Geophy. Res. Lett. , 22, 17 (1995).

Zeng, Y., J. G. Anderson and G. Yu, A composite source model for computing realistic synthetic strong ground motions, Geophy. Res. Lett, 21, 725 (1994).

Zeng, Y. and J. G. Anderson, A composite source model of the 1994 Northridge earthquake using genetic algorithms, Bull. Seism. Soc. Am. 86, S71 (1996).

Table 1: Station Information

Name	Location (Latitude, Longitude)		NE[a]	Strong-motion Station (source[b]-site name)	PGA[c] (cm/s^2)	PGV (cm/s)	ASW Ratio		Site Geology[d]
CPCP	34.2114	-118.6081	11	USC-station #53	320	28.7	0.48	Q	sediment
JFPP	34.3120	-118.4960	9	USGS-Jensen Filter Plant	416	40.8	0.25	Q	sediment
KSRG	34.0596	-118.4736	11	USGS-LA, Brentwood VA Hosp.	143	14.9	1.02	Q	sediment
LA00	34.1062	-118.4542	20	SCEC-Stone Canyon Reservoir	307	24.1	1.00	M	hard rock
LA01	34.1317	-118.4394	16	USC-station #13	388	36.2	0.43	T	soft rock
LA03	34.0900	-118.3390	9	CDMG-LA, Hollywood Storage Bldg.	256	15.1	0.97	Q	sediment
LA04	34.0700	-118.1500	6	CDMG-Alhambra, Fremont School	81	5.4	1.01	Q	sediment
MKDR	34.2173	-118.5235	7	USC-station #3	355	26.3	0.39	Q	sediment
MPKP	34.2871	-118.8816	10	CDMG-Moorpark	221	16.0	0.73	Q	sediment
NHFS	34.1988	-118.3978	13	USC-station #9	258	14.8	0.81	Q	sediment
NWHP	34.3880	-118.5332	16	CDMG-Newhall	540	60.2	0.22	Q	sediment
OVHS	34.3285	-118.4460	3	CDMG-Sylmar County Hosp.	594	45.9	0.64	Q	sediment
PDAM	34.3341	-118.3980	10	CDMG-Pacoima Dam Downstream	369	27.0	1.07	M	hard rock
SFYP	34.2369	-118.4391	5	CDMG-Arleta	256	22.3	0.58	Q	sediment
SMC	34.0122	-118.4913	5	CDMG-Santa Monica City Hall	498	23.5	0.69	Q	sediment
SMIP	34.2632	-118.6673	6	USC-station #55	475	41.4	0.40	T	sediment
SSAP	34.2309	-118.7135	13	USGS-Santa Susana	234	11.8	0.74	M	hard rock
SSC	34.0467	-118.3557	9	USC-station #91	395	28.8	0.76	Q	sediment
TAG	34.1604	-118.5343	6	CDMG-Tarzana	1150	61.4	0.20	Q	soft rock
VAN	34.2493	-118.4777	8	USGS-LA, Sepulveda VA Hosp.	706	59.5	0.46	Q	sediment
WVES	34.0050	-118.2790	3	USC-station #22	251	17.7	1.15	Q	sediment

a: Number of aftershock events used at that station.

b: The source of strong motion data is as follows: USC - University of Southern California; SCEC - Southern California Earthquake Center; CDMG - California Division of Mines and Geology; USGS - United States Geological Survey.

c: PGA and PGV are the arithmetic averages of the peak ground acceleration and velocity of two horizontal components, respectively. The seismograms were filtered in frequency band of 0.1 - 15.0 Hz in time doman before obtaining peak values.

d: M=Mesozoic and older rocks, T=Tertiary sediments, Q=Quaternary sediments. The averaged shear wave velocity in the upper 30 meters is 333m/s for Quaternary sediments , 406m/s for Tertiary and 589m/s for Mesozoic according to Park and Elrick (1998).

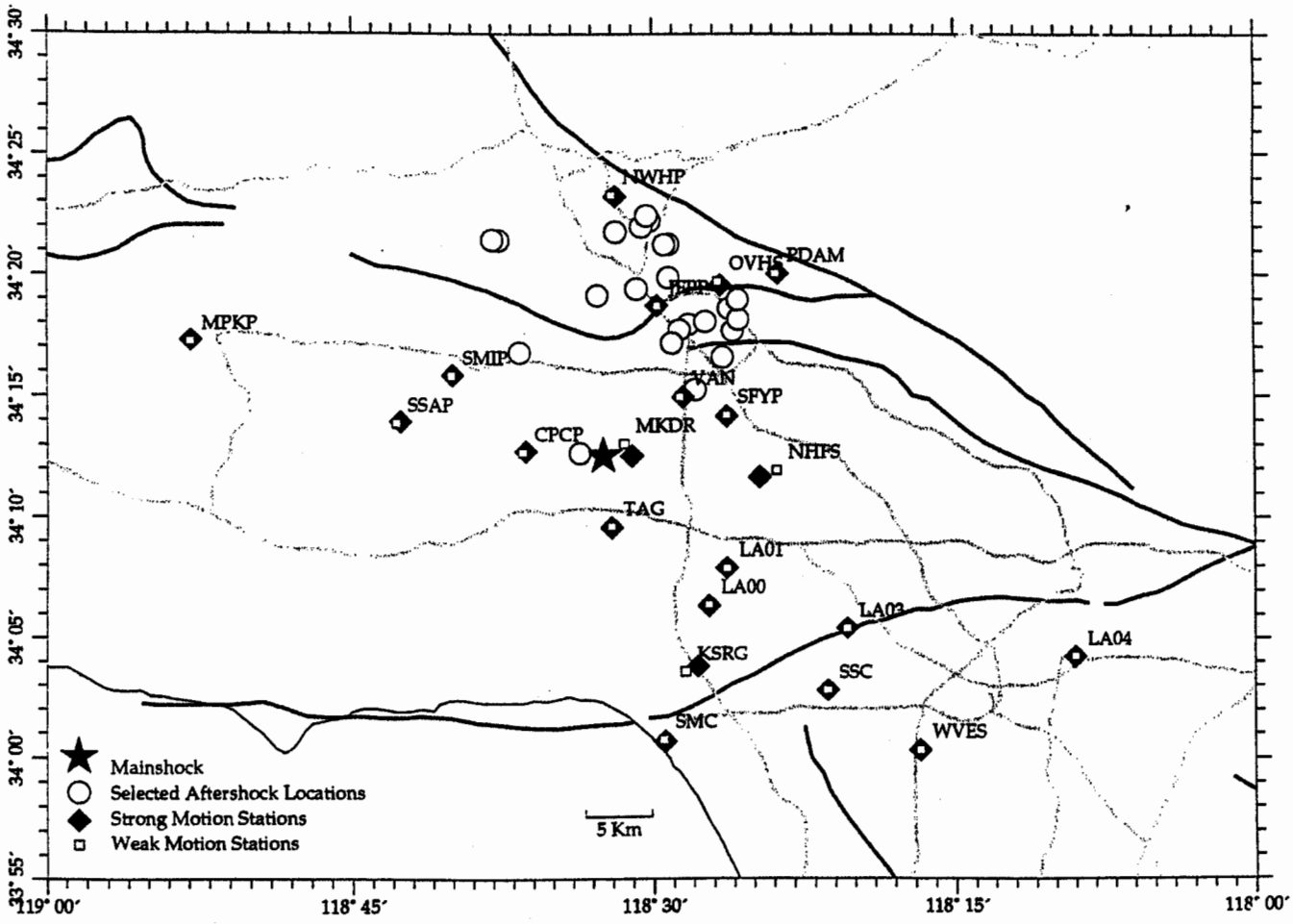

Figure 1: Map view of the event and station distributions used in this study.

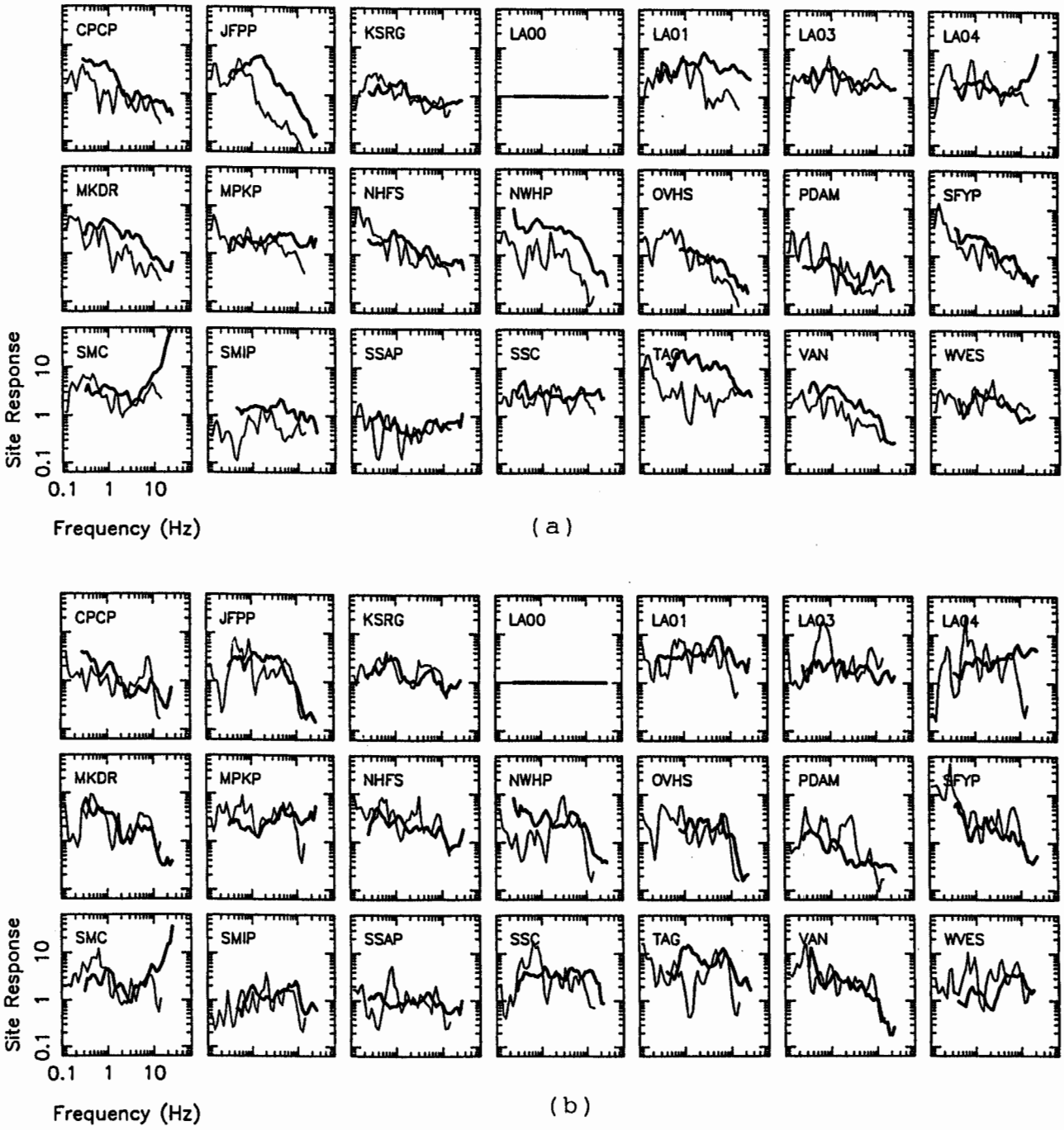

Figure 2: Comparisons of weak and strong motion site amplifications at their co-located sites. The thick and thin lines represents the site amplification obtained from weak motion and strong motion data, respectively. (a) Average of the horizontal components. (b) Vertical component.

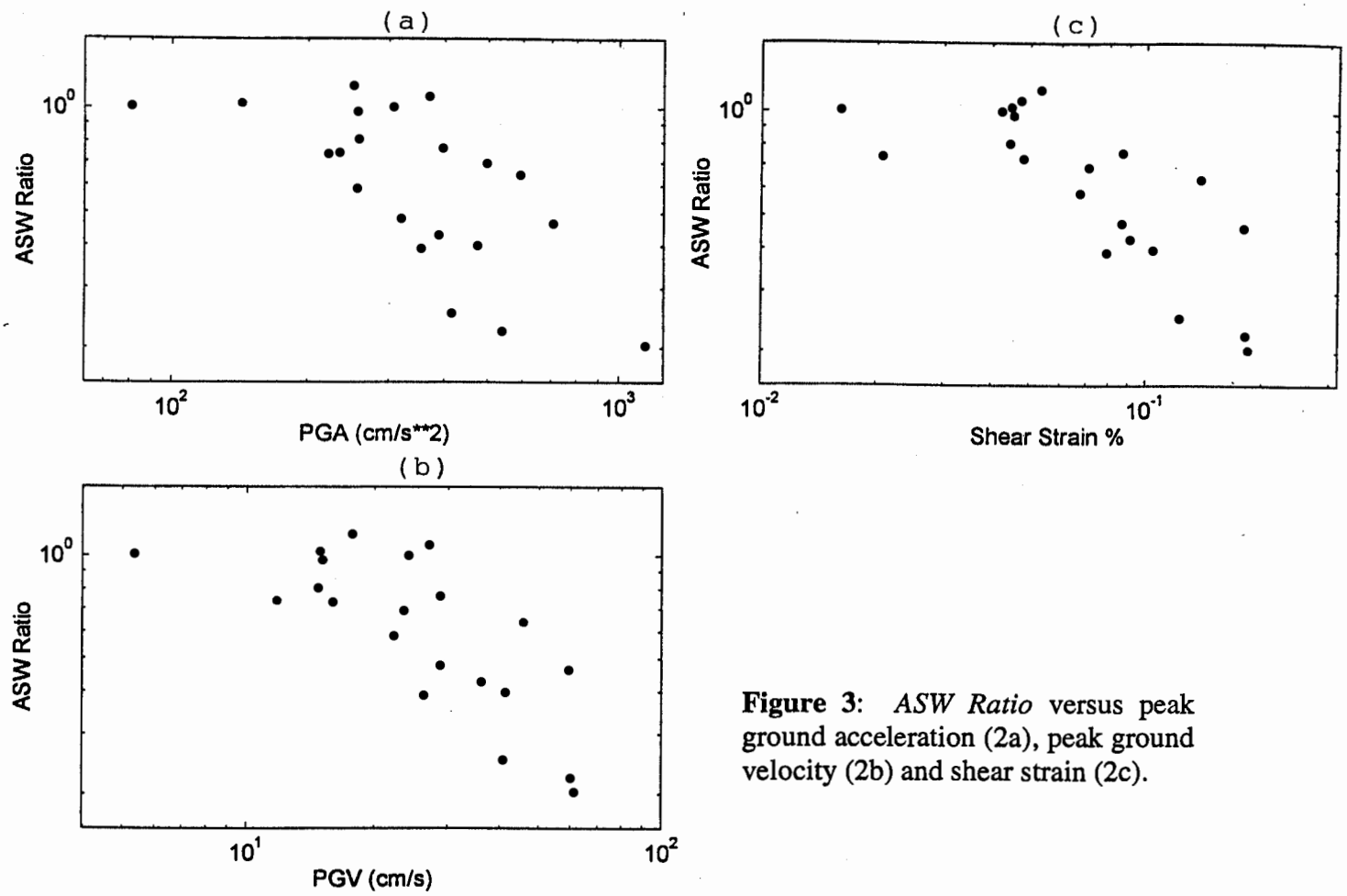

Figure 3: *ASW Ratio* versus peak ground acceleration (2a), peak ground velocity (2b) and shear strain (2c).

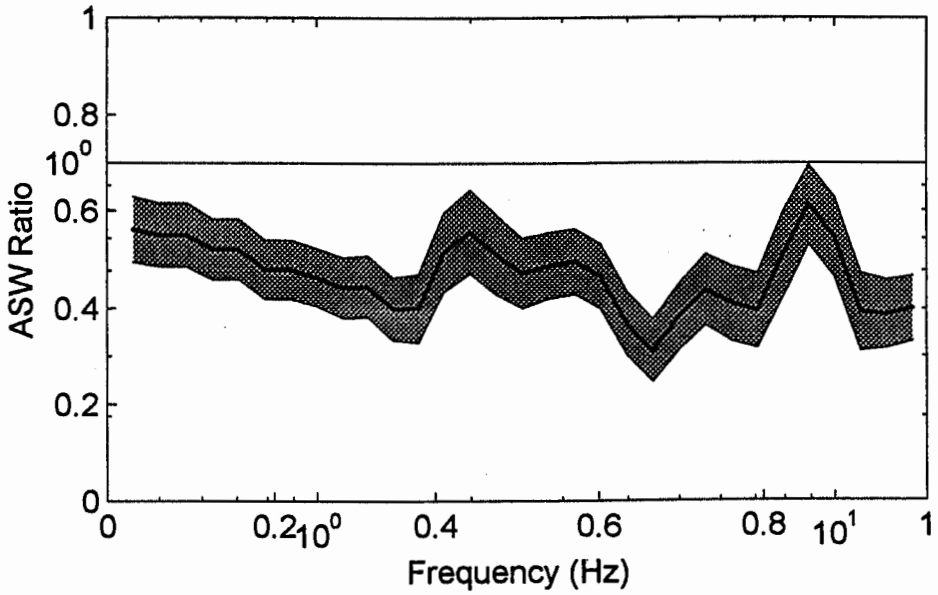

Figure 4: Ratio of strong to weak motion site response versus frequency averaged over 15 sediment sites we used (see Table 2 for station site condition. Station SMC is excluded since it may have focusing effect due to subsurface structure according to Gao et al. (1996)). The shaded area indicates the 95% confidence zone.

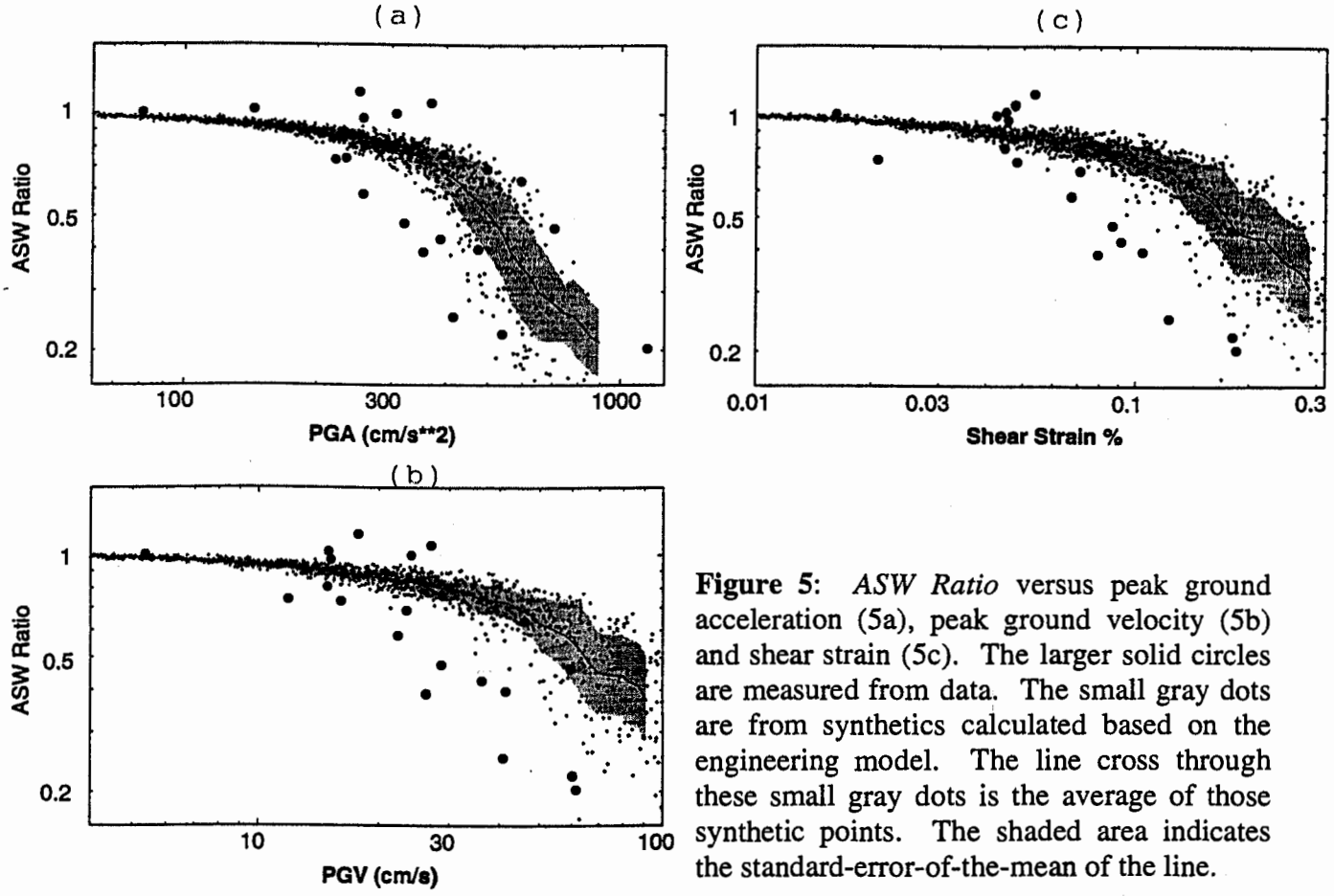

Figure 5: *ASW Ratio* versus peak ground acceleration (5a), peak ground velocity (5b) and shear strain (5c). The larger solid circles are measured from data. The small gray dots are from synthetics calculated based on the engineering model. The line cross through these small gray dots is the average of those synthetic points. The shaded area indicates the standard-error-of-the-mean of the line.

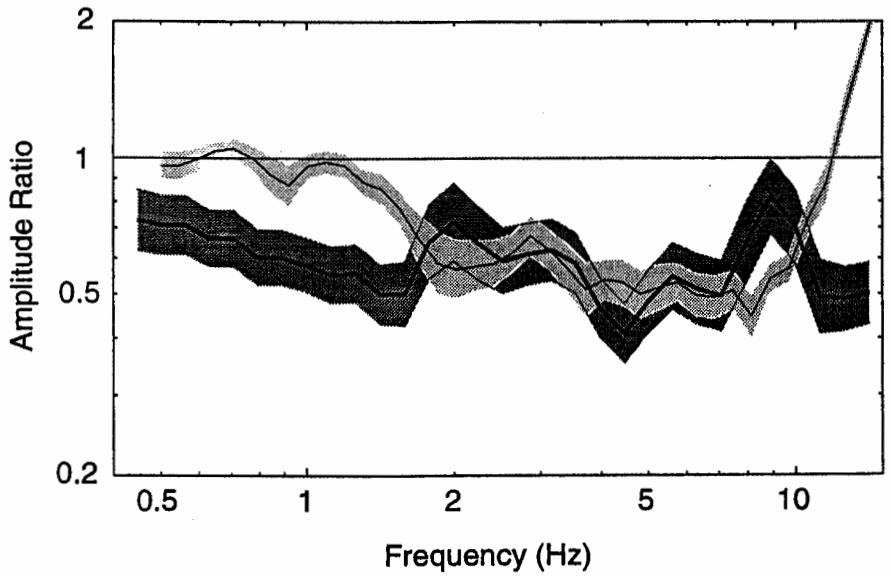

Figure 6: Ratio of strong to weak motion site response versus frequency averaged over 15 sediment sites we used. The thick line is from data and the thin line is from synthetics. The shaded area indicates the 95% confidence zone.

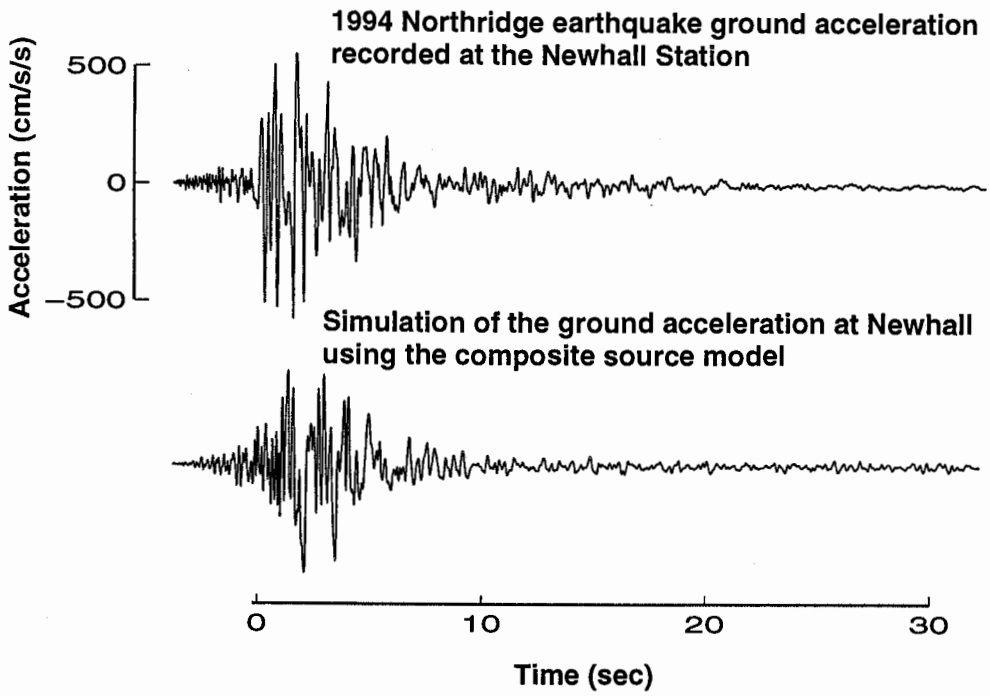

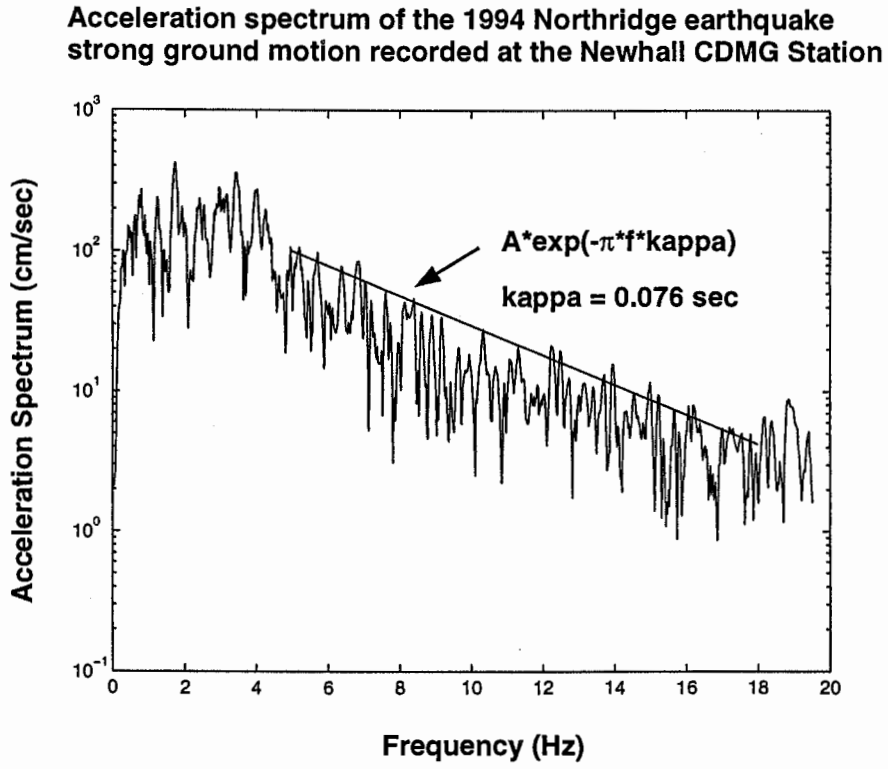

Figure 7. Top panel shows a comparison between an observed strong motion accelerogram and a synthetic one for the Northridge earthquake. The lower panel show the spectrum of the accelerogram and its kappa estimated from the spectral decay at high frequency.

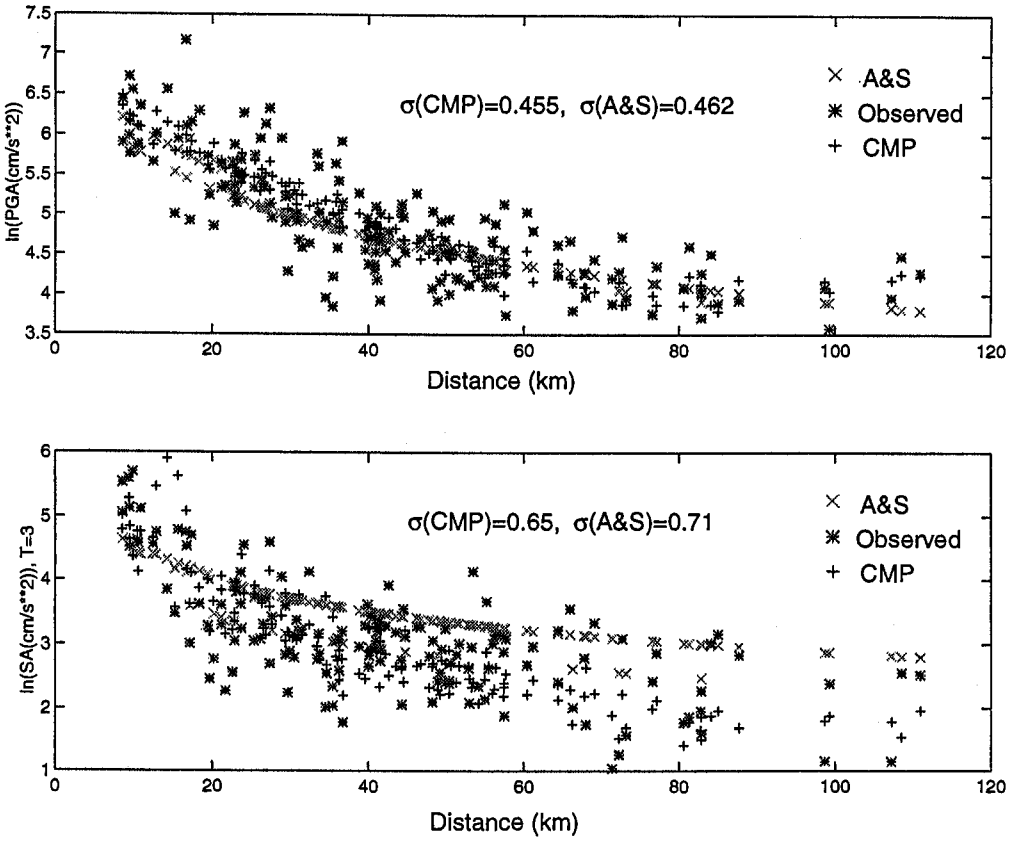

Figure 8. Comparison between observed and predicted peak ground motion parameters for the Northridge earthquake, 1994. The upper panel is for the peak ground acceleration and the low panel is for the spectra acceleration with 5% damping at 3 second period.

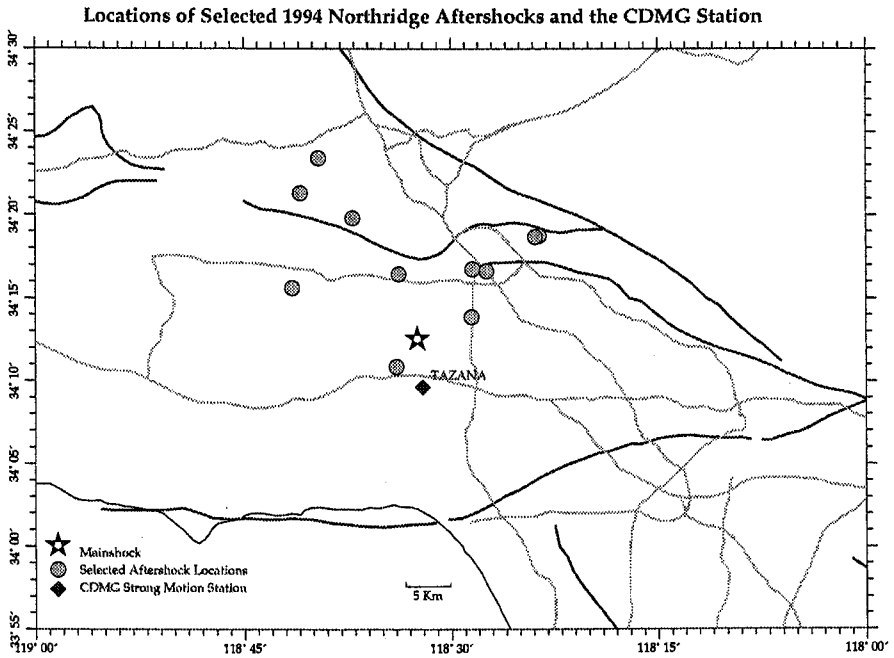

Figure 9. Map view of the Northridge aftershocks and station distribution used for this study.

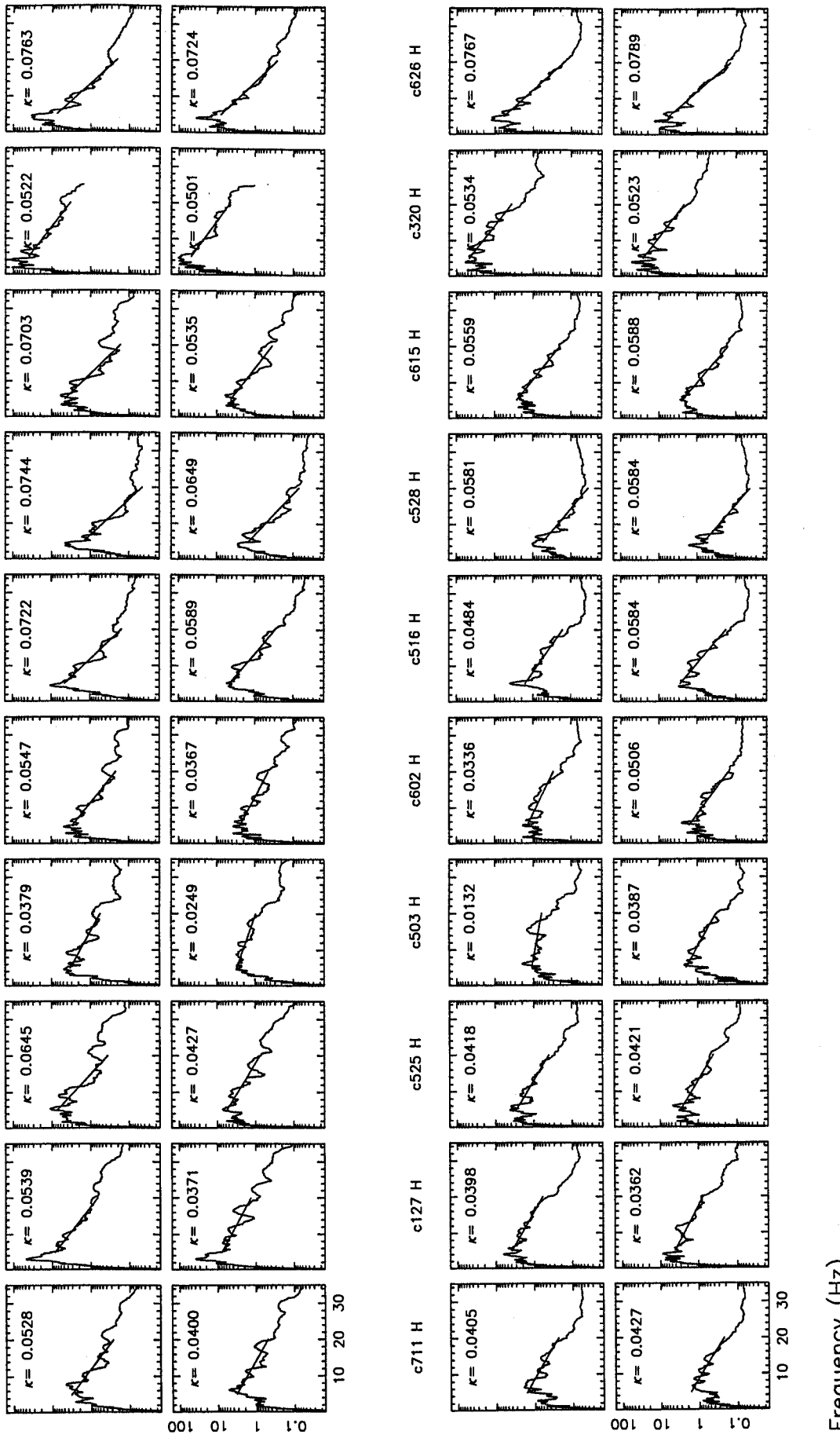

Figure 10: Acceleration spectra of the 10 aftershocks and their spectral fits that produce the individual κ measurements. These 10 aftershocks are recorded in both station NUR and CLU from Jan. 27, 1994 and July, 11, 1995 (CSMIP data report OSMS 96-06, Darragh et al., 1996).

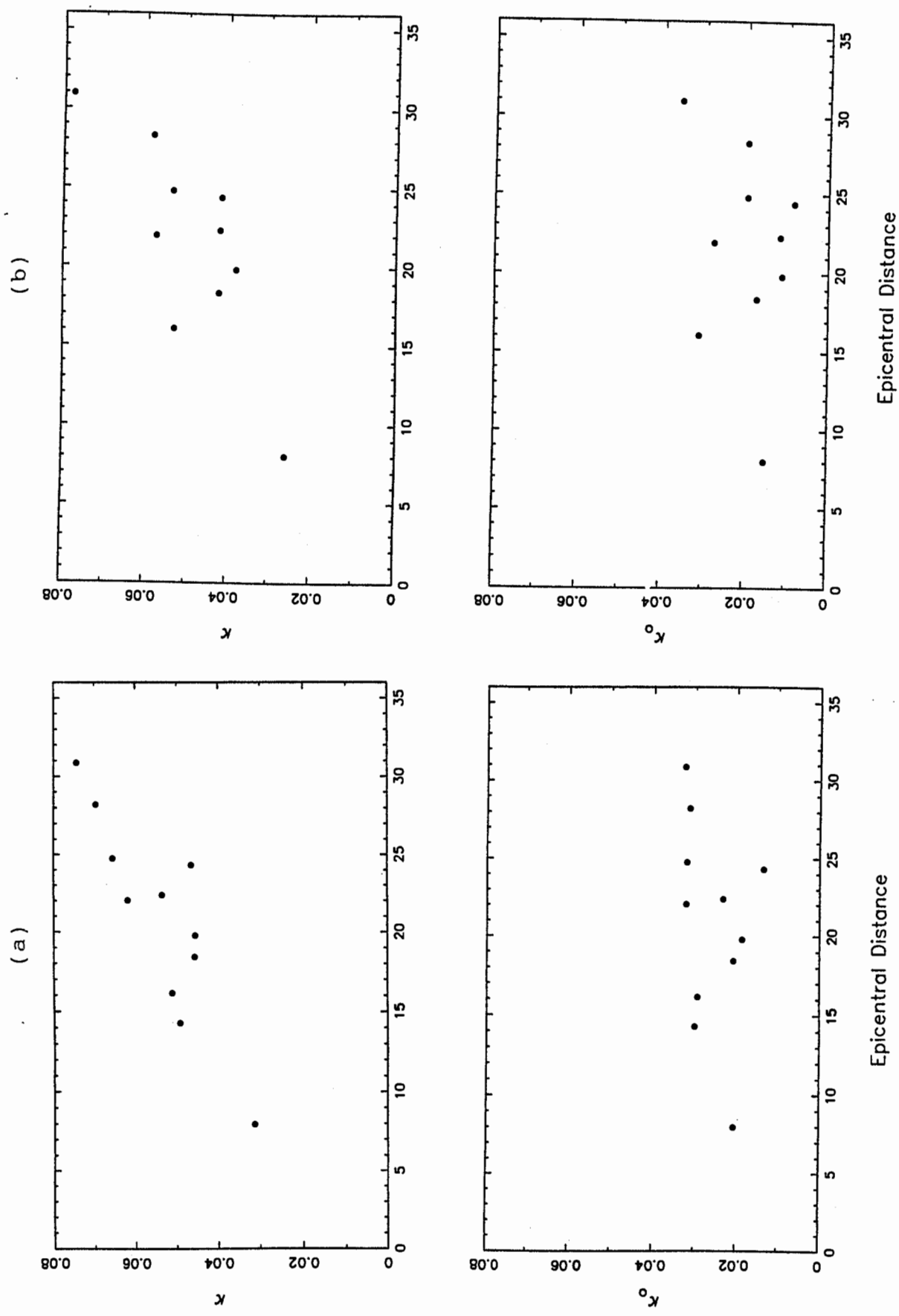

Figure 11: Estimated κ and κ_0 versus distance, (a) for station NUR; (b) for station CLU.

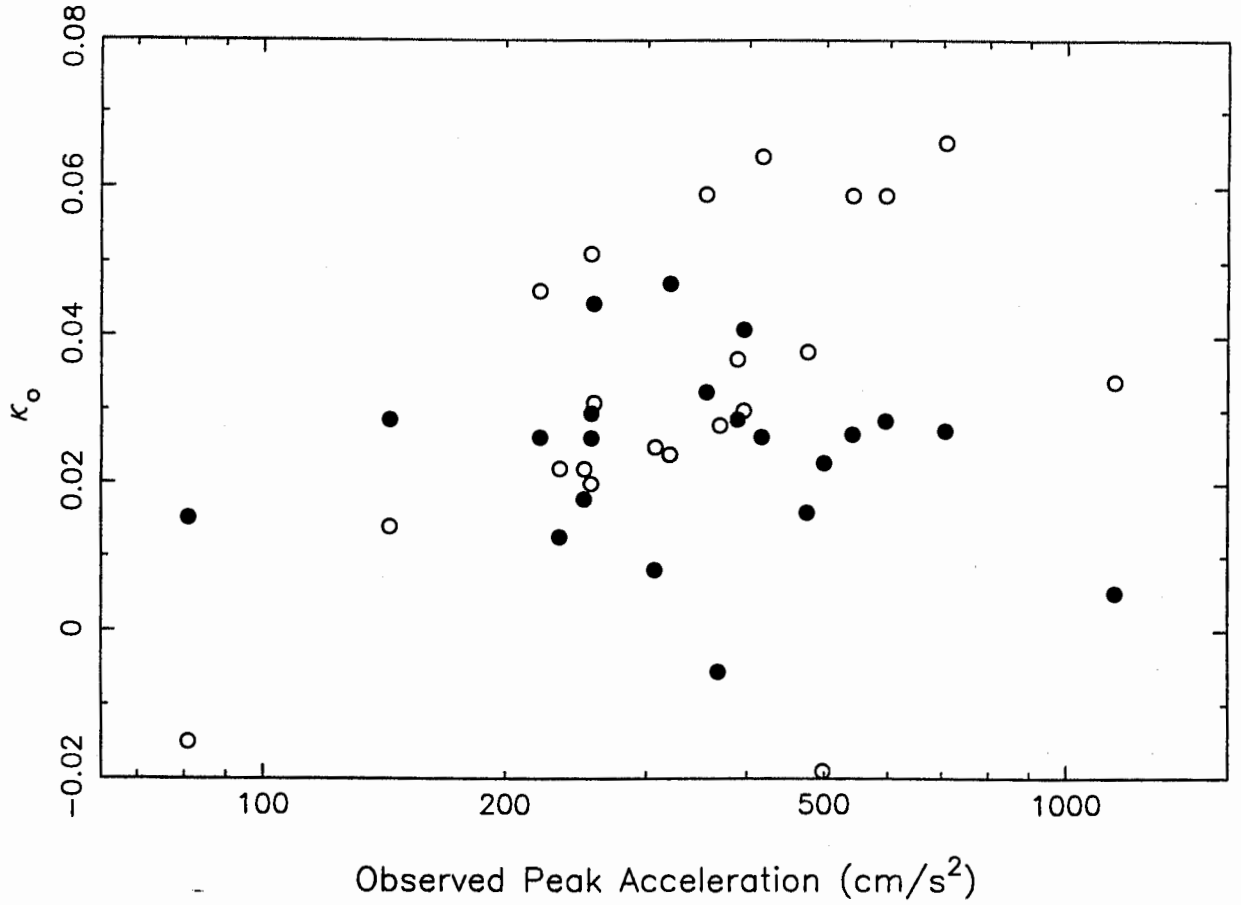

Figure 12: Estimated κ_o from strong motion stations (solid circle) and weak motion stations (open circle) versus observed PGA during the Northridge mainshock at these stations.

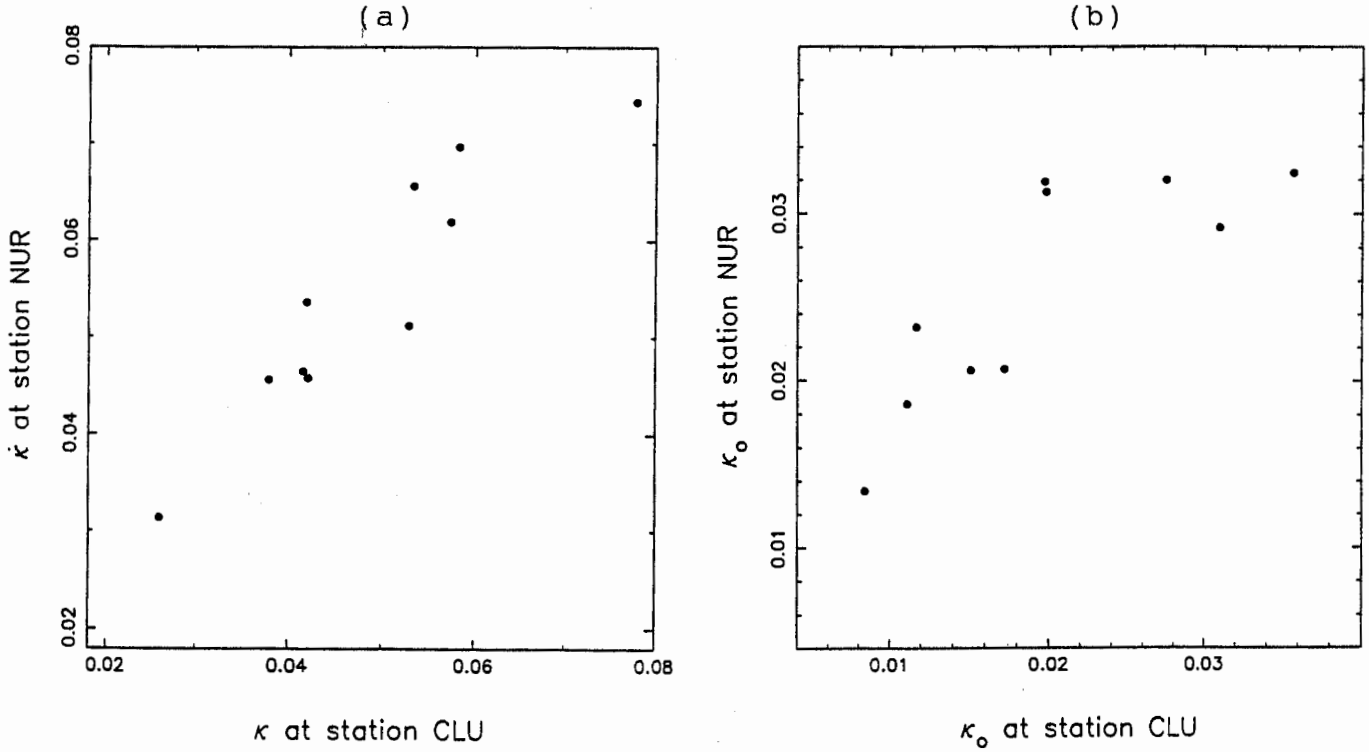

Figure 13: (a) Comparison of estimated κ between station NUR and CLU; (b) comparison of estimated κ_o between NUR and CLU.

VERTICAL GROUND MOTION: CHARACTERISTICS, RELATIONSHIP WITH HORIZONTAL COMPONENT, AND BUILDING-CODE IMPLICATIONS

Y. Bozorgnia[1], K.W. Campbell[2], and M. Niazi[3]

ABSTRACT

In this study, the characteristics of peak vertical ground acceleration and vertical response spectra are examined and the differences between the vertical and horizontal components are investigated. This was accomplished with a comprehensive database of 2,823 free-field components (three per recording) of uncorrected peak ground acceleration from 48 worldwide earthquakes and 1,308 free-field components of corrected peak ground acceleration and response spectral acceleration from 33 worldwide earthquakes, all recorded within 60 km of the causative fault from earthquakes ranging from 4.7 to 7.7 in magnitude. Peak and spectral acceleration attenuation models were developed for both the vertical and horizontal components as a function of magnitude, source-to-site distance, type of faulting, and local soil conditions. An analysis of residuals indicated that the vertical-to-horizontal (V/H) spectral ratios predicted by these attenuation relationships show no significant bias with respect to observed V/H and the modeled parameters. The study clearly demonstrates the strong dependence of V/H on oscillator period, source-to-site distance, and local soil conditions. V/H shows a weaker and more limited dependence on magnitude and type of faulting. The largest short-period V/H ratios are observed to occur on Holocene Soil at short periods and short distances where they can reach values in excess of 1.5 at 0.1-sec period. The largest long-period V/H ratios are observed to occur on Hard Rock where they can reach values as high as 0.7. Generally V/H is 0.5 or less at the longer periods (0.3 to 2.0 sec). We conclude that the standard engineering practice of assigning V/H a value of two-thirds is unconservative at short periods, especially for unconsolidated soil, but conservative at long periods, and should be modified. We propose a simplified model for estimating a design vertical response spectrum for engineering purposes from a simplified model of V/H that better fits the observed trends in V/H. The procedure seems to have merit and will be refined in a future study.

INTRODUCTION

Previous studies of recorded free-field ground motion have revealed that the vertical component is generally richer in high-frequency energy than the horizontal component and its amplitude at these frequencies can exceed that of the horizontal component. These differences are especially evident in vertical and horizontal response spectra from recordings located close to the causative fault.

Niazi and Bozorgnia (1989, 1990, 1991, 1992) analyzed over 700 horizontal and vertical response spectra from 12 earthquakes recorded by the SMART-1 strong-motion array in Taiwan. In subsequent studies, Bozorgnia and Niazi (1993) examined 159 horizontal and vertical

[1] Managing Engineer, Exponent Failure Analysis Associates, Menlo Park, California
[2] Vice President, EQE International, Inc., Evergreen, Colorado
[3] Principal, Berkeley Geophysical Consultants, Berkeley, California

response spectra from the 1989 Loma Prieta, California, earthquake and Bozorgnia and others (1995) analyzed 123 horizontal and vertical response spectra of 41 soil sites from the Northridge, California, earthquake. Ansary and Yamazaki (1998) analyzed 2,166 horizontal and vertical response spectra from 387 earthquakes recorded at 76 Japan Meteorological Agency (JMA) sites in Japan. All of these investigators came to the same conclusion: that the vertical-to-horizontal (V/H) spectral ratio of strong ground motion is a strong function of oscillator period with short periods having higher ratios than long periods. They also found that V/H spectral ratios are only weakly correlated with magnitude, especially beyond the immediate vicinity of the fault. Those studies that looked at near-source recordings additionally found that V/H ratios of peak ground acceleration and response spectra were also a strong function of source-to-site distance and could approach or exceed a value of 1.0 at short periods.

Several investigators have developed attenuation relationships for both horizontal and vertical components of strong ground motion (e.g., Campbell, 1982; Abrahamson and Litehiser, 1989; Sadigh and others, 1993; Abrahamson and Silva, 1997; Campbell, 1997; Ansary and Yamazaki, 1998). Predicted accelerations and response spectra from these attenuation relationships confirm the above conclusions regarding the V/H ratio. Amirbekian and Bolt (1998) have also examined the differences between the spectral characteristics of near-source vertical and horizontal ground motions from a seismological point of view. They concluded that the high-amplitude, high-frequency vertical accelerations that are observed on near-source accelerograms are most likely generated by the conversion of shear waves to compressional waves (S-to-P conversion) within the transition zone between the underlying bedrock and the overlying softer sedimentary layers.

The main objective of this study was to identify the general characteristics and differences of vertical and horizontal response spectra in terms of some fundamental properties of the earthquakes and stations that recorded them. These properties include earthquake magnitude, source-to-site distance, type of faulting, and local soil conditions. This objective was accomplished by analyzing near-source ground motions of numerous worldwide earthquakes. The specific tasks involved in accomplishing this objective were as follows:

1. We compiled a comprehensive database of near-source vertical and horizontal time histories and response spectra, building on our previous study of the horizontal component of peak ground acceleration (Campbell and Bozorgnia, 1994; Campbell, 1997).
2. We used the compiled database to develop attenuation relationships for the vertical and horizontal components of peak ground acceleration and acceleration response spectra taking into account the effects of magnitude, distance to the causative fault, type of faulting, and local soil conditions.
3. We used the vertical and horizontal attenuation relationships to examine and evaluate the differences between the spectral characteristics of the vertical and horizontal ground motions and to propose a model for estimating V/H.
4. We used the observed and modeled characteristics of V/H to evaluate two simplified procedures for developing a vertical response spectrum from a horizontal response spectrum for practical engineering and building-code applications by (a) shifting the horizontal response spectrum to shorter periods and adjusting its amplitude or (b) applying a simplified V/H spectral ratio to the horizontal spectrum.

STRONG-MOTION DATABASE

This study utilized a comprehensive worldwide database of near-source accelerograms that were recorded between 1957 and 1995. The database is an expanded and updated version of the one that was used by two of the authors to develop a near-source attenuation relationship for peak horizontal acceleration (Campbell and Bozorgnia, 1994; Campbell, 1997). It was expanded to include response spectral ordinates and significant earthquakes that have occurred since 1992 (Table 1). The strong-motion parameters analyzed in this study include uncorrected peak ground acceleration (Uncorrected PGA), corrected peak ground acceleration (Corrected PGA), and 15 components of 5%-damped response spectral acceleration (SA) at natural oscillator periods of 0.04, 0.05, 0.075, 0.1, 0.15, 0.2, 0.3, 0.4, 0.5, 0.75, 1.0, 1.5, 2.0, 3.0, and 4.0 sec. The terms "Uncorrected" and "Corrected" refer to the standard levels of accelerogram processing referred to as Phases 1 and 2. Uncorrected PGA is measured directly from the accelerogram or, if the accelerogram has been processed, from the baseline and instrument corrected acceleration record. Corrected PGA is measured from the acceleration record after it has been band-passed filtered and decimated to a uniform time interval.

The database of Uncorrected PGA includes 941 near-source recordings, each having two horizontal and one vertical component (2,823 individual components altogether) from 48 worldwide earthquakes ranging from 4.7 to 7.7 in magnitude. This corresponds to a 50% increase in the number of Uncorrected PGA values that had been used in our previous study. The database of Corrected PGA and SA consists of 436 near-source recordings (1,308 individual components) from 33 worldwide earthquakes ranging from 4.7 to 7.7 in magnitude. It is important to note that the Uncorrected database has over double the number of recordings as the Corrected database. The importance of this difference on the regression results will become evident later in the paper. The distribution of these recordings with respect to magnitude and distance is given in Figure 1.

All of the earthquakes occurred in a shallow crustal tectonic environment. All of the recordings are considered to be free field, defined as ground level of an instrument shelter or a building less than three stories high (less than seven stories high if located on Hard Rock). Recordings on dam abutments were included to enhance the database of rock recordings. Recordings obtained in the basements of buildings of any size or at the toe or base of a dam were excluded.

The magnitude measure used to characterize the size of an earthquake is moment magnitude (M_W). The distance measure is defined as the shortest distance from the area of seismogenic rupture on the causative fault to the recording site, hereafter referred to as distance to seismogenic rupture (R_S). R_S was restricted to 60 km or less to avoid the complicating problems related to the arrival of multiple reflections from the lower crust, as was clearly observed during the 1989 Loma Prieta earthquake (Somerville and Yoshimura, 1990; Campbell, 1991). This distance range is believed to include most ground shaking of engineering interest, except for possibly long-period spectral accelerations on extremely poor soil.

The types of faulting were classified into three categories defined as Strike Slip, Reverse, and Thrust. The Strike Slip faulting category includes primarily vertical or near-vertical faults with predominantly lateral slip. The Reverse category includes steeply dipping faults with either predominantly reverse slip or nearly equal amounts of reverse and lateral slip (reverse-oblique slip). The Thrust category includes shallow dipping faults with predominantly thrust mechanisms. The last category includes blind-thrust events such as the 1983 Coalinga, 1987

Whittier Narrows, and 1994 Northridge earthquakes. Since there is only one normal-faulting event in the database, this earthquake was placed in the Strike Slip category. There are 20 Strike Slip, 7 Reverse, and 6 Thrust events in the Corrected database.

Local soil conditions were classified into four categories defined as Holocene Soil, Pleistocene Soil, Soft Rock, and Hard Rock. The Holocene Soil category includes soil deposits of Holocene age (11,000 years or less) generally described on geologic maps as recent alluvium. The Pleistocene Soil category includes soil deposits of Pleistocene age (11,000 to 1.5 million years) generally described on geologic maps as older alluvium and terrace deposits. The Soft Rock category primarily includes sedimentary rock deposits of Tertiary age (1.5 to 100 million years). The Hard Rock category primarily includes older sedimentary rock deposits, metamorphic rock, and crystalline rock. There are 239 Holocene Soil, 84 Pleistocene Soil, 61 Soft Rock, and 52 Hard Rock recordings in the Corrected database.

REGRESSION ANALYSIS

An initial attempt at developing an attenuation relationship directly in terms of the V/H ratio failed. The relationship between V/H and magnitude, source-to-site distance, type of faulting, and local soil conditions was too complicated to model independently. Instead, we decided to develop a consistent set of attenuation relationships for the horizontal and vertical components of PGA and SA and use these to estimate V/H. This approach was later validated from an analysis of residuals.

After considerable exploratory analysis, the following equation was finally selected to represent the attenuation of PGA and SA for both horizontal and vertical components:

$$\begin{aligned} \ln Y = {} & c_1 + c_2 M_W + c_3 (8.5 - M_W)^2 + c_4 \ln (\{R_S^2 + [(c_5 S_{HS} + c_6 \{S_{PS} + S_{SR}\} + c_7 S_{HR}) \\ & \exp (c_8 M_W + c_9 \{8.5 - M_W\}^2)]^2\}^{1/2}) + c_{10} F_{SS} + c_{11} F_{RV} + c_{12} F_{TH} \\ & + c_{13} S_{HS} + c_{14} S_{PS} + c_{15} S_{SR} + c_{16} S_{HR} \end{aligned} \quad (1)$$

where Y is either the vertical component (Y_V) or the geometric average of the two horizontal components (Y_H) of PGA or SA in g (g = 981 cm/sec^2); M_W is moment magnitude, R_S is the distance to seismogenic rupture in km; S_{HS} = 1 for Holocene Soil, S_{PS} = 1 for Pleistocene Soil, S_{SR} = 1 for Soft Rock, S_{HR} = 1 for Hard Rock, and $S_{HS} = S_{PS} = S_{SR} = S_{HR} = 0$ otherwise; F_{SS} = 1 for Strike Slip faulting, F_{RV} = 1 for Reverse faulting, F_{TH} = 1 for Thrust faulting, and $F_{SS} = F_{RV} = F_{TH} = 0$ otherwise; and c_1 through c_{16} are regression coefficients.

The exponential magnitude term on the second line of Equation (1) accounts for the magnitude dependence of Y as a function of distance. After some preliminary analyses, we determined that the coefficients in this term should be set so that Y is independent of M_W at $R_S = 0$, referred to as magnitude saturation. It is equivalent to setting $c_8 = -c_2/c_4$ and $c_9 = -c_3/c_4$. The coefficients c_5 through c_7 determine the degree of distance saturation of Y for a given magnitude. As modeled, differences in these coefficients will allow the value of Y between different soil categories to vary with distance, permitting the possibility of nonlinear soil behavior.

The regression analysis was performed using the generalized nonlinear regression module in SYSTAT, a commercially available statistical analysis software package offered by SPSS, Inc. of Chicago, Illinois. The loss function used in the analysis was ordinary least squares. As in our previous study, no weights were applied during the analysis because we believed that the distribution of Uncorrected recordings with respect to magnitude and distance was not

significantly biased. However, inspection of Figure 1 indicates that this is not necessarily true for the Corrected database. The use of weights or a similar procedure, such as two-step or random-effects regression, will be explored in a future study.

When all of the coefficients were allowed to be freely determined during the regression analysis, the analysis commonly became unstable. This was due mainly to the tradeoff between c_2 through c_7 during the regression (recall that c_8 and c_9 were constrained). To make the regression more stable, c_2 was set equal to the value determined from the better-constrained analysis of Uncorrected PGA.

We found that there was a considerable degree of period-to-period variability in the regression coefficients that caused the predicted spectra to be very jagged near the limits of the magnitude and distance ranges. In order to reduce this jaggedness to an acceptable degree, some of the coefficients were smoothed. In order to make the spectra completely smooth at all magnitudes and distances, the coefficient smoothing would have to be done iteratively over the entire period range. We believed that this more rigorous smoothing process was not necessary to meet the objectives of the current study. Methods for producing smoothed response spectra suitable for design will be explored in a future study. The partially smoothed regression coefficients for the horizontal and vertical components of PGA and SA that were used in the present study of V/H are listed in Table 2. Because of the extremely small number of 0.04-sec SA values, no amount of smoothing could bring it into line. Therefore, this spectral ordinate was removed from the analysis.

The difference in the regression results for the horizontal component of Uncorrected and Corrected PGA is demonstrated in Table 2 and in Figure 1. Figure 1 indicates that this difference is largest at short distances and small magnitudes where there are fewer recordings. Similar differences are observed for the vertical component (not shown). The plots of the normalized residuals clearly show the narrower magnitude range for the Corrected data. The residuals, which represent the difference between the observed and predicted values of ln Y, were normalized by dividing them by the standard error of the Uncorrected PGA regression analysis. In this way one can visually compare the scatter in the residuals on a consistent basis. The residual plots together with the standard errors and r^2 values (goodness of fit) in Table 2 indicate that both the Uncorrected and Corrected PGA fits are equally good, given their respective databases. The differences are principally the result of the bias in the number and distribution of recordings in the Corrected database.

Figures 2 and 3 show how the predicted horizontal and vertical response spectra scale with magnitude, distance, local soil conditions, and type of faulting. The horizontal spectra clearly show a trend towards increasing predominate period with increasing magnitude. This trend is largely missing in the vertical spectra. The dependence of predominant period on distance for both the vertical and horizontal spectra is negligible, except possibly at 60 km. It should also be noted that the predominate periods of the horizontal spectra (0.2 to 0.5 sec) are longer than those of the vertical spectra (around 0.1 sec).

The behavior of SA with soil conditions is also significantly different between the horizontal and vertical spectra. The horizontal spectra show relatively little difference between the different soil categories at short periods for the distance shown (R_S = 10 km). However, the horizontal Hard Rock spectrum is much smaller than that of the other soil categories at longer periods. The vertical spectra, on the other hand, are all quite similar for the different soil categories, except for

the larger amplitude for Holocene Soil at short periods. Both the horizontal and vertical spectra show the same tendency towards higher amplitudes for Reverse and Thrust faulting at short and moderate periods. At periods greater than about 1.0 sec, however, these differences become negligible. This trend of decreasing difference in SA with increasing period for different types of faulting is consistent with the expected effects of dynamic stress drop and the expectation that Reverse and Thrust faulting is generally associated with higher stress drops.

V/H RATIO

The horizontal and vertical regression results can be used to derive an attenuation relationship for V/H by subtracting the logarithm of the vertical and horizontal components of Y calculated from Equation (1), giving:

$$\ln V/H = \ln Y_V - \ln Y_H \quad (2)$$

The plots of the normalized residuals of ln V/H versus magnitude and distance shown in Figures 4 and 5 demonstrate the validity of Equation (2) as an unbiased predictor of V/H. Note, however, that the difference between the values of V/H using the Corrected and Uncorrected databases can be as much as 20%, more than for horizontal and vertical SA. Other plots (not shown) clearly confirm that the prediction of V/H from Equation (2) is equally unbiased with respect to SA at other periods, types of faulting, and soil categories. The bias and standard errors derived from these residuals are listed in Table 3. Note that the standard errors are somewhat smaller than those from the horizontal regression.

To further verify the validity of Equation (2), we compared the standard errors and scaling characteristics derived from this equation with those determined from our preliminary regression on V/H. Although the regression results for V/H were erratic, they did confirm that Equation (2) fit the observed values of V/H just as well as a model derived from a direct regression on ln V/H.

Figure 6 demonstrates the attenuation characteristics of V/H for Strike Slip faulting and Holocene Soil. This figure clearly shows that V/H attenuates rather steeply with distance at short periods, but that this rate decreases with increasing period until at periods between 0.3 and 1.0sec V/H begins to increase with distance. As subsequent plots will show, this transition from decreasing to increasing V/H with distance actually occurs between 0.3 and 0.4 sec. V/H scaling with magnitude also decreases with distance, becoming insignificant at 0.3 sec. On these and subsequent plots, horizontal lines are plotted at V/H = 0.5, 0.67, and 1.0 for reference.

Figures 7 and 8 demonstrate the effect of soil conditions on V/H as a function of magnitude and distance, respectively. Also shown on Figure 7 is the effect of fault type. The effect of the type of faulting was found to be independent of magnitude, distance, and soil conditions, so this effect can be shown on a single plot. Only at very short and very long periods is V/H different for the three faulting categories. At short periods, Strike Slip faulting has higher V/H but differences between Reverse and Thrust faulting are barely distinguishable. The differences at long periods might not be significant, since there are fewer recordings at these periods. Soil effects are most pronounced for Holocene Soil (at short periods) and Hard Rock (at long periods). The difference in Holocene Soil diminishes with decreasing magnitude and increasing distance, however, the difference in Hard Rock remains relatively constant at all magnitudes and distances. At small magnitudes and large distances, the only effect of local soil conditions that remains is higher V/H on Hard Rock a periods exceeding about 0.2 sec.

The dependence of V/H on magnitude and distance for each of the soil categories are better demonstrated in Figures 9 and 10, respectively. The effect of magnitude (shown for R_S = 10 km) is most significant for Holocene Soil at periods shorter than 0.3 sec. The other soil categories show very little magnitude scaling and what scaling exists becomes negligible at larger distances. The effect of distance is also most pronounced for Holocene Soil, but the other soil categories show significant scaling at longer periods where V/H increases with distance. Once a distance of 60 km is reached, most of the dependence of V/H on distance at short periods has ended but differences at longer periods remain significant.

SIMPLIFIED VERTICAL SPECTRUM

For practical engineering applications, and especially when vertical response spectra are not available, it is desirable to develop a vertical response spectrum from an approximate relationship between the vertical and horizontal spectrum. In this section, we examine two such simplified methods.

The first method is to shift the horizontal spectrum to shorter periods and then reduce its amplitude to approximate the vertical spectrum. The method was proposed by Watabe and others (1990) and later evaluated by Bozorgnia and others (1996). Shifting the horizontal spectrum to shorter periods is consistent with the fact that vertical ground motion is richer in high-frequency energy than horizontal ground motion. Based on the observed differences between the spectral content of vertical and horizontal spectra for the 1994 Northridge earthquake, Bozorgnia and others (1996) suggested a period shift factor of 2.0. Amirbekian and Bolt (1998) also found an approximate ratio of 2.0 between the vertical and horizontal values of the spectral corner frequency f_{max}.

Based on these past studies, we examine the following simplified procedure for estimating a vertical spectrum from a horizontal spectrum: (1) shift the horizontal acceleration spectrum to a shorter period by dividing each period by a factor of 2.0, and (2) reduce the spectral ordinates of the shifted horizontal spectrum by the V/H ratio of PGA. It should be noted that the PGA ratio is a function of source-to-site distance. Figure 11 shows the results of applying this simplified procedure. The agreement between the predicted and shifted spectra is reasonably good at M_W 6.5 for Holocene Soil and at M_W 7.5 for Hard Rock. However, the same level of agreement is not achieved for other magnitudes and soil categories. This simplified method is, therefore, limited in its usefulness. A more general agreement between the predicted and shifted horizontal spectrum might be possible if a variable period shift is used. This latter approach will be explored in a future study.

The second method is to apply a simplified V/H spectral ratio to the horizontal spectrum. As previously discussed, the V/H spectral ratio is a strong function of period, source-to-site distance, and local soil conditions, and more weakly dependent on magnitude and type of faulting. However, for practical engineering applications it is desirable to model only those factors that have the greatest influence on the V/H and make conservative assumptions regarding the influence of the other factors. Figure 12 shows our attempt at defining a simplified model for estimating V/H. Since the behavior of the observed V/H spectral ratio with distance is much different for Holocene Soil than for the other three soil categories, a separate model is proposed for this category. The dependence of V/H on distance is generally similar for Pleistocene Soil, Soft Rock, and Hard Rock, but less than that for Holocene Soil. Figure 12 also shows the

comparison between the simplified V/H spectral model and predicted V/H for different magnitudes and soil conditions. For Holocene Soil, the proposed V/H ratio of 0.5 is relatively conservative at mid periods and can, therefore, be extended to periods longer than 1.0 sec. However, for the other three soil categories, the predicted V/H ratio is greater than 0.5 beyond 1.0 sec, approaching a value of 0.7 at about 4.0 sec.

BUILDING-CODE APPLICATION

In this section we evaluate the definition of vertical ground motion in the 1997 Uniform Building Code (UBC-97). We compare vertical response spectra calculated using the simplified V/H spectra given in Figure 12 with vertical spectra calculated from Equation (1) and similar spectra developed by applying a constant factor of two-thirds to the UBC-97 horizontal spectrum. However, examination of the effects of vertical ground motion on the response of various structural systems is out of scope of the current study.

The fact that the relationship between the vertical and horizontal response spectra is dependent on source-to-site distance at relatively short distances is recognized in UBC-97. Section 1631.2 of that code states that *"The vertical component of ground motion may be defined by scaling corresponding horizontal accelerations by a factor of two-thirds. Alternative factors may be used when substantiated by site-specific data. Where the Near-Source Factor, N_a, is greater than 1.0, site-specific vertical response spectra shall be used in lieu of the factor of two-thirds."* The Near-Source Factor N_a is specified in Table 16-S of UBC-97 and is greater than 1.0 for the following cases:

- Seismic Source Type A when the closest distance to a known seismic source is < 10 km
- Seismic Source Type B when the closest distance to a known seismic source is < 5 km

For the above cases, according to UBC-97, site-specific vertical response spectra shall be used. Otherwise, the vertical spectrum may be defined by scaling the corresponding horizontal spectrum by a factor of two-thirds. Seismic Source Types A and B are defined in Table 16-U of UBC-97. Seismic Source Type A is a fault that is capable of producing large magnitude events and that has a high rate of seismic activity, defined as a fault having $M \geq 7.0$ and SR (slip rate) $\geq$ 5 mm/yr. Seismic Source Type B is a fault other than Types A and C, where Type C is a fault that is not capable of producing large magnitude earthquakes and that has a relatively low rate of seismic activity (i.e., $M < 6.5$, SR $\leq$ 2 mm/yr). Therefore, Seismic Source Type B is a fault for which either $M \geq 7.0$ and SR < 5 mm/yr, or $M < 7.0$ and SR > 2 mm/yr, or $M \geq 6.5$ and SR < 2 mm/yr.

Figure 13 compares vertical response spectra calculated using three different methods. The first method predicts the vertical spectrum using Equation (1). The second method calculates the vertical spectrum by multiplying the design horizontal response spectrum developed in accordance with Figure 16-3 of UBC-97 by two-thirds. The third method calculates the vertical spectrum by multiplying the simplified V/H spectrum from Figure 12 by the UBC-97 horizontal design spectrum. Compared to the predicted vertical spectrum for Holocene Soil, the two-thirds scaled UBC-97 horizontal spectrum for Soil Profile Type S_D, which is consistent with the Holocene Soil category defined in this study, is generally unconservative around the 0.1-sec spectral peak of the predicted vertical spectrum. It should be noted that structural members may have vertical natural periods in this period range (Bozorgnia and others, 1998). For the other soil

categories, the two-thirds scaled UBC-97 horizontal spectrum might result in more reasonable values. For example, as Figure 13 shows, there is better agreement between the predicted Hard Rock spectrum and the two-thirds scaled UBC-97 horizontal spectrum for Soil Profile Type S_B.

In reviewing similar comparisons between the vertical spectrum predicted from Equation (1) and the vertical spectrum calculated by applying the simplified V/H spectrum to the UBC-97 horizontal design spectrum, we come to the general conclusion that the latter is relatively conservative. The degree of conservatism varies with the type of faulting and the source-to-site distance. This conservatism is probably caused by the inherent conservatism in the UBC-97 horizontal design spectrum and, therefore, might be acceptable. This approach seems to have merit and will be refined in a future study.

CONCLUSIONS AND RECOMMENDATIONS

Based on the results of our study, we offer the following conclusions and recommendations regarding the prediction of the vertical response spectrum and the V/H spectral ratio:

1. The Corrected database is severely limited for small magnitudes ($M_W < 6.0$) at moderate distances and for large magnitudes ($M_W > 7.0$) at all distances, which has resulted in a bias in the attenuation relationships for PGA, SA, and V/H spectral ratio compared to a similar analysis using the Uncorrected database. The Uncorrected database compiled for this study has over two times the number of recordings as the Corrected database. In order to make the regression analysis on Corrected PGA and spectral acceleration more reliable, consideration should be given to extending the accelerogram processing to a wider range of magnitudes and distances.
2. The standard low-pass filter applied during Phase 2 of the accelerogram processing (around 20 to 25 Hz) is not sufficient to capture all of the significant high-frequency energy contained in near-source recordings of vertical ground motion. This is exacerbated by the need to remove those recordings that have low-pass filters less than 25 Hz, which reduced the number of available recordings to the point that the 0.04-sec spectral ordinate became unstable in the regression analysis and could not be used. In order to capture all significant high-frequency energy in near-source vertical recordings, the low-pass filter should be extended to as high a frequency as allowed by the processing noise.
3. An analysis of residuals determined that the estimation of the V/H spectral ratio from attenuation relationships developed independently from the horizontal and vertical components of PGA and SA are unbiased, so that these attenuation relationships can be used to estimate V/H.
4. The V/H spectral ratio is a strong function of oscillator period, source-to-site distance, and local soil conditions, and a weaker function of magnitude and type of faulting. The largest short-period V/H ratios are observed to occur on Holocene Soil at short periods and short distances where they can reach values in excess of 1.5 at 0.1-sec period. The largest long-period V/H ratios are observed to occur on Hard Rock where they can reach values as high as 0.7. Generally V/H is 0.5 or less at the longer periods (0.3 to 2.0 sec).
5. The concept of shifting the horizontal response spectrum to shorter periods and reducing its amplitude to approximate the vertical response spectrum is only valid over a limited range of magnitudes, distances, and soil conditions. In order for this procedure to work for a broader

range of conditions, it will need to be modified to account for differences in these parameters.

6. We conclude that the standard engineering practice of assigning the V/H ratio a value of two-thirds is unconservative at short periods, especially for unconsolidated soil and in the near-source region, but conservative at long periods, and should be modified. Such a modification is recommended in the 1997 Uniform Building Code when the site is located close to a fault, but UBC-97 gives no guidance on how that should be done. We propose a simplified method for estimating a design vertical response spectrum for engineering purposes from a simplified model of V/H that better fits the observed trends in V/H. The procedure seems to have merit and will be refined in a future study.

ACKNOWLEDGEMENTS

This study was supported by the California Department of Conservation, Division of Mines and Geology, Strong Motion Instrumentation Program, Contract 1097-606. The support is gratefully acknowledged.

REFERENCES

Abrahamson, N.A., and J.J. Litehiser (1989). "Attenuation of vertical peak acceleration," *Bulletin of the Seismological Society of America*, Vol. 79, p. 549–580.

Abrahamson, N.A., and W.J. Silva (1997). "Empirical response spectral attenuation relations for shallow crustal earthquakes," *Seismological Research Letters*, Vol. 68, p. 94–127.

Amirbekian, R.V., and B.A. Bolt (1998). "Spectral comparison of vertical and horizontal seismic strong ground motions in alluvial basins," *Earthquake Spectra*, Vol. 14, p. 573–595.

Ansary, M.H., and F. Yamazaki (1998). "Behavior of horizontal and vertical SV at JMA sites, Japan," *Journal of Geotechnical and Geoenvironmental Engineering*, Vol. 124, p. 606–616.

Bozorgnia, Y., and M. Niazi (1993). "Distance scaling of vertical and horizontal response spectra of the Loma Prieta earthquake," *Earthquake Engineering and Structural Dynamics*, Vol. 22, p. 695–707.

Bozorgnia, Y., M. Niazi, and K.W. Campbell (1995). "Characteristics of free-field vertical ground motion during the Northridge earthquake," *Earthquake Spectra*, Vol. 11, p. 515–525.

Bozorgnia, Y., M. Niazi, and K.W. Campbell (1996). "Relationship between vertical and horizontal ground motion for the Northridge earthquake," in *Proceedings, 11th World Conference on Earthquake Engineering*, Acapulco, Mexico.

Bozorgnia, Y., S.A. Mahin, and A.G. Brady (1998). "Vertical response of twelve structures recorded during the Northridge earthquake," *Earthquake Spectra*, Vol. 14, p. 411–432.

Campbell, K.W. (1982). "A Study of the near-source behavior of peak vertical acceleration", (Abs.), *EOS*, Vol. 63, p. 1,037.

Campbell, K.W. (1991). "An empirical analysis of peak horizontal acceleration for the Loma Prieta, California, earthquake of 18 October 1989," *Bulletin of the Seismological Society of America*, Vol. 81, p. 1838–1858.

Campbell, K.W. (1997). "Empirical near-source attenuation relationships for horizontal and vertical components of peak ground acceleration, peak ground velocity, and pseudo-absolute acceleration response spectra," *Seismological Research Letters*, Vol. 68, p. 154–179.

Campbell, K.W., and Y. Bozorgnia (1994). "Near-source attenuation of peak horizontal acceleration From worldwide accelerograms recorded From 1957 to 1993", in *Proceedings, Fifth U.S. National Conference on Earthquake Engineering*, 1993, Chicago, Ill.

Niazi, M., and Y. Bozorgnia (1989). "Behavior of vertical ground motion parameters in the near field," (Abs.), *Seismological Research Letters*, Vol. 60, No. 1.

Niazi, M., and Y. Bozorgnia (1990). "Observed ratios of PGV/PGA and PGD/PGA for deep soil sites across SMART-1 array, Taiwan," in *Proceedings, 4th U.S. National Conference on Earthquake Engineering*, Palm Springs, Calif., Vol. 1, p. 367–374.

Niazi, M., and Y. Bozorgnia (1991). "Behavior of near-source peak vertical and horizontal ground motions over SMART-1 array, Taiwan," *Bulletin of the Seismological Society of America*, Vol. 81, p. 715–732.

Niazi, M., and Y. Bozorgnia (1992). "Behavior of near-source vertical and horizontal response spectra at SMART-1 array, Taiwan," *Earthquake Engineering and Structural Dynamics*, Vol. 21, p. 37–50.

Sadigh, K., C.-Y. Chang, N.A. Abrahamson, S.J. Chiou, and M.S. Power (1993). "Specification of long-period ground motions: updated attenuation relationships for rock site conditions and adjustment factors for near-fault effects," in *Proceedings, ATC-17-1 Seminar on Seismic Isolation, Passive Energy Dissipation, and Active Control*, San Francisco, Calif., Applied Technology Council Report ATC-17-1, Vol. 1, p. 59–70.

Somerville, P., and J. Yoshimura (1990). "The influence of critical MOHO reflections on strong ground motions recorded in San Francisco and Oakland during the 1989 Loma Prieta earthquake," *Geophysical Research Letters*, Vol. 17, p. 1203–1206.

Uniform Building Code (1997). International Conference of Building Officials, Whittier, CA, Volume 2.

Watabe, M., M. Tohido, O. Chiba, and R. Fukuzawa (1990). "Peak accelerations and response spectra of vertical strong motions from near-field records in USA," in *Proceedings, 8th Japan Earthquake Engineering Symposium*, Vol. 1, p. 301–306.

Table 1—Earthquakes Used in the Current Study

Earthquake	Location	Corrected	Year	M_W	Type of Faulting
Daly City	California	Yes	1957	5.3	Reverse Oblique
Parkfield	California	Yes	1966	6.1	Strike Slip
Koyna	India	Yes	1967	6.3	Strike Slip
Lytle Creek	California	Yes	1970	5.3	Reverse
San Fernando	California	Yes	1971	6.6	Reverse
Sitka	Alaska	Yes	1972	7.7	Strike Slip
Stone Canyon	California	Yes	1972	4.7	Strike Slip
Managua	Nicaragua	Yes	1972	6.2	Strike Slip
Point Magu	California	No	1973	5.6	Reverse
Hollister	California	Yes	1974	5.1	Strike Slip
Oroville	California	Yes	1975	6.0	Normal
Kalapana	Hawaii	No	1975	7.1	Thrust
Gazli	Uzbekistan	Yes	1976	6.8	Reverse
Caldiran	Turkey	Yes	1976	7.3	Strike Slip
Mesa de Andrade	Mexico	No	1976	5.6	Strike Slip
Santa Barbara	California	Yes	1978	6.0	Thrust
Tabas	Iran	Yes	1978	7.4	Thrust
Bishop	California	No	1978	5.8	Strike Slip
Malibu	California	No	1979	5.0	Reverse
St. Elias	Alaska	No	1979	7.6	Thrust
Coyote Lake	California	Yes	1979	5.8	Strike Slip
Imperial Valley	California	Yes	1979	6.5	Strike Slip
Livermore	California	No	1980	5.8	Strike Slip
Livermore Aftershock	California	No	1980	5.4	Strike Slip
Westmorland	California	No	1981	6.0	Strike Slip
Morgan Hill	California	Yes	1984	6.2	Strike Slip
Nahanni	Canada	Yes	1985	6.8	Thrust
North Palm Springs	California	Yes	1986	6.1	Strike Slip
Chalfant Valley	California	No	1986	6.3	Strike Slip
Whittier Narrows	California	Yes	1987	6.1	Thrust
Whittier Narrows Aftershock	California	Yes	1987	5.3	Reverse Oblique
Elmore Ranch	California	Yes	1987	6.2	Strike Slip
Superstition Hills	California	Yes	1987	6.6	Strike Slip
Spitak	Armenia	Yes	1988	6.8	Reverse Oblique
Pasadena	California	No	1988	5.0	Strike Slip
Loma Prieta	California	Yes	1989	6.9	Reverse Oblique
Malibu	California	No	1989	5.0	Thrust
Manjil	Iran	Yes	1990	7.4	Strike Slip
Upland	California	Yes	1990	5.6	Strike Slip
Sierra Madre	California	Yes	1991	5.6	Reverse
Landers	California	Yes	1992	7.4	Strike Slip
Big Bear	California	Yes	1992	6.6	Strike Slip
Joshua Tree	California	No	1992	6.2	Strike Slip
Petrolia	California	Yes	1992	7.1	Thrust
Petrolia Aftershock	California	No	1992	7.0	Strike Slip
Erzincan	Turkey	Yes	1992	6.7	Strike Slip
Northridge	California	Yes	1994	6.7	Thrust
Kobe	Japan	Yes	1995	6.9	Strike Slip

Table 2—Results of Regression Analysis of Horizontal and Vertical Components of PGA and SA

Period (sec)	c_1	c_2	c_3	c_4	c_5	c_6	c_7	c_8	c_9	c_{10}	c_{11}	c_{12}	c_{13}	c_{14}	c_{15}	c_{16}	No.	σ	r^2
Mean Horizontal Component																			
Unc PGA	-2.896	0.812	0.000	-1.318	0.187	-0.029	-0.064	0.616	0.000	0	0.179	0.307	0	-0.062	-0.195	-0.320	960	0.509	0.955
Cor PGA	-4.033	0.812	0.036	-1.061	0.041	-0.005	-0.018	0.766	0.034	0	0.343	0.351	0	-0.123	-0.138	-0.289	443	0.465	0.949
0.05	-3.740	0.812	0.036	-1.121	0.054	0.000	-0.024	0.724	0.032	0	0.302	0.362	0	-0.140	-0.158	-0.205	435	0.485	0.940
0.075	-3.076	0.812	0.050	-1.252	0.121	-0.005	-0.035	0.648	0.040	0	0.243	0.333	0	-0.150	-0.196	-0.208	439	0.497	0.923
0.10	-2.661	0.812	0.060	-1.308	0.166	-0.009	-0.052	0.621	0.046	0	0.224	0.313	0	-0.146	-0.253	-0.258	439	0.503	0.901
0.15	-2.270	0.812	0.041	-1.324	0.212	-0.033	-0.044	0.613	0.031	0	0.318	0.344	0	-0.176	-0.267	-0.284	439	0.519	0.862
0.20	-2.771	0.812	0.030	-1.153	0.098	-0.012	-0.020	0.704	0.026	0	0.296	0.342	0	-0.148	-0.183	-0.359	439	0.526	0.844
0.30	-2.999	0.812	0.007	-1.080	0.064	-0.010	-0.027	0.752	0.007	0	0.359	0.385	0	-0.162	-0.157	-0.585	439	0.512	0.859
0.40	-3.511	0.812	-0.015	-0.964	0.019	0	0	0.842	-0.016	0	0.379	0.438	0	-0.078	-0.129	-0.557	439	0.532	0.871
0.50	-3.556	0.812	-0.035	-0.964	0.019	0	0	0.842	-0.036	0	0.406	0.479	0	-0.122	-0.130	-0.701	439	0.535	0.890
0.75	-3.709	0.812	-0.071	-0.964	0.019	0	0	0.842	-0.074	0	0.347	0.419	0	-0.108	-0.124	-0.796	438	0.566	0.917
1.0	-3.867	0.812	-0.101	-0.964	0.019	0	0	0.842	-0.105	0	0.329	0.338	0	-0.073	-0.072	-0.858	438	0.582	0.935
1.5	-4.093	0.812	-0.150	-0.964	0.019	0	0	0.842	-0.155	0	0.217	0.188	0	-0.079	-0.056	-0.954	428	0.557	0.960
2.0	-4.311	0.812	-0.180	-0.964	0.019	0	0	0.842	-0.187	0	0.060	0.064	0	-0.124	-0.116	-0.916	405	0.543	0.971
3.0	-4.817	0.812	-0.193	-0.964	0.019	0	0	0.842	-0.200	0	-0.079	0.021	0	-0.154	-0.117	-0.873	333	0.561	0.976
4.0	-5.211	0.812	-0.202	-0.964	0.019	0	0	0.842	-0.209	0	-0.061	0.057	0	-0.054	-0.261	-0.889	275	0.579	0.978
Vertical Component																			
Unc PGA	-2.807	0.756	0	-1.391	0.191	0.044	-0.014	0.544	0	0	0.091	0.223	0	-0.096	-0.212	-0.199	941	0.548	0.964
Cor PGA	-3.108	0.756	0	-1.287	0.142	0.046	-0.040	0.587	0	0	0.253	0.173	0	-0.135	-0.138	-0.256	439	0.520	0.958
0.05	-1.918	0.756	0	-1.517	0.309	0.069	0.010	0.498	0	0	0.058	0.100	0	-0.195	-0.274	-0.219	434	0.592	0.934
0.075	-1.504	0.756	0	-1.551	0.343	0.115	0.067	0.487	0	0	0.135	0.182	0	-0.224	-0.303	-0.263	436	0.602	0.910
0.10	-1.672	0.756	0	-1.473	0.282	0.062	0.001	0.513	0	0	0.168	0.210	0	-0.198	-0.275	-0.252	436	0.591	0.900
0.15	-2.323	0.756	0	-1.280	0.171	0.045	0.008	0.591	0	0	0.223	0.238	0	-0.170	-0.175	-0.270	436	0.574	0.899
0.20	-2.998	0.756	0	-1.131	0.089	0	-0.013	0.668	0	0	0.234	0.256	0	-0.098	-0.041	-0.311	436	0.551	0.915
0.30	-3.721	0.756	0.007	-1.028	0.050	0	-0.007	0.736	0.007	0	0.249	0.328	0	-0.026	0.082	-0.265	436	0.509	0.941
0.40	-4.536	0.756	-0.015	-0.812	0.012	0	0	0.931	-0.018	0	0.299	0.317	0	-0.017	0.022	-0.257	436	0.521	0.949
0.50	-4.651	0.756	-0.035	-0.812	0.012	0	0	0.931	-0.043	0	0.243	0.354	0	-0.020	0.092	-0.293	436	0.515	0.957
0.75	-4.903	0.756	-0.071	-0.812	0.012	0	0	0.931	-0.087	0	0.295	0.418	0	0.078	0.091	-0.349	435	0.556	0.962
1.0	-4.950	0.756	-0.101	-0.812	0.012	0	0	0.931	-0.124	0	0.266	0.315	0	0.043	0.101	-0.481	435	0.562	0.967
1.5	-5.073	0.756	-0.150	-0.812	0.012	0	0	0.931	-0.184	0	0.171	0.211	0	-0.038	-0.018	-0.518	420	0.581	0.973
2.0	-5.292	0.756	-0.180	-0.812	0.012	0	0	0.931	-0.222	0	0.114	0.115	0	0.033	-0.022	-0.503	395	0.591	0.977
3.0	-5.748	0.756	-0.193	-0.812	0.012	0	0	0.931	-0.238	0	0.179	0.159	0	-0.010	-0.047	-0.539	321	0.617	0.978
4.0	-6.042	0.756	-0.202	-0.812	0.012	0	0	0.931	-0.248	0	0.237	0.134	0	-0.059	-0.267	-0.606	274	0.636	0.980

Table 3—Statistical Summary of Predicted V/H

Period (sec)	No.	Bias (ln V/H)	Bias (Factor)	σ
Unc PGA	941	-0.0121	0.99	0.432
Cor PGA	439	-0.0074	0.99	0.422
0.05	432	0.0003	1.00	0.465
0.075	436	-0.0081	0.99	0.470
0.10	436	-0.0098	0.99	0.469
0.15	436	-0.0110	0.99	0.493
0.20	436	-0.0100	0.99	0.480
0.30	436	-0.0094	0.99	0.463
0.40	436	-0.0074	1.00	0.483
0.50	436	-0.0044	1.00	0.491
0.75	435	-0.0057	0.99	0.487
1.0	435	-0.0033	1.00	0.514
1.5	419	-0.0183	0.98	0.487
2.0	393	-0.0292	0.97	0.454
3.0	313	-0.0370	0.96	0.437
4.0	262	0.0055	1.01	0.451

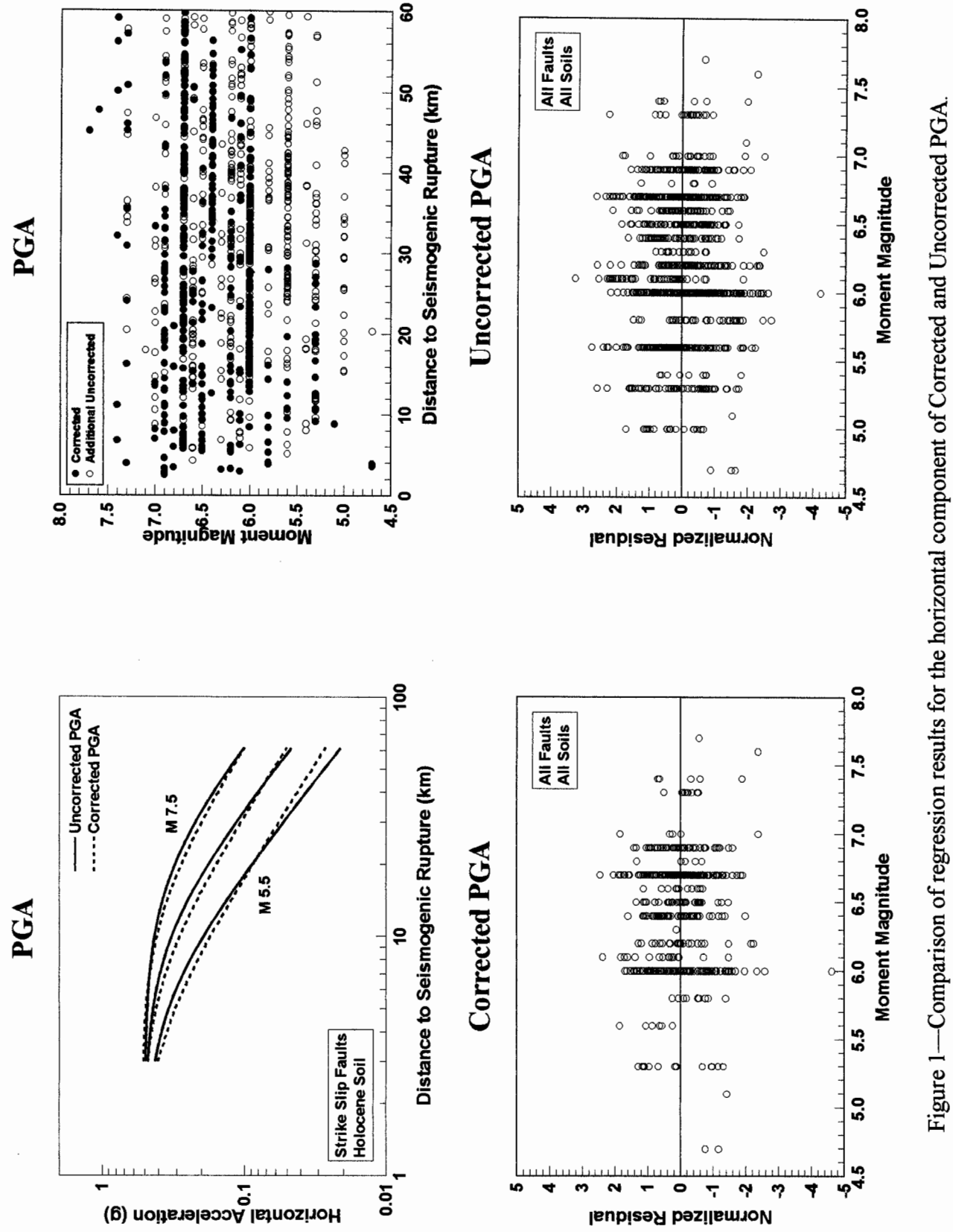

Figure 1—Comparison of regression results for the horizontal component of Corrected and Uncorrected PGA.

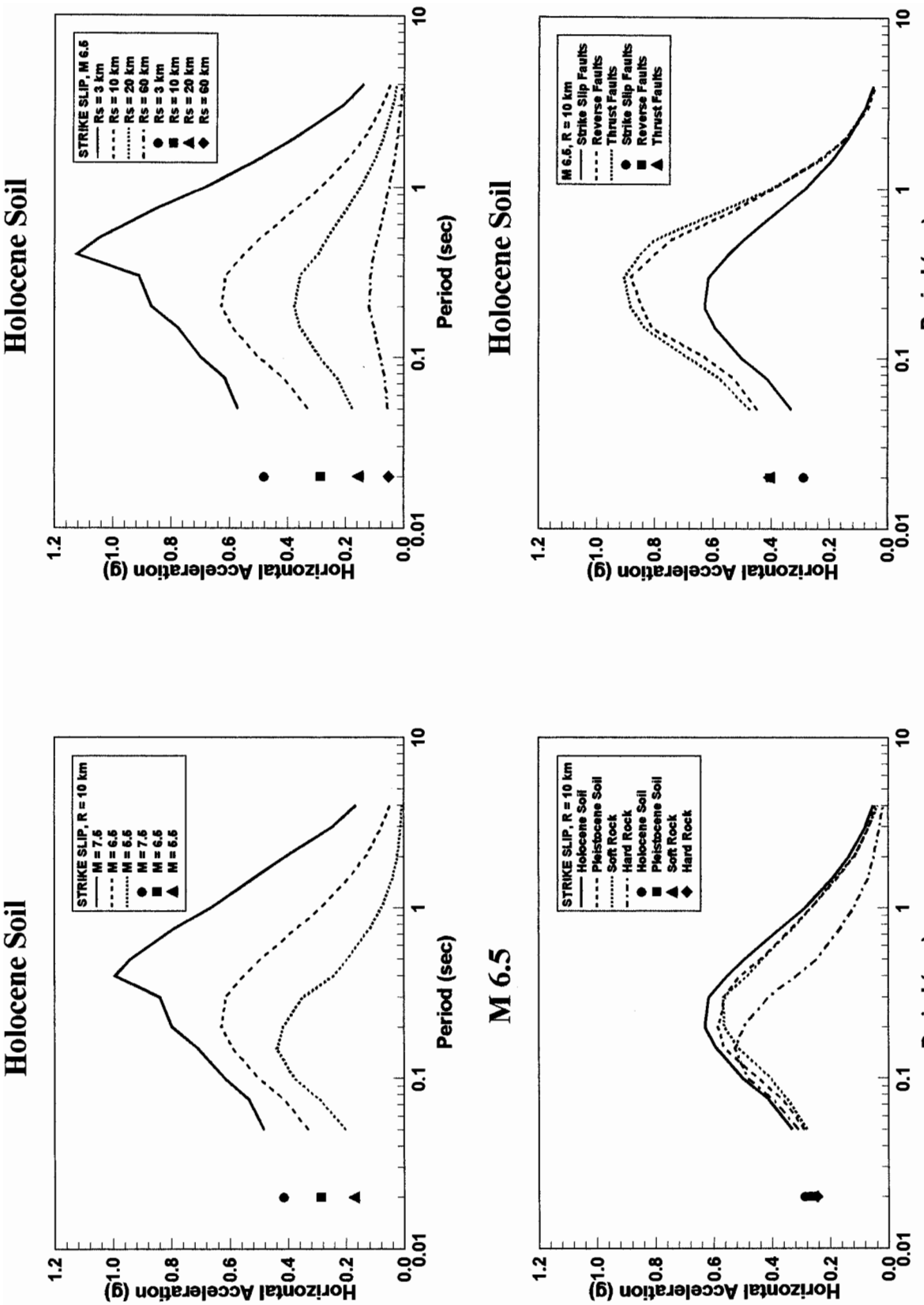

Figure 2—Dependence of horizontal SA on moment magnitude, source-to-site distance, local site conditions, and type of faulting.

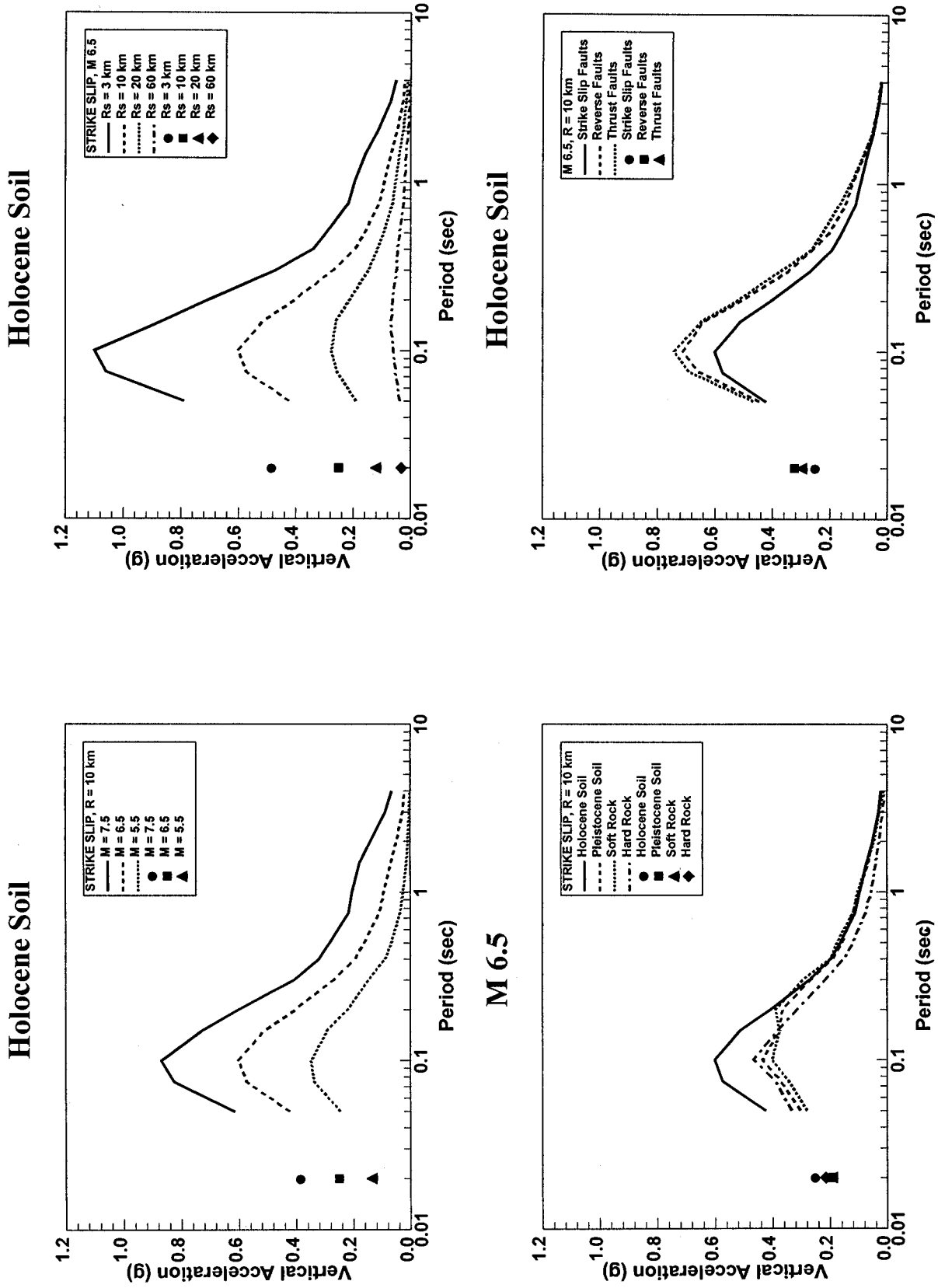

Figure 3—Dependence of vertical SA on moment magnitude, source-to-site distance, local site conditions, and type of faulting.

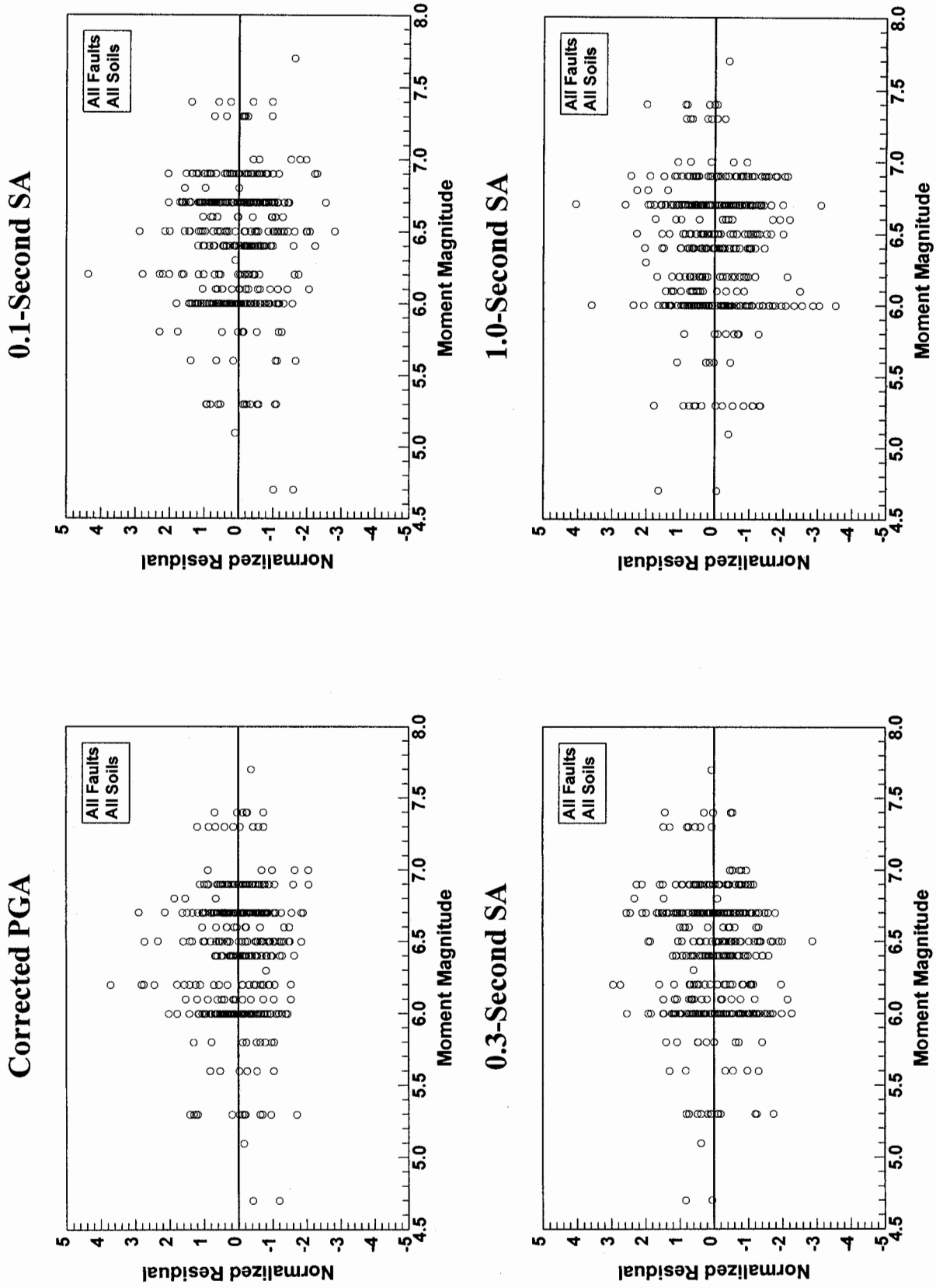

Figure 4—Normalized residuals of V/H versus moment magnitude.

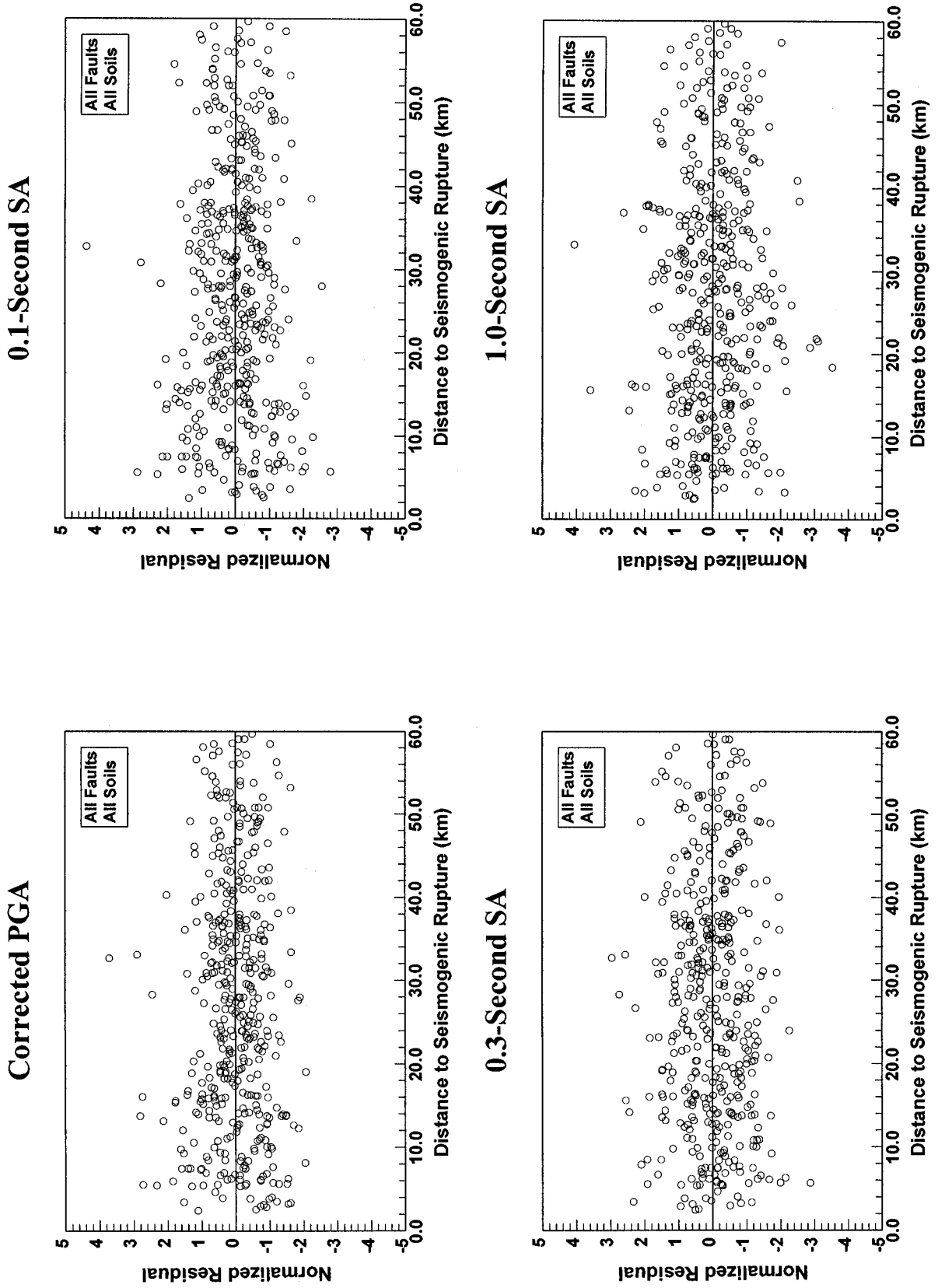

Figure 5—Normalized residuals of V/H versus source-to-site distance.

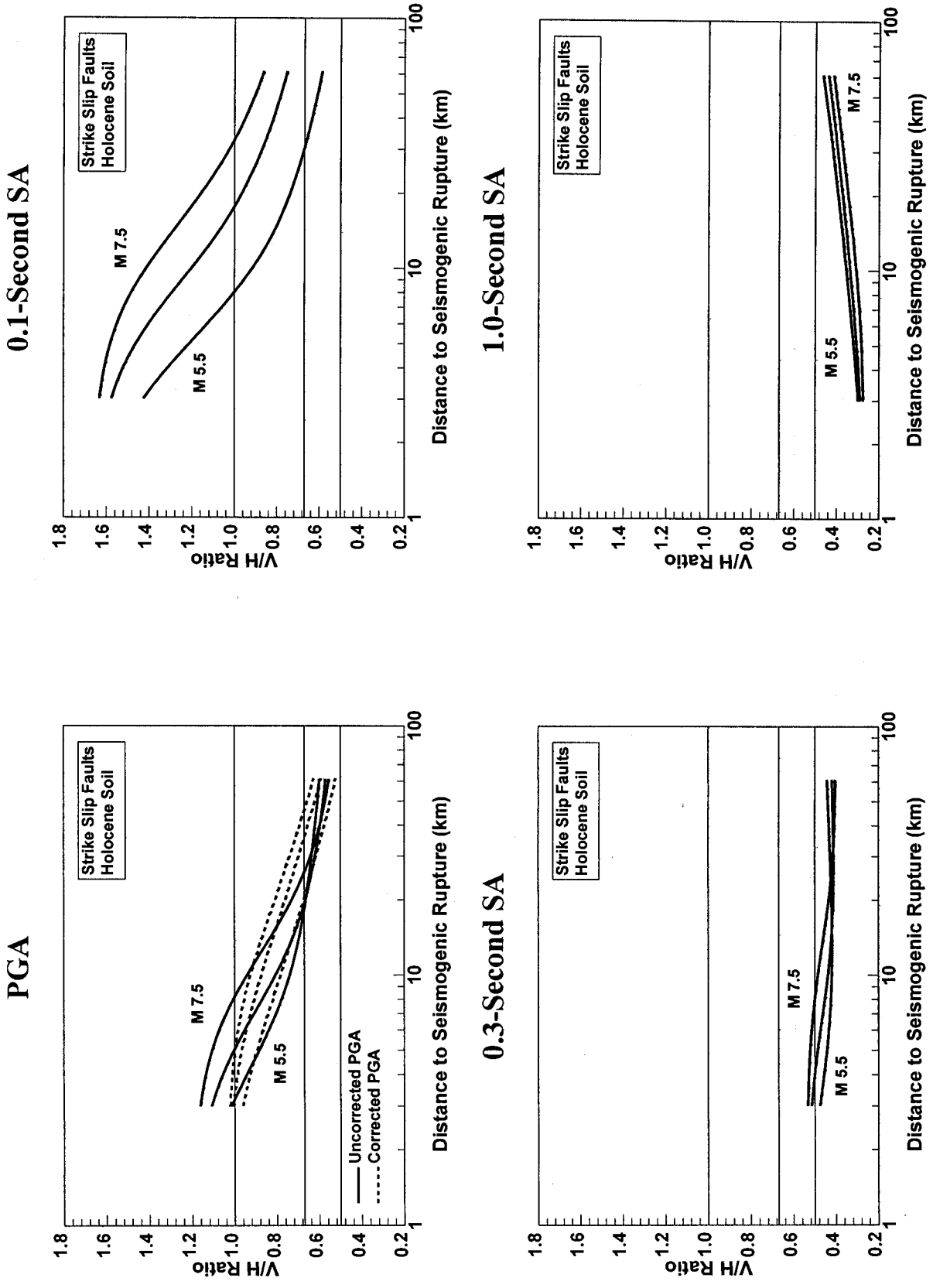

Figure 6—Behavior of V/H spectral ordinates with source-to-site-distance.

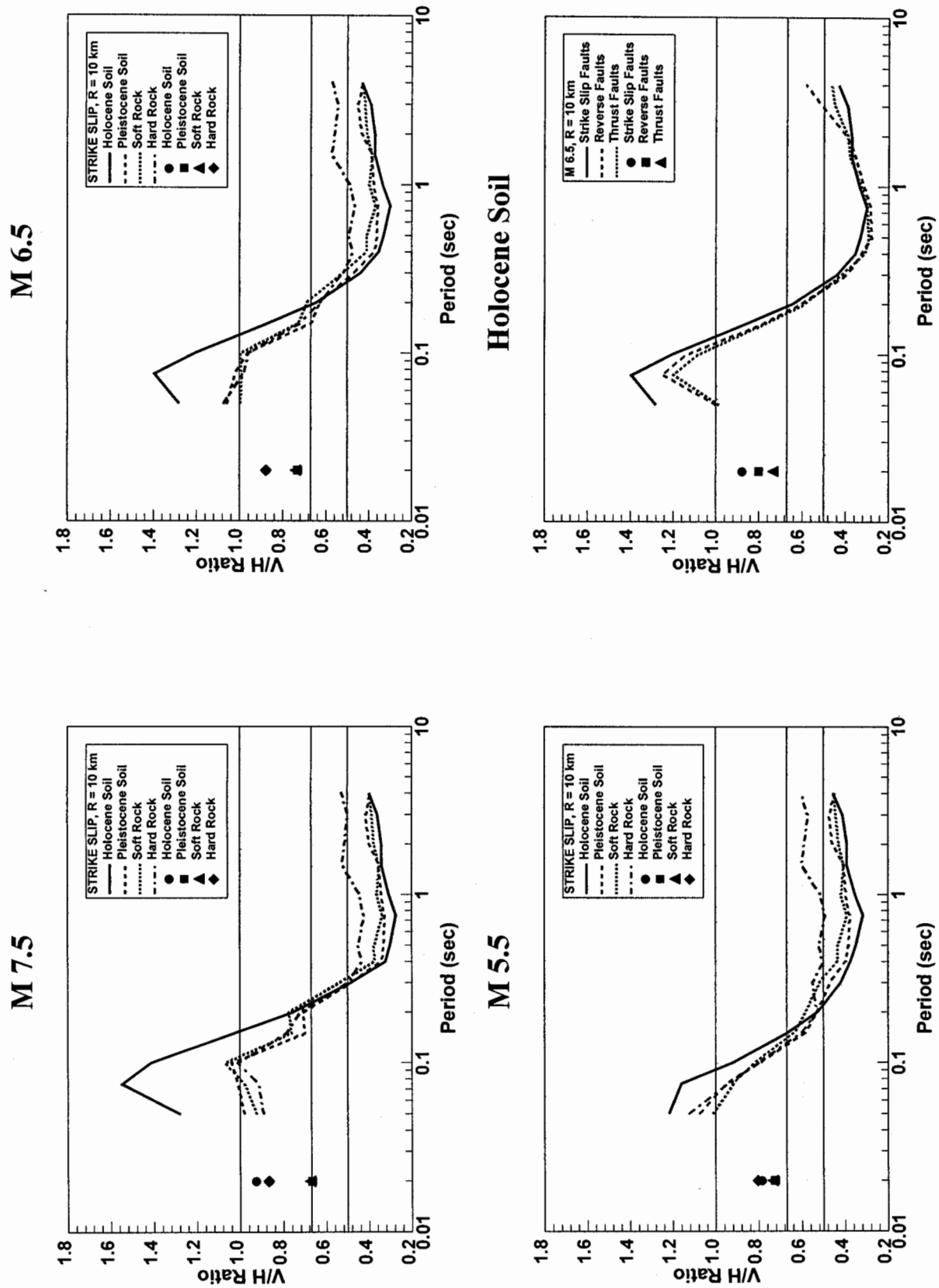

Figure 7—Behavior of V/H spectral ratio with moment magnitude, local soil conditions, and type of faulting.

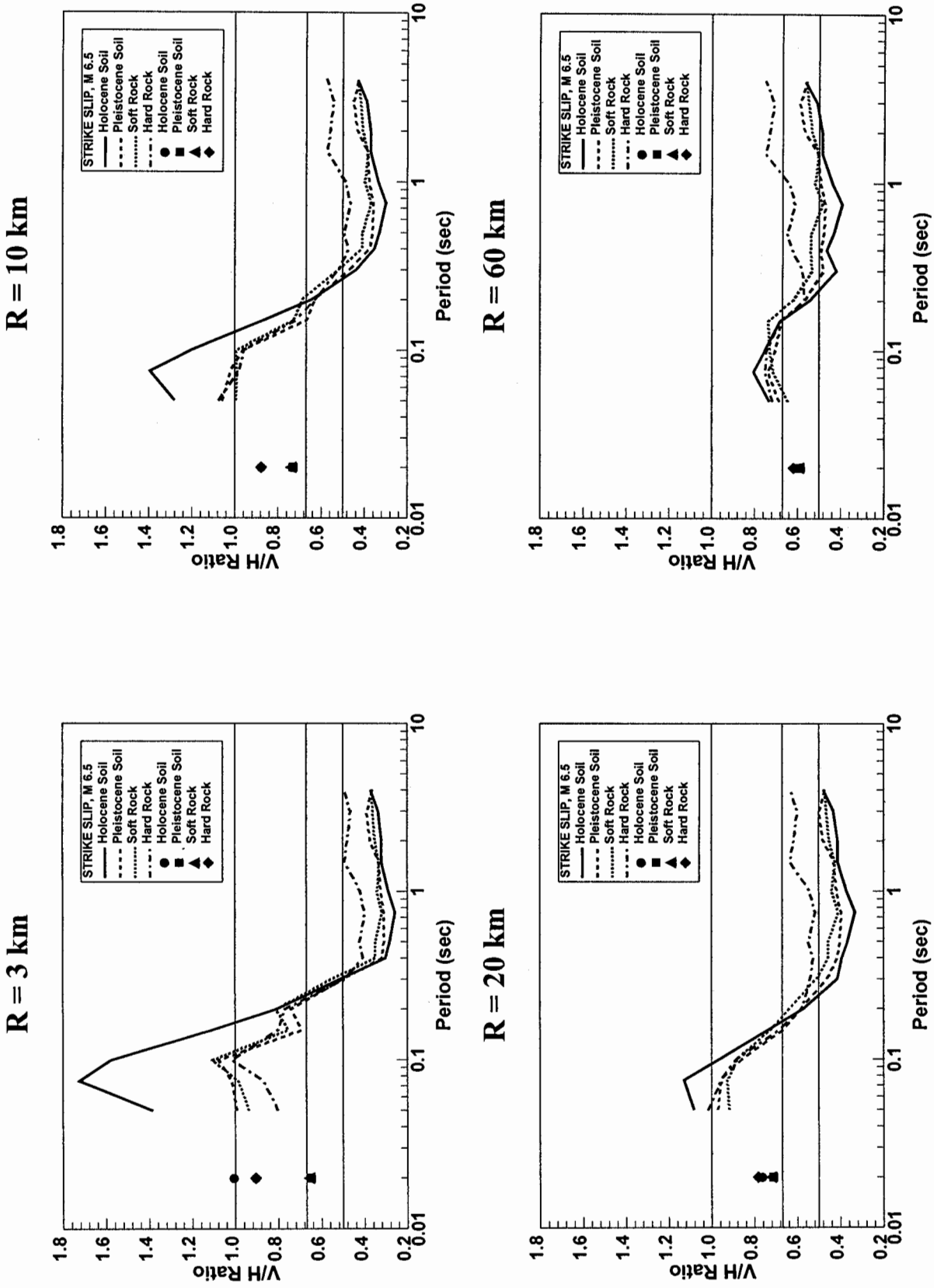

Figure 8—Behavior of V/H spectral ratio with source-to-site distance and local soil conditions.

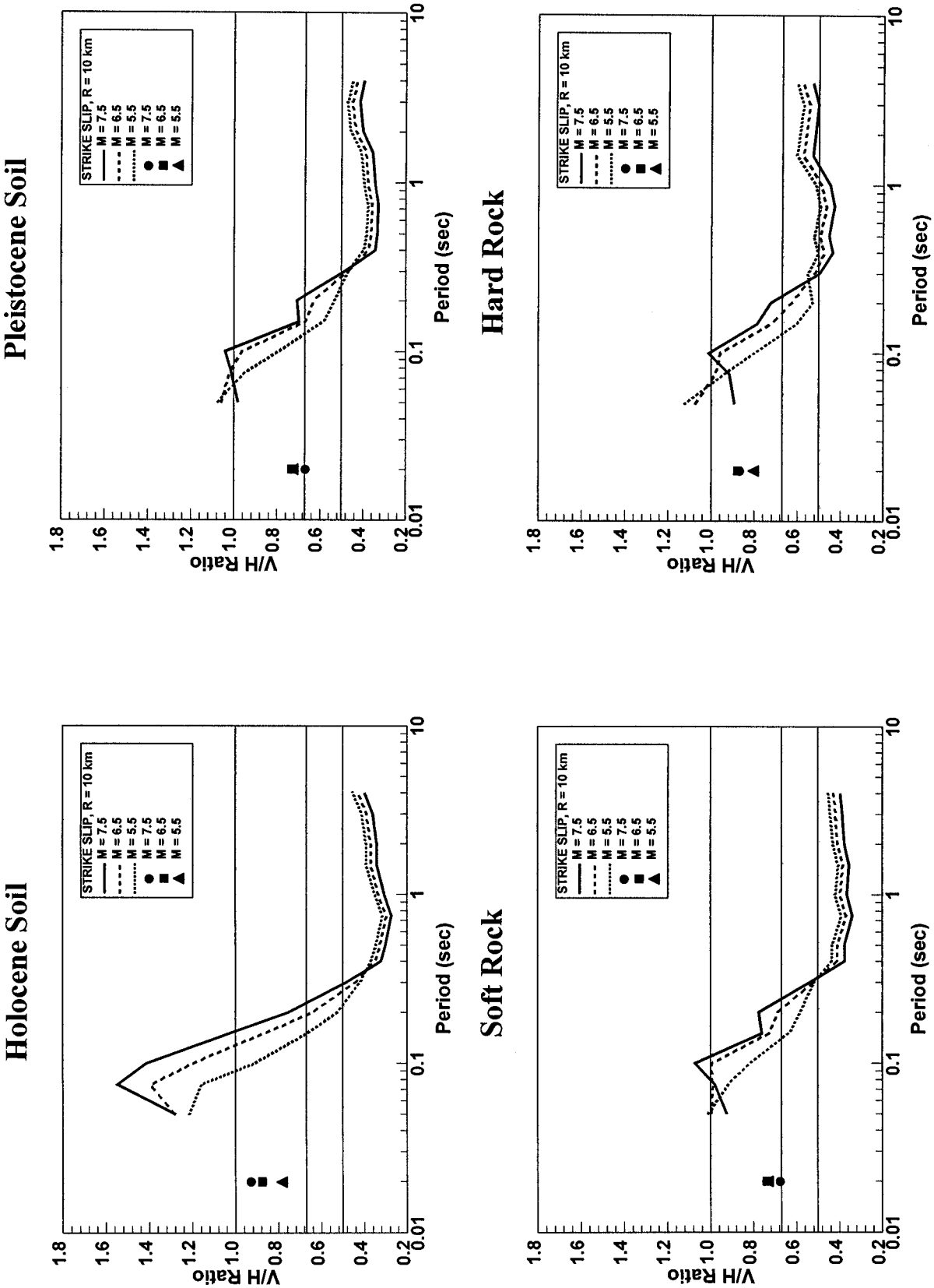

Figure 9—Behavior of V/H spectral ratio with local soil conditions and moment magnitude.

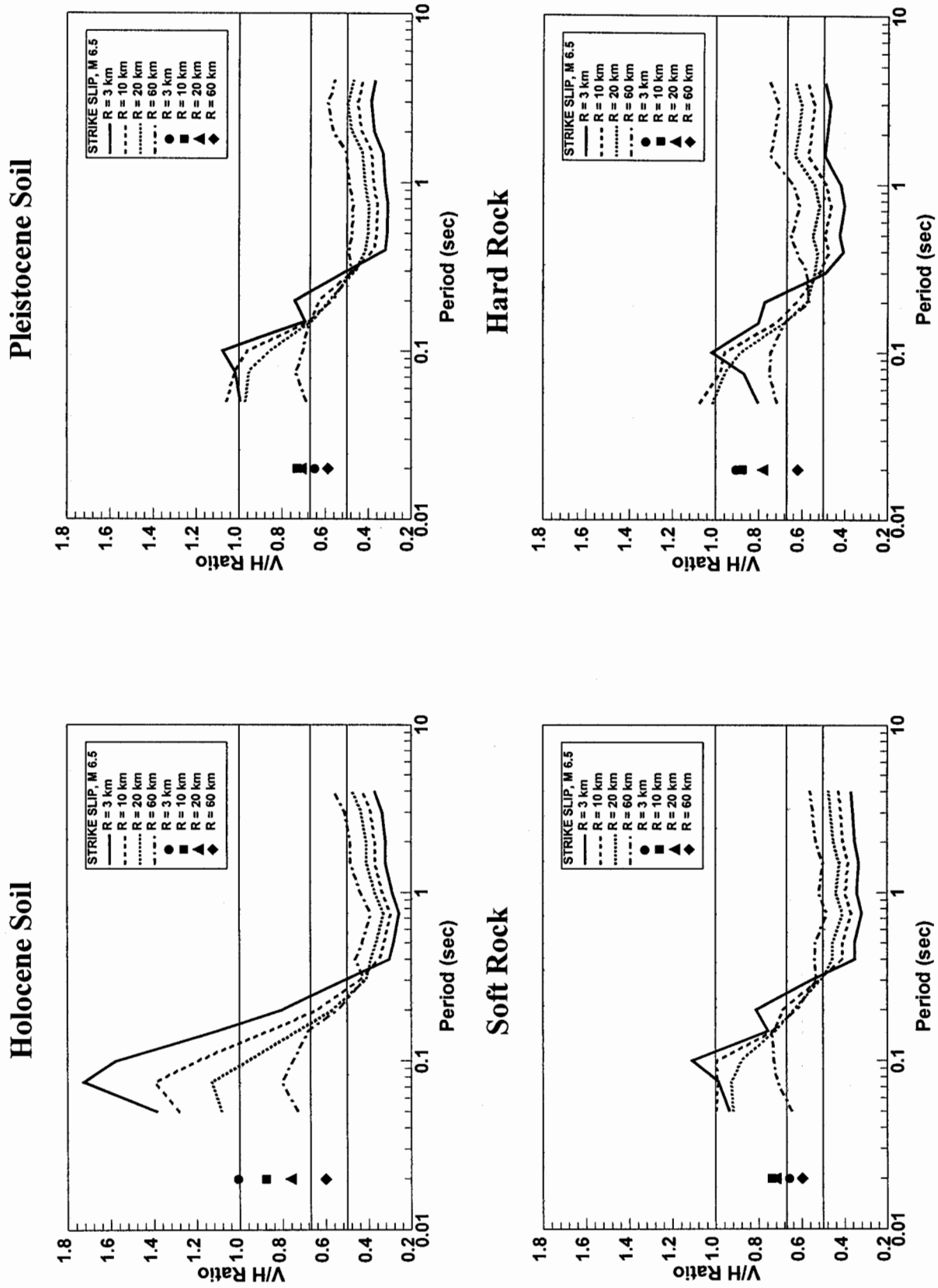

Figure 10—Behavior of V/H spectral ratio with local soil conditions and source-to-site distance.

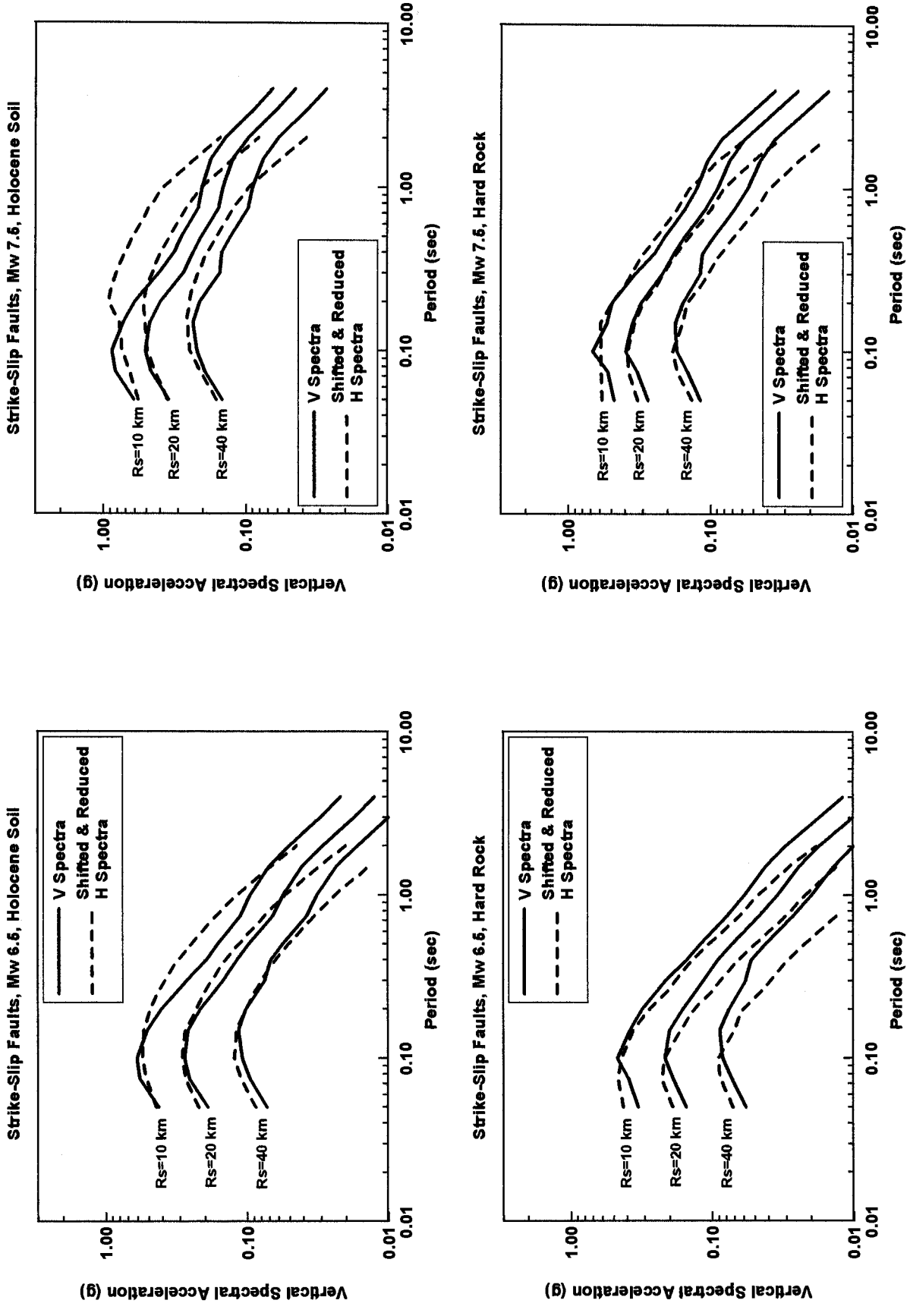

Figure 11—Vertical response spectra and shifted & reduced horizontal spectra.

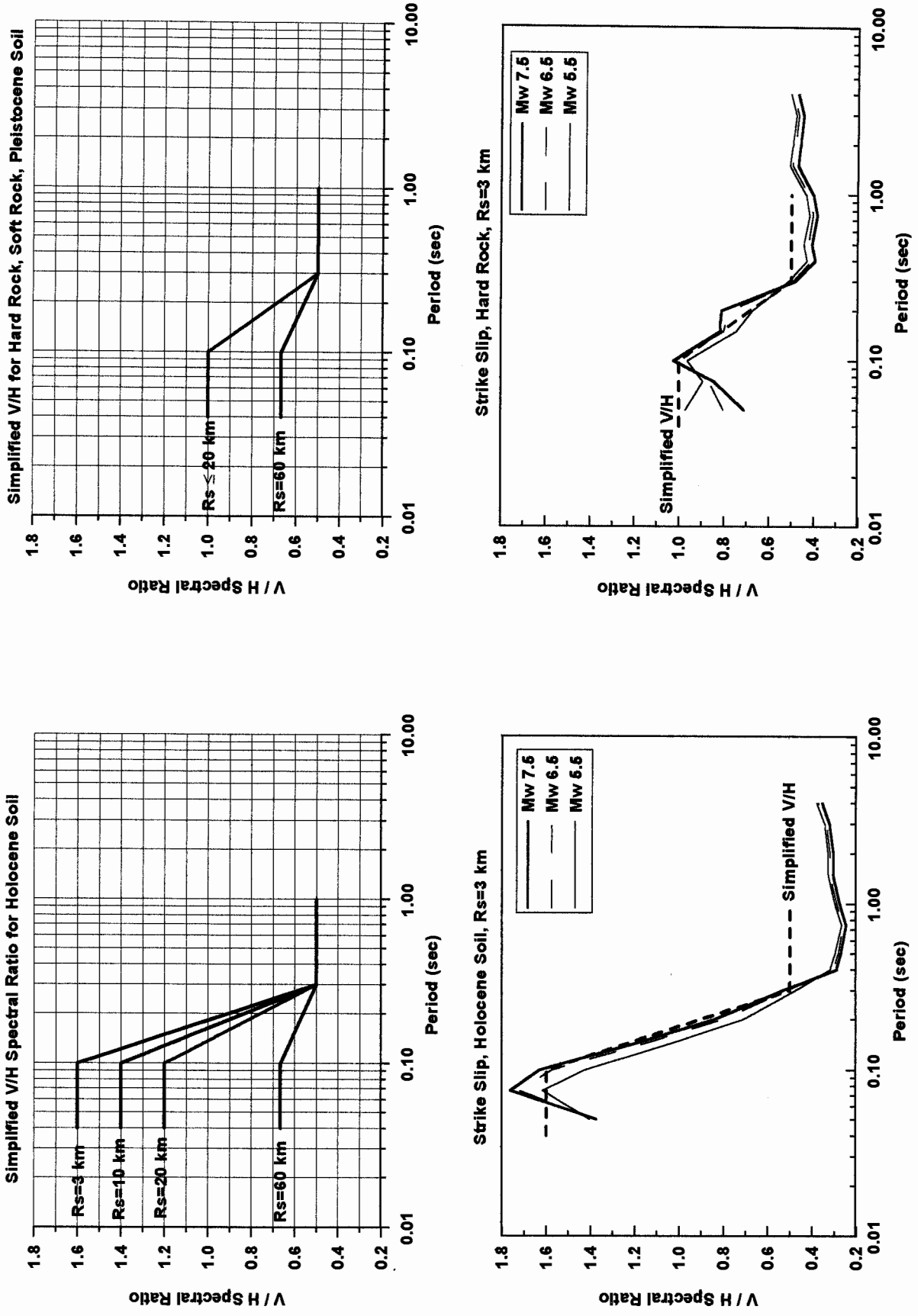

Figure 12—Predicted and simplified V/H spectral ratios.

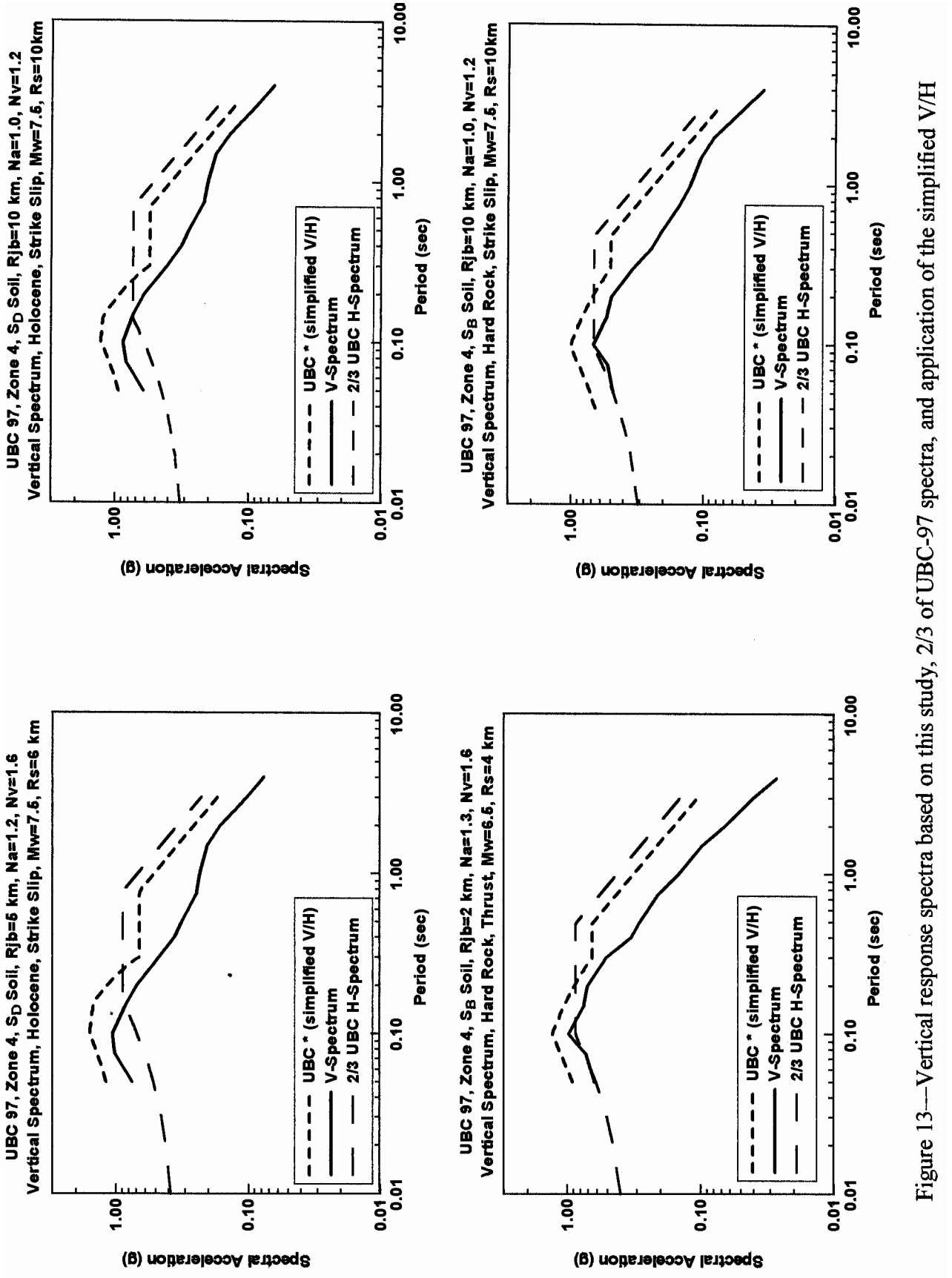

Figure 13—Vertical response spectra based on this study, 2/3 of UBC-97 spectra, and application of the simplified V/H

SEISMIC PERFORMANCE OF FOUR INSTRUMENTED STEEL MOMENT RESISTING BUILDINGS DURING THE JANUARY 17, 1994 NORTHRIDGE EARTHQUAKE

Farzad Naeim, Roy M. Lobo, Konstantinos Skliros and Marcello Sgambelluri

Research and Development Department
John A. Martin and Associates, Inc.

ABSTRACT

This paper presents a summary of our comprehensive evaluation of the seismic performance of four instrumented steel moment resisting frame buildings during the 1994 Northridge earthquake. The buildings were inspected and repaired, where necessary, according to the requirements of the FEMA-267 Interim Guidelines [FEMA, 1995]. The basic premise of performance based seismic engineering is the ability to predict performance given the base earthquake ground motion and building characteristics. These four buildings provided a perfect vehicle to compare the current status of analytical abilities versus this basic requirement for achieving a meaningful performance based design. To this end, not only we developed and studied numerous linear and nonlinear, static and dynamic computer models of these buildings, but we evaluated the relevant provisions of the leading traditional as well as performance based codes and standards. As this paper indicates, we are not far from the ability to understand, model, and explain global performance of structures. However, we are farther away from accurate prediction of location and extent of local damages within a structure. It is hoped that future work by us and other researchers will remedy this shortcoming in the near future.

INTRODUCTION

Our purpose of this study was to evaluate seismic performance of these four instrumented buildings, compare the observed performance with those predicted by model codes and guidelines, and where applicable suggest modifications to the prevailing analysis and design techniques and code provisions. In this paper, we contrast the results obtained by evaluation of the actual performance of these buildings with the design requirements embodied in the UBC-97 Code [ICBO, 1997] and FEMA-273 Guidelines [FEMA, 1997].

The four instrumented Los Angeles SMRF office buildings evaluated in this study were chosen by CSMIP, they are: (1) a 20 story building located in Encino, (2) a 10 story building in Tarzana, (3) an eight story building in North Hollywood, and 4) a 16 story building located in Sherman Oaks. The buildings were inspected after the Northridge earthquake for potential damage using the procedures outlined by SAC Interim Guidelines [FEMA 267, 1995]. The structural engineers who inspected and/or repaired each building were consulted. Their observations were documented and the structural plans and their repair drawings and reports were acquired.

The Northridge earthquake strong-motion recordings, obtained from the sensors installed at the buildings, were obtained from CSMIP. The accelerations were recorded in by tri-channel accelerometers (two horizontal components and one vertical) located on the ground, at mid level and on the roof of each building. It is worthy of mentioning that the instruments at various floors of these buildings were not time-synchronized. That is, the zero time for the sensors located at various floors did not exactly coincide (because it takes time for the seismic waves to reach the upper floors from the ground level). Interestingly, however, this proved not to be a significant problem in engineering evaluation of the seismic response for these buildings.

ANALYTICAL MODELS

Numerous analytical models for each building were created for linear and nonlinear, static and dynamic analyses. The models were calibrated by comparing the recorded building response with the response obtained from analysis. The comparisons included, but were not limited to, building periods, drifts, higher-mode response, time histories and known location of damaged joints, if any. The observed building performances as evidenced by post earthquakes investigations and recorded by installed instruments were compared with analytical results and code provisions. The most calibrated model for each building was used for these comparisons. In comparisons with UBC-97, we used elastic demand capacity ratios, demand plastic moment ratios, inter-story drifts, redundancy requirements and other UBC-97 special provisions. In application of the FEMA-273 guidelines, the desired performance objective was assumed to be the Basic Safety Objective. We used the nonlinear static procedure for this evaluation. The buildings were pushed to the desired target displacement and the plastic rotations were compared with the acceptance criteria associated with that performance level.

The general procedure utilized for construction and calibration of various computer models of the buildings is shown in Figure 1. The primary lateral resisting system for all the buildings consists of Special Moment Resisting Frames (SMRF). One of the buildings had shear walls and cross braces at the lower levels which are also modeled as part of the lateral resisting system. We evaluated the contribution of the gravity framing to the lateral stiffness for one of the buildings (the North Hollywood building). The difference in the responses with and without the inclusion of the gravity framing was minimal (between 2% to 5%). Furthermore, the response of calibrated analytical models for other three buildings, without explicit inclusion of the gravity framing, matched the recorded response very well both in the frequency and time domains. Therefore, there was no need for explicit inclusion of the gravity framing in computer models of these buildings.

Initially, we created two distinct three-dimensional computer models of each building using the SAP2000 computer program [Computers and Structures, 1997]. The only difference between these two models was in the way the beam-column panel zone was defined. For the first model (Model 1) we assumed the beam-column panel zone to be fully rigid. In the second model (Model 2) we assumed no rigid end zones for beams (column-center to column-center length). Using the recorded ground motions from the Northridge earthquake, we performed a series of elastic time-history analyses and compared the analytical results with the recorded responses. Based on these comparisons, we constructed a third, best fit model (Model 3) using calibration techniques.

We investigated the influence of vertical ground motion on seismic response of the Tarzana building since this building was subjected to the most severe vertical ground motion in the group of buildings studied. Our analysis indicated the effects of vertical ground motion to be insignificant for this building in terms of increases in both stresses and displacements. Therefore, the effects of vertical ground motion were not included in performance analysis of other buildings.

For three of the four buildings (Tarzana, North Hollywood and Sherman Oaks), the precise locations of the seismographs/accelerometers were unavailable. Therefore, they were initially assumed at the center of mass of the respective floors. We evaluated the torsional components of the response obtained from our analytical models and found them to be insignificant. That is, there was no appreciable difference in the displacements in a particular direction measured at the corners of the building. The exact amount of torsional displacements experienced by these buildings during the earthquake could not be determined from the instrumented response because there was only one sensor located at a floor and the torsional component of the response was not explicitly recorded. The symmetrical configuration of all four buildings and the excellent agreement achieved between the recorded and analytical responses, however, strongly suggests that torsion was not a significant contributor to seismic response of these buildings during the 1994 Northridge earthquake.

We compared the acceleration, velocity and displacement responses for Model 1 and Model 2 with the recorded responses. If the predominant period of the building as interpreted from the recorded time-histories, throughout the duration of response, was bounded by the predominant periods of Models 1 and 2, the response was considered as essentially elastic. The reason is that in this case the predominant period of the building through the duration of response could be matched by adjusting the effective rigidity of the beam-column panel zones. The amplitudes then could be matched by adjusting modal damping values. This approach was used via a series of iterative schemes for development of a best fit model or Model 3. In contrast, if the recorded response indicated that the building was more flexible (even during just a portion of the response duration) than Model 2, a nonlinear model was required. This is due to the fact that in such cases the recorded response could not have been matched merely by adjusting the rigid end zones.

We examined the results from the time history analysis for Model 3 subjected to Northridge earthquake input ground motion with respect to the following parameters:

1. zones of high demand as suggested by analysis versus post earthquake inspection results.
2. Sensible estimates of effectiveness of the beam-column rigid zones based on connection details utilized in each building.
3. The values of equivalent modal damping needed to match analytical and recorded response amplitudes, and
4. Sensitivity of models to minor modeling variations.

The expected, rather than nominal, yield strengths were used for calculation of member capacities throughout. These are 1.5 times the yield strength for A36 steel and 1.15 times the yield strength for A50 steel [AISC 1997].

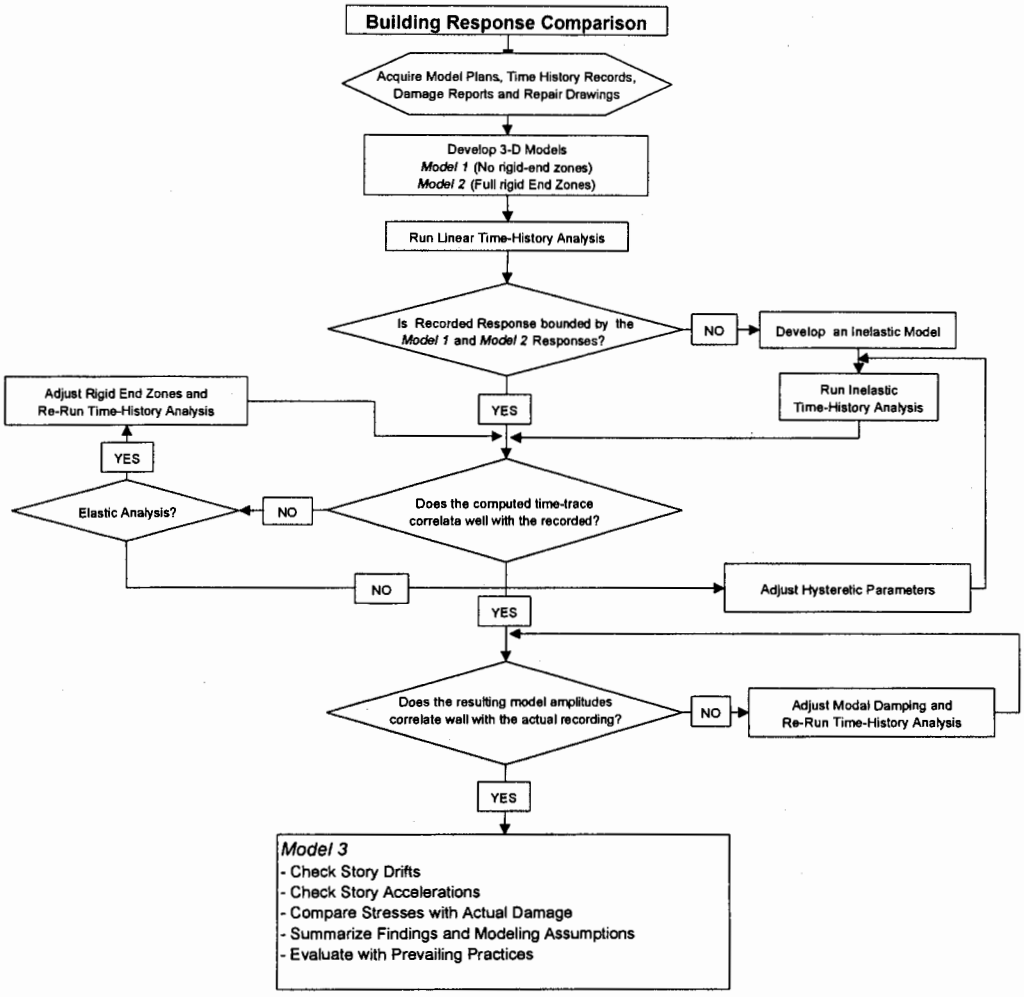

Figure 1. Procedure for Construction and Calibration of Analytical Models.

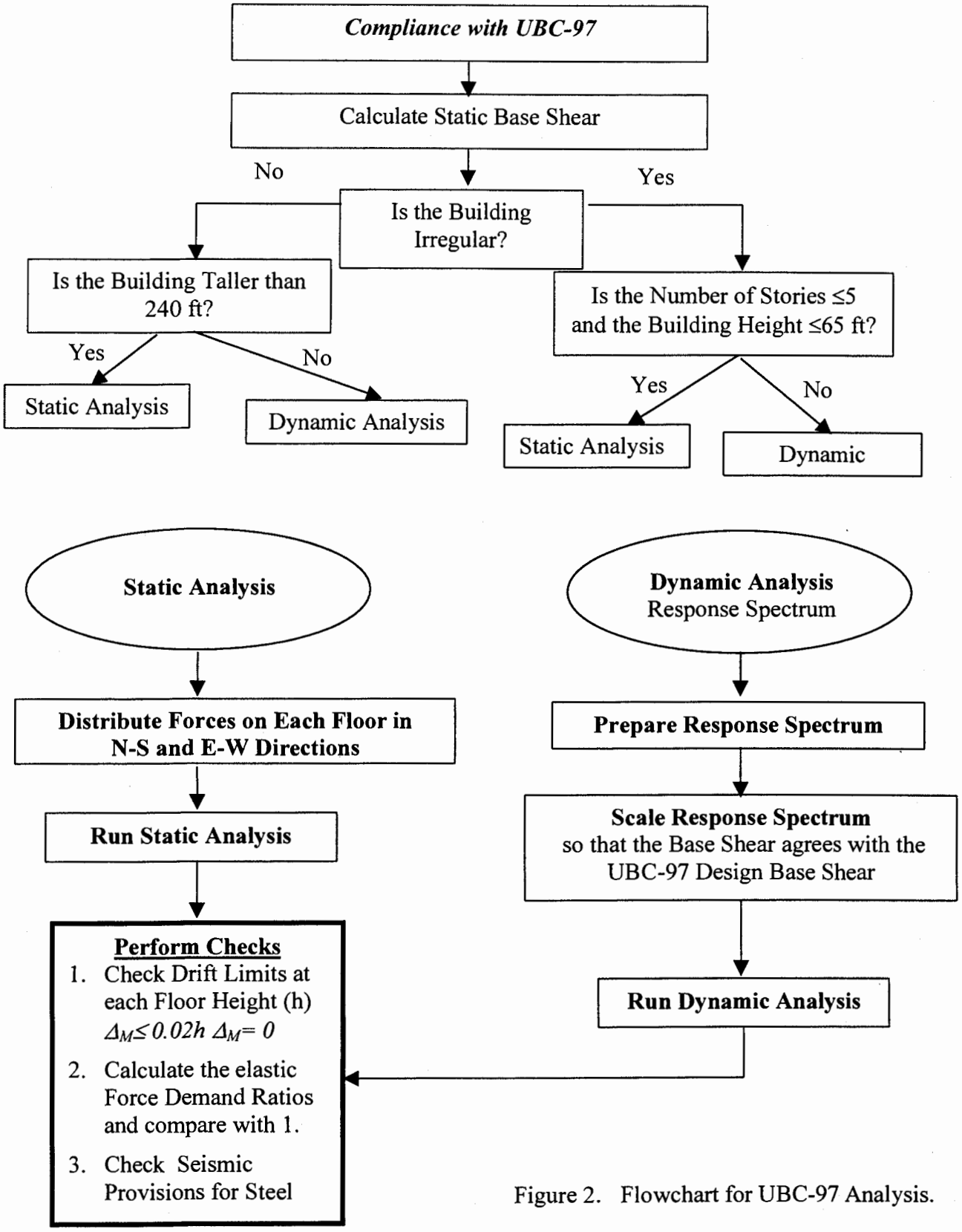

Figure 2. Flowchart for UBC-97 Analysis.

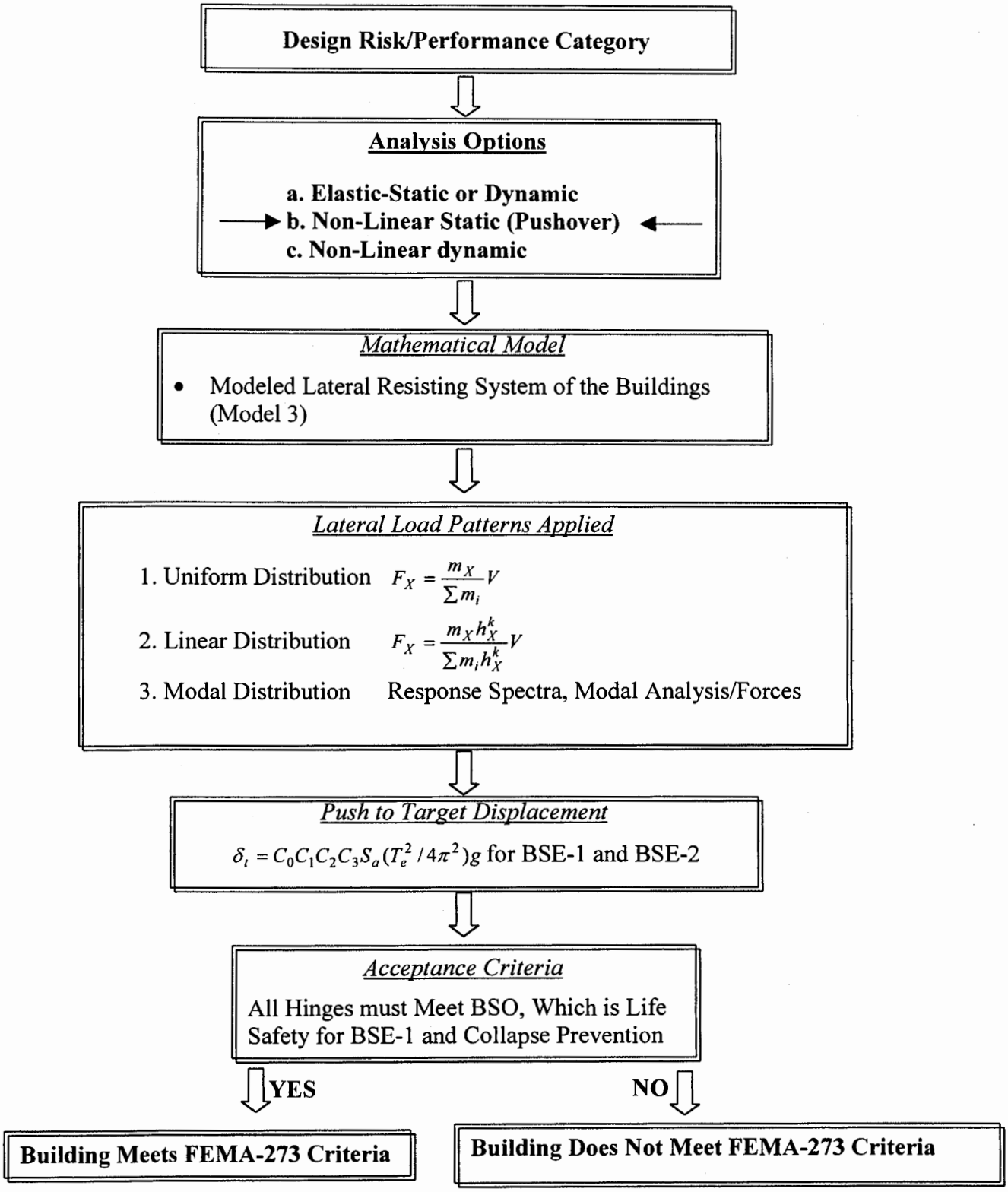

Figure 3. Flowchart for FEMA-273 Analysis

We analyzed and compared the status of all four buildings with respect to the UBC-97 and FEMA-273 requirements. This comparison can serve several purposes:

- Establishment of the relation between the demand imposed by the ground motion experienced during the 1994 Northridge earthquake to code level demands that buildings are to be designed for and withstand
- Identification of the relevance and relative importance of various codified detailed design procedures in seismic performance of existing structures
- Evaluation of reliability, or lack thereof, of codified procedure in identifying the weak links in the structure and the zones of high demand
- Comparing relative accuracy of specific, calibrated, analyses for actual earthquake ground motions to generic codified analyses in terms of ability to identify potential zones of damage
- Identification of those code provisions that are either over-conservative or under-conservative and development of alternate, more accurate, code provisions.
- Identification of areas that need improvement to accelerate realization of effective and reliable performance based design alternatives.

Flowcharts showing the general procedure of code comparisons are presented in Figures 2 and 3 for UBC-97 and FEMA-273 , respectively.

The idealized force deformation relation for each element defining its acceptance criteria is shown in Figure 4. All the elements in the model are primary members. The acceptance criteria for the beams and columns are taken from Table 5-4 of FEMA-273. The maximum plastic rotations corresponding to the Life-Safety (LS) and Collapse Prevention (CP) requirements as well as the plastic hinge properties are calculated as a function of the width-thickness ratio (b/t) of each section under the guideline specifications

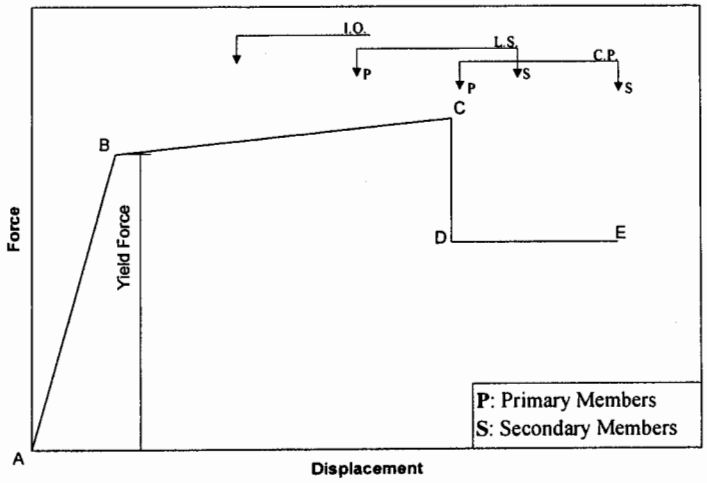

Figure 4. Component or Element Deformation Limits According to FEMA 273.

THE ENCINO BUILDING

This building consists of a twenty-story tower and an attached four-story parking garage. The structure of the tower is rectangular in plan and over 249 feet tall. The lateral resisting system of the building is provided by Steel Moment Resisting Frames (SMRF). The floor slabs consist of 5 in. thick light-weight concrete with no metal deck. The four story parking structure is offset to the east of the tower, but shares a continuous floor diaphragm with it. The parking structure has its own SMRF system. The parking structure has two four-bay moment frames in the North-South and East-West directions, respectively. The tower has four four-bay frames in the North-South direction and two seven-bay frames in the East-West direction over the first four floors. The frames are cutback by one bay on the upper floors in the North-South direction. There is a bank vault in the Southwest corner of the tower with four concrete shear walls at the first floor and two X-braces on the second floor.

A view of our three-dimensional model showing the lateral resisting system is presented in Figure 5. A plan view of the building showing the lateral frames, corresponding gridlines and column orientations may be seen in Figure 6. The beam-column connections are typical pre-Northridge SMRF connections. Continuity plates exist only on the upper five floors of the tower (floors 16 to 20). There are four non-prismatic girders per floor that are located on gridlines 4 and 7 and span from lines A to D and E to G. The rolled steel sections are Grade A572 steel and the plate girders, used for the non-prismatic members, are made of A36 steel. Tri-channel seismic sensors are located in the basement (arcade) level, 10th floor, and roof.

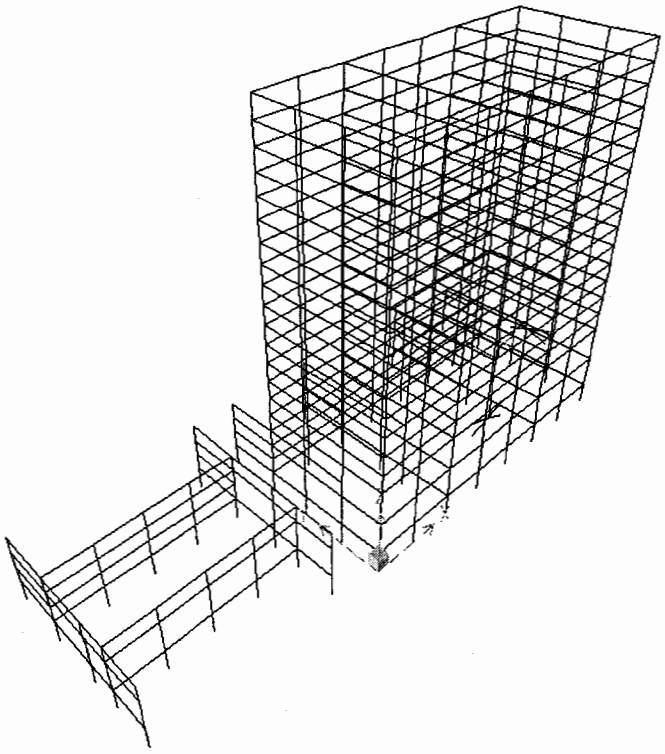

Figure 5. Three-dimensional Model of the Encino Building.

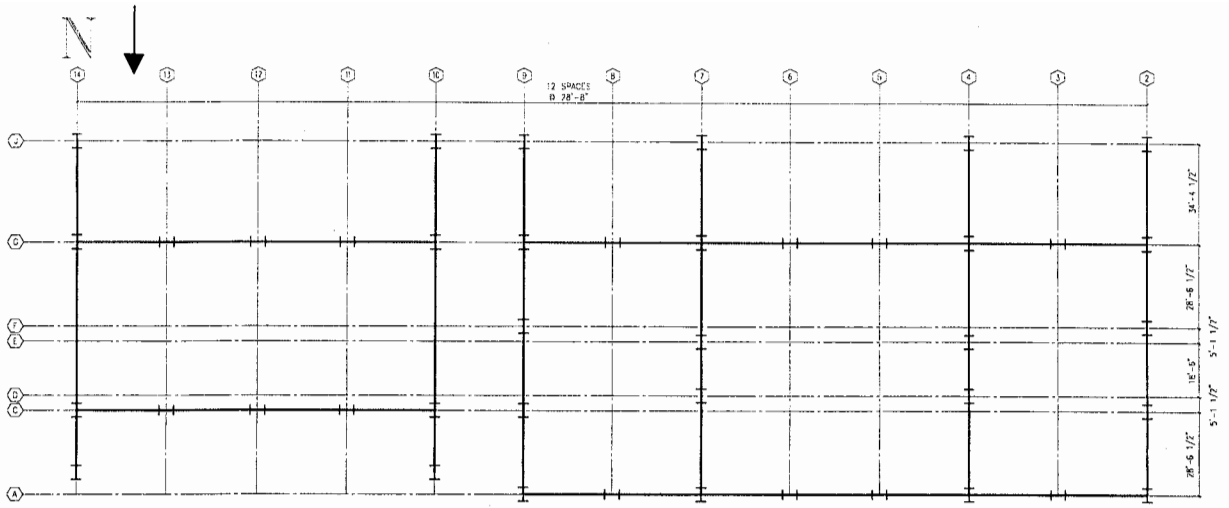

Figure 6. Plan View of Seismic Frames and Gridlines for the Encino Building.

The assumed damping levels and member end rigid zone factors used for various analytical models are shown in Table 1. Our best-fit model corresponded to 95% effective rigid end-zone for columns and 100% for beams.

Table 1. Rigid End Zone Factors and Modal Damping in the Models.

Model	Rigid End Zone Factors	Analysis	Modal Damping
Model 1	All Elements=100%	Elastic 3D	
Model 2	All Elements=0%	Elastic 3D	
Model 3	All Beams 100 % Columns Moment connection in 2 directions 3 and 4 way=100% Corner=95% Moment connection in 1 direction With Continuity Plates=5% Without Continuity Plates=2.5%	Elastic 3D	NS: 3% 1st ,3rd ,and 6th, all others 10% damped EW: 2.5% 1st and 5th, all others 10% damped

A comparison of the periods interpreted from recorded data by from the transfer function analysis and our best-fit model for the first three modes of vibration are given in Table 2. The largest percent difference is only 11.3%. This closeness indicated that the vibration periods of the computer model correlated well with the periods of the actual building.

Table 2. Comparison of Vibration Periods for *Model 3* and the Periods for the Recorded Response using the FFT Method.

North-South				East-West			
Mode	**Modal Periods (SAP2000)** (*sec*)	**Modal Periods (FFT Analysis)** (*sec*)	**Diff.** (%)	**Mode**	**Modal Periods (SAP2000)** (*sec*)	**Modal Periods (FFT Analysis)** (*sec*)	**Diff.** (%)
1	2.754	2.596	5.7	2	2.530	2.242	11.3
4	0.967	0.937	3.1	5	0.930	0.931	1.1
7	0.573	0.531	7.3	8	0.558	0.538	3.6

The recorded ground motions at the arcade level of this building are presented in Figure 7.

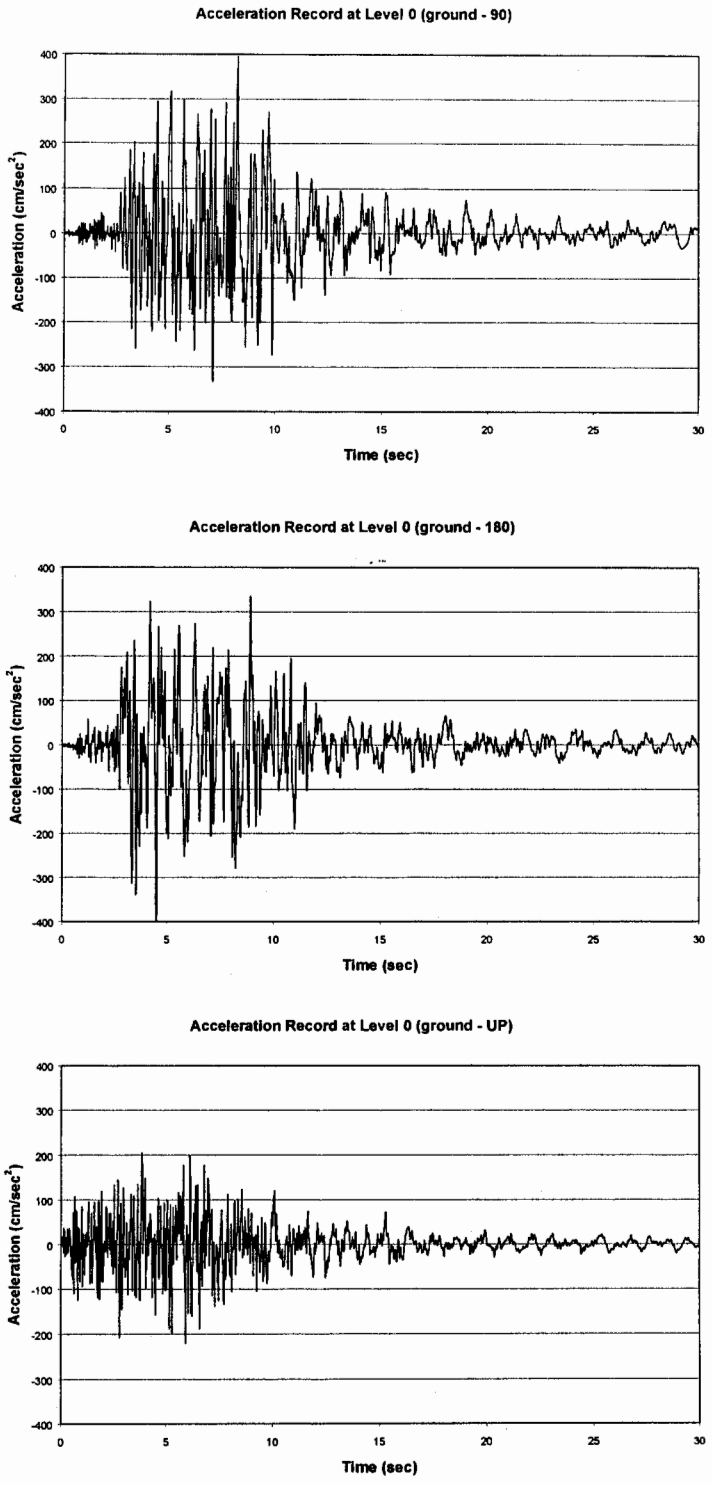

Figure 7. Recorded Northridge Ground Motions at the Arcade Level for the Encino Building.

After the Northridge earthquake, the building moment connections were inspected for damage. A summary of the different types of damage found and the corresponding (SAC) identifications are given in Table 3. The overall damage statistics is given in Table 4. The type 1D damage was small enough that it was not repaired. Therefore, the 1D type damage is excluded from any of the comparisons made in this study. Figures 8A through 8D show the different locations of observed damage on the moment resisting frames. Note that not all connections were inspected following the Northridge earthquake. The most severe damage was experienced in the columns on the North-South lateral frame along line 2, where the crack propagated all the way into the column web.

Table 3. Identification of Damage.

ID Name	SAC Identification Definitions
1D-W4	Light beam flange weld cracking
C2	Column flange damage: Complete flange tear out from beam flange weld
C3	Column flange damage: Partial cross-flange crack in HAZ
P5	Column Web Damage: Partial depth cracking originating from cracked col. Flange
W4	Beam Flange Damage: Crack at column interface (in weld)

(A) Damage on Gridlines 2 and 9

(B) Damage on Gridlines 4 and 7

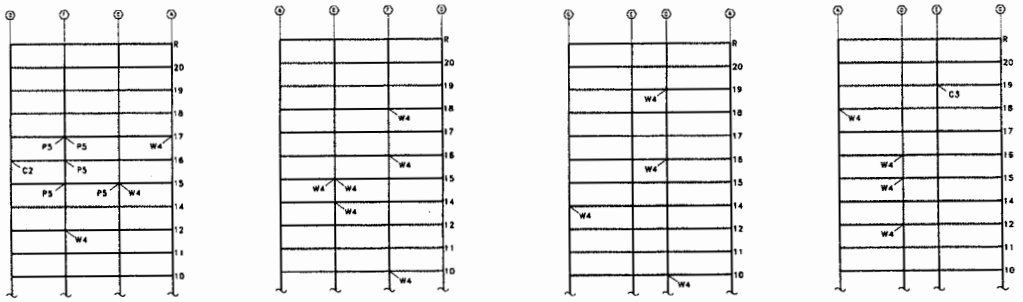

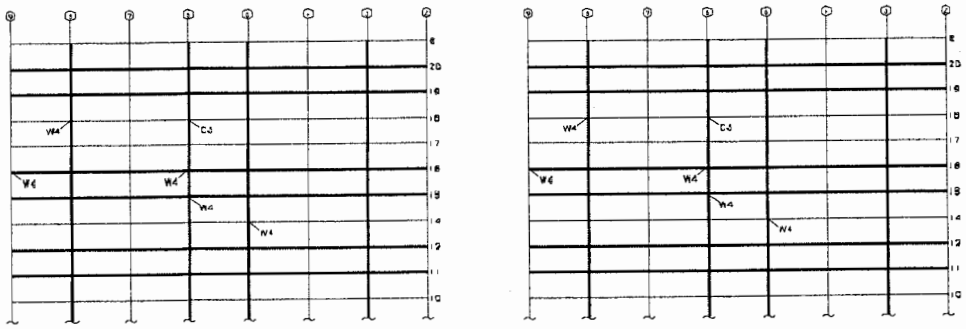

(C) Damage on Gridlines A

(D) Damage on Gridlines G

Figure 8. Damage revealed by inspection of the Encino Building.

Table 4. Summary of Damaged Connections.

East-West				North-South			
Member	**Total Number of Connections**	**Number of Damaged Connections**	**Ratio (%)**	**Member**	**Total Number of Connections**	**Number of Damaged Connections**	**Ratio (%)**
Columns	512	0	0	Columns	256	5	1.9
Beams	448	11	2.5	Beams	384	19	5

Responses computed by our best-fit model are contrasted with those experienced by the building during the Northridge earthquake in Figures 9 to 11. The accuracy of the analytical model in capturing the essence of building response is clear. There are some spikes in the analytical acceleration responses that are probably due to higher modes. Increasing the damping in the higher modes decreases the amplitudes of these spikes. These higher modes are probably highly damped in the actual structure as evident from of the recorded acceleration responses. The calculated displacement response amplitudes in the North-South direction show some departure from the recorded response from about 15 to 25 seconds. This is probably due to some inelastic response in this range. This, however, did not significantly affect the overall stiffness of the structure. Additional damping by yielding of some of the non-structural elements could have also resulted in the difference in the responses. Although the North-South direction experienced some inelastic behavior, the difference in the elastic response of the computer model to the inelastic behavior of the building is very small. In addition, there are no noticeable differences in the East-West direction response between the analytical and recorded response, although there was damage.

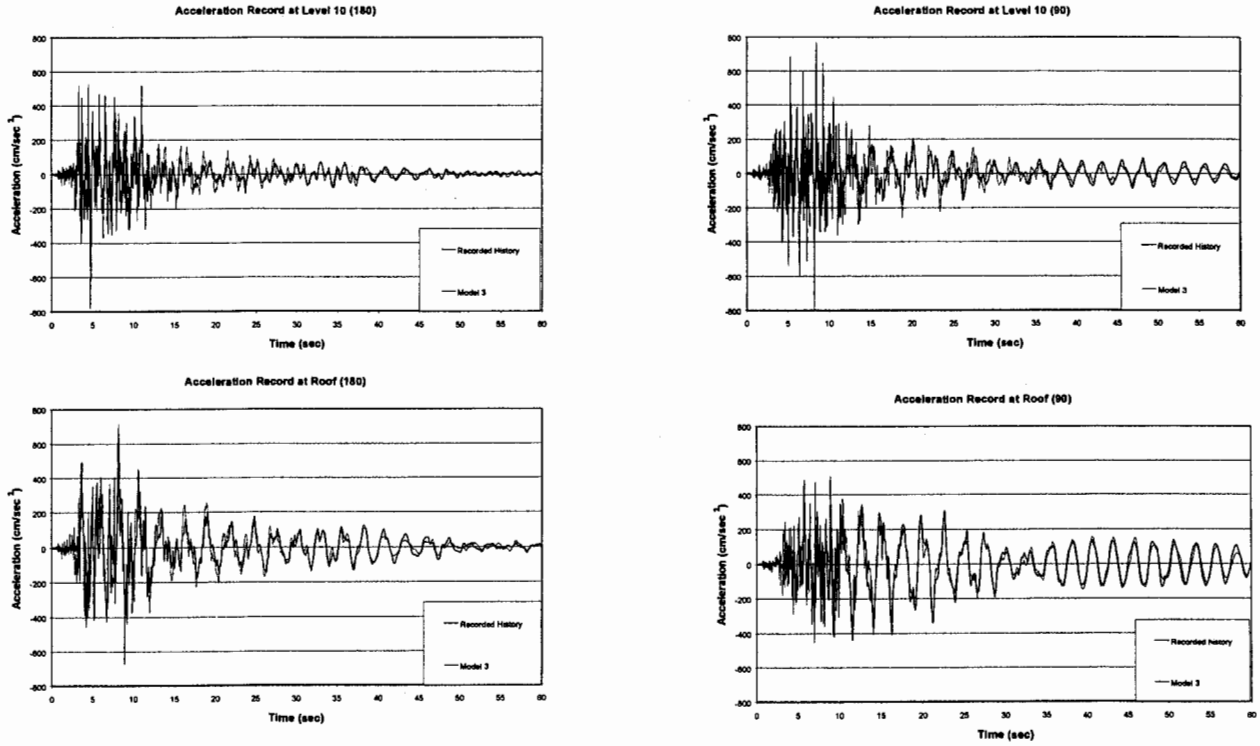

Figure 9. Acceleration Time Histories for the Encino Building.

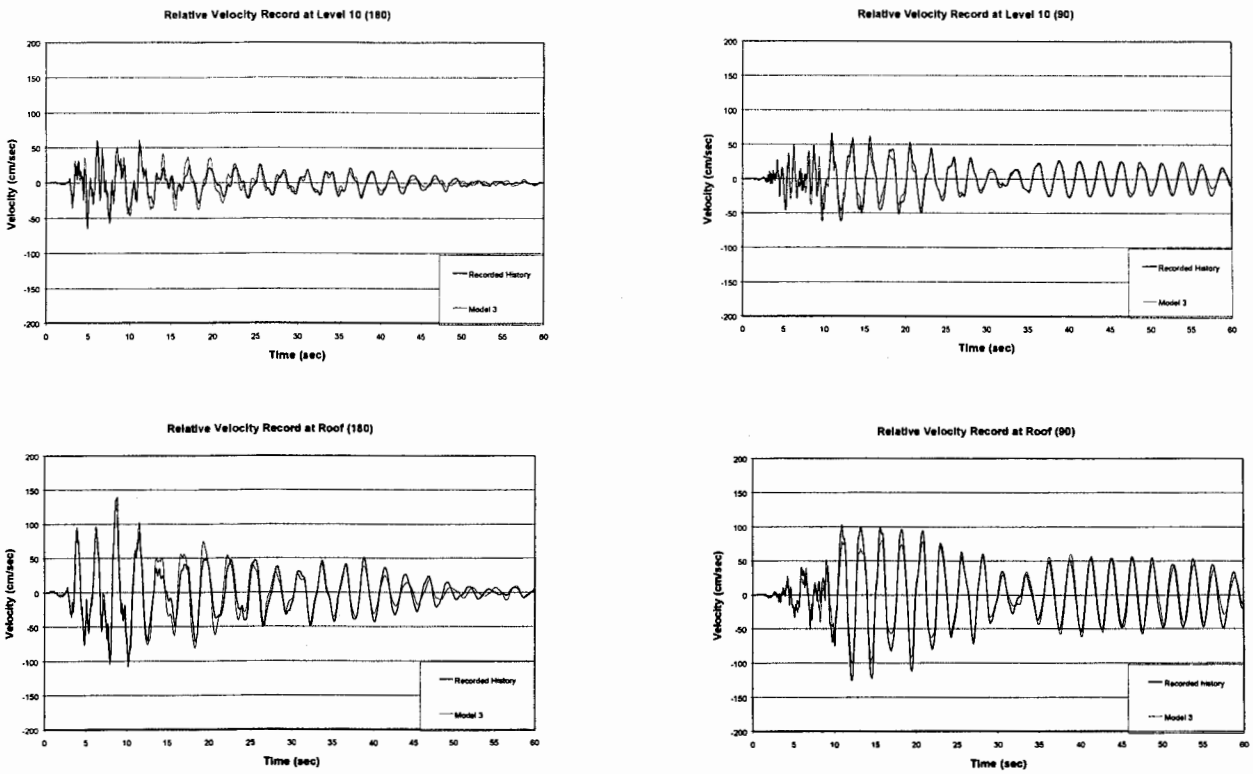

Figure 10. Velocity Time Histories for the Encino Building.

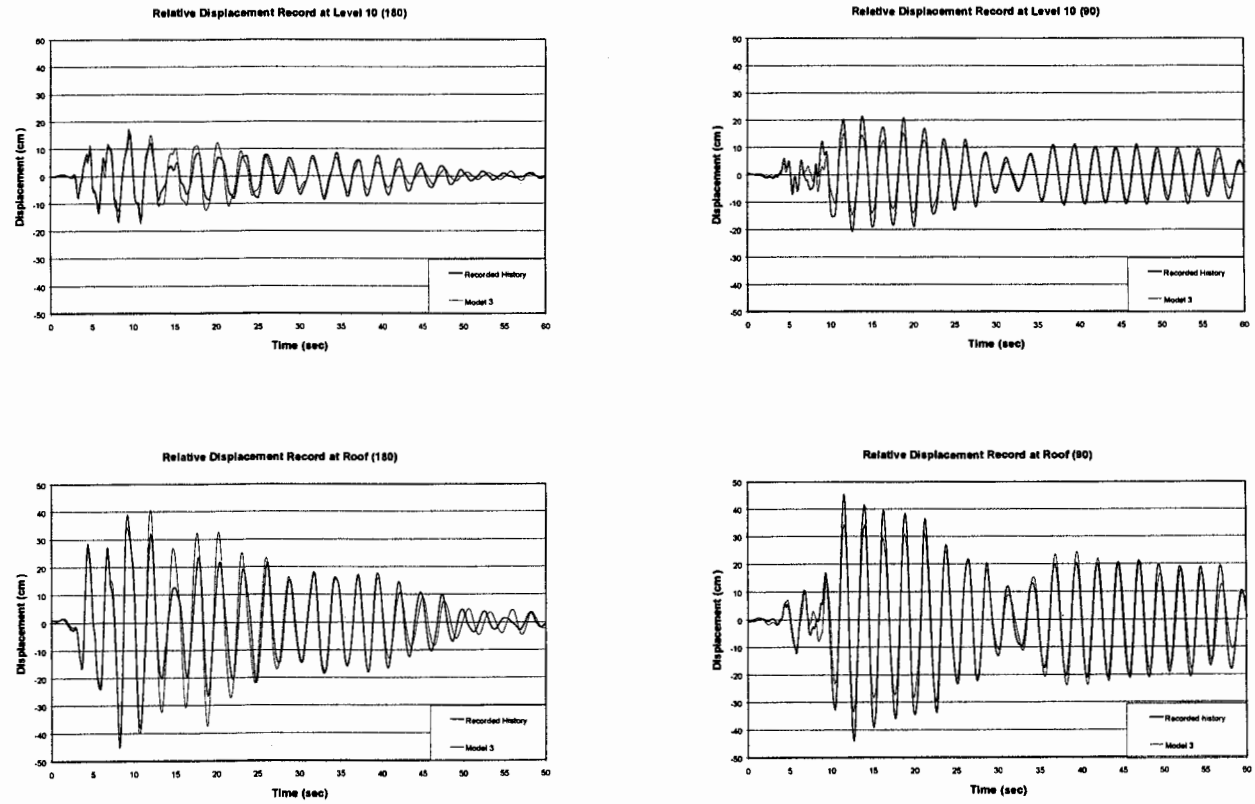

Figure 11. Displacement Time Histories for the Encino Building.

The Elastic Demand Ratios (EDR) are calculated from the Time History analyses in order to determine if the zones of excess correlate with the observed pattern of damage to the building. This is one way of establishing how effective, or ineffective, our analytical indicators of damage are for prediction of likely damages to this SMRF building. These EDR are calculated using the Load and Resistant Factor Design (LRFD) method with capacities for the EDR calculated using the expected yield strengths. Columns on lines 2, 4, 7, 9 which are common to seismic frames in each direction are the only members that have EDR greater than unity. No damage was observed in these columns. These columns had to resist biaxial moments, driving up the calculated demands. EDR calculations in time history analysis are inherently conservative. This is due to the fact that in using EDR formulas, the maximum actions (i.e., flexure or axial load) throughout the time history response are used while it is obvious that such maximums do not necessarily concurrent in time. The greater the number of actions combined to calculate EDR, the more exaggerated this conservativeness may become. That is why, calculated EDR for columns subjected to biaxial bending may be larger than other columns not because of higher actual demand but due to the bias in the conventional way EDR is calculated. For this reason, we also use a second damage indicator, Demand-Capacity Ratio (DCR). This second indicator, although is unconservative because it does not consider flexure-axial load interaction, does not suffer from the EDR bias mentioned above. When considered together, EDR and DCR can effectively bound the actual demand ratio imposed on a member.

The damaged members had ratios below unity and not appreciably higher than the undamaged members. For example, the EDR corresponding to the severely damaged column (F-2 on the 16th floor) is 0.67 and the undamaged column (F-9 on the 16th floor) on the opposite side of the building had a ratio of 0.64. Furthermore, both of these ratios are well below the values commonly attributed to onset of significant plastic deformations. For Example, the Tri-services Manual [Department of Defense; 1986] considers EDR below 2.0 to be an indicator of essentially elastic behavior. The EDR are unable to predict, with any degree of certainty, damage to the Encino building. This is primarily due to premature failure of structural members at seismic demands significantly lower than what was predicted by design assumptions. None of the demand capacity ratios exceeded unity, which is another indicator that if members had performed as expected no damages should have occurred. This, obviously, contradicts the actual state of the building after the Northridge earthquake.

UBC-97 analyses indicated that the building satisfied UBC-97 strength requirements but failed the code drift requirements at the upper 15 floors. The building also passed UBC-97 panel zone thickness requirements and continuity plate requirements. Strong column weak girder provision was satisfied everywhere except at the roof.

FEMA-273 push-over analysis predictions where in close agreement with the results of dynamic time history analyses. As with the time history analysis, this method was unable to pin-point the exact location of damaged joints. In our opinion, this is not a weakness of the method but the premature failure of the joints which was responsible for the lack of coherency. The FEMA-273 push-over curves identifying the demand and capacity curves, BSE-1 and BSE-2 target displacements, as well as the base shear and displacements observed during the Northridge earthquake are shown in Figures 12 and 13.

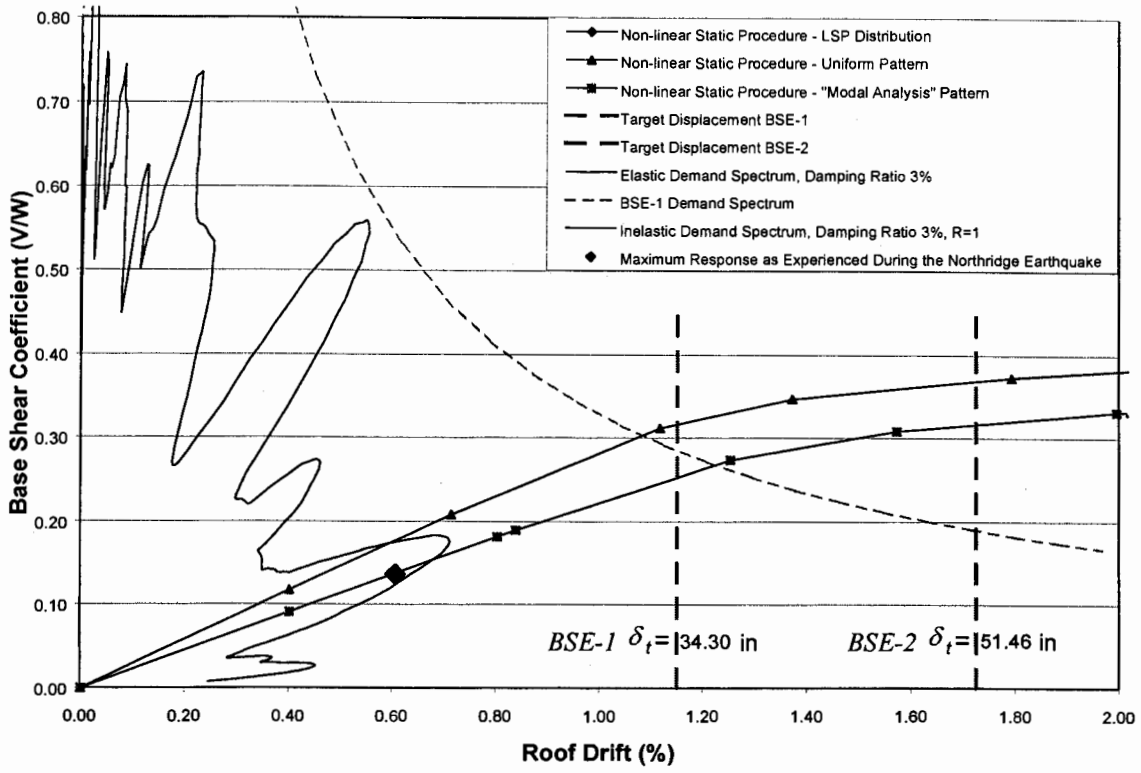

Figure 12. Demand-Capacity Spectrum for the North-South Direction of the Encino Building.

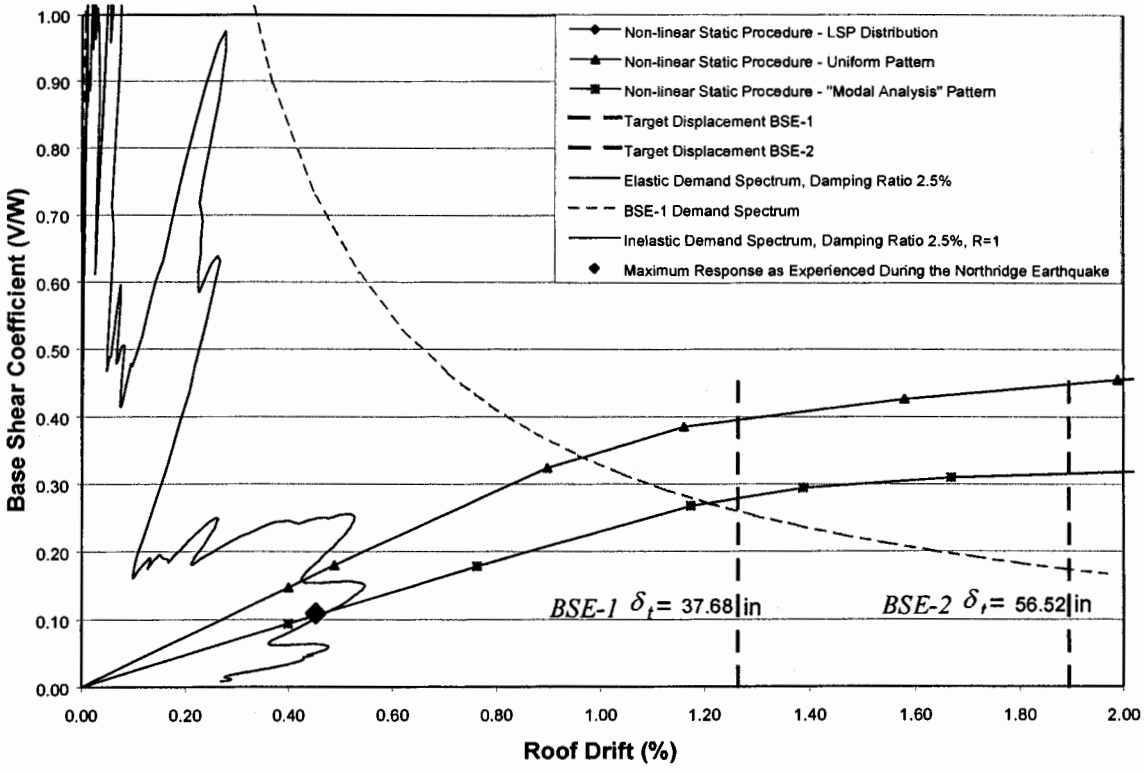

Figure 13. Demand-Capacity Spectrum for the East-West Direction of the Encino Building.

THE TARZANA BUILDING

The lateral resisting system of this ten-story Steel Moment Resisting Frame (SMRF) office building consists of three moment resisting frames in the North-South direction and six in the East-West direction. All beam-column connections in the building are moment resisting. The column spacings are 30 ft. on center. The floor plan of the lateral resisting system and the column orientations are shown in Figure 14. The first floor height is 16 ft. The remaining stories are 13 feet tall. The columns typically have continuity plates, but no doubler plates and use typical pre-Northridge rigid connections. The beams are made of A36 structural steel and columns are Grade A572 (Grade 50). The floor system consists of a 6¼" thick composite metal deck (a 3", 24-gauge metal deck, overlaid by 3¼" lightweight concrete).

The seismic sensors for this building are located at the base, the fifth floor, and the roof. The exact locations of the sensors were not identified. This did not prove to be a major issue in our investigation of this building. A sketch of the computer model of this building identifying the locations of discovered damages is shown in Figure 14.

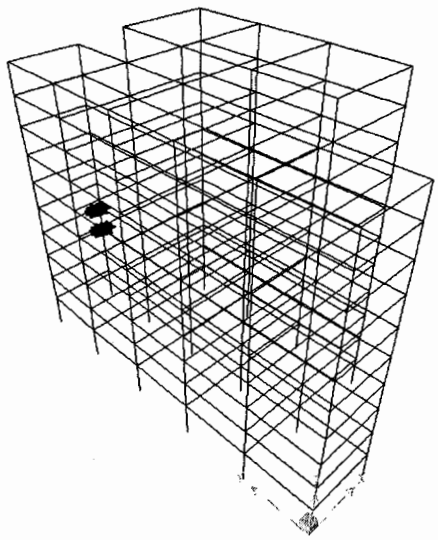

Figure 14. Computer Model of the Tarzana Building with Damaged Joints Identified.

The recorded response of this building indicated noticeable inelasticity. Therefore, our best-fit model for this building is a nonlinear model with hysteretic degradation characteristics. The hysteretic model chosen for this study is the multi-linear model, similar to that referred to in previous versions of IDARC2D as the three-parameter model [Kunnath et. al. 1992]. The member capacity is defined by a moment-curvature envelope with positive and negative moment capacities equal to the plastic moment of the section. We set the post yield stiffness at 3% of the riginal elastic stiffness. The stiffness degradation used is severe (see Table 5) with the value of parameter α (Figure 15) set to 1.7 in the East-West model and 3.0 in the North-South model. No strength degradation ($\beta=0$) or slip ($\gamma=1$) is considered for the hysteretic parameters, because this best simulates the observed behavior. The best results were obtained by assuming no end-rigid zones in the East-West direction and fully rigid end zones in the North-South Direction. Rayleigh damping was used and the best fit model reported 3% damping in the East-West

direction and 7% in the North-South direction, respectively. The effective periods of vibration from the nonlinear analytical model are compared to those from data interpretations in Table 6. The recorded earthquake ground motions at the base of the building are shown in Figure 16. We created a separate computer model to investigate the effects of the vertical ground motion. In this model, we divided the floor slabs into individual panel elements with the masses assigned per unit volume. The individual floor slabs supported between frame grids were subdivided into a four by four grid system to ensure sufficient vertical degrees of freedom to capture the vertical effects of the ground motion. Our study showed that the change in the peak lateral displacements due to vertical effects to be insignificant. In fact, the time history responses using the vertical excitation were almost indistinguishable from the responses using only the horizontal excitations. There was a maximum increase of 6% in the Demand Capacity Ratio (DCR) of the beams at the mid-span, with an average difference of only 0.18%. At the beam-ends, there was only 2% difference in the DCR, with an average difference of 0.17%.

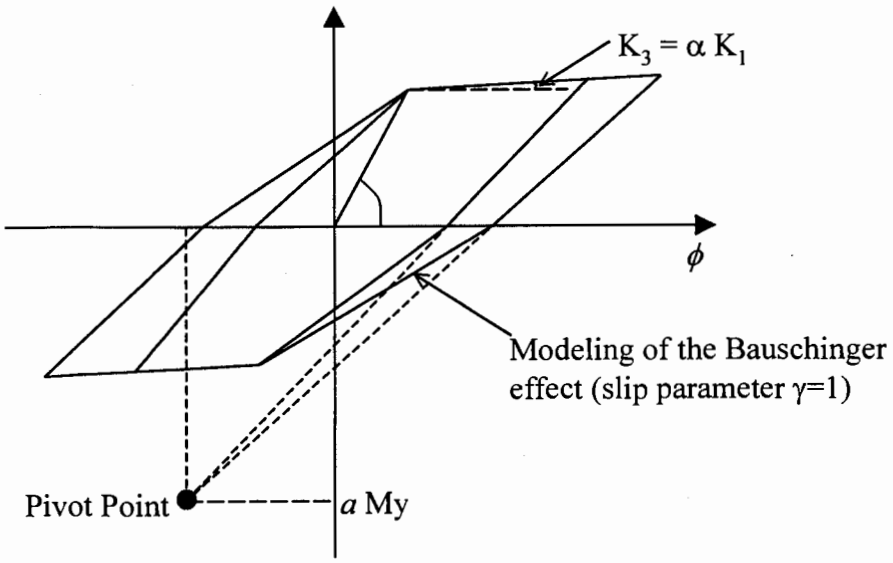

Figure 15. Hysteretic Model Used for this Study.

Table 5. Suggested Hysteretic Parameters for the Multi-linear Model.

PARAMETER	SLIGHT	MODERATE	SEVERE
Stiffness Degradation - α	2000	10	2
Strength Degradation - β	0.4	0.8	1.5
Slip - γ	$\cong$ 1	0.5	0.2

Table 6. Comparison of the Periods for Model 3 with the Periods from the Recorded Response for the Tarzana Building.

East-West				North-South			
Mode	**Vibration Periods (IDARC2D)** (*sec*)	**Vibration Periods (FFT Analysis)** (*sec*)	**Diff.** (%)	**Mode**	**Vibration Periods (IDARC2D)** (*sec*)	**Vibration Periods (FFT Analysis)** (*sec*)	**Diff.** (%)
1	2.349	2.272	3.24	1	2.153	2.222	3.11
2	0.796	0.833	4.48	2	0.721	0.75	3.87
3	0.458	0.602	1.07	3	0.412	Not identified	

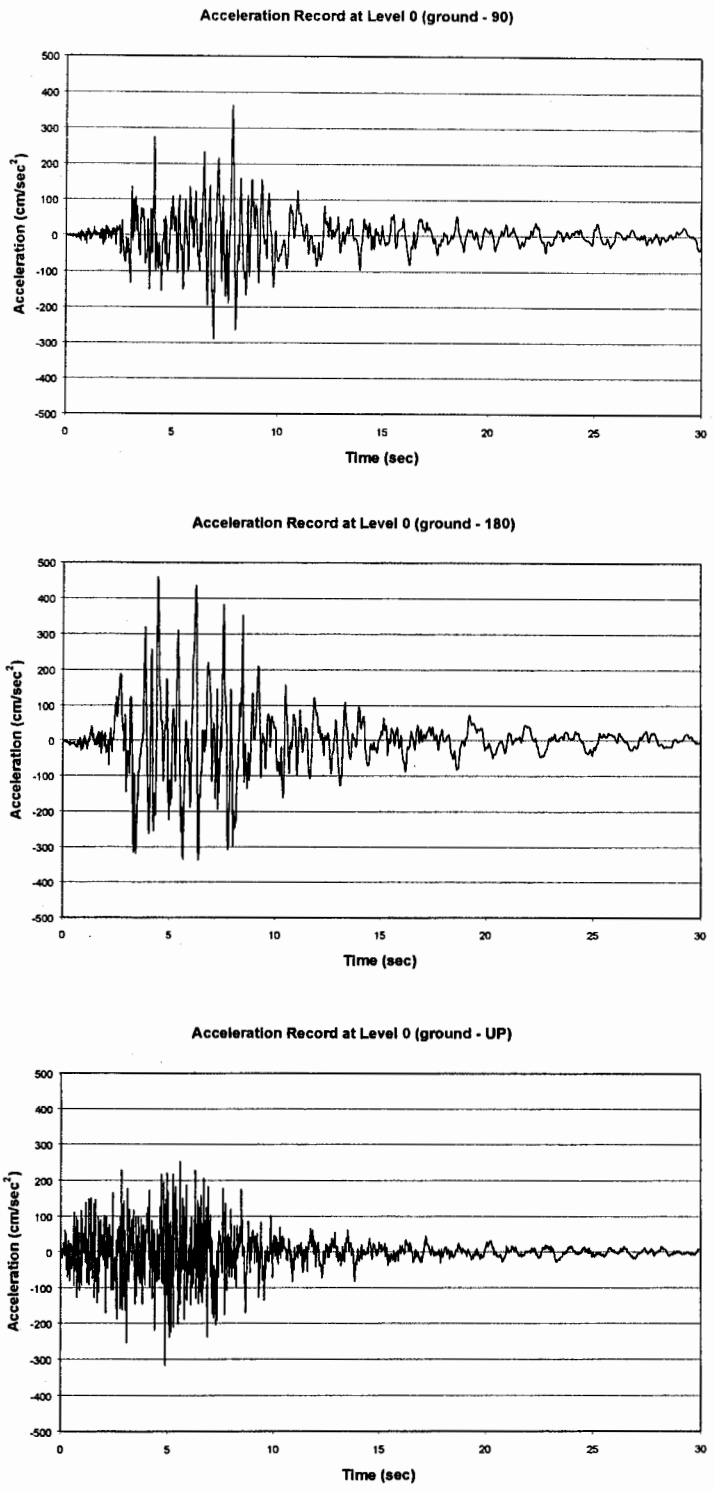

Figure 16. Recorded Northridge Ground Motions at the Base of the Tarzana Building.

The observations made with respect to reliability of EDR and DCR as well as UBC-97 analysis predictions apply equally as well to this building. All these procedures predict damage at locations where no damage occurred. Once again the FEMA-273 push-over analysis results provided a very accurate estimate of the overall response of the structure although the exact locations of the plastic hinges predicted by the push-over analyses did not correspond to the actual damage locations.

The nonlinear analytical response is compared to the observed response in Figure 17. The FEMA-273 push-over curves identifying the demand and capacity curves, BSE-1 and BSE-2 target displacements, as well as the base shear and displacements observed during the Northridge earthquake are shown in Figures 18 and 19.

The building passed the panel zone thickness, continuity plate, and strong column weak girder requirements of the UBC-97 code.

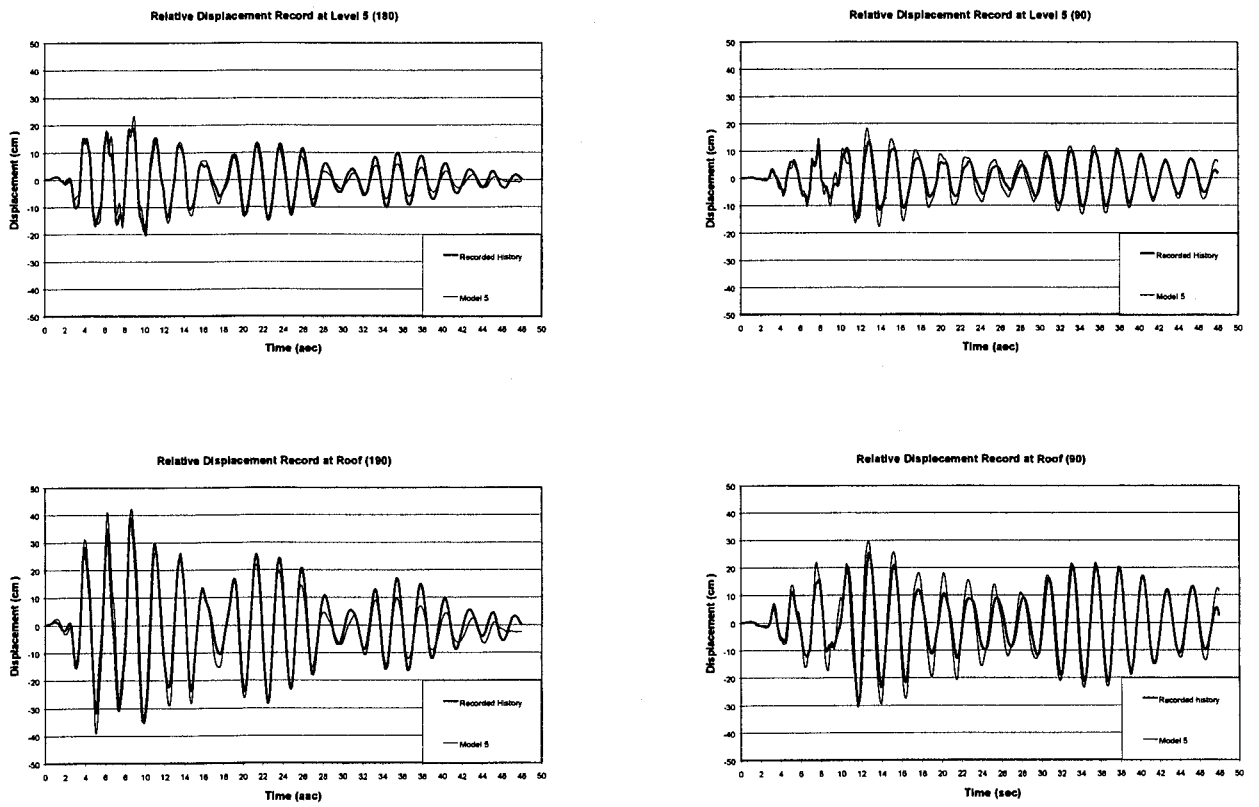

Figure 17. Displacement Time Histories from Northridge Earthquake for Model 3.

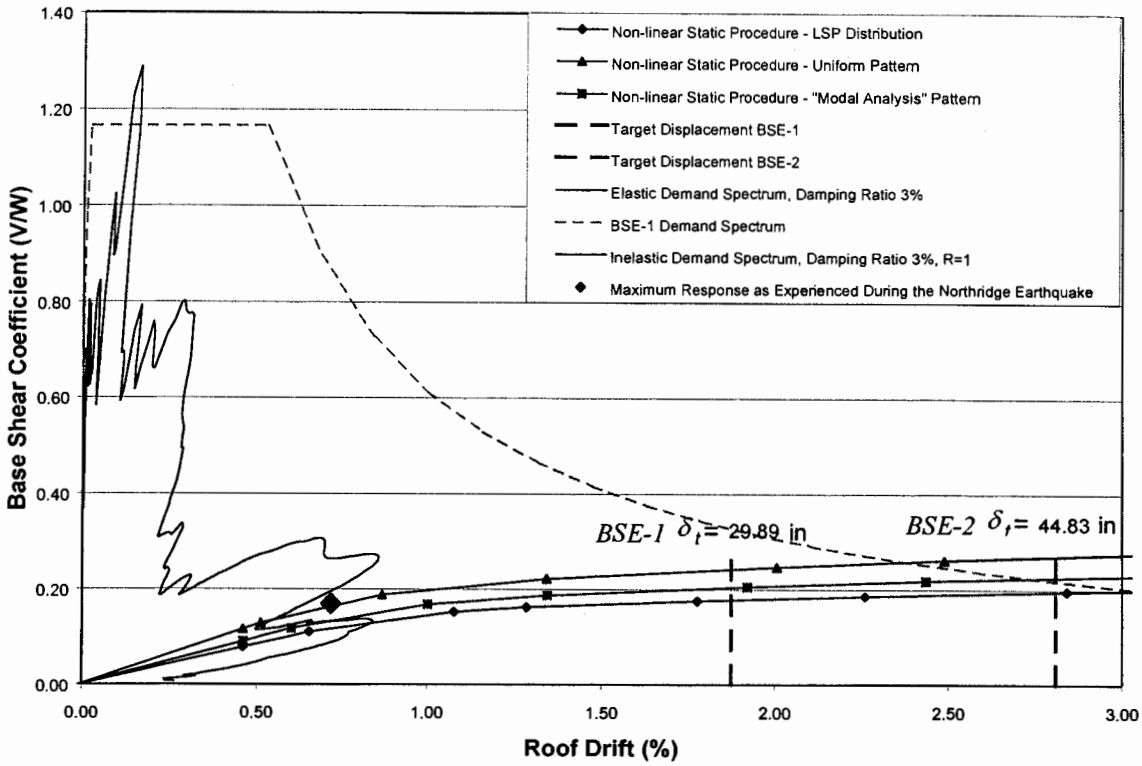

Figure 18. Demand-Capacity Spectra for the East-West Direction of the Tarzana Building.

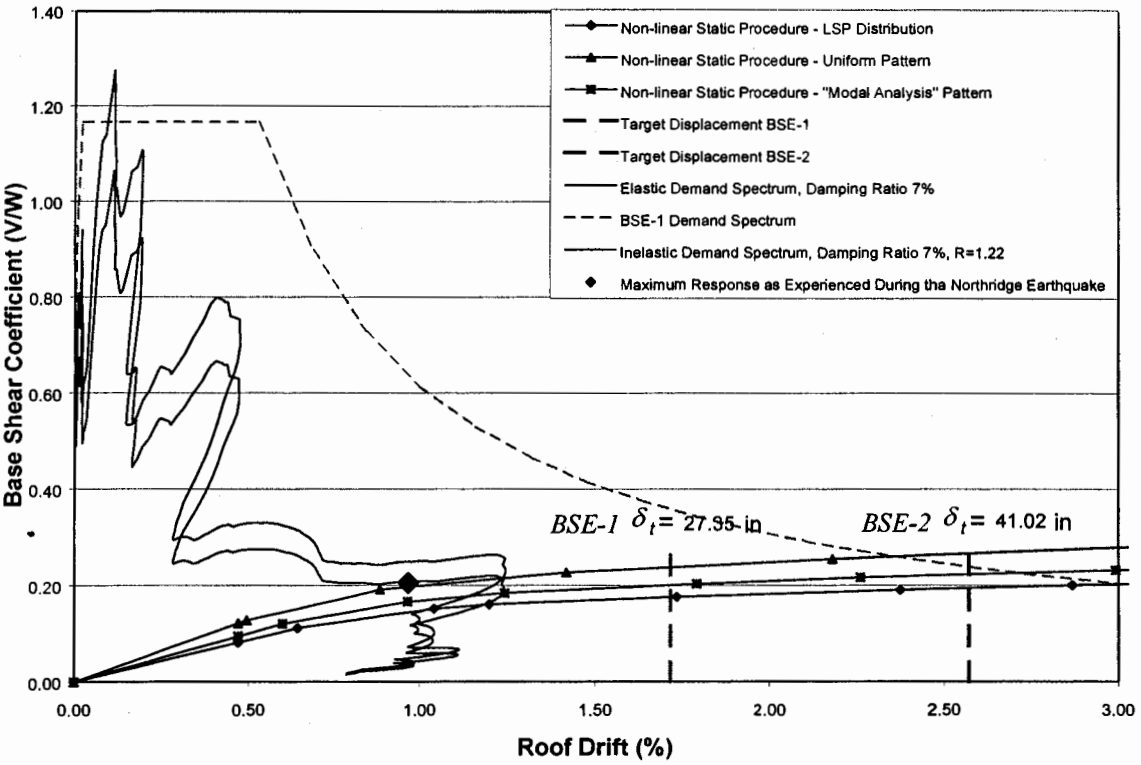

Figure 19. Demand-Capacity Spectra for the North-South Direction of the Tarzana Building.

THE NORTH HOLLYWOOD BUILDING

The lateral resisting system of this eight-story Steel Moment Resisting Frame (SMRF) office building consists of three moment resisting frames in the North-South direction and six in the East-West direction. It is rectangular in plan, with approximate plan dimensions of 71 ft. by 192 ft. The lateral resistance in the North-South direction is provided by four single bay moment resisting frames along the centerline. In the East-West direction, two bay moment resisting frames at the North and South edges of the building provide the lateral resistance.

The beam column connections are typical pre-Northridge SMRF connections. The structural steel used is either Grade A36 or Grade A572 (Grade 50) as specified on the structural plans. The floor system at all floors except the roof is composed of QL-99-20 steel deck overlaid with 3¼" lightweight concrete. The roof is a combination of a QL-99-20 steel deck overlaid with 3¼" lightweight concrete and a TUFCOR 24 GA. metal deck with 2¼'' zonolite. Seismic sensors are located at the base, the fifth floor and the roof. The exact locations of the sensors were not identified in the documentation we were able to obtain, but this proved not to be of a practical concern for this building.

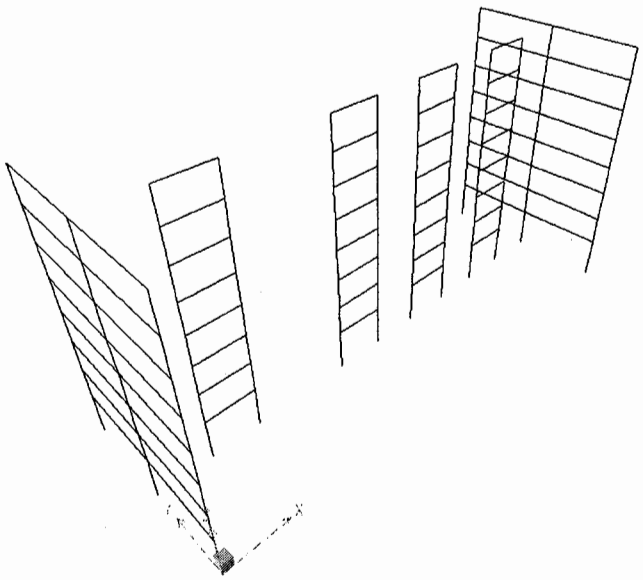

Figure 20. Three Dimensional Model of the North Hollywood Building.

The effectiveness of the beam-column rigid end zones for our best-fit model (*Model 3*) is calibrated at 80% of the full rigid zone length for the East-West direction frames and 85% for the North-South direction frames. The damping ratios used for the fundamental periods of *Model 3* were set at 5% for the East-West direction and 4% for the North-South direction. All higher modes are damped at 10% so that the contribution of the high frequency response in the acceleration time histories is not overstated. A summary of the modeling assumptions is presented in Table 7.

Table 7. Modeling Differences Between the Various Models for the North Hollywood Building.

Model	Rigid Zones	Analysis	Yield Stress (*ksi*)	Modal Damping
Model 1	All Elements	Elastic 3D	-	EW: 5% 1st, all others 10% damped NS: 4% 1st, all others 10% damped
Model 2	None	Elastic 3D	-	
Model 3	80 % EW 85% NS	Elastic 3D	-	

Model 3, has a fundamental period of 2.57 seconds in the East-West and 2.19 in the North-South direction. The natural periods of the building were also interpreted from the recorded response to the Northridge earthquake using the transfer functions of the story accelerations with respect to input base motion in the frequency domain . The periods calculated using this method match well with the periods obtained from the modal analysis for *Model 3* (see Table 8).

Table 8. Comparison of the Vibration Periods for Model 3 and the Periods Obtained from the Recorded Response Using the Fast Fourier Transform (FFT) Method.

East-West				North-South			
Mode	Vibration Periods (SAP2000) (*sec*)	Vibration Periods (FFT Analysis) (*sec*)	Diff. (%)	Mode	Vibration Periods (SAP2000) (*sec*)	Vibration Periods (FFT Analysis) (*sec*)	Diff. (%)
1	2.565	2.6	1.3	2	2.189	2.111	3.6
4	1.028	1.039	1.1	5	0.746	0.771	3.2
7	0.583	0.540	7.3	8	0.412	Not Identified	

The earthquake ground motions recorded at the base of the building during the 1994 Northridge earthquake are shown in Figure 21. The results for the best-fit model (*Model 3*) are compared to the recorded response if Figures 22 and 23. The time history signatures closely follow the recorded responses. Therefore, its appears that there was little inelasticity in the North Hollywood building and its behavior was essentially elastic during the Northridge earthquake.

There are 92 moment resisting frame connections in the North Hollywood building, 64 of which are in the North-South and 28 in the East-West direction. This building was inspected for damage after the earthquake with 11 connections tested in the North-South direction and 6 in the East-West direction using visual and ultrasonic examination. The inspection results showed no detectable defects or damage caused by the earthquake. Essentially similar conclusion may be drawn from the displacement responses obtained by our best-fit elastic model which coincides with the real recordings. The observations made with respect to reliability of EDR and DCR as well as UBC-97 analysis predictions apply equally as well to this building. All these procedures predict damage at locations where no damage occurred. Once again the FEMA-273 push-over analysis results provided a very accurate estimate of the overall response of the structure although the exact locations of the plastic hinges predicted by the push-over analyses did not correspond to the actual damage locations. The FEMA-273 push-over curves identifying the demand and capacity curves, BSE-1 and BSE-2 target displacements, as well as the base shear and displacements observed during the Northridge earthquake are shown in Figures 24 and 25.

A summary of analytical indicators of this building's response is presented in Table 9.

Table 9. Summary of the North Hollywood Building Analysis.

	Northridge Earthquake		
	Observed Damage?	**Elastic Demand Ratios (Model 3)**	**Design/Capacity Ratios (Model 3)**
Remarks	**No** –Elastic Response--	Ratios >1 in Beams and Columns	Ratios >1 in Beam and Column Structural Elements

	UBC-97					
				Special Provisions		
	EDR	**Drift Limits**	**Redundancy Factors**	**Panel zones**	**Continuity Plates**	**Column-Beam Moment Ratios**
Compliance	**No** EDR>1 in Several Elements	**No** Limit Exceeded at all Levels	**>1.25** Exceed Code Limitations	**OK**	**OK** Provided where needed	**No** Failed to pass the test on the top 2 floors

	FEMA-273		
	Life Safety-BSE-1	**Collapse Prevention-BSE-2**	**Demand-Capacity Spectra**
Compliance	**OK**	Failed in East West Direction	Elastic Behavior.

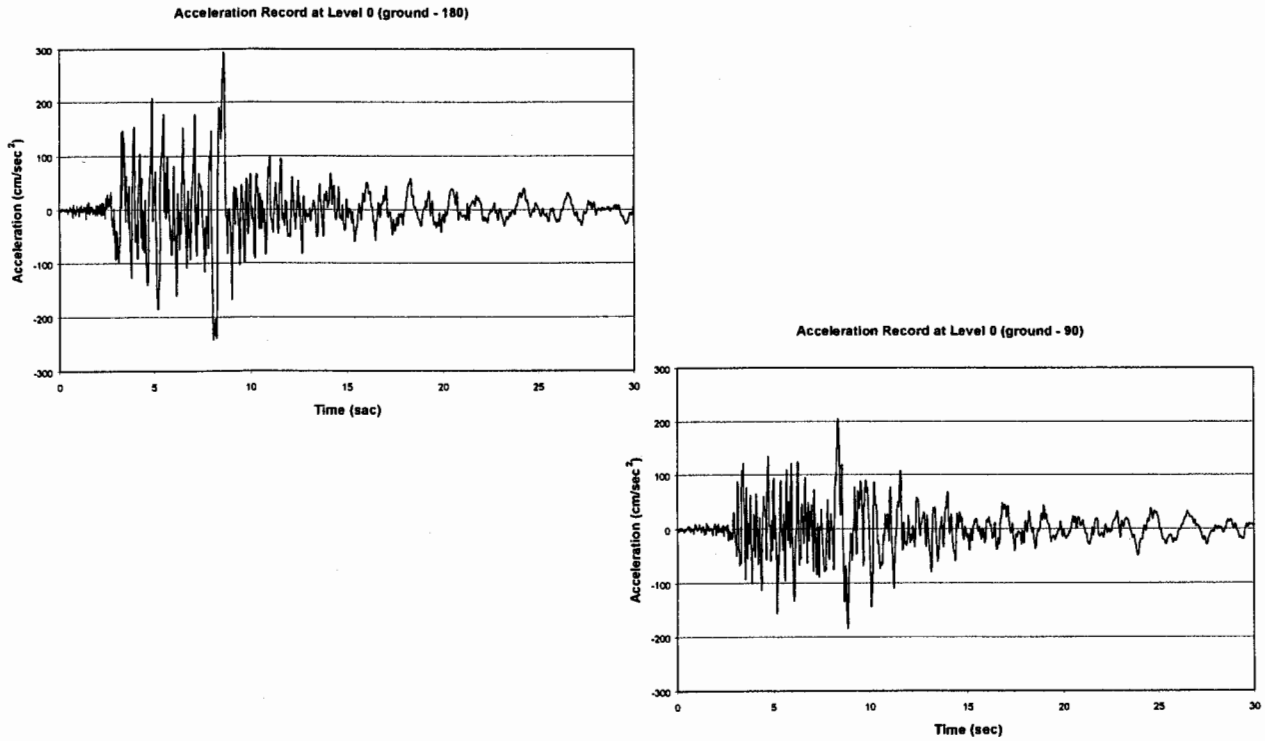

Figure 21. Recorded Northridge Ground Motions at the Base of the North Hollywood Building.

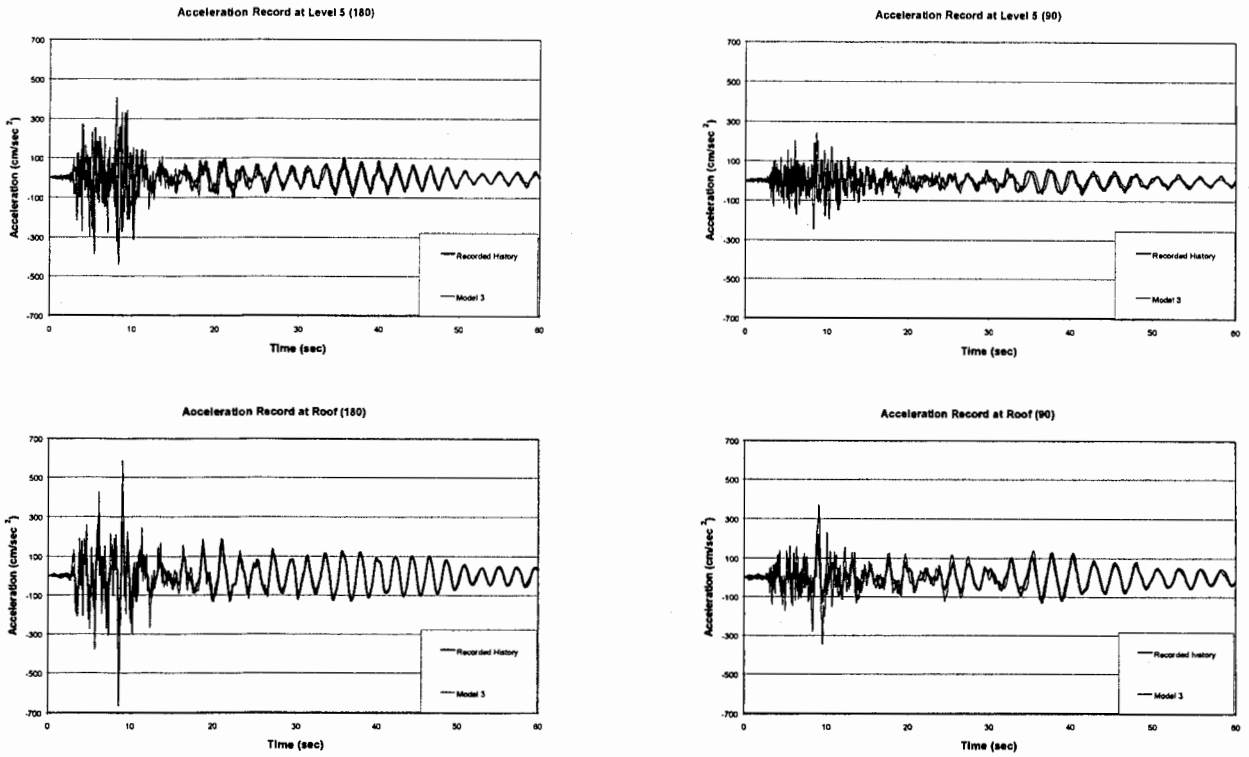

Figure 22. Acceleration Time Histories from Northridge Earthquake for Model 3.

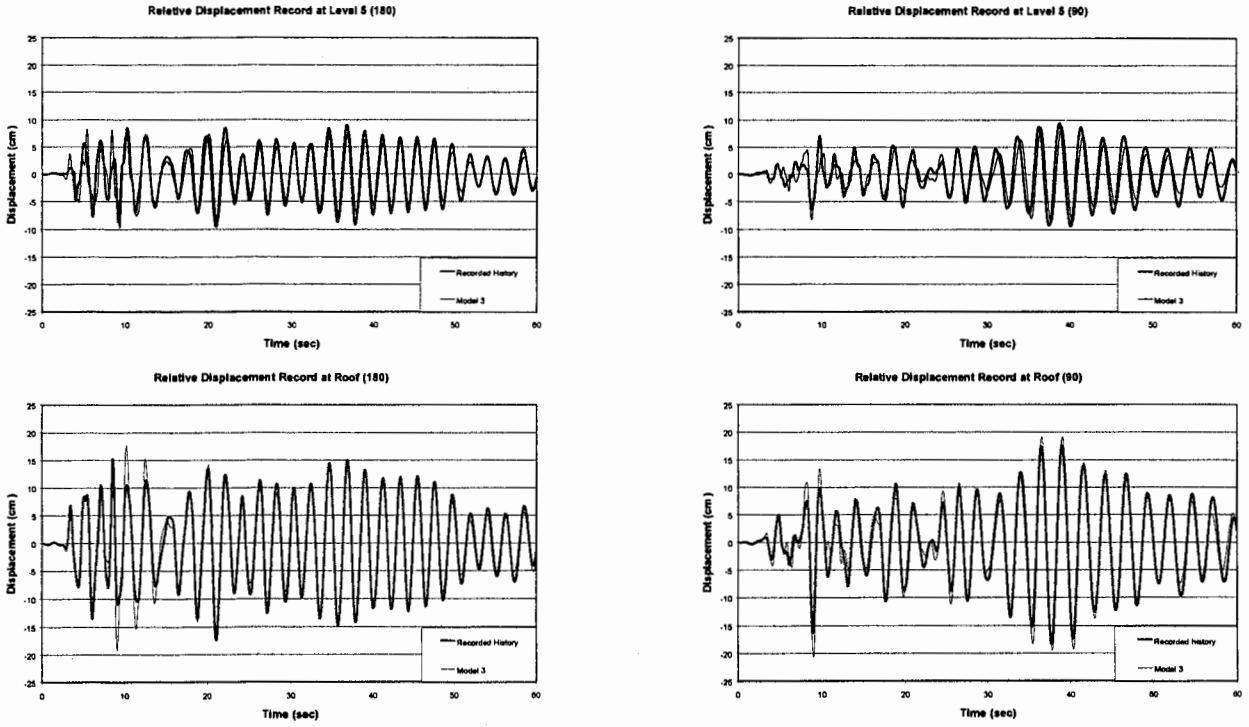

Figure 23. Displacement Time Histories from Northridge Earthquake for Model 3.

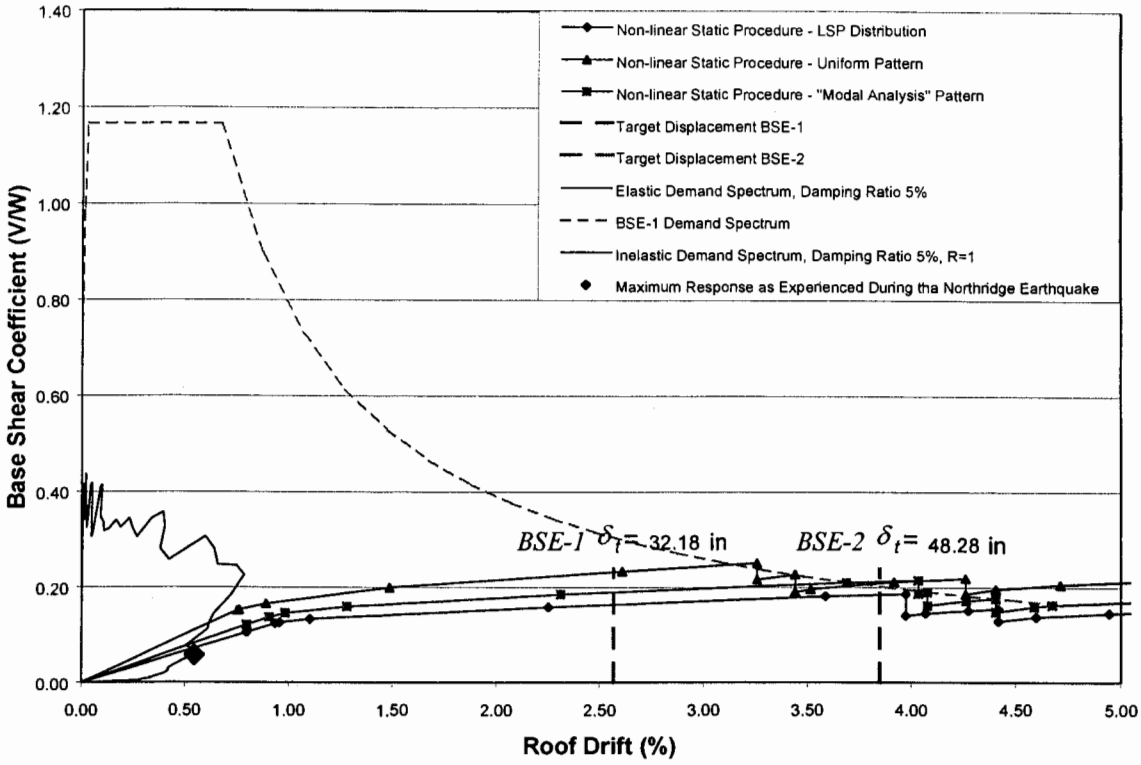

Figure 24. Demand-Capacity Spectra for the East-West Direction.

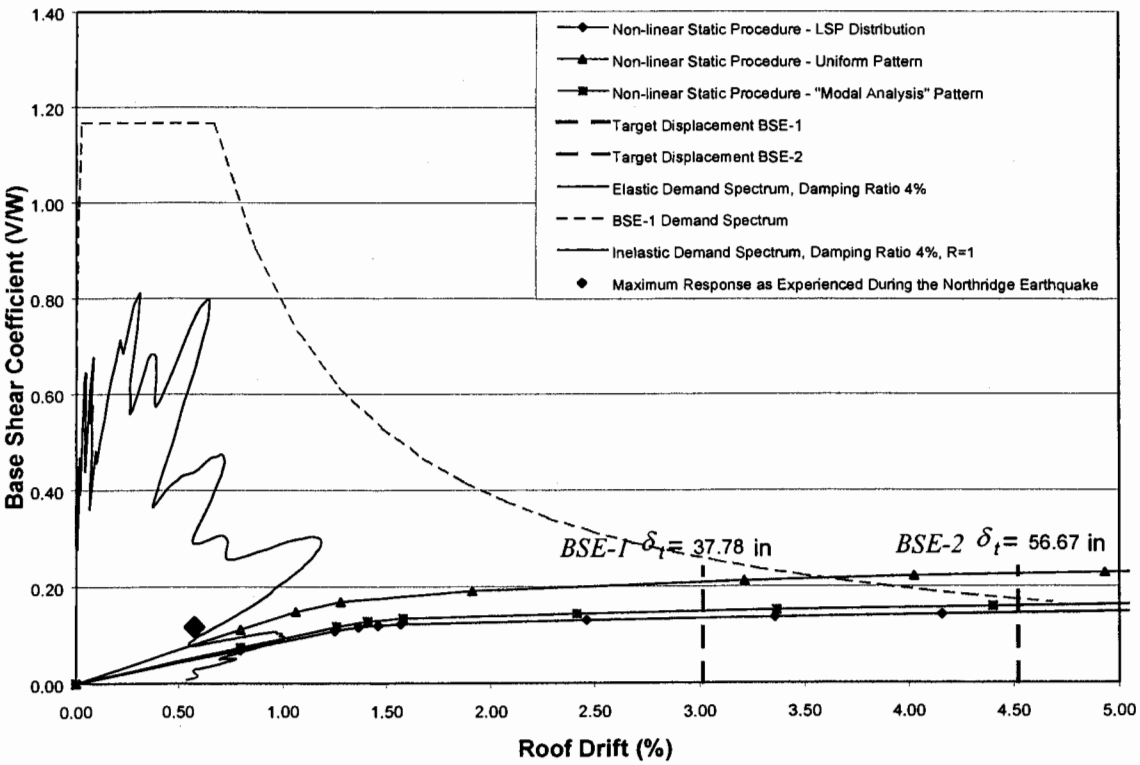

Figure 25. Demand-Capacity Spectra for the North-South Direction.

THE SHERMAN OAKS BUILDING

This is a sixteen-story Steel Moment Resisting Frame (SMRF) office building. It is rectangular in plan, with approximate plan dimensions of 129 ft. by 152 ft. The lateral resisting system of the structure consists of two pairs of identical multiple bay moment resisting frames along the perimeter of the building, in the North-South and the East-West directions with typical pre-Northridge rigid connections. The structural steel is either Grade A36 or Grade A572 (Grade 50) as specified on the construction drawings. The floor system at all floors except the roof is composed of QL-3-20 GA 1½" steel deck overlaid with 2½" lightweight concrete. For the roof, a QL-3-18 GA 1½" steel deck overlaid with 4½" lightweight concrete was used. Seismic sensors are located at the base, the eighth floor and the roof. The exact locations of the sensors were not identified, but surprisingly this proved not to be a practical concern for this building. A view of the computer model for this building is shown in Figure 26.

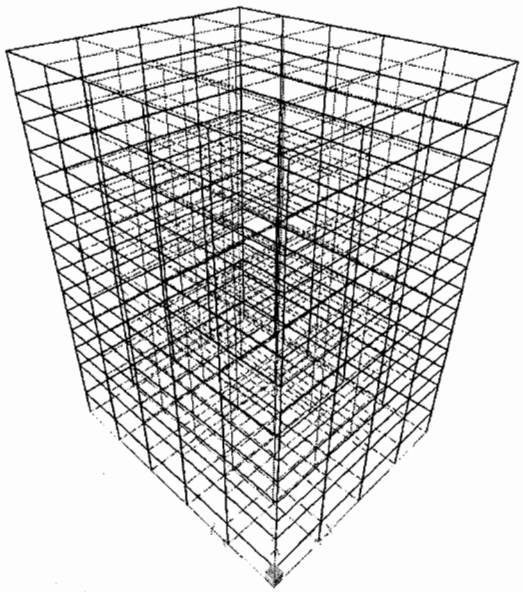

Figure 26. Three Dimensional Model of the Sherman Oaks Building.

The effectiveness of the rigid zones for the best fit model (*Model 3*) is 80% of the full rigid zone length for the East-West direction frames and 34% for the North-South direction frames. The damping ratios used for the first two modes of *Model 3* in the East-West direction were set at 2% and 3% and in the North-South direction at 1% and 3%. All higher modes were damped at 6%, so that the contribution of the high frequency response in the acceleration time histories is not exaggerated. A summary of the modeling differences between the models is presented in Table 10.

Table 10. Modeling Differences Between the Various Models.

Model	Rigid Zones	Analysis	Yield Stress (*ksi*)	Modal Damping
Model 1	All Elements	Elastic 3D	-	1%EW, 2% NS
Model 2	None	Elastic 3D	-	1%EW, 2% NS
Model 3	80 % EW 34% NS	Elastic 3D	-	EW: 2% 1st, 3% 2nd, 6% all others NS: 1% 1st, 3% 2nd, 6% all others

The vibration periods obtained from data interpretation are compared to those obtained by analysis in Table 11. The earthquake ground motions recorded at the base of the building are presented in Figure 27.

Table 11. Comparison of the Vibration Periods for Model 3 and the Periods Obtained from the Recorded Response Using the Fast Fourier Transform (FFT) Method.

North-South				East-West			
Mode	Vibration Periods (SAP2000) (*sec*)	Vibration Periods (FFT Analysis) (*sec*)	Diff. (%)	Mode	Vibration Periods (SAP2000) (*sec*)	Vibration Periods (FFT Analysis) (*sec*)	Diff. (%)
1	3.610	3.55	1.8	2	3.267	3.0	9.0
4	1.234	1.13	9.2	5	1.104	1.083	1.9
7	0.689	0.66	4.2	8	0.629	0.66	5.1

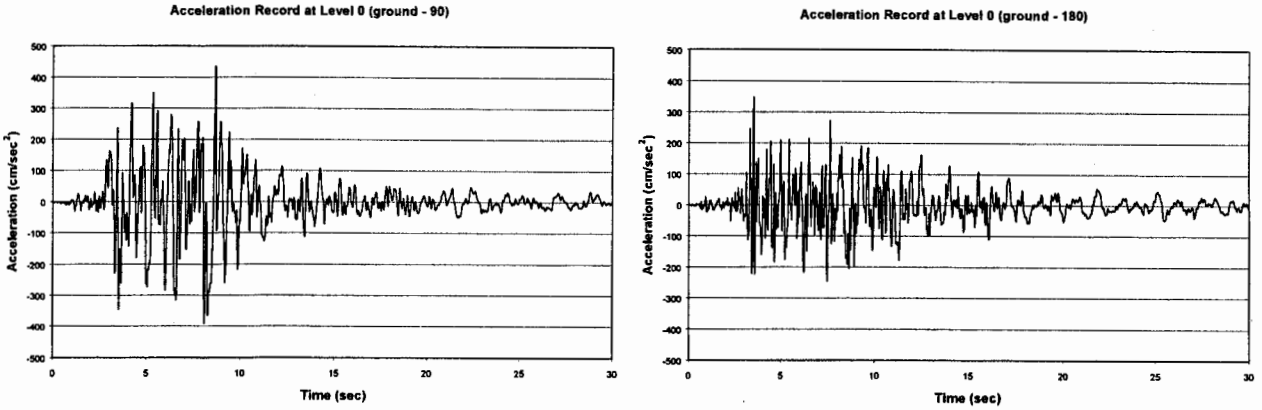

Figure 27. Recorded Northridge Ground Motions at the Base of the Sherman Oaks Building.

Details of performance analyses of this building may be found in our report to CSMIP [Naeim and others, 1999]. In this paper, however, we concentrate on what seems to be a clear case of resonant building response and possibly the first such response ever reported for a building in southern California.

The only difference between our various elastic analytical models for this building was the percentage of effectiveness assigned to beam-column end zones. In the case of this building, such an adjustment not only made the anticipated differences in the vibration periods, but made a huge difference in the amplitude of the observed response.

The response for Model 1 (Figure 28) shows that from the initial portion of the response the actual structure is more flexible than that predicted by this model. The response at the latter half does not come anywhere close to the actual response either because of resonant response not being captured. The response for *Model 2* (see Figure 29) shows that this model is unable to capture the response in the latter portion of the analysis, even though the initial portion seems to follow closely the initial response. The response for Model 3 (Figure 30), however, clearly matches the observed response showing that this building behaved in an essentially elastic manner during the Northridge earthquake.

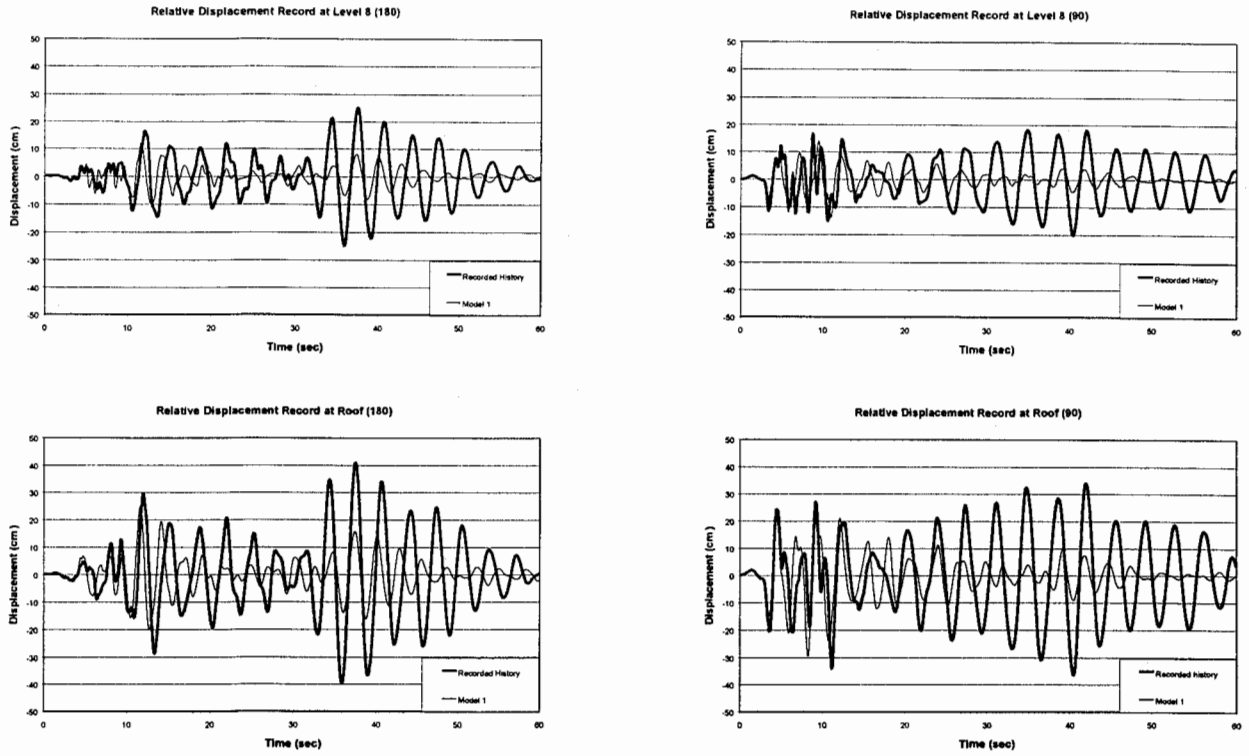

Figure 28. Displacement Time Histories from Northridge Earthquake for Model 1.

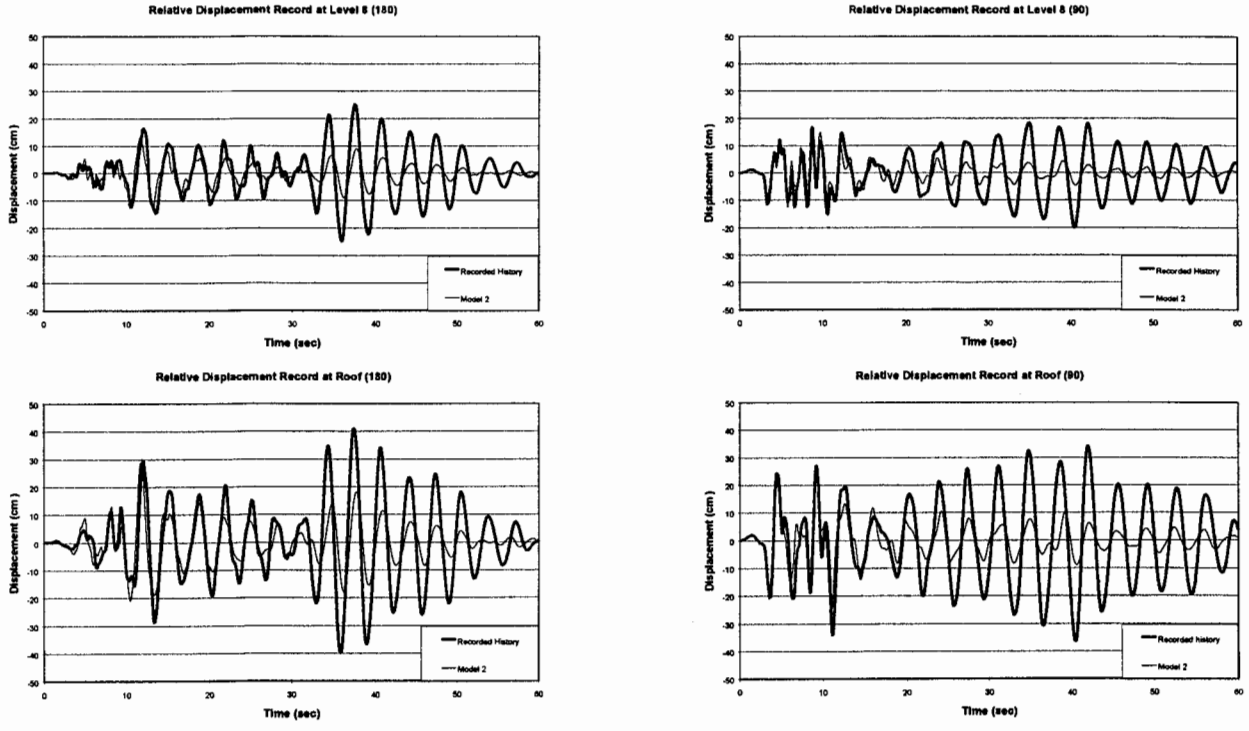

Figure 29. Displacement Time Histories from Northridge Earthquake for Model 2.

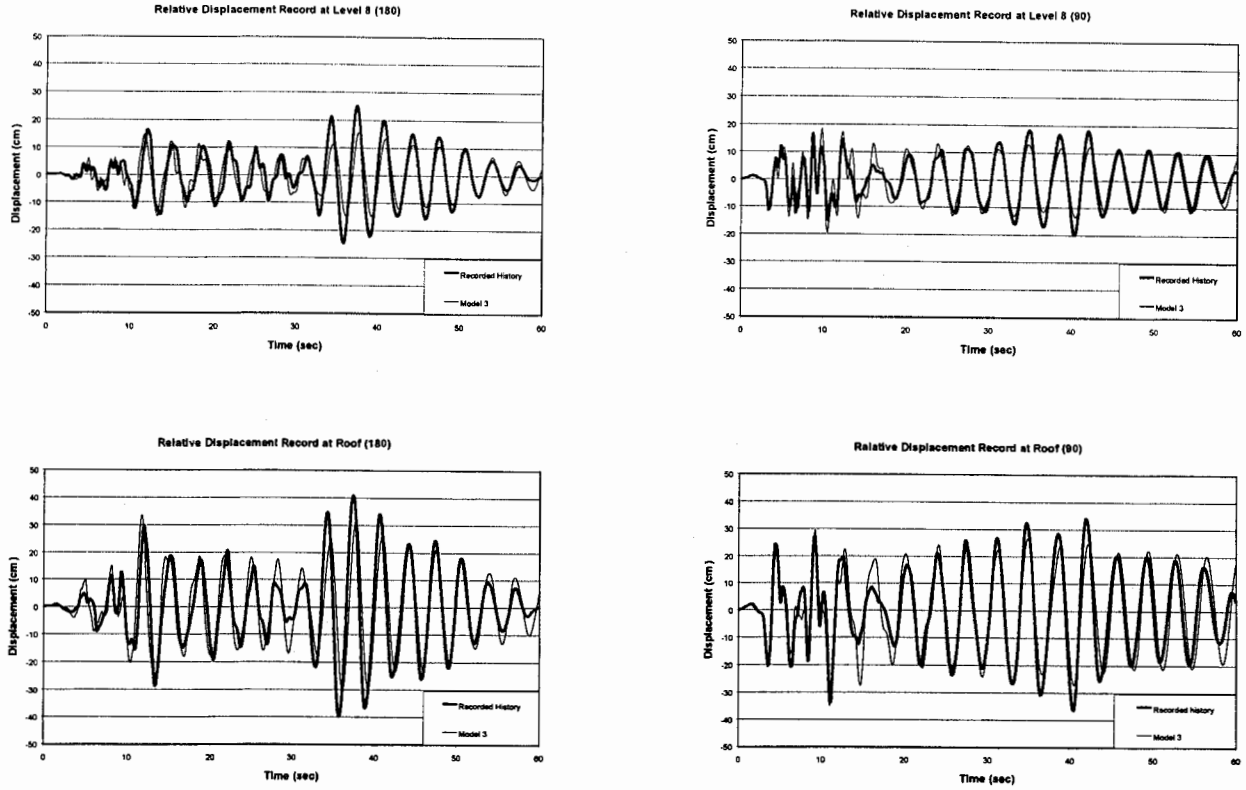

Figure 30. Displacement Time Histories from Northridge Earthquake for Model 3.

CONCLUSIONS

We have studied the seismic performance of four instrumented steel moment resisting buildings during the 1994 Northridge earthquake. These commercial buildings ranged from 8 stories to 20 stories in height and all had rectangular and regular plans, although two had elevation irregularities. The buildings were instrumented at the ground floor, a floor near the mid-height, and at the roof. For three of the four buildings the precise location of the instruments in plan was not known. However, due to insignificant contribution of torsion to seismic response of these buildings, that did not prevent us from being able to effectively and accurately match the observed response by analytical means. Furthermore, the sensors at various floors were not linked to a common timer and therefore the timing of their recordings were not synchronized. Although it was initially expected that the phase lag present between the roof records and the base may present some problems in matching the analytical and recorded responses, lack of synchronization proved not to be a significant issue.

Among the four buildings evaluated in this study, the Tarzana building experienced the most severe horizontal and vertical ground motion at the base. Therefore, the effects of vertical accelerations on seismic performance of this building were evaluated and proved to be insignificant.

Gravity framing has been known to have some participation in the seismic response. For the buildings investigated in this report, however, the observed response could be matched

analytically both in terms of frequency content and response amplitude without the need for explicit modeling of the gravity frames. This was achieved simply by adjusting the effective width of the beam and column panel zones and using appropriate modal damping ratios.

One of the buildings located in Sherman Oaks exhibited strong evidence of resonant behavior as a result of the long-period content of the base motion which was close to the fundamental period of the building. To our knowledge, this is the first time that resonant behavior of a building in response to a southern California earthquake has been documented and reported.

We performed linear and nonlinear, static and dynamic analyses of these buildings and compared the design details and performance with those suggested or anticipated by the provisions of the UBC-97 code and FEMA-273 guidelines. Generally speaking, the nonlinear static procedure as suggested by the FEMA-273 guidelines provided the most accurate reflection of the observed response. This is true even for the 20 story building which had significant higher mode participation. Due to the conservative nature of the prevailing methods of calculating elastic demand ratios (EDR) in time history analysis, as explained previously in this report, time history analysis overestimated the seismic demand imposed on beams and columns and was not as good as the pushover-method in predicting the state of individual elements. This is true in spite of the fact that the time history displacement response of our calibrated models matched the observed response very closely.

It is fair to say that none of the methods utilized were accurate enough in pin-pointing the exact locations of the observed damage. More research is needed to overcome this shortcoming which has been reported by many investigators [see Naeim and others 1995, 1997].

The UBC-97 methodology consistently underestimated the force demand and significantly over-estimated the drift demands. Underestimating the force demand by UBC-97 is understandable in the light of the code reduction factor and expectation of nonlinear behavior where most of these buildings remained essentially elastic in spite of damage to some joints. UBC's overestimating of the demand may require a revision of the code drift demand provisions since they do not seem realistic.

ACKNOWLEDGEMENTS

The authors wish to express their gratitude to the following individuals and organizations:

- California Strong Motion Instrumentation Program (CSMIP) for funding this research and its staff particularly Dr. Anthony Shakal and Dr. Moh Huang for their assistance and valuable advice.
- John A. Martin and Associates, Inc., for supplementing the project budget with providing substantial additional funding.
- The distinguished members of the project advisory committee: Mr. Chris Poland (Chair), Dr. Ken Honda, Dr. Charles Kircher, and Mr. Donald Jephcot for their constructive suggestions during the course of this investigation.

Structural engineering teams who conducted post-earthquake investigations and repair of the four buildings studied in this project and graciously shared their knowledge of the buildings, as well as, the as-built and repair drawings with the project team. They are:

- Kariotis & Associates Structural Engineers, for the Encino building
- Englekirk and Sabol Consulting Structural Engineers, for the Sherman Oaks building
- Myers Nelson Houghton Inc., for the North Hollywood building
- John A. Martin and Associates Inc., for the Tarzana building

The Contents of this report were developed under Contract No. 1097-607 from the California Department of Conservation, Division of Mines and Geology, Strong Motion Instrumentation Program. However, these contents do not necessarily represent the policy of that agency nor endorsement by the State Government.

REFERENCES

1. International Conference of Building Officials (1997), *1997 Uniform Building Code*, ICBO, Volume 2, Whittier, California.
2. NEHRP (1997), *NEHRP Guidelines for the Seismic Rehabilitation of Buildings*, FEMA Publication 273, Washington D.C.
3. SAC Joint Venture (1995), *Interim Guidelines: Evaluation, Repair, Modification and Design of Welded Steel Moment Frame Structures,* FEMA Publication 267, Sacramento, California.
4. Computers and Structures (1997), SAP 2000 Integrated Finite Element and Design of Structures, Berkeley, California.
5. Naeim, F., Lobo, R. F., Battelle, G., Lee, H. (1998), *JAMA SDS/Floor Mass, Mass Moment of Inertia and CG Calculation Subsystem*, Report of John A. Martin & Associates, Los Angeles, California.
6. American Institute of Steel Construction, *Load & Resistance Factor Design*, 1995
7. Applied Technology Council, ATC 40 (1996), *Seismic Evaluation and Retrofit of Concrete Buildings*,
8. Reinhorn, A. M. (1996), "Introduction to Dynamic and Static Inelastic Analysis Techniques," Los Angeles Tall Buildings Structural Design Council.
9. Krawinkler, H., Nasser, A. A. (1992), "Seismic Design Based on Ductility and Cumulative Damage Demand and Capacities," *Nonlinear Seismic Analysis and Design of Retrofit Concrete Buildings,* Elsevier Science Publishers Ltd., New York, New York, 23-40
10. Departments of the Army, the Navy, and the Air Force (1986), *Technical Manual, Seismic Design for Buildings,* Washington D.C.
11. American Institute of Steel Construction (1997), *Seismic Provisions for Structural Steel Buildings,* Chicago, Illinois.
12. Naeim F., Di Julio, Roger Jr., Benuska Kalman, Reinhorn, A. M., Li, C. (1995), *Evaluation of the Seismic Performance of an Eleven Story Steel Moment Frame Building during the 1994 Northridge Earthquake,* Report No. SAC 95-04 Part II, SAC Joint Venture.
13. Valles-Matrox, R. E., Reinhorn, A. M., Kunnath, S. K., Li, C., Madan, A. (1996), *IDARC2D version 4.0: A Computer Program for the Inelastic Damage Analysis of Buildings,* Report No. NCEER-96-0010, NCEER Technical Report, State University of New York at Buffalo, Buffalo, New York.

EVALUATION OF SOIL-STRUCTURE INTERACTION EFFECTS FROM STRONG MOTION RECORDINGS

J. P. Stewart
Department of Civil & Environmental Engineering
University of California, Los Angeles

ABSTRACT

This paper reviews the results of recent studies that have investigated the effects of soil-structure interaction (SSI) on the seismic response of building structures using recorded strong motions. Two manifestations of SSI are described: (1) inertial interaction effects on the effective first-mode period and damping ratio of buildings, and (2) variations between foundation-level and free-field ground motions. Inertial interaction effects are seen to increase with the ratio of soil-to-structure stiffness, and are reasonably well predicted with simplified analytical formulations similar to those in the NEHRP Provisions (BSSC, 1997). Ground motions in structures are seen to generally be less than free-field motions. Foundation embedment and frequency are shown to significantly affect the variations between these motions.

INTRODUCTION

Documentation of seismic case history data is a critically important step towards understanding and reliably characterizing complex problems in geotechnical earthquake engineering. Few empirical studies of soil-structure interaction (SSI) have been previously performed, although the literature on analytical procedures for SSI is extensive.

This paper is a summary of some previous and ongoing work at UCLA that is seeking to document SSI effects from strong motion recordings. The paper is divided into two main sections. The first section reviews inertial interaction effects on structural response. These effects are quantified in terms of the ratio of flexible- to fixed-base first mode period $\tilde{T}/T$ and foundation damping factor $\tilde{\zeta}_0 = \tilde{\zeta} - \zeta/(\tilde{T}/T)^3$, where ζ and $\tilde{\zeta}$ = fixed- and flexible-base first mode damping ratio, respectively. The subject of the second section is foundation/free-field ground motion variations that result from kinematic interaction (embedment, base-slab averaging) and inertial interaction.

INERTIAL INTERACTION EFFECTS ON FIRST-MODE VIBRATION PARAMETERS

Evaluation of Modal Parameters from Strong Motions Recordings

Three cases of base fixity are of interest in analyses of SSI: (1) fixed-base, representing only the flexibility of the structure, (2) flexible-base, representing the combined flexibility of the

complete soil-structure system, and (3) pseudo flexible-base, representing flexibility in the structure and rocking in the foundation. Pseudo flexible-base parameters are of interest because they can sometimes be used to approximate flexible-base parameters or to estimate either fixed- or flexible-base parameters.

Stewart and Fenves (1998) evaluated the types of input and output strong motion recordings that should be used in system identification analyses to evaluate fixed-, flexible- and pseudo flexible-base vibration parameters of structures. While roof translations are always used as output, the input motions for various base fixity conditions vary as indicated in Fig. 1. Recordings of free-field, foundation, and roof-level translations, as well as base rocking, are needed to evaluate directly both fixed- and flexible-base modal parameters of a structure. The system identification procedures used to evaluate modal parameters for a given input and output are described by Stewart and Fenves (1998).

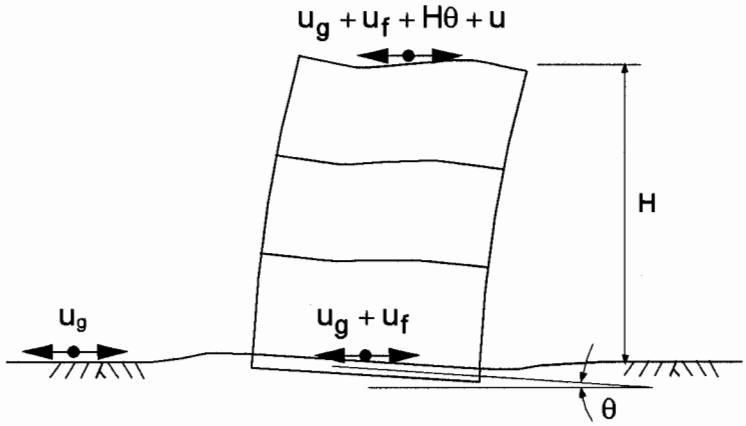

Fig. 1: Input and output motions for system identification

Instrumented building sites often lack sensors for recording base rocking or free-field translations. For such cases either fixed-base parameters (missing base rocking) or flexible-base parameters (missing free-field translations) cannot be evaluated directly from system identification analyses. Stewart and Fenves (1998) derived expressions to estimate either flexible- or fixed-base parameters using "known" modal parameters for the two other cases of base fixity. The estimation procedures operate on the premise that differences between known parameters can be used to calibrate the foundation impedance at the structure's period; the calibrated impedance can then be used to estimate the unknown parameters. These estimation procedures extend significantly the number of sites for which SSI effects can be empirically evaluated.

Database

Two classes of sites are considered: Class 'A' sites, which have a free-field accelerograph and a structure instrumented to record base and roof translations (and in some cases, base rocking as well), and Class 'B' sites, which have structures instrumented to record base rocking as well as base and roof translations, but have no free-field accelerographs. Criteria employed in the selection of 'A' sites are described by Stewart et al. (1999a).

Suitable free-field instruments were sought for virtually all instrumented structures in California, and 44 sites were identified (plus one additional structure in Taiwan). An additional 13 structures in California were considered in this study as 'B' sites. For the 57 sites, 74 processed data sets are available as a result of multiple earthquake recordings at 13 sites. Fifteen California earthquakes contributed data to this study with magnitudes ranging from 4.8 to 7.3. Moderate to low level shaking (pga < 0.1 to 0.2g) is well represented in the database (50 data sets), while a moderate amount of data (24 data sets) is available for more intense shaking (pga > 0.2g). The foundation conditions at the sites include 23 buildings with piles or piers, and 34 with footings, mats, or grade beams. Most buildings are not embedded (36) or have shallow single-level basements (14). Only seven buildings have multi-level basements. The buildings range from single story warehouses to high-rise office buildings. Lateral force resisting systems include shear walls, frames, and base isolation.

Evaluation of Period Lengthening and Foundation Damping

Period lengthening ratios and foundation damping factors derived from fixed- and flexible-base modal vibration parameters obtained from system identification analyses are shown in Fig. 2. These parameters are plotted against the dimensionless structure-to-soil stiffness ratio $1/\sigma = h/(V_S \cdot T)$, where h = effective structure height and V_S = effective soil shear wave velocity. Also shown are second-order polynomials fit to the data by regression analysis, and analytical results by Veletsos and Nair (1975) for h/r = 1 and 2 (where r = foundation radius). Both $\tilde{T}/T$ and $\tilde{\zeta}_0$ are seen to increase with $1/\sigma$, and the best fit lines through the data are similar to the Veletsos and Nair curves.

There is significant scatter in the data in Fig. 2, although much of this results from systematic variations in $\tilde{T}/T$ and $\tilde{\zeta}_0$ associated with factors such as structure aspect ratio, embedment, foundation type, and foundation shape and flexibility effects. In addition, $\tilde{\zeta}_0$ is influenced by the hysteretic soil damping (β), which varies with soil type.

Results from several sites help to illustrate the strong influence of $1/\sigma$ on inertial interaction effects. The most significant inertial interaction occurred at site A46 ($\tilde{T}/T \approx 4$ and $\tilde{\zeta}_0 \approx 30\%$), which has a stiff ($T \approx 0.1$ sec) cylindrical concrete structure (h=14.3 m) and relatively soft soils ($V_S \approx 85$ m/s), giving a large $1/\sigma$ of about 1.5. Conversely, the inertial interaction effects are negligible at site A21 ($\tilde{T}/T \approx 1$ and $\tilde{\zeta}_0 \approx 0\%$), which has a relatively flexible ($T \approx 0.8$-1.0 sec) base-isolated structure (h=6.7 m) that is founded on rock ($V_S \approx 300$ m/s), giving a much smaller $1/\sigma$ value of 0.02-0.03. These two sites represent the extremes of inertial interaction. More typical SSI effects occur at sites B14 ($\tilde{T}/T = 1.14$ and $\tilde{\zeta}_0 \approx 3.4\%$) and A1-tr ($\tilde{T}/T = 1.57$ and $\tilde{\zeta}_0 \approx 15.4\%$). The structures at both sites are shear wall buildings with periods of T = 0.49 and 0.15 sec, respectively, and are founded on medium-stiff soils (V_S = 256 and 213 m/s), combining to give $1/\sigma \approx 0.12$ at B14 and $1/\sigma \approx 0.29$ at A1-tr. The results from these four sites illustrate that both $\tilde{T}/T$ and $\tilde{\zeta}_0$ increase with increasing $1/\sigma$.

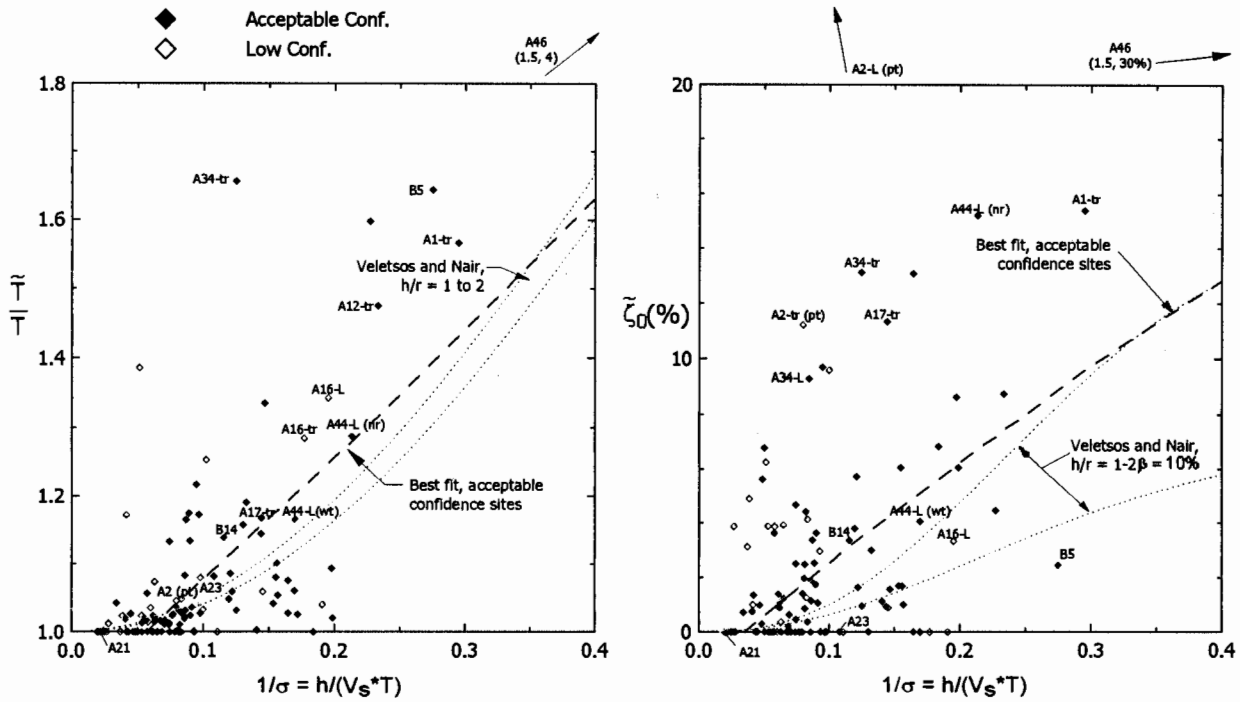

Fig. 2: Period lengthening ratios and foundation damping factors for sites sorted by confidence level (tr=transverse, L = longitudinal)

Comparison to Analysis

For analysis of inertial interaction effects, the objectives are predictions of first-mode period lengthening ratio $\tilde{T}/T$ and foundation damping factor $\tilde{\zeta}_0$. As shown in Fig. 3, simple procedures for evaluating these effects employ a model consisting of a single degree-of-freedom structure resting on a foundation-soil system represented by an impedance function. The impedance function is calculated for a rigid disk foundation resting either at the surface of (Veletsos and Nair, 1975) or embedded into (Bielak, 1975) a uniform visco-elastic halfspace.

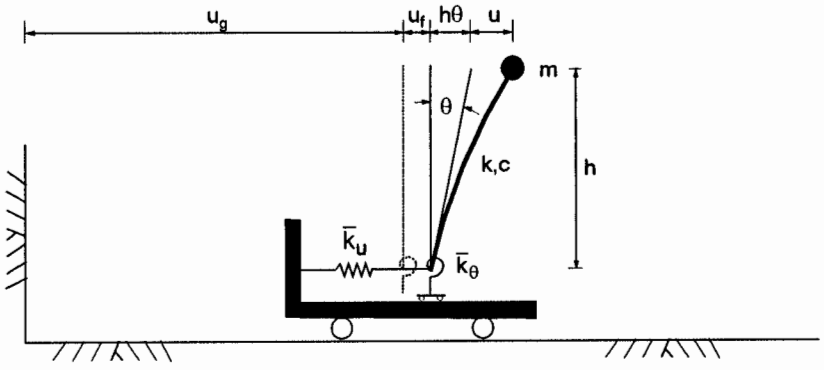

Fig. 3: Simplified model for analysis of inertial interaction

The foundation impedance function is evaluated at the flexible-base period of the structure, $\tilde{T}$. The frequency dependent and complex-valued impedance terms are expressed in the form

$$\bar{k}_j = k_j(a_0, \upsilon) + i\omega c_j(a_0, \upsilon) \tag{1}$$

where j denotes either deformation mode u (translation) or θ (rocking), ω is angular frequency (radians/sec.), a_0 is a dimensionless frequency defined by $a_0 = \omega r/V_S$, r = foundation radius, and υ = soil Poisson ratio. Terms k_j and c_j consist of a combination of static foundation stiffness (K_j) and dynamic modifiers α_j and β_j as follows:

$$k_j = \alpha_j K_j \qquad\qquad c_j = \beta_j \frac{K_j r}{V_s} \tag{2}$$

The terms α_j and β_j express the frequency dependence of the impedance, and are computed differently for surface (Veletsos and Verbic, 1973) and embedded (Bielak, 1975) foundations. Foundation radii are computed separately for translational and rotational deformation modes to match the area (A_f) and moment of inertia (I_f) of the actual foundation (i.e. $r_u = \sqrt{A_f/\pi}$, $r_\theta = \sqrt[4]{4I_f/\pi}$). The Bielak formulation includes a rigorous model of dynamic basement wall-soil interaction, assuming perfect wall-soil bonding. An approximate analysis of embedment effects can be made with the Veletsos and Nair model by increasing the static stiffness according to the well known guidelines of Kausel (1974), and using α_j and β_j terms for surface foundations (Elsabee and Moray, 1977).

Stewart et al. (1999a) outlined several considerations associated with the application of these procedures to realistic foundation and soil conditions. These can be summarized as follows:

1. *Representation of nonlinear soil response and nonuniform soil profiles as a visco-elastic halfspace*. Strain dependent soil properties are evaluated here with site response analyses which are used to calculate an equivalent hysteretic damping ratio and a degraded shear wave velocity profile. The effective profile velocity is taken as the profile depth divided by the shear wave travel time through the degraded profile. Profile depth is taken as $r_u = \sqrt{A_f/\pi}$.

2. *Representation of non-circular foundations*. While noncircular foundations with aspect ratios < 4:1 can generally be represented as equivalent disks (Roesset, 1980), radiation dashpot coefficients for rocking can be underestimated by such procedures (Dobry and Gazetas, 1986). Correction factors can be adapted from the Dobry and Gazetas results.

3. *Representation of flexible foundations*. The impedance of flexible base mats with thin perimeter walls or rigid concentric interior and perimeter walls can be reasonable well represented by rigid foundation models (Liou and Huang, 1994; Riggs and Waas, 1985). However, the rigid disk model is inadequate for buildings with rigid central cores, and should be modified according to the results of Iguchi and Luco (1982).

The basic procedures for a rigid disk foundation on the surface of, or embedded into, a halfspace were modified according to (1) to (3) above, and are subsequently referred to as the "modified Veletsos" (MV) and "modified Bielak" (MB) formulations.

Period lengthening ratios and foundation damping factors were evaluated by the Modified Veletsos (MV) procedure. For embedded foundations, similar comparisons using the Modified Bielak (MB) procedure are described by Stewart et al. (1999b).

Deviations in MV predictions of $\tilde{T}/T$ and $\tilde{\zeta}_0$ relative to empirical values are shown in Fig. 4 for sites with acceptable and low confidence designations. Also plotted are best fit second-order polynomials established from regression analyses on data from acceptable confidence sites. For most sites, the predictions are accurate to within absolute errors of about ±0.1 in $\tilde{T}/T$ and ±3% damping in $\tilde{\zeta}_0$ for $1/\sigma = 0$ to 0.4. The regression curves indicate no significant systematic bias in predictions of either $\tilde{T}/T$ or $\tilde{\zeta}_0$ up to $1/\sigma = 0.4$. However, there is a downward trend in the best fit curve for damping for $1/\sigma > 0.5$ (beyond the range on Fig. 4) due to a significant underprediction of $\tilde{\zeta}_0$ at site A46 ($1/\sigma = 1.5$) which results from a pronounced embedment effect at this site that is not fully captured by the MV formulation.

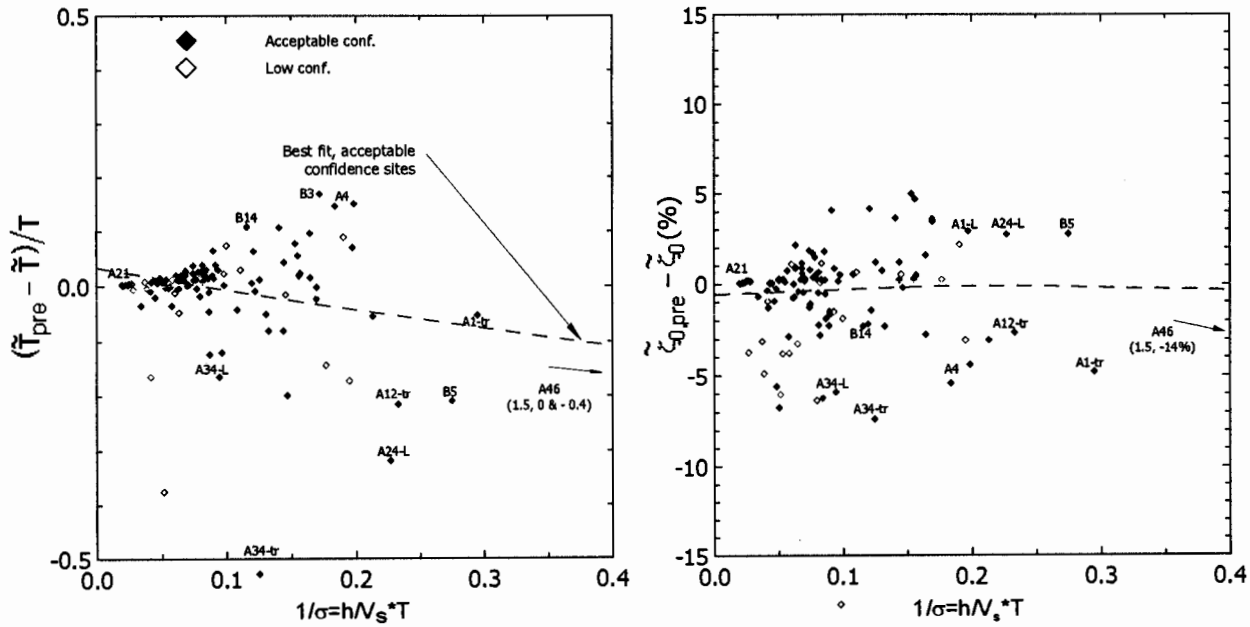

Fig. 4: Errors in "modified Veletsos" formulation for sites sorted by confidence level

The results from several sites help illustrate the general findings of Fig. 4. The minimal inertial interaction effects at site A21 ($1/\sigma = 0.02$ to 0.03, $\tilde{T}/T \approx 1$ and $\tilde{\zeta}_0 \approx 0\%$) are well predicted by the MV analyses, as is typical for sites with $1/\sigma < 0.1$. The predictions are also generally satisfactory for sites with intermediate $1/\sigma$ values such as B14 and A1-tr ($1/\sigma = 0.12$, $1/\sigma = 0.29$). At these sites, period lengthenings of 1.14 and 1.57 are over- and under-predicted by

absolute differences of about 0.11 and 0.06, respectively, while foundation damping factors of 3.4 and 15.4% are underpredicted by absolute differences of 2.3 and 4.8%, respectively. The large inertial interaction effects at site A46 ($1/\sigma = 1.5$, $\tilde{T}/T \approx 4.0$ and $\tilde{\zeta}_0 \approx 30\%$) are predicted to within an absolute difference of about 0.4 for period lengthening, but damping is underpredicted by an absolute difference of about 14%. With the exception of the damping results at site A46 (where there is a significant embedment effect), these results indicate that predictions of $\tilde{T}/T$ and $\tilde{\zeta}_0$ by the MV procedure are reasonably good considering the breadth of conditions represented in the database.

There are several noteworthy outliers in Fig. 4. When the residuals in Fig. 4 are considered with respect to the magnitude of the observed SSI effect, the most significant outliers for period lengthening are seen to be site A34 and several long period structures (A4, B3). The unusual results at site A34 may be associated with erroneously high shear wave velocity measurements. The long period structures at sites A4 and B3 are founded on soft Bay Mud soils in the San Francisco Bay Area, and were subject to negligible period lengthening (a common system identification result for all long-period structures). The soft soils at sites A4 and B3 lead to overpredictions of period lengthening, suggesting an error in the model. It appears from these data that the simple single-degree-of-freedom models on which the MV and MB formulations are based are incapable of adequately modeling SSI effects in long period structures with significant higher mode responses.

VARIATIONS BETWEEN FOUNDATION AND FREE-FIELD GROUND MOTIONS

It is widely known that soil-structure interaction modifies foundation-level motions relative to free-field motions (Kramer, 1996; Chopra, 1995), with both amplification and de-amplification of foundation-level motion possible across different frequency ranges. Two mechanisms of SSI generate the deviations between foundation and free-field motions:

- *Inertial Interaction*: Inertia developed in the structure due to its own vibrations gives rise to base shear and moment, which in turn causes displacements and rocking of the foundation relative to the free-field. These relative displacements can lead to amplification of foundation-level motion relative to the free-field at the fundamental-mode period of the structure ($\tilde{T}$).
- *Kinematic Interaction*: An assemblage of stiff foundation elements located on or in soil moves as a constrained body. Since free-field motions are generally spatially and temporally incoherent, motions on surface foundations are typically filtered with respect to free-field motions through a process termed "base slab averaging" by Seed (1986). Embedded foundations are subject to additional ground motion filtering associated with the reduction of ground motion amplitude with depth. Kinematic effects are most pronounced at high frequencies.

At a site with recordings of both free-field and foundation-level motions, variations between these motions result from a composite of kinematic and inertial effects, as well as random variations resulting from spatial incoherence effects.

Fig. 5 compares maximum horizontal acceleration (MHA) and spectral acceleration at the first-mode building period ($S_a@\tilde{T}$) for a data set consisting of 'A' sites in the aforementioned database (both transverse and longitudinal data are included). The MHA data in Fig. 5 generally indicate de-amplification of foundation-level MHA, and a perceptible increase in the level of de-amplification with increasing MHA. Filtering of foundation motion is significantly smaller in the $S_a@\tilde{T}$ data. The MHA de-amplification reflects the significant influence of kinematic interaction at high frequencies. The relatively modest de-amplification of $S_a@\tilde{T}$ results from both foundation motion amplification associated with inertial interaction, which is most pronounced at $\tilde{T}$, and the reduced kinematic effect at longer spectral periods.

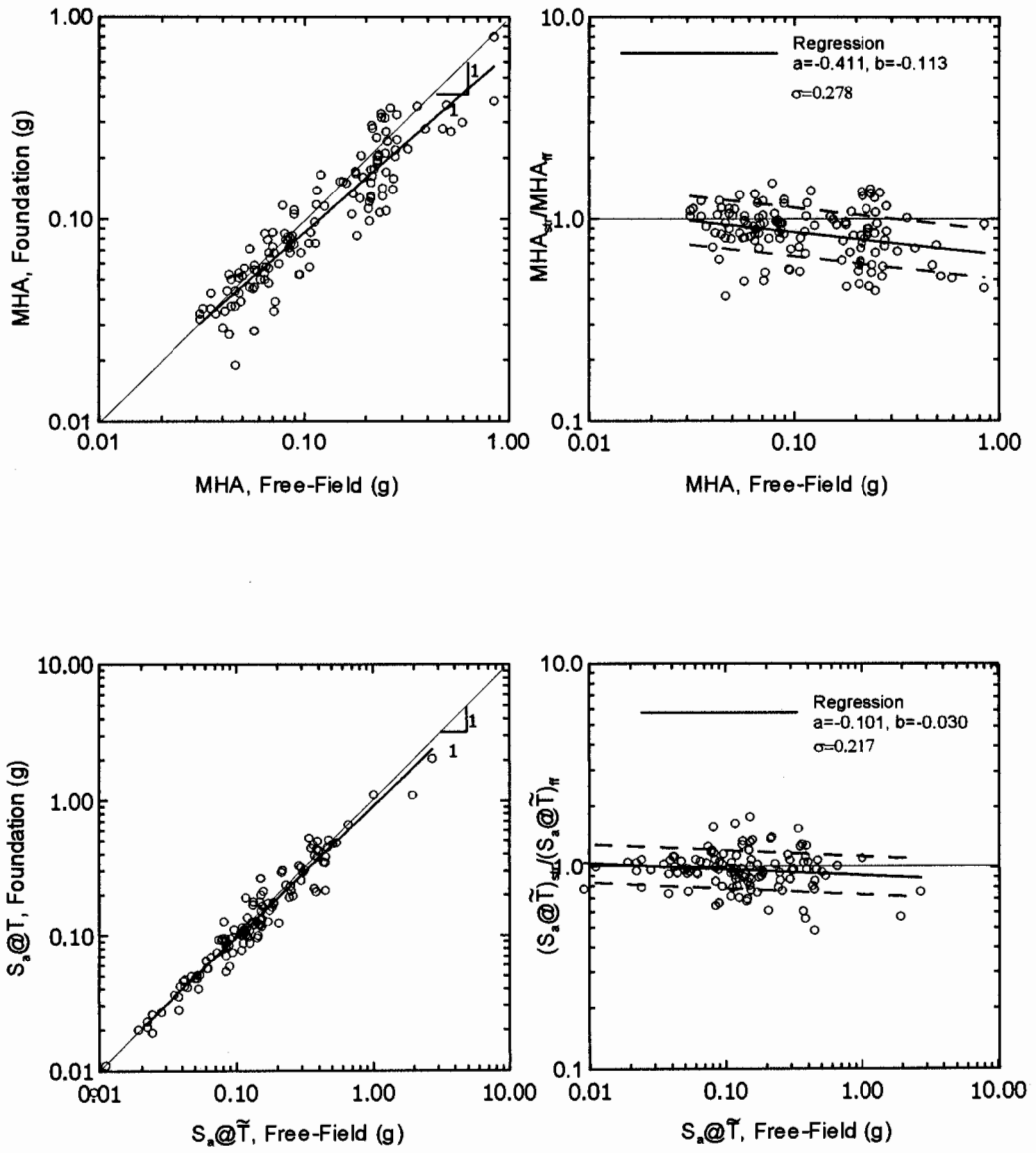

Fig. 5: Variation between free-field and foundation-level MHA and 5% damped $S_a@\tilde{T}$, full data set

In order to elucidate trends in the data plotted in Fig. 5, linear regression analyses were performed to fit an equation of the following form to the data,

$$\ln(ratio) = a + b\ln(ff) \tag{3}$$

where *ratio* is the ratio of foundation/free-field motion and *ff* is the amplitude of the free-field motion. The result of this regression is plotted in Fig. 5. More complex equation forms were investigated, but did not significantly reduce residuals. The residuals between the data and regression results are essentially log-normally distributed. Accordingly, the standard error of the regression, denoted henceforth as σ, is computed from the log of the residuals, with the results listed in Fig. 5. Regression results $\pm\ \sigma$ are plotted in Fig. 5 as dashed lines. It may be noted that the error term for MHA (σ=0.278) significantly exceeds that for $S_a@\tilde{T}$ (σ=0.217), suggesting a higher level of data noise at high frequencies where spatial incoherence effects are most pronounced.

Elsabee and Morray (1977) and Day (1978) found from finite element analyses of cyclindrical embedded foundations that embedement ratio (*e/r*) is a significant parameter controlling the filtering of embedded foundation-level motion relative to free-field motion. Fig. 6 compares ratios of MHA and $S_a@\tilde{T}$ data for the full data set sorted according to $e/r = 0$, $e/r > 0$ & < 0.5, and $e/r > 0.5$. Also plotted in Fig. 6 are regression results fitting Eq. 3 for the different data bins. The $S_a@\tilde{T}$ data for $e/r > 0$ & < 0.5 has negligible deviations from the $e/r = 0$ data. The MHA deviations for these two *e/r* bins are larger, but are still modest. Although the data for $e/r > 0.5$ is sparse, significant and consistent de-amplification is apparent both in MHA and $S_a@\tilde{T}$ relative to $e/r < 0.5$. Therefore, it appears that *e/r* is an important index controlling foundation/free-field ground motion variations.

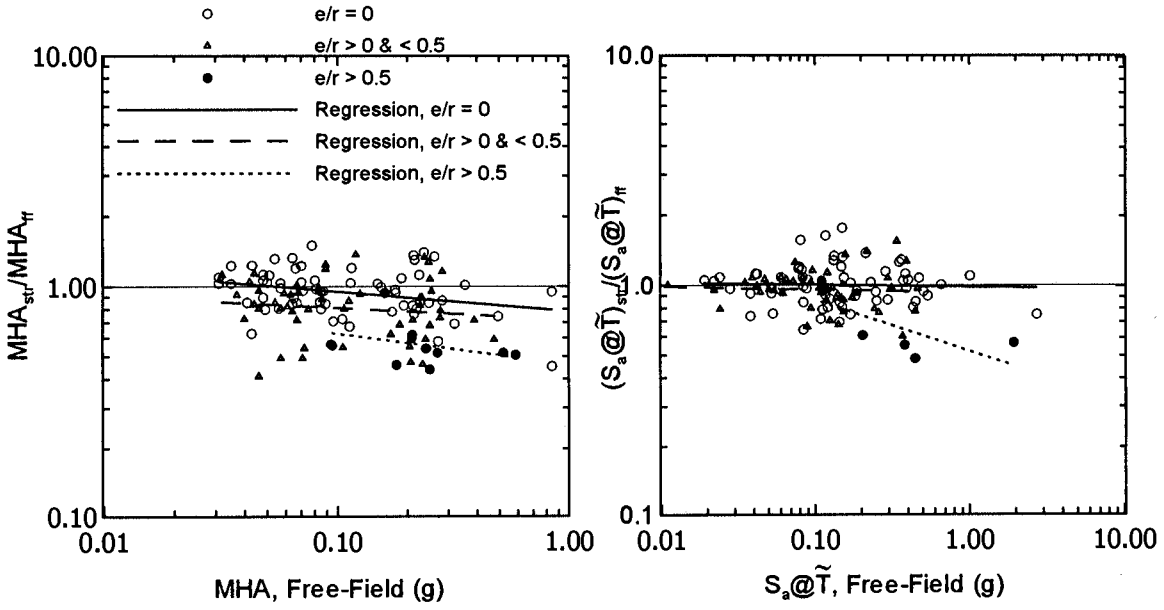

Fig. 6: Ratio of foundation-level/free-field motion, complete data set, sorted by e/r

As noted previously, inertial interaction effects in buildings are strongly a function of $1/\sigma$. Data from sites with $e/r < 0.5$ are sorted into bins with $1/\sigma < 0.1$ and $1/\sigma > 0.1$ and are plotted in Fig. 7 along with regressions according to Eq. 1. The results indicate that motions in buildings with $1/\sigma > 0.1$ are larger than motions with negligible inertial interaction. This suggests that structural vibrations enhance foundation-level motions in buildings with significant inertial interaction, which is expected. However, the inertial interaction effect on foundation-level ground motions is fairly small.

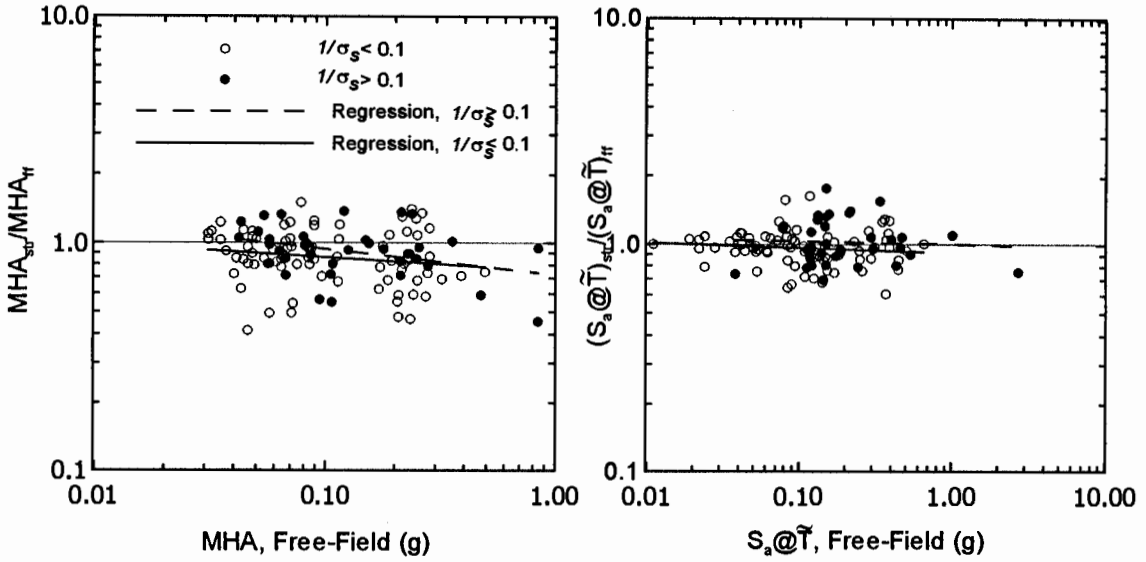

Fig. 7: Ratio of foundation-level/free-field motion, data set with e/r < 0.5, sorted according to $1/\sigma < 0.1$ and $1/\sigma > 0.1$

Veletsos and Prasad (1989) and Veletsos et al. (1997) investigated with theoretical analysis base slab averaging effects for rigid foundations subjected to nonvertically incident and incoherent wave fields. It was found that the filtering of translational motion on base slabs increases with dimensionless frequency, $\tilde{a}_0$, defined for circular foundations as,

$$\tilde{a}_0 = \frac{\omega r}{V_s}\sqrt{\kappa^2 + \sin^2 \alpha_v} \qquad (4)$$

where κ=an incoherence parameter for the incident waves which varies between 0 and 1.0, and α_v=vertical angle of incidence of waves. Stewart (1999) found a strong effect of $\tilde{a}_0$ on foundation/free-field ground motion ratios at various spectral frequencies (ω), but the effect was traced principally to ω (i.e. variations with $\tilde{a}_0/\omega$ were negligible). Accordingly, base slab averaging effects can be grossly approximated using single median values of spectral acceleration ratio and standard error terms evaluated across a range of spectral periods (T=0.18, 0.32, 0.56, 1.0, 1.8, and 3.0 s) using data with $e/r < 0.5$. The results are compiled in Fig. 8, and show decreasing bias and standard error with increasing spectral period up to $T \approx 0.5$ s. These results

suggest that for $T \geq \sim 0.5$ s, median foundation-level spectral accelerations are within about 5 percent of free-field spectral accelerations, and that the standard error of the ratio is small ($\sigma \approx$ 0.18 to 0.22). This finding is consistent with Campbell (1984), who also found negligible de-amplification for spectral periods larger than 1 s.

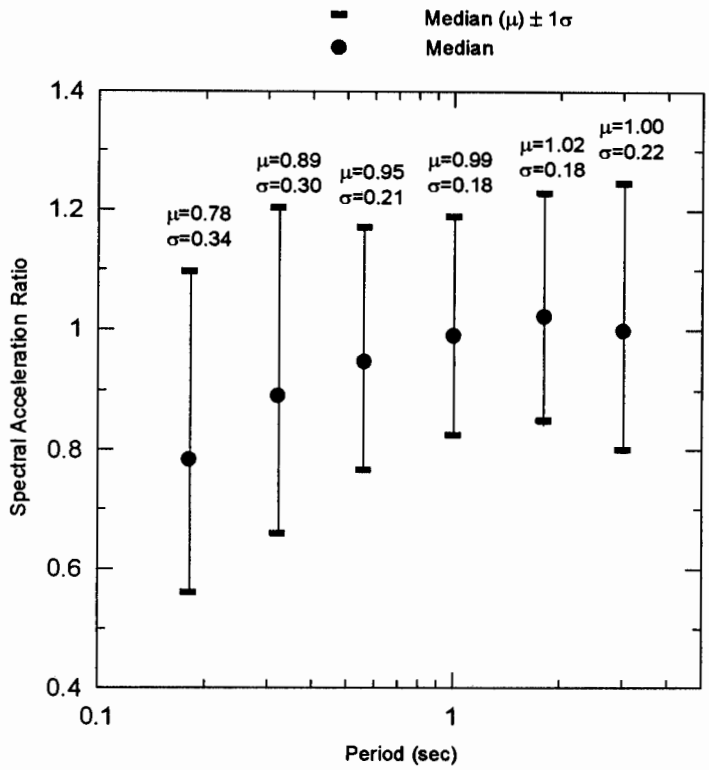

Fig. 8: Statistical values of 5% damped spectral acceleration ratio for various spectral periods, data set with $e/r < 0.5$

CONCLUSIONS

Based on the database of 57 sites compiled for this study, the factor with the greatest influence on $\widetilde{T}/T$ and $\widetilde{\zeta}_0$ is the ratio of structure-to-soil stiffness as quantified by the parameter $1/\sigma = h/(V_S \cdot T)$. When $1/\sigma$ is nearly zero, $\widetilde{T}/T$ and $\widetilde{\zeta}_0$ values are about unity and zero, respectively, whereas at the maximum observed value of $1/\sigma = 1.5$ at site A46, interaction effects dominated the structural response ($\widetilde{T}/T \approx 4$ and $\widetilde{\zeta}_0 \approx 30\%$). Additional factors which can significantly affect inertial interaction include the structure's aspect ratio (h/r) and foundation embedment and flexibility.

Variations between foundation and free-field motions result from kinematic and inertial soil-structure interaction effects. While inertial interaction can lead to minor amplification of foundation motion relative to the free-field, kinematic effects, which de-amplify high frequency motions, are generally more significant.

ACKNOWLEDGMENTS

Support for this work was provided by a CAREER award from the National Science Foundation (Award No. CMS 9733113). The views and conclusions contained in this document are those of the author and should not be interpreted as necessarily representing the official policies, either expressed or implied, of the U.S. Government.

REFERENCES

Bielak, J. (1975). "Dynamic behavior of structures with embedded foundations," *J. Eq. Engrg. Struct. Dynamics*, 3(3), 259-274.

Building Seismic Safety Council, BSSC (1997). "NEHRP Recommended provisions for seismic regulations for new buildings and other structures, Part 1, Provisions and Part 2, Commentary" *Rpt. No. FEMA 302*, Federal Emergency Management Agency, Washington D.C.

Campbell, K.W. (1984). "Near-source attenuation of strong ground motion for moderate to large earthquakes—An update and suggested application for the Wasatch Fault Zone of Norhcentral Utah," *in* Evaluation of Regional and Urban Earthquake Hazards and Risk in Utah, W.W. Hays and P.L. Gori (eds.), Proc. 26th NEHRP Workshop, Salt Lake City, Utah, Rpt. No. USGS OFR 84-763.

Chopra, A.K. (1995). *Dynamics of Structures.* Prentice Hall, Upper Saddle River, NJ, pg. 192.

Day, S.M. (1978). "Seismic response of embedded foundations," *Proc. ASCE Convention*, Chicago, IL, October, Preprint 3450.

Dobry, R. and Gazetas, G (1986). "Dynamic response of arbitrarily shaped foundations," *J. Geotech. Engrg.*, ASCE, 112(2), 109-135.

Elsabee, F. and Morray, J.P. (1977). "Dynamic behavior of embedded foundations," *Rpt. No. R77-33*, Dept. of Civil Engrg., Massachusetts Inst. Technology.

Iguchi, M. and Luco, J.E. (1982). "Vibration of flexible plate on viscoelastic medium," *J. Engrg. Mech.*, ASCE, 108(6), 1103-1120.

Kausel, E. (1974). "Forced vibrations of circular foundations on layered media," *Rpt. No. R74-11*, Dept. of Civil Engrg., Massachusetts Inst. Technology.

Kramer, S.L. (1996). *Geotechnical Earthquake Engineering.* Prentice Hall, Upper Saddle River, NJ, pg. 294-303.

Liou, G.-S. and Huang, P.-H. (1994). "Effect of flexibility on impedance functions for circular foundations," *J. Engrg. Mech.*, ASCE, 120(7), 1429-1446.

Roesset, J.M. (1980). "A review of soil-structure interaction," *in* Soil-structure interaction: the status of current analysis methods and research, J.J. Johnson, ed., *Rpt. No. NUREG/CR-1780 and UCRL-53011*, U.S. Nuclear Regulatory Com. and Lawrence Livermore Lab.

Riggs, H.R. and Waas, G. (1985). "Influence of foundation flexibility on soil-structure interaction," *J. Eq. Engrg. Struct. Dynamics*, 13(5), 597-615.

Seed, H.B. (1986). "Influence of local soil conditions on ground motions and building damage during earthquakes," 8th Nabor Carillo Lecture, 13th Nat. Mtg. Of Mexican Society for Soil Mech., Sinaloa, Mexico, November.

Stewart, J.P., Fenves, G.L. and Seed, R.B. (1999a). "Seismic Soil-Structure Interaction in Buildings. I: Analytical Aspects," *J. Geotech.. & Geoenv. Engrg.*, ASCE, 125 (1), 26-37.

Stewart, J.P., Seed, R.B., and Fenves, G.L. (1999b). "Seismic Soil-Structure Interaction in Buildings. II: Empirical Findings," *J. Geotech. & Geoenv. Engrg.*, ASCE, 125 (1), 38-48.

Stewart, J.P. and Fenves, G.L. (1998). "System Identification for Evaluating Soil-Structure Interaction Effects in Buildings from Strong Motion Recordings," *Earthquake Engineering and Structural Dynamics*, 27, 869-885.

Stewart, J.P. (1999). "Variations between foundation-level and free-field earthquake ground motions," *Earthquake Spectra*, EERI (in review).

Veletsos, A.S. and Prasad, A.M. (1989). "Seismic interaction of structures and soils: stochastic approach," *J. Struct. Engrg.*, ASCE, 115(4), 935-956.

Veletsos, A.S., Prasad, A.M., and Wu, W.H. (1997). "Transfer functions for rigid rectangular foundations," *J. Earthquake Engrg. Struct. Dynamics*, 26 (1), 5-17.

Veletsos, A.S. and Nair V.V. (1975). "Seismic interaction of structures on hysteretic foundations," *J. Struct. Engrg.*, ASCE 101(1), 109-129.

Veletsos, A.S. and Verbic, B. (1973). "Vibration of viscoelastic foundations," *J. Eq. Engrg. Struct. Dynamics*, 2(1), 87-102.

EVALUATATION OF RESPONSE OF A TALL CONCRETE FRAME BUILDING TO MULTIPLE EARTHQUAKES

G. Hart, M. Skokan, and A. Dumortier.
Department of Civil and Environmental Engineering
University of California, Los Angeles

And

S. Huang, Hart Consultant Group, Los Angeles

ABSTRACT

The response of an instrumented reinforced concrete moment-resisting frame (RCMRF) building, located in Southern California, was investigated to show how instrumented response can significantly improve the accuracy of performance based design. RCMRF buildings are particularly difficult to model and therefore this uncertainty reduction is very important. A model of the building using FEMA 273 recommended structural design variables is used as a baseline model. Performance based design estimates are made using this model and then compared with estimates made using improved models that benefit from the measured 1987 Whittier and the 1994 Northridge earthquake response of the building.

INTRODUCTION

The primary objective of the structural engineer for a new or seismic rehabilitation building is the development of a building design whose performance can be accurately estimated during a range of earthquakes. The goal of performance prediction can only be achieved when the design is based on a proper analytical model of the building system and the earthquake ground motion that the building can be expected to experience during its design life. It is obvious that an improved model of an existing building for PML studies can be done more accurately if the model incorporates measured building responses. This paper describes work in progress in this area. The reader is referred to paper approved for publication but in early under expansion with the same title in the Wiley journal entitled "Structural Design of Tall Buildings."

The SEAOC Vision 2000 report (OES, 1995) outlines a framework for implementing the performance base design concept. One of the first steps in performance based design is the selection of performance objectives, each of which requires the selection of a seismic hazard level and performance level. The seismic hazard level is defined by the selection of a return period for the earthquake motion and the performance level specifies a level of structural and non-structural damage by both qualitative and quantitative measures. For each of the selected performance objectives, an analysis of the building is performed using the specified level of seismic hazard and the performance of the building compared to the acceptance criteria for the specified performance level. It is during this phase of the performance base design procedure that the importance of a proper analytical model of the building is very critical.

In this research, the response of an instrumented RCMRF building, located in Southern California, was estimated and compared to the performance of linear elastic analytical models of the building developed with the benefit of measured building response. RCMRF buildings are particularly difficult to model when the objective is to predict the performance of the building. It is difficult to quantify the stiffness of the beams and columns in a linear elastic computer model primarily because the stiffness of each element is highly dependant on the level of strain induced by flexural and axial loads. The baseline model used in this research is based on FEMA 273 and represents a model that does not benefit from building instrumented response measurements. Improved building models are developed using the 1987 Whittier and 1994 Northridge earthquakes and these show the improved response. Furthermore, the contribution of the floor slab to the stiffness of the beams, the effect of confinement on the behavior of the columns, and the stiffness of the beam-column joints, further increases the complexity of the modeling decisions.

BUILDING DESCRIPTION

The focus of this study is a 20-story reinforced concrete frame hotel (Figure 1) located in North Hollywood, California, approximately 19 km from the epicenter of the 1994 Northridge Earthquake. Constructed in 1968, this building was the first to be designed using the 1966 Los Angeles building code that prescribed ductility requirements for reinforced concrete moment resisting frames (Wayman, 1968; Steinmann, 1998). As a result, the design features a strong column-weak beam concept, under-reinforced beams to assure steel yielding prior to concrete crushing, full hoop ties in the beam-column joints, continuous top and bottom beam bars through the joints, and column bar splices at the mid-height (Wayman, 1968).

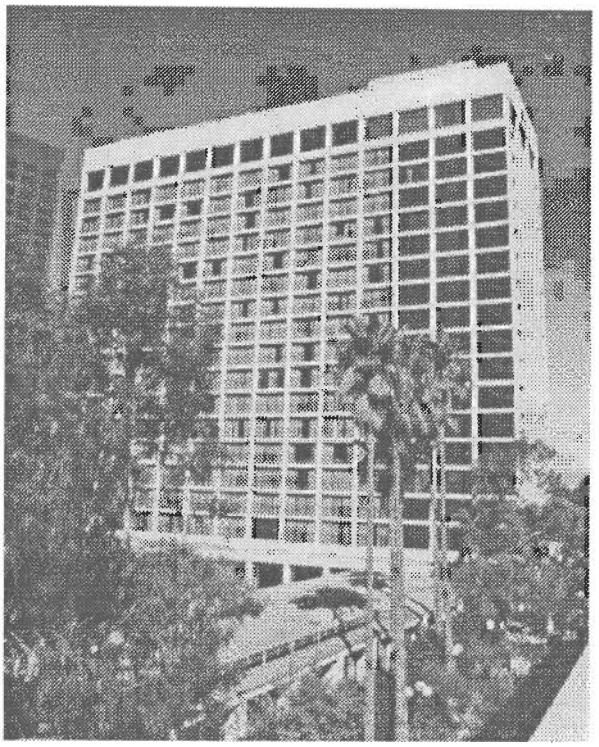

Figure 1 20-Story North Hollywood Building

All concrete is composed of lightweight aggregate with 3,000 psi and 4,000 psi compressive strength at 28 days. The reinforcing steel was specified to be both high-strength ASTM 432 grade with 60,000 psi yield strength and ASTM A-15 grade with 40,000 psi yield strength. The typical floor elevation is 8'-9" and a typical bedroom floor plan is shown in Figure 2. Below grade, perimeter concrete shear walls and spread footings support the 210-ft structure.

SEISMIC BUILDING RESPONSE

The case study building used in this research is a 20-story North Hollywood building that is instrumented with strong motion sensors by the California Strong Motion Instrumentation Program (CSMIP). Sixteen strong motion sensors, as shown in Figure 3, are located over the height of the building, with three sensors placed at each of four floors (3rd' 9th, 16th, and Roof) and four sensors located at the basement level. Strong motion records are available from five major earthquakes over the past 30 years including: 1971 San Fernando, 1987 Whittier, 1992 Landers, 1992 Big Bear, and 1994 Northridge.

Records from the 1987 Whittier and the 1994 Northridge earthquakes are addressed in this research. The ground acceleration time histories in the North-South and East-West directions are shown for the Whittier and Northridge earthquakes in Figures 4 and 5, respectively. Note that for both events, the East-West direction peak ground acceleration (PGA) is larger, and in the

case Northridge, the East-West PGA is approximately three times larger. In terms of PGA, it is also observed that Northridge was clearly stronger than the Whittier event. A previous paper entitled "Response Evaluation of a 20-Story Concrete Frame Building to the Northridge and Other Earthquakes" presented at the 1998 SMIP annual meeting describes the building response in some details. Only the highlights are presented here.

Figure 6 shows the roof relative displacement ratio history at the center-of-mass location. The center-of-mass displacement history was calculated by transforming the displacement history from the three roof sensors using the methodology outlined by Naeim (1997). Figure 6 also indicates the displacement ratio suggested by the Vision 2000 report for the Fully Operational and Operational performance levels. In general, the displacement ratios fall within the definition of the Fully Operational performance level, however, one strong pulse in the North-South direction displaces the building to a 0.4% displacement ratio. This is near the displacement ratio used to define the Operational performance level. A goal of performance based design is to accurently calculate a response for the future earthquakes for evaluation of the type shown in Figure 6.

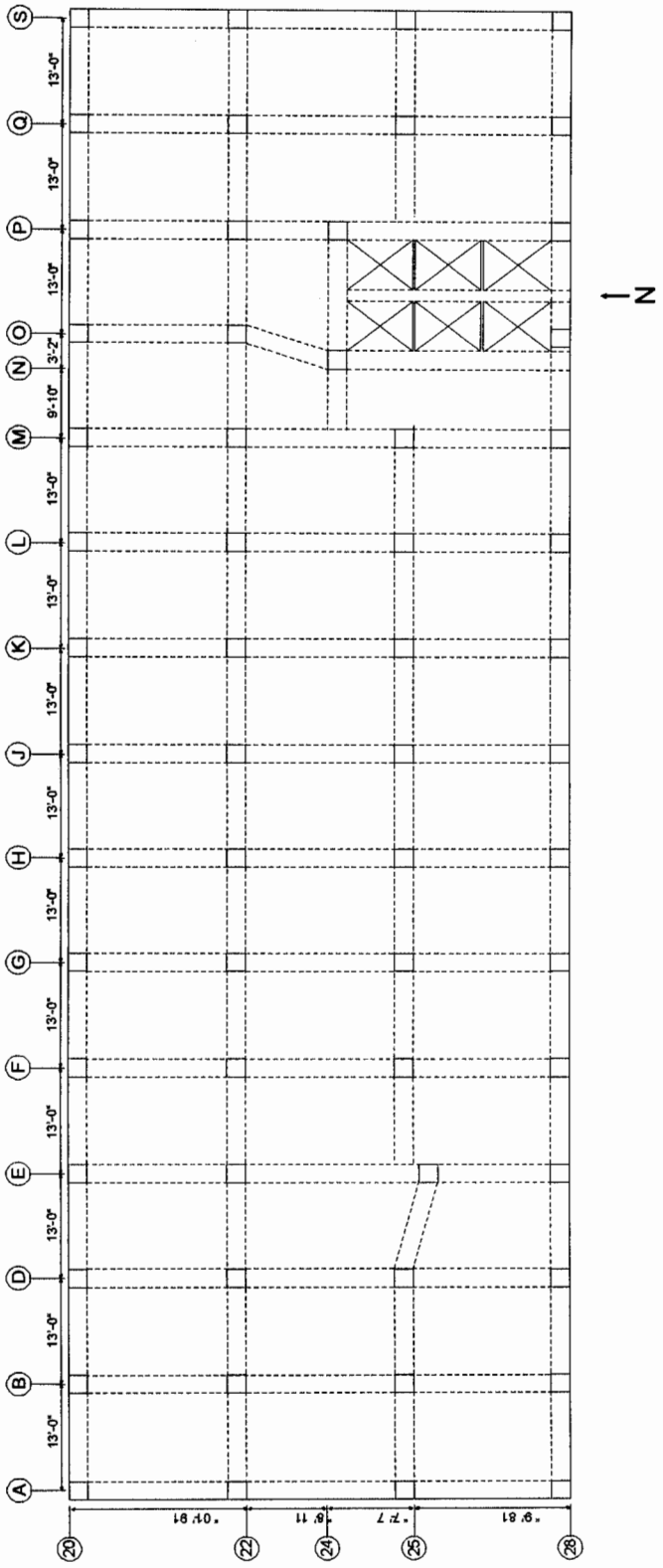

Figure 2 Typical Bedroom Floor Plan

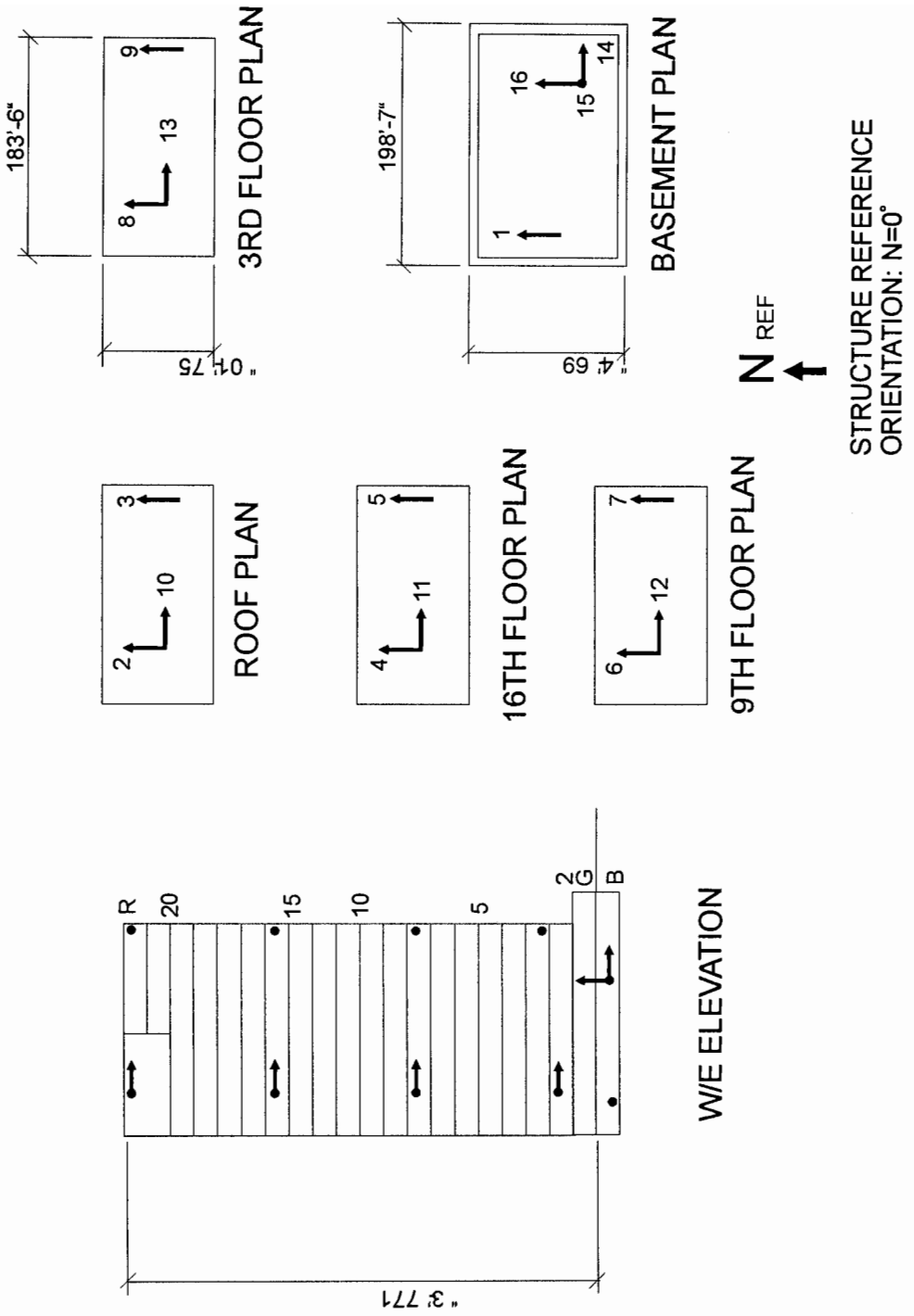

Figure 3 Sensor Locations

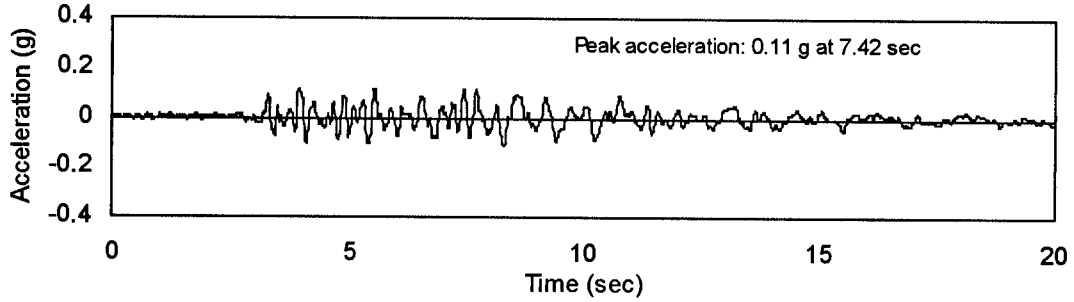

(a) North-South (Longitudinal) Direction (Channel 16)

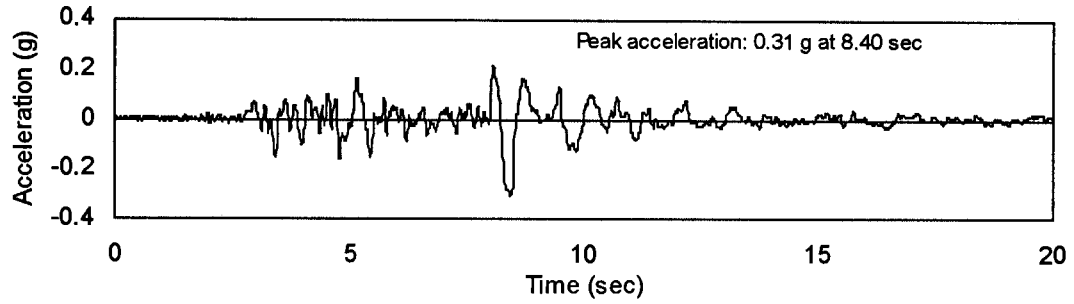

(b) East-West (Transverse) Direction (Channel 14)

Figure 4 1994 Northridge Earthquake Acceleration Time Histories at Ground Level

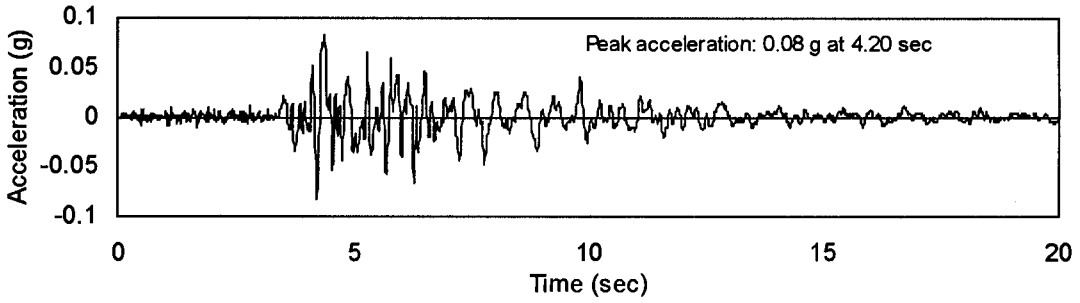

(a) North-South (Longitudinal) Direction (Channel 16)

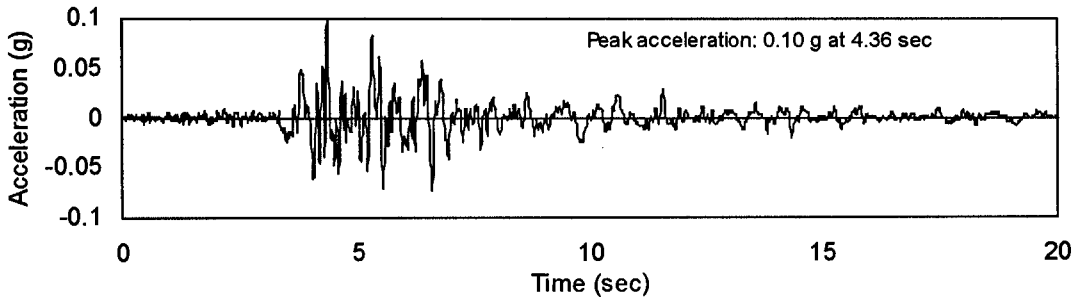

(b) East-West (Transverse) Direction (Channel 14)

Figure 5 1987 Whittier Earthquake Acceleration Time Histories at Ground Level

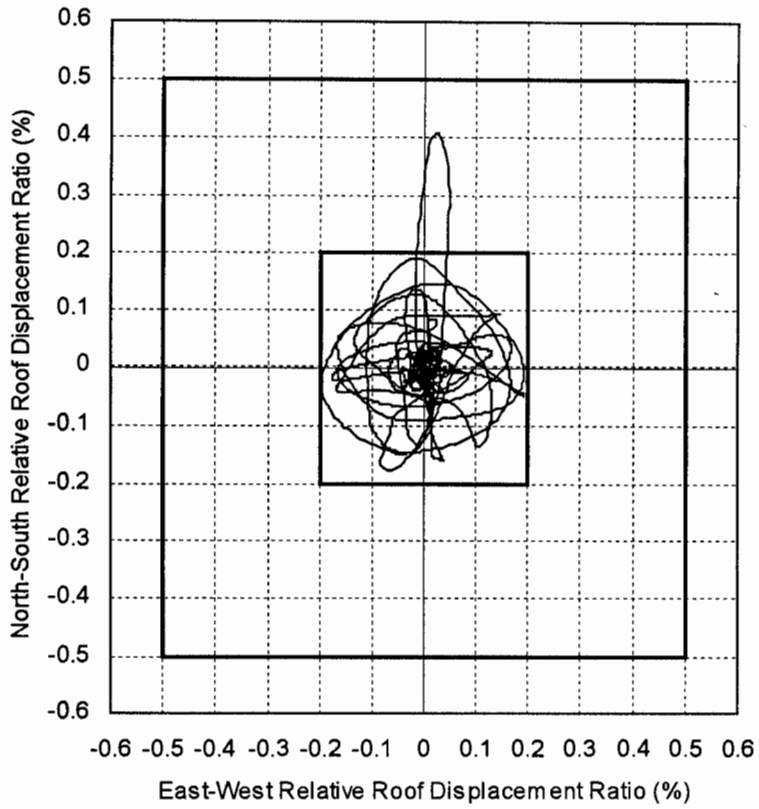

Figure 6 Northridge earthquake relative roof displacement ratio history with Vision 2000 (OES, 1995) performance level drift ratios

Studies of the instrumented response of the case study building (Goel, et. al, 1997; Naeim, 1997) have yielded estimates of the fundamental translational periods of vibration of the building. In addition, the studies by Goel, et. al. have resulted in estimates of the percentage of critical damping for these fundamental periods. The results of the work by Goel, et. al. are provided in Table 1. The results show that the periods of vibration in the transverse and longitudinal building directions are approximately equal. Note also that the fundamental periods estimated for the Northridge earthquake are approximately 18% larger than for the Whittier earthquake. This is most likely due to the fact that the displacement demands from the Northridge earthquake were significantly greater than during the Whittier earthquake.

Table 1 Translational periods of vibration and percentage of critical damping (Goel, et. al, 1997)

Earthquake Record	North-South (Longitudinal)		East-West (Transverse)	
	Period (sec)	Damping (%)	Period (sec)	Damping (%)
1987 Whittier	2.15	---	2.21	---
1994 Northridge	2.60	5.9	2.62	6.5

Using the ground acceleration records for the Whittier and Northridge earthquakes, the 5% damped response spectra were calculated and are given in Figure 7 along with the UBC design spectrum for soil type 2. For the fundamental periods estimated by Goel, et. al., notice that the spectral accelerations are well below the values that given by the UBC design spectrum.

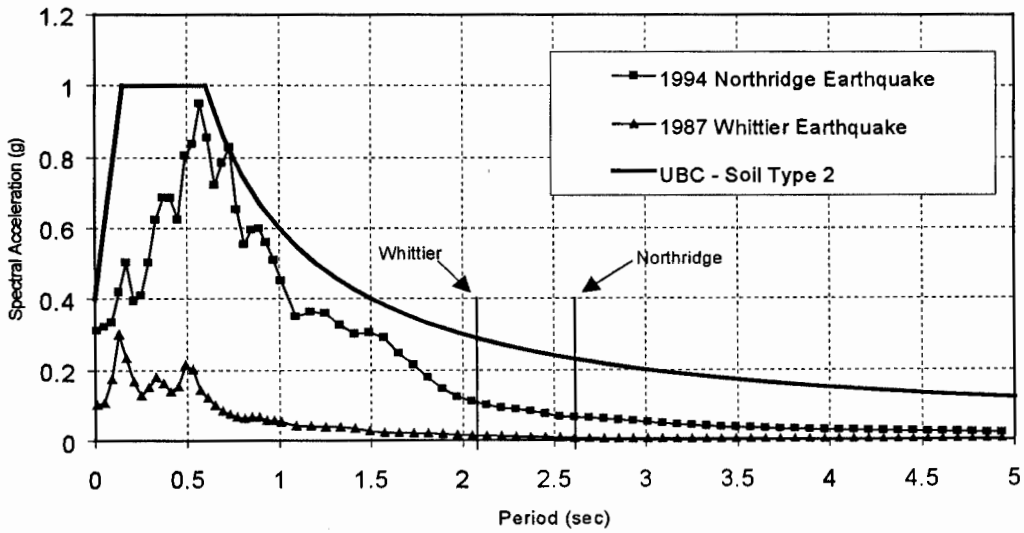

(a) North-South (Transverse) direction

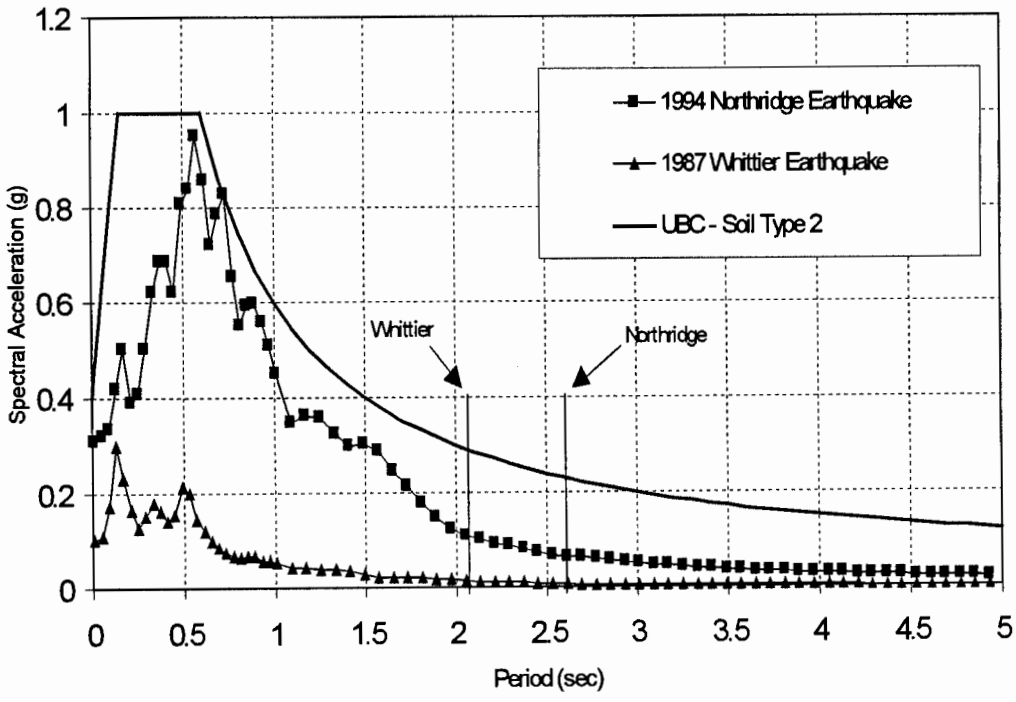

(b) East-West (Longitudinal) direction

Figure 7 5% damped response spectra at ground level

BASELINE, PRE EARTHQUAKES, ANALYTICAL COMPUTER MODELS

The case study building was analyzed using the three-dimensional linear elastic computer program ETABS (CSI, 1997). All of the beams and columns of the moment resisting frames were included in the model along with the walls at the basement level.

The floor diaphragms were assumed to be rigid and assigned a mass, center-of-mass location, and mass moment of inertia based on detailed calculations assuming point masses at the column locations. Since the structural elements are composed of lightweight concrete, 105 pcf was assumed for the unit weight of all concrete. In addition, the weight of partitions, exterior cladding, and specific mechanical equipment was included along with 15 psf to account for mechanical, electrical, ceiling and floor finishes, and other miscellaneous items.

The *FEMA 273 Stiffness* model is considered to be the **Baseline** model. In the model, the beams and columns are assigned an effective moment of inertia based on a percentage of the gross moment of inertia suggested by the *NEHRP Guidelines for the Seismic Rehabilitation of Buildings - FEMA 273* (ATC, 1997). FEMA 273 suggests the use of 50% of gross for beams, 70% of gross for columns in axial compression, and 50% of gross for columns in axial tension. Since the axial load in the columns will vary throughout the analysis, 60% of gross was assumed for the column stiffness in this model.

PREDICTED BUILDING RESPONSE

The Baseline model described in the previous section was used to calculate the natural frequencies and mode shapes for the building. Table 2 gives the periods of vibration and the percentage of participating mass in each direction for the first nine modes. They are also presented in Table 3 for a sensitivity study where key structural model variables were slightly changed from the FEMA values. The structural parameters considered were the rigid end zone (REZ), the inertia of the columns and the beams, and the modal damping. For each change of parameter, the maximum displacements predicted by the analyses were compared to the maximum recorded displacements at each instrumented floor. The results are displayed in Figure 8.

This led the writers to investigate the influence of each parameter on the structural response of the building in more details. The parameters were then varied from the FEMA model one at a time, from their minimum to their maximum values, and values of displacements were calculated and compared to the maximum recorded displacements. The stiffness of the beam-column joints was varied to reflect a range of behavior. This was accomplished by varying the length of the rigid end zone (REZ) at the beam-column intersections. In the *100% REZ* model, the entire beam-column intersection was assumed to rigid, the *50% REZ* model assumes that only one-half of the beam-column intersection is rigid, and the *Centerline* model assumes no rigidity of the beam-column intersection. As one would expect, as the stiffness of the beams, columns, and REZ's decreases, the periods of vibration tend to increase. Different reduction factors were also applied to the inertia of the columns and the beams, and the modal damping was also varied. The

results plotted on Figure 9 through 14 show that the inertia of the columns and the beams have a greater influence on the structural response than the REZ and damping.

The results reported here are a portion of the ongoing research which is working towards improving the accuracy of performance based design. Further refinement is still underway and will be reported in future report.

Table 2 Periods of Vibration and Participating Mass from the Baseline Model

Mode #	FEMA			
	Period (Sec)	Participating Mass (%)		
		N-S	E-W	Rotation
1	3.03	36.5	1.1	30.4
2	2.86	24.1	28.5	17.8
3	2.82	9.8	40.6	18.9
4	1.03	9.0	0.0	3.0
5	0.95	1.1	6.0	3.3
6	0.93	0.9	4.6	5.5
7	0.61	4.1	0.0	0.3
8	0.57	0.1	3.3	1.4
9	0.57	0.2	1.8	3.3

Table 3 Periods of Vibration and Participating Mass from the Sensitivity Study of the Baseline Model

Mode #	FEMA with 75% REZ			
	Period (Sec)	Participating Mass (%)		
		N-S	E-W	Rotation
1	3.14	34.7	1.6	31.7
2	2.98	14.1	51.1	5.4
3	2.93	21.6	17.6	30.0
4	1.07	8.8	0.1	3.1
5	1.00	0.8	7.5	2.0
6	0.97	1.2	3.0	6.7
7	0.64	4.1	0.0	0.3
8	0.60	0.1	4.0	0.7
9	0.59	0.2	1.0	3.9

Mode #	FEMA with 80% I Column			
	Period (Sec)	Participating Mass (%)		
		N-S	E-W	Rotation
1	2.94	36.5	1.0	29.9
2	2.78	25.8	23.2	20.6
3	2.74	7.5	45.2	15.8
4	0.99	9.0	0.1	3.1
5	0.92	1.1	6.1	3.2
6	0.90	0.9	4.6	5.5
7	0.58	4.2	0.0	0.4
8	0.55	0.2	3.5	1.4
9	0.54	0.2	1.8	3.5

Mode #	FEMA with 70% I Beam			
	Period (Sec)	Participating Mass (%)		
		N-S	E-W	Rotation
1	2.70	40.4	0.9	27.4
2	2.55	25.9	18.2	26.8
3	2.51	4.6	52.1	13.5
4	0.93	9.5	0.0	2.6
5	0.86	1.1	4.8	4.6
6	0.84	0.6	5.8	4.7
7	0.55	4.1	0.0	0.2
8	0.52	0.1	2.3	2.0
9	0.51	0.1	2.4	2.6

Mode #	FEMA with 10% Damping			
	Period (Sec)	Participating Mass (%)		
		N-S	E-W	Rotation
1	3.03	36.5	1.1	30.4
2	2.86	24.1	28.5	17.8
3	2.82	9.8	40.6	18.9
4	1.03	9.0	0.0	3.0
5	0.95	1.1	6.0	3.3
6	0.93	0.9	4.6	5.5
7	0.61	4.1	0.0	0.3
8	0.57	0.1	3.3	1.4
9	0.57	0.2	1.8	3.3

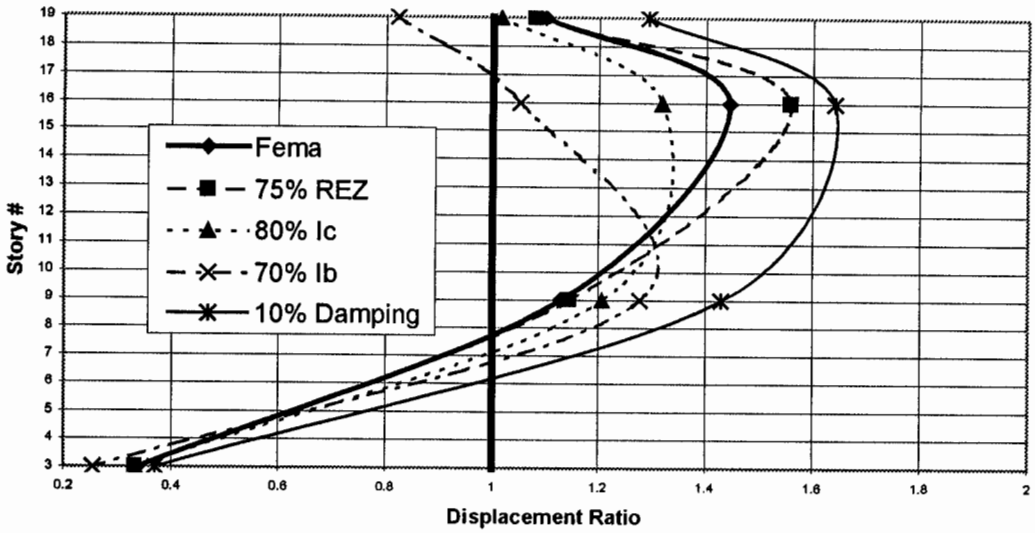

(a) North-South Direction

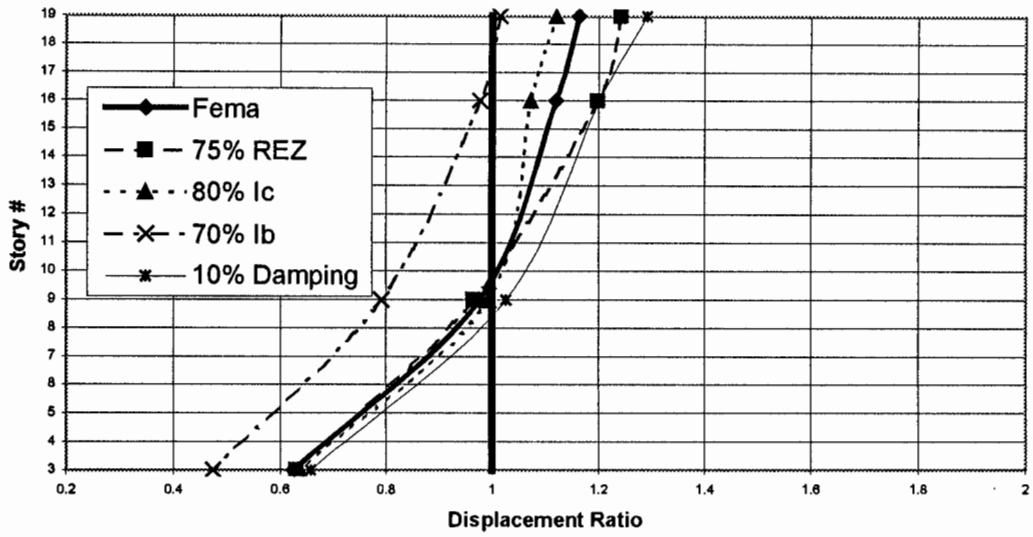

(b) East West Direction

Figure 8 Maximum Recorded / Maximum Predicted Floor Displacement Ratios - Whittier EQ -

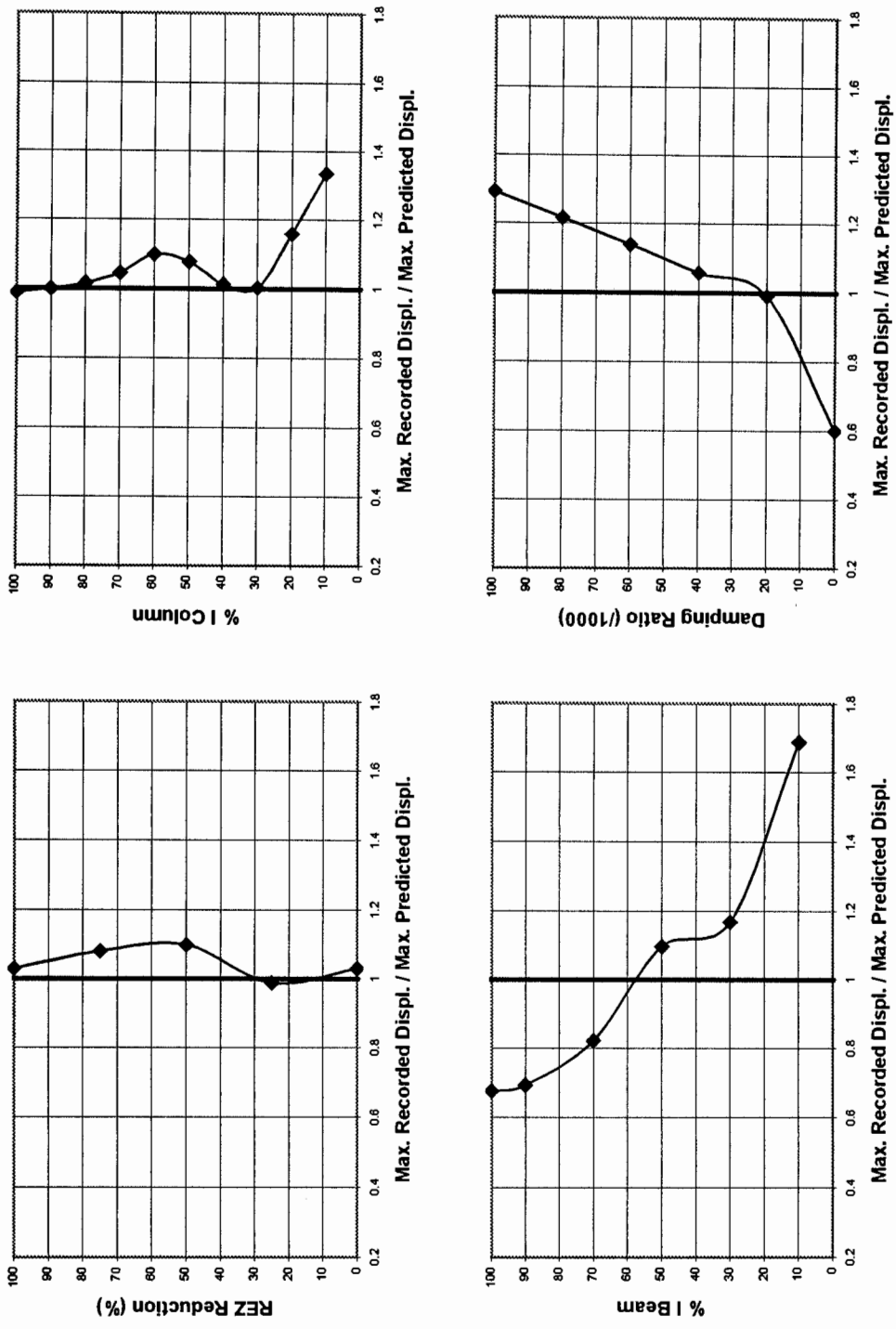

Figure 9 Roof Maximum Recorded / Maximum Predicted Displacement Ratios – Whittier EQ. – North-South Direction

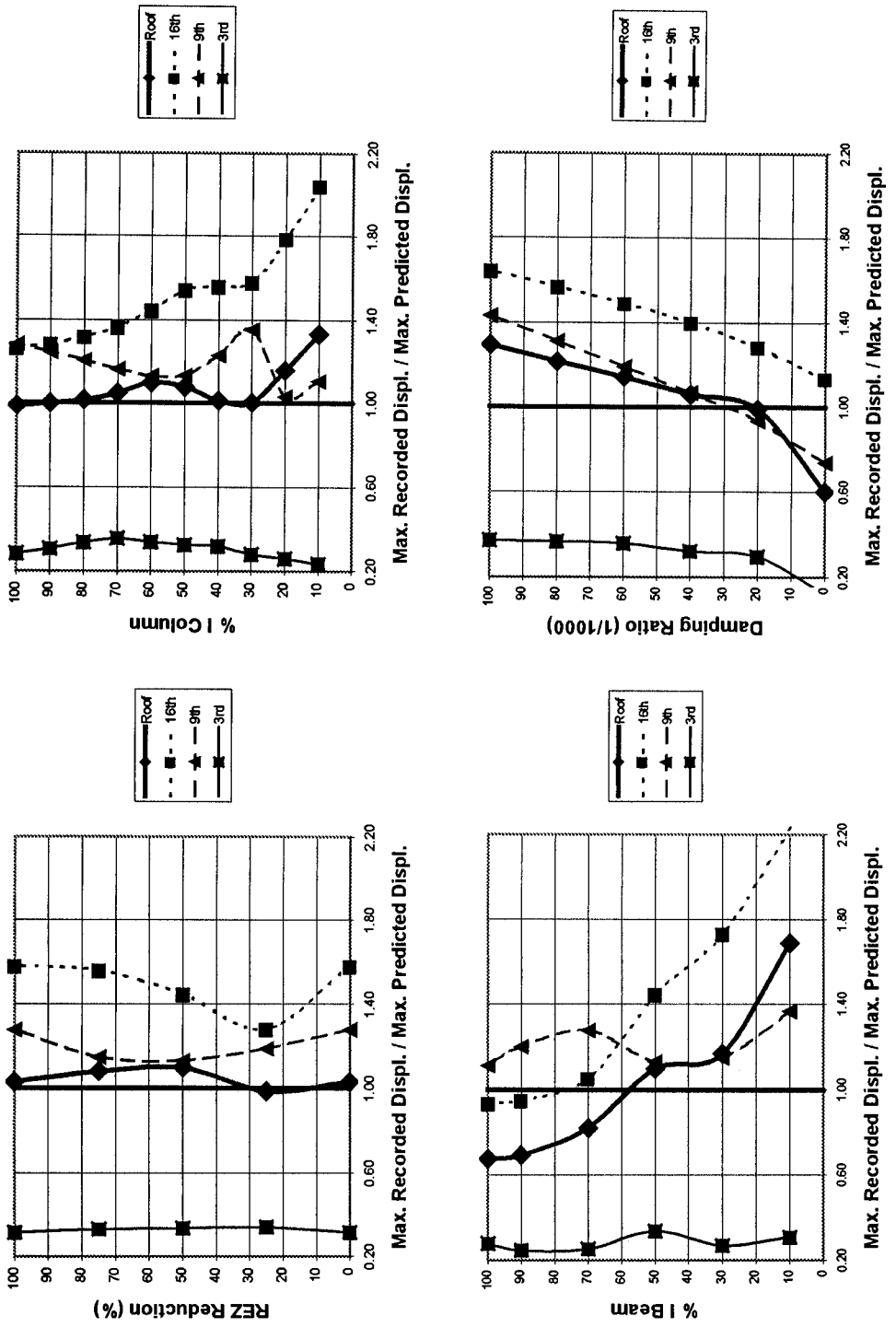

Figure 10 Story Maximum Recorded / Maximum Predicted Displacement Ratios – Whittier EQ. – North-South Direction

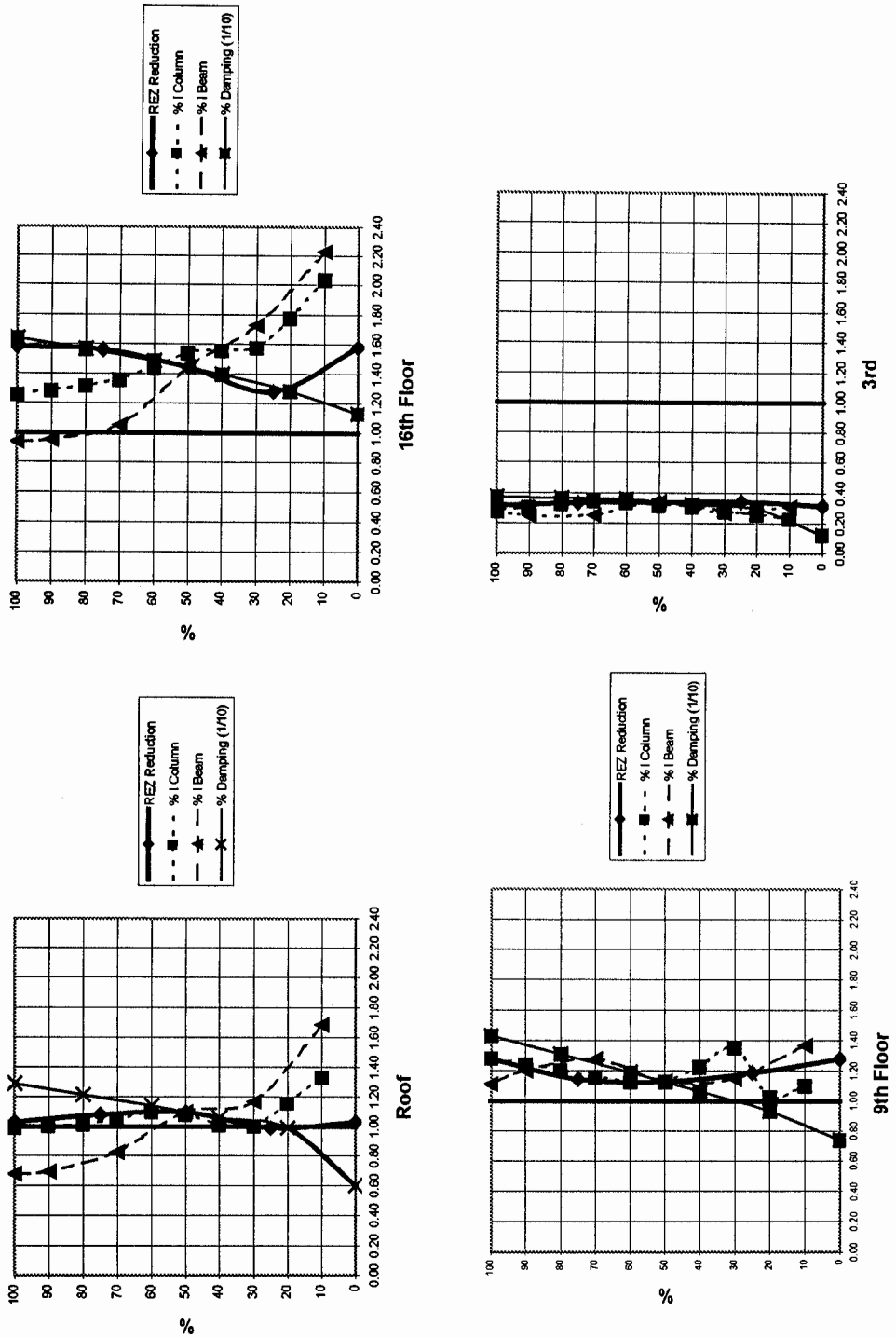

Figure 11 Maximum Recorded / Maximum Predicted Displacement Ratios – Whittier EQ. – North-South Direction

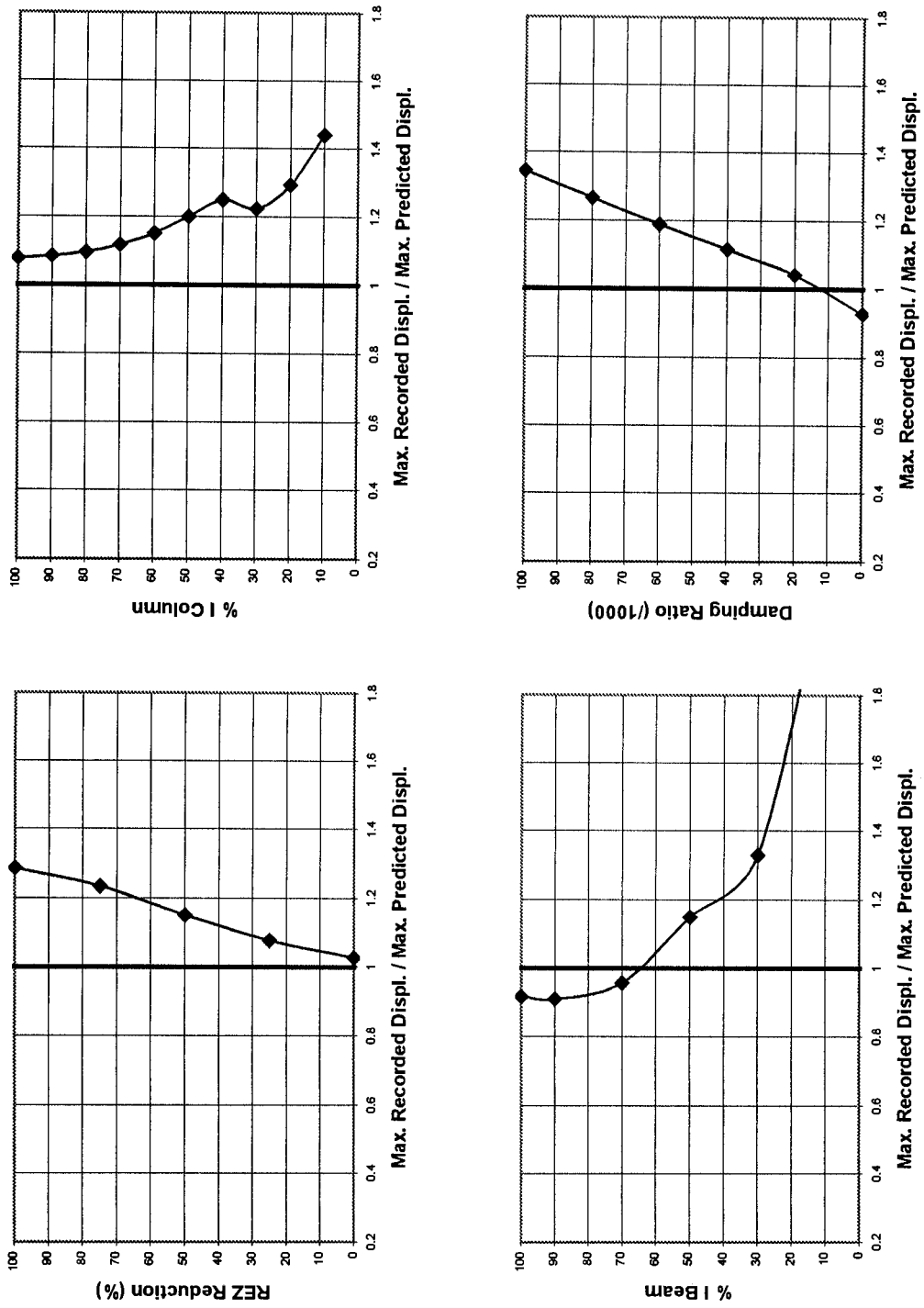

Figure 12 Roof Maximum Recorded / Maximum Predicted Displacement Ratios – Northridge EQ. – North-South Direction

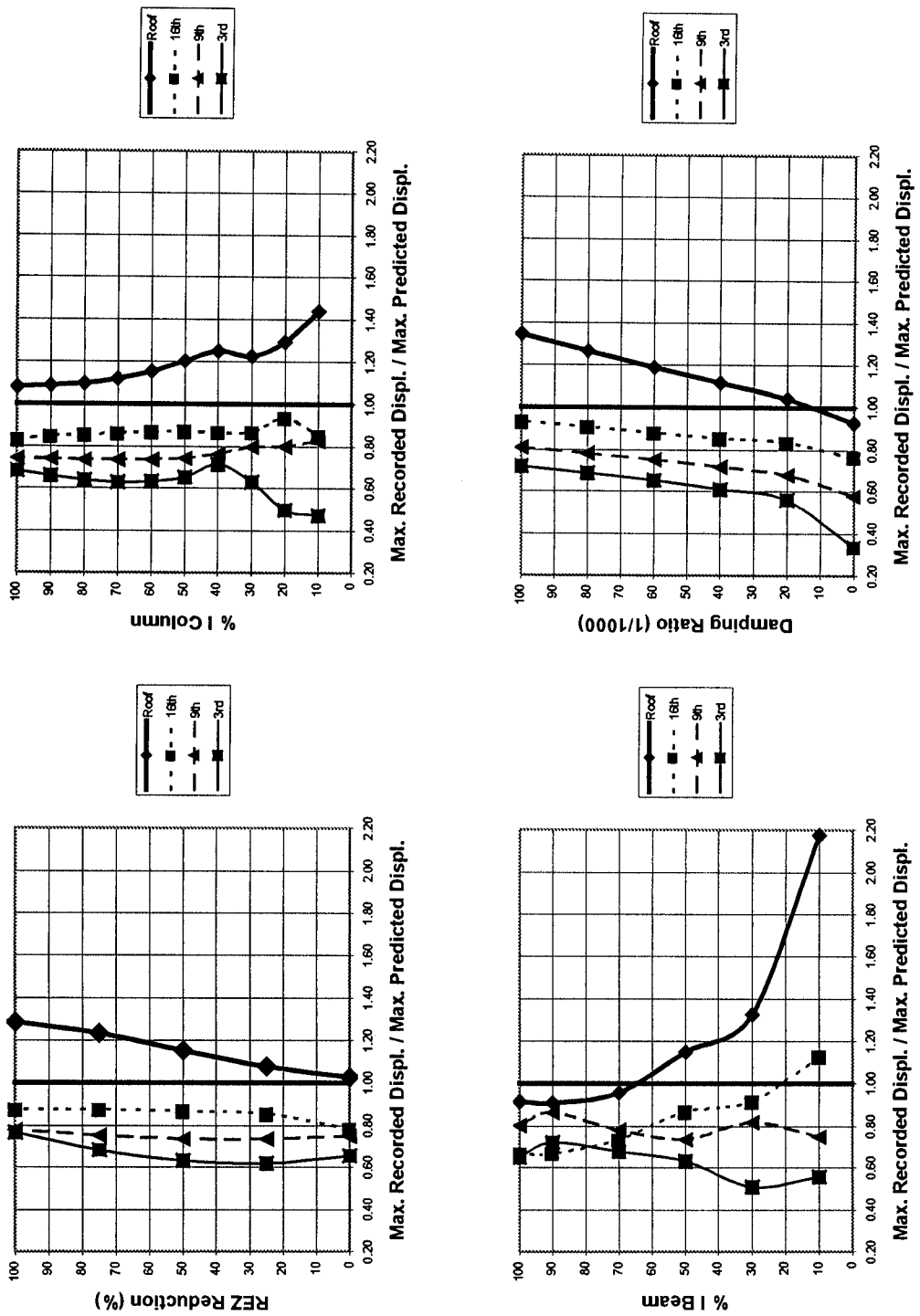

Figure 13 Story Maximum Recorded / Maximum Predicted Displacement Ratios – Northridge EQ. – North-South Direction

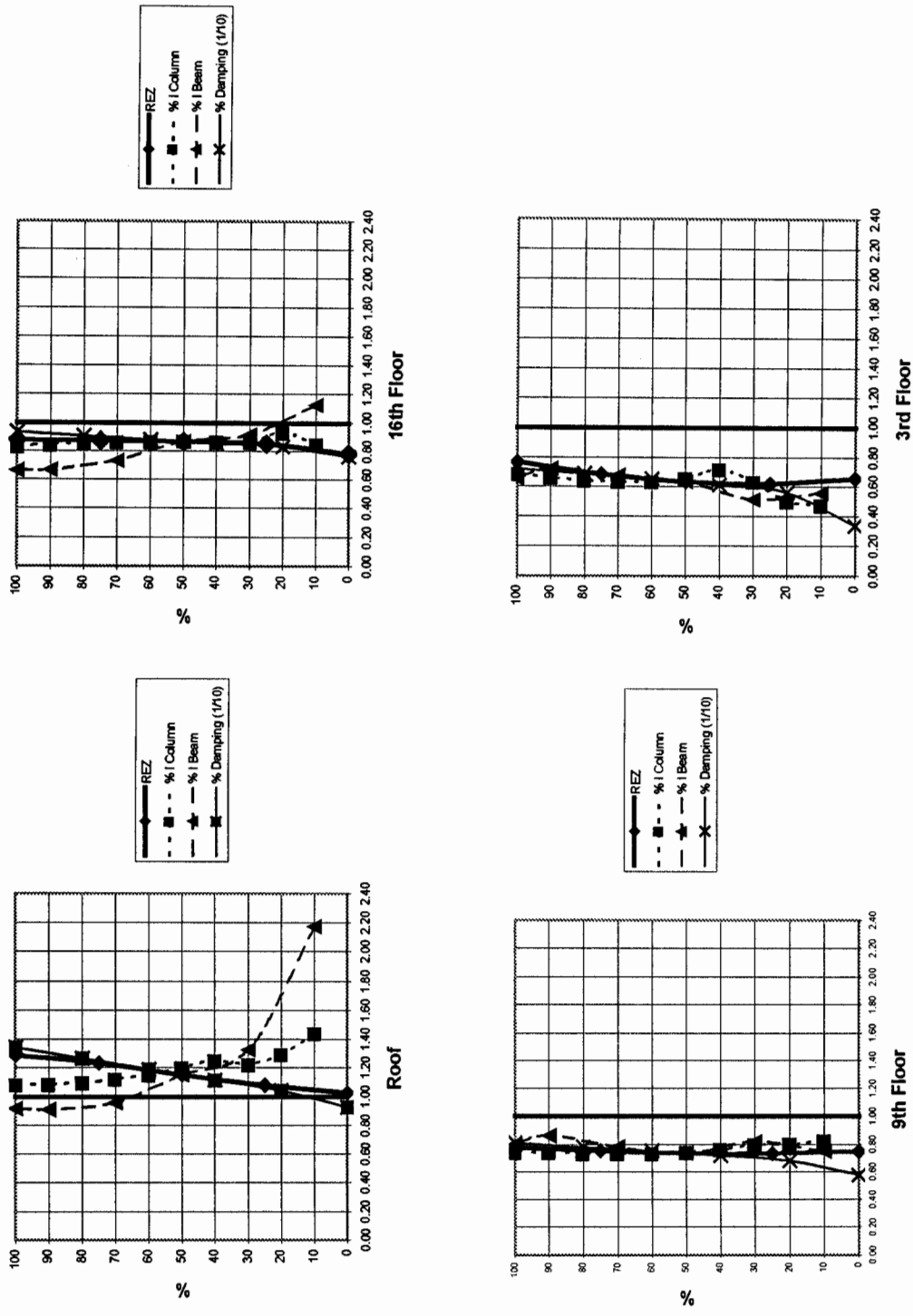

Figure 14 Maximum Recorded / Maximum Predicted Displacement Ratios – Northridge EQ. – North- South

ACKNOWLEDGEMENTS

Funding for this research was provided by the State of California, Department of Conservation, Division of Mines and Geology, Strong Motion Instrumentation Program (SMIP). The authors wish to acknowledge the assistance and commitment of Dr. Marshall Lew, Dr. Farzad Naeim, Prof. Gerard Pardoen, Dr. Tom Sabol, Dr. Roger Li, Dr. Roy Lobo, Ms. Julia Li, Ms. Mary Elise Richter, and Mr. Insuck Song through the course of this research. Dr. Moh Huang of SMIP was essential in obtaining the recorded motions and the structural/architectural plans for this building. The efforts of Ms. Mary Elise Richter in the preparation of this paper are greatly appreciated.

REFERENCES

ATC. (1997). *NEHRP Guidelines for the Seismic Rehabilitation of Buildings, Volume I, Guidelines*. FEMA 273. Federal Emergency Management Agency.

CSI (1997) "ETABS – Extended Three Dimensional Analysis of Building Systems – Nonlinear Version 6.21," Computers & Structures, Inc.

Goel, R.K. and Chopra, A.K. (1997). "Vibration Properties of Buildings Determined From Recorded Earthquake Motions," *Report No. EERC/UCB-72/22*, Earthquake Engineering Research Center, University of California, Berkeley, California.

Naeim, F. (1997). "Instrumented Buildings Information System, January 14, 1994, Northridge, California Earthquake, Version 1.0," John A. Martin & Associates.

Paulay, T. and Priestley, M.J.N. (1992). *Seismic Design of Reinforced Concrete and Masonry Buildings*, Wiley Interscience, 744 pp.

OES. (1995). California Office of Emergency Services, *Vision 2000: Performance Based Seismic Engineering of Buildings*. Prepared by Structural Engineers Association of California, Sacramento, California.

Saatcioglu, M. and Razvi, S.R. (1992). "Strength and Ductility of Reinforced Concrete," *Journal of Structural Engineering*, Vol. 118, No. 6, pp. 1590-1607.

Steinmann, H.G. (1998). Personal Communication.

Wallace, J.W. (1992). "BIAX: Revision 1 – A Computer Program for the Analysis of Reinforced Concrete and Reinforced Masonry Sections," *Report No. CU/CEE-92/4*, Clarkson University, Potsdam, New York.

Wing, W.C. (1968). "Hotel Pioneers Earthquake Code," *Engineering News Record*, Feb. 22.

THE CONSORTIUM OF ORGANIZATIONS FOR STRONG-MOTION OBSERVATIONS SYSTEMS (COSMOS) MISSION AND OBJECTIVES

Bruce A. Bolt, President

1. Introduction

Many present will remember, and even have taken part in, the sequence of meetings, working groups, committees, and report writings over thirty or more years that were aimed at funding, strengthening, and consolidating the diverse strong-motion instrument systems in the earthquake vulnerable parts of the United States. There was therefore widespread satisfaction with the announcement in 1998 that a Consortium of Organizations for Strong-Motion Observation Systems (COSMOS) had been formed. The decisive initiative was a National Science Foundation Vision 2005 report written during a 1977 national workshop, chaired by J. Carl Stepp. This initiative went hand in hand with a statement (October 1997) on the future of the U.S. National Strong-Motion Program, under the auspices of the U.S. Geological Survey, prepared by a committee chaired by Roger Borcherdt (*U.S.G.S. Open File Report 97-530B*).

A further auspicious alignment of interests took place with the preparation by the U.S. Geological Survey of a comprehensive review of seismic monitoring in the United States and the publication of "An Assessment of Seismic Monitoring in the United States: Requirement for an Advanced National Seismic System," (U.S.G.S., February 1999). This document went forward to the U.S. Congress with notable success. It dealt with all aspects of earthquake monitoring, including emergency response for volcanic eruptions, tsunamis, hazard assessment, and earthquake engineering. It considered seismographic observatories of the classical type, with sensitive seismographs providing continuous surveillance of earthquakes in the United States and around the world. But it also gave due weight to strong-motion monitoring systems with accelerometers, specifically designed to record the near-source ground motion associated with earthquakes greater than about magnitude 5. "An Assessment..." noted that strong-motion recordings provide "fundamental data for engineering design and construction practices and for seismic design criteria for building codes." It went on to state that "the primary data and results from the systems are records of strong shaking and empirical relationships, showing the attenuation of strong-ground shaking at increased distance from the source."

A part of the 1999 U.S. Geological Survey document was its brief history of the seismic monitoring networks in the United States. It noted that two distinct systems—for weak and strong motion—had developed in the country, growing out of differences in monitoring, research interests, and instrumentation. I would agree with this generalization, but remark that there have always overlaps, particularly at some seismological centers, among which I include the one I directed for almost thirty years at the University of California at Berkeley. In the UCB network, every attempt was made to operate a range of seismographs so that not only microscopic ground motions from remote earthquakes could be recorded, but also the very strong shaking near the source of even great earthquakes, such as the 1906 San Francisco earthquake.

In its assessment of the progress of the modernization of seismic networks, the U.S. Geological Survey report specifically mentioned COSMOS and its goal of providing a continuous link between the users of strong-motion data and organizations, both public and private and both state and federal, which operate strong-motion networks across the country. Its vision plan required combining and integrating seismographic monitoring on all scales, "with strong-motion recording and structural response monitoring focussed on urban areas of risk."

In a meeting in August 1999 in Colorado, called by Dr. John Filson for the U.S. Geological Survey, discussion took place on the report to Congress on the implementation plans for the Advanced National Seismic System. While the final report, stating the conclusions of this workshop is not yet to hand, they include an important role for COSMOS.

2. Purposes of COSMOS

Details on the mission and purposes of COSMOS are found in its Charter (attainable from the COSMOS office: COSMOS, c/o PEER, Bldg. 454, 1301 S. 46th Street, Richmond, California, 91804, and from the COSMOS web site, http://www.cosmos-eq.org/), which was adopted by professionals attending a meeting of the Stepp committee in Oakland, California, on 19 December 1997. Subsequently this Charter was endorsed by four core strong-motion systems operators: California Division of Mines and Geology, the U.S. Army Corps of Engineers, the U.S. Bureau of Reclamation, and the U.S. Geological Survey.

The COSMOS Charter sets out as a prime objective the reduction of the catastrophic effects of earthquakes in life and property, the protection of economic health, and public safety from future earthquakes. It mentions specifically:

(1) the acquisition and dissemination of critical sets of *in situ* measurements of damaging ground shaking and the resultant response of the built environment;
(2) the advancement of programs to acquire and disseminate the measurements, to develop adequate resources to acquire and disseminate rapidly strong-motion data, and to avoid missing infrequent earthquakes;
(3) the rapid dissemination of strong-motion information through the optimum use of modern technologies, including a virtual data dissemination system of national and international extent;
(4) the stimulation of the use of strong-motion data for design of new facilities and evaluation of existing facilities; and
(5) the advancement of the use of strong-motion measurements and information for post-earthquake response and recovery.

The urgent need for all these objectives has been brought home with terrible emphasis in the recent, tragic and devastating Izmit earthquake in Turkey (M_W = 7.4, 8/17/99). In the shaken region, our Turkish colleagues and their collaborators operated systems of strong-motion instruments. Even in such an emergency, they were able to make accelerograms of the strong ground motions available in digital form on the World Wide Web in the days immediately following the disaster. These records will be invaluable in future studies of the seismic shaking that caused the destruction.

3. The Incorporation of COSMOS

As mentioned above, the seminal Charter of COSMOS was prepared in final form by the end of 1997. Subsequent meetings of interested parties took place, which led to the decision in early 1999 at the Annual Meeting at the Earthquake Engineering Research Institute in San Diego, California, to set up a nonprofit public-interest corporation in the State of California, which would adopt the Charter and carry out its mandates. The need for such an independent, private corporation had emerged as essential after discussions of the ways in which funding could flow from members for support and expenses for COSMOS and its policy committees. In particular, the retention of an Executive Director, responsible for the development of the program, was believed to be essential; past efforts at integration often failed through weak administration and lack of coordination.

Consequently, in the first half of 1999, under an interim Board (President, Bruce A. Bolt, Secretary, William U. Savage, Treasurer, Chris D. Poland, and an Interim Executive Director, Carl Stepp) Bylaws were drawn up that meet California incorporation law and tax code, and are compatible with the Charter. In August 12, 1999, official confirmation of the Incorporation of the Consortium was received from the Secretary of State in Sacramento.

At the meeting tomorrow on 16 September 1999, COSMOS will have its inaugural General Meeting, with a much broader membership as here-for-too. The meeting has been advertised in brochures, on the World Wide Web (http://www.cosmos-eq.org/), and in the notification of the SMIP 99 meeting. It is expected that at that time a slate for the Board of Directors will be put before the members present; the Board of Directors will then elect officers according to the Bylaws of the Corporation. At the same time, some key committees, as foreshadowed by the Charter, will be put into place. These include the election of a Strong-Motion Program Board (SMPB) and a Senior Advisory Council (SAC). It is to be hoped that members present at the 15 September 1999 meeting of SMIP 99 interested in the future enhanced effectiveness of strong-motion systems in the United States will attend the General Meeting.

As this interim period comes to an end, a number of organizations must be thanked for grassroots support that enabled the organization to be established. First is the Pacific Earthquake Engineering Research Center (PEER), particularly Jack Moehle, Director, where COSMOS has an office. Secondly, we have had crucial financial support from contracts with the California Strong-Motion Instrumentation Program and with the U.S. Geological Survey, Roger Borcherdt helped in critical ways, as did Grant Lindley in setting up the World Wide Web for COSMOS. We have been given a computer system by the Bureau of Reclamation and financial grants from Pacific Gas & Electric Co., Degenkolb Engineers, and Kinemetrics, Inc. At the meeting at PEER on 16 September, members will be asked to confirm a fee schedule for differing categories of membership in order to maintain the Consortium as an active partner in meeting the challenge of earthquake loss reduction in the U.S. over future years. The help of everyone present here and of the organizations many of you represent is earnestly solicited.

4. Future of COSMOS

Even while COSMOS was being constructed, it has been active in a number of ways. There is clearly much to do and it will be a busy time in the year ahead. First and foremost will be policy contributions to the establishment of the Advanced National Seismic System after Congress appropriates funds to the U.S. Geological Survey. COSMOS representatives will take a significant place in the organizational structure of the National System.

COSMOS has already started on the development of a model for a virtual strong-motion data center for data dissemination through the Internet. The organization is grateful to Ralph Archuleta, Roger Borcherdt, and Anthony Shakal for acting as a Working Committee on this project. In a few minutes, the meeting will hear about their findings.

Finally, COSMOS has been concerned even at this early stage with the definition of standards for the various networks that comprise the variety of systems of strong-motion accelerometers and associated instruments across the country. It has also taken preliminary steps to integrate the U.S. systems with those of our neighbors in the Americas and overseas.

I assure the membership that the present officers and those that emerge from the meeting tomorrow envisage a vigorous attack on the problems of strong-motion recording in the U.S. As the new millennium unfolds, we look forward to a much more effective national strong-motion program to serve the scientific, engineering, and emergency-response interests of the country.

TOWARD A COMMON FORMAT FOR STRONG-MOTION DATA

A.F. Shakal, California Strong Motion Instrumentation Program,
Calif. Dept. Conservation/Div. Mines & Geology
and

R.D. Borcherdt, National Strong Motion Program,
United States Geological Survey

Abstract

The need for a common format for the earthquake engineering use of strong-motion data has become increasingly apparent during the last several years. An early goal of the Consortium of Organizations for Strong Motion Observation Systems is the development of a consensus format for data products. The current number and variety of formats arose largely through the nature of the growth of strong motion recording and processing. As new networks or processing facilities began many produced data in a format of their own convenience since no standard had been established. As a first step toward developing a common format, a Format Working Group met at PEER in January 1999.

The introduction of new standard formats should bear positive results in data exchange for both the data-producing organizations and the data users. A common format does not bar the use of individual formats by data producers, but rather provides for a common, minimum basic format for use of strong-motion data in earthquake engineering. Once a common format achieves adequate consensus, converters are planned to be made available at the COSMOS Virtual Data Center which will perform translations of data formats, so that from a user perspective, the data will appear to be all of one "virtual" format.

Introduction

Analysis and study of strong-motion data has been important since the first strong-motion records were obtained in the 1933 Long Beach earthquake. Early strong-motion records were processed by various means, including manual numerical integration and mechanical analyzers. As digital computers became more common in the 1960s, attempts to process the records using digital computers became common. Several important records had been recorded, including the 1940 El Centro record, which led to a variety of studies but the digitized data was not distributed in a standard format. Since those beginnings, a large number of records have been recorded. A large number of data formats have also come into use, making the translation of data between formats cumbersome and limiting. As more data becomes available, either more translation will be necessary, or the data will not be put to its fullest use. This makes conversion, sometimes called filtering, between formats more and more important.

Conversion or Filtering Between Formats

Before considering individual formats or possible standards, it may be beneficial to consider a framework for the release of data in a common format. This will also put into perspective the role of individual formats in this framework.

A schematic of the interaction between existing formats and a common format is shown in Figure 1. In this scenario, data produced by networks or researchers would be converted to a common format, either at their facility or at the COSMOS Virtual Data Center. Converters, or filters, would be built that perform the conversion between the original formats and the common format. Once the data can be converted in this way to the common format, everyone can use the data without further difficulty.

An additional aspect is derivative-product formats. For example, a post-converter could be made available that would convert the standard format to that needed, for example, by SAP, for structural analysis projects, or by Shake, for site response projects.

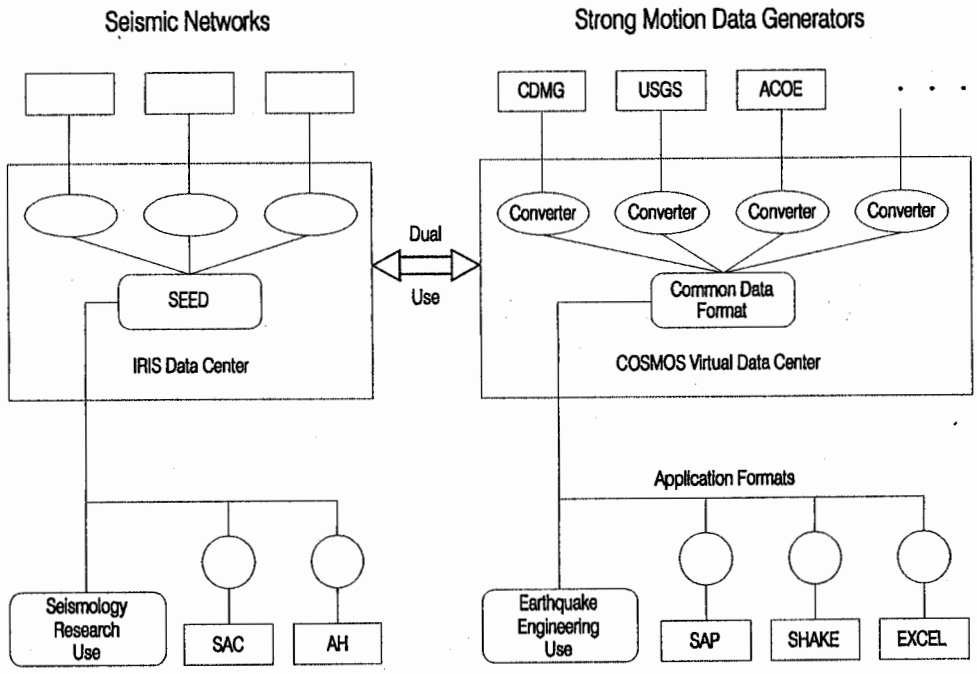

Figure 1. Schematic diagram showing the proposed interaction between strong motion network data production and a common strong motion format on the right, the parallel arrangement in place for seismic data on the left, and the connection between the two.

The most important secondary conversion would be the conversion to and from the main format used by IRIS (Institutions for Research in Seismology) and other seismological

networks, called SEED (Standard for Exchange of Earthquake Data). The use of SEED by IRIS for seismology research data in many ways parallels the framework proposed for strong-motion data conversion and use in earthquake engineering.

A common format allows convenient "dual use" of recorded data. If data recorded by strong-motion networks can be converted between SEED and the strong motion format, the path is paved for dual use of the data recorded. That is, low level data recorded by traditional strong motion networks, for whom the data may only be of secondary interest, can, through the use of a common format, easily be converted to SEED, and from that to SUDS, GEOS, or any other format, making the data convenient for effective utilization by a wide range of investigators. Similarly, data recorded by seismic networks with broadband instruments that record data of potential value in earthquake engineering can convert the data in a single translation, from SEED to the common strong motion format, and the data will be available for use in earthquake engineering. This linking between a common strong motion format and a common seismology format is important for the advance of both earthquake engineering and seismology research.

A necessary component for the model in Figure 1 to come into being is the development of a common format for strong motion data that is accepted by an adequate number of data producers. In order to move toward that goal, it is useful to review the existing formats and their evolution.

Standardized Processing - Caltech Blue Book Project

Until the late1960s, there was no standard processing or formatting of strong-motion records. The Coast and Geodetic Survey obtained many records, but a need developed for standardized processing, so that investigators would be analyzing the same time histories and spectral inputs in various engineering and or response studies. The records obtained from El Centro in 1940, Kern County in 1952, and Parkfield in 1966 made clear the need for uniform processing, particularly because of the unexpected amplitudes and spectral levels

A project initiated in 1969 at Caltech with National Science Foundation funding focused on computer processing of all records available at the time in a standardized way (e.g., Hudson et al., 1969; 1971). The San Fernando earthquake occurred during the course of the project and caused a large increase in the number of records and included the largest motions recorded up to that time.

The Caltech project was very productive, and the series of reports produced, all in blue cover, gave the project its unofficial name, "Blue Book". The complete results were released by means of printed reports as well as by computer tapes and cards, which allowed major progress by many investigators performing analytical studies of the data. The records processed during this period were the foundation of many studies in the following years.

Standard Data Products

The results of processing were released in the Blue Book project at several specific processing stages and the names for these have become traditional:

- Volume 1 Raw acceleration as digitized, usually given as acceleration-time pairs, and expressed in units of acceleration; no instrument correction or filtering applied. The background and original output format are described in Hudson et al. (1969).

- Volume 2 Processed or "corrected" acceleration, velocity and displacement; the final time-history product. The acceleration, velocity and displacement all have constant time steps, though they may be different. Important parameters describing the processing steps are also included. The original format of these files is given in Trifunac and Lee (1973).

- Volume 3 Spectral data, including response spectrum values for five damping values (0, 2, 5, 10, and 20%) and 91 periods (from 0.04 seconds to 15.5 seconds). Spectral acceleration (Sa), velocity (Sv) and displacement spectra (Sd), and pseudo acceleration (PSA) and velocity (PSV), and Fourier amplitude spectra are included in the file.

Several additional numbered products were generated during the Caltech project, but they are not commonly used today. Nearly all strong motion programs, worldwide, currently generate these three primary products. These three products are sometimes denoted as Phase 1, 2, 3 rather than Volume 1, 2, 3 data (e.g., Brady et al., 1980).

One of the benefits of the Blue Book project was that all the data was released with a standard format. As a result, when the project ended the vast majority of strong motion data, world wide, was available in a single format. For the first time, many investigators could study all of the data, and with a single program analyze records from many earthquakes, recorded by many agencies.

As a result of the growth of networks and processing centers, by early 1990s the situation was much changed from the early 1970s. There was now a variety of formats, some very close to the Blue Book format, and some quite different. The format used by CDMG is given in Shakal and Huang (1985), and Brady and Converse (1992) discuss a format used by the USGS.

This problem was an early focus of the Consortium of Organizations for Strong Motion Observation Systems (COSMOS), and in fact was one of the factors motivating the creation of the consortium. The creation of COSMOS, and the initial development of a Virtual Data Center described in these proceedings, puts strong motion data exchange on the threshold of new effectiveness and user convenience.

The Virtual Data Center being developed will allow convenient access to data recorded by different networks. But the current individual formats will limit and hold back the possible advances. There is a clear need for a common, standard format. For a common format to be established, certain basic properties are suggested.

Properties of a Standard Strong Motion Format

A successful common strong motion data format for earthquake engineering use needs to have a certain set of properties, and several of these properties are suggested below.

1. The format must include a minimum set of information about the record, the recording station, the recording instrument, and the causative earthquake.

2. Data in the format should be readily convertible to the most common formats used in seismology research (SEED, or mini-Seed), and thus to other seismological formats (SUDS, GEOS, SAC, etc.). The data should also be readily convertible to common engineering applications formats (SAP, Shake, etc.) as well basic applications tools like spreadsheets (Excel).

3. The format should include an adequate amount of text and information at the beginning to provide the user key information and assurances about the data

4. The format should have easily accessible information for use in metadata information collections and databases.

5. The format should share as much as possible with the legacy formats, and be consistent with past evolution. The format should also be convertible back to the old formats, so legacy programs can use newly recorded data.

6. The format should have adequate resolution, or precision, so there is no loss of accuracy in the data being written, to control noise source and propagation. The format needs to handle very small motion, since current earthquake engineering research often extends to very low levels of motion (e.g., studies of linearity).

7. The format should be flexible, to allow a range of inputs and allow tomorrow's data, if possible. It should accommodate physical parameters in addition to acceleration (relative displacement, pore pressure, etc.) at the Volume 1 level.

8. The format should, so far as possible, meet the needs of groups across the strong motion community, world wide, and allow the expression of aspects which are unique to specific seismic and political environments.

Early strong motion format design in the Blue Book project was quite deliberate, with the needs and convenience of the users firmly in mind. It is suggested that this focus on user needs and convenience should be preserved in arriving at a new common format.

Structure of Proposed Format

Consistent with the original Blue Book format design, it is suggested that the file format for Volume 2 data, the most commonly used data, have the two main sections: a header followed by data, with the header made up of three parts: text, integer, and real valued:

A. Header Section
   1. Text section
   2. Integer values section
   3. Real values section

B. Data Section
   1. Acceleration segment
   2. Velocity segment
   3. Displacement segment

A1. Text Section of Header

The purpose of the text header is to provide information that is intrinsically textual in nature, for use in titles and labels of plots, and for human reading. It is proposed that the length and information content in this section be at the discretion of the data generator, as long as the required basic information is present. The required fields, such as station name, earthquake name, etc., need to be present and in the prescribed locations. The first line of the text section should include the number of lines contained in the text section. For reference, a text header from the Blue Book series is included in Appendix A.

A2. Integer Section of Header

The integer section provides items of information about a record that are intrinsically integer. The data-generating agency may include as many parameters as desired, provided that a minimum set of defined parameters are present. The Blue Book format allowed for 100 integer parameters at the Volume 2 stage. In any case, the number of parameters should be given as one of the parameters. A list of proposed integer parameters is included as Appendix B.

A3. Real Section of Header

The real-values section provides information that is intrinsically real. As for the integer-values section, the data-producer may include as many parameters as desired, provided a minimum set of parameters are present. A proposed list of real-valued parameters is given in Appendix C. Many of the parameters also appear in previous formats, but some need to be augmented or redefined for the new digital data types.

The data follows the header section, and the three data segments comprise the greater part of the data file. The first line of each data segment contains basic information about the data points that follow in the file:

- the number of data points in the segment, N;
- the sampling rate (no. of points per second);
- the physical units of the data, and
- the numeric format in which the data is written, n points per line.

Note that including the numeric format here allows the format to be specified to match the precision or accuracy of the data itself. For example, some formats use a format of 10F8.3 (i.e., 10 values per line, each 8 digits wide, with 3 decimal digits of precision for acceleration). Thus, values could range from +/- 1.000g down to +/-0.001g. For modern digital recorders, this resolution is not adequate. But with a dynamically-specifiable fixed numeric format, the data producer can write the data in the most appropriate format, as 5F15.7 for example, preserving the resolution. The user's program must then read the format before it reads the data. With this approach, flexibility and preservation of accuracy is maintained.

Overall File Structure

It has been suggested that a strong motion data file contain data for only one component of an accelerogram. That is, the accelerogram from a 3-channel freefield accelerogram would be contained in three files, one for each component. For a structural record, which may have 20 channels, for example, the data will be released as 20 separate files, each containing one channel. Several parameters specific for structures are included in the parameter specifications; these would be blank or zero for non-structural stations.

The format of Volume 1 and Volume 3 files can be specified in a similar way, and the headers would be largely coincident with the Volume 2 header. The Volume 2 format is used as an example; the principles agreed to for that format would carry forward to the other files.

More fundamental files than the user-oriented data products discussed here are also needed. These files contain the data in the most raw and elemental way; the data in these files would still be in digital counts as recorded, for example. In the context of the products discussed here, they could be referred to as Volume 0 files, since they are precursors to the Volume 1 files. These files would be maintained by the data-generating agencies. Their format need not be common, since they are specific to the instruments and network configurations of a specific network. Nonetheless, they can be archived as the most basic record, much like accelerogram film itself is preserved for analog recorders, even though the film has been digitized and the data has been processed and released. These fundamental files will not interfere with the common data format for earthquake engineering users, which is the focus of this effort.

Summary

A common format for strong motion data is needed to allow effective utilization of the data being recorded by the various networks in the United States and worldwide. This does not require data-generating agencies to stop using the formats they are currently using, but only requires that a common standard be agreed to, and that converters be available to convert data from their formats to the common format. From a user perspective, this step will represent a breakthrough in the convenient and rapid of new data. Definition of this format, with adequate flexibility and power to handle past data and needs of the present and immediate future, is an important task to accomplish. Some suggestions toward that goal are included here from an initial Workshop. The next steps include broad input from a larger user workshop, and finalization of a proposed format by a COSMOS and its member agencies.

Acknowledgements

The ideas and suggestions from the Working Group were important to the progress to date. Participants included N.Abrahamson and W. Savage (PG&E), R. Graves (Woodward Clyde), A. Tumarkin (UCSB), W. Joyner (USGS), M. Huang and V. Graizer (CDMG) and the authors.

References

Brady, A., V. Perez and P. Mork (1980). The Imperial Valley earthquake, October 15, 1979, Digitization and processing of accelerograph records, U.S. Geological Survey, Seismic Engineering Data Report, Open File Report 80-703.

Converse, A.M. and A.G. Brady (1992) BAP: Basic strong-motion accelerogram processing software, USGS Open File Report 92-296A.

Hudson, D., A. Brady and M. Trifunac (1969). Strong-motion earthquake accelerograms, digitized and plotted data, Vol. I, Parts A-Y, Calif. Inst. Technology, EERL reports.

Hudson, D., A. Brady, M. Trifunac and A. Vijayaraghavan (1971). Strong-motion earthquake accelerograms, Corrected accelerograms and integrated velocity and displacement curves, Vol. II, Parts A-Y, Calif. Inst. Technology, EERL Reports.

Shakal, A. and M.J. Huang (1985) Standard tape format for CSMIP strong-motion data tapes, CDMG/SMIP Report OSMS 85-03, 26 pp.

Appendix A - Example Header

(For purposes of illustration, a header from a data file produced during the Blue Book project is shown. The record happens to be the Pacoima Dam record from the San Fernando earthquake of 1971.)

```
CORRECTED ACCELEROGRAM  IIC041  71.001.0    COMP S16E   FILE  1 CORRESPONDING TO
FILE   1  OF UNCORRECTED ACCELEROGRAM DATA OF VOL. I-C, EERL 71-20
SAN FERNANDO EARTHQUAKE
FEBRUARY 9, 1971 - 0600 PST
IC041   71.001.0 R                                                    18
STATION NO. 279   34 20 06N,118 23 48W                               38
PACOIMA DAM, CAL.                                                     17
COMP S16E                                                             9
SAN FERNANDO EARTHQUAKE   FEB 9, 1971 - 0600 PST                      48
EPICENTER  34 24 00N,118 23 42W                                       31
INSTR PERIOD   0.0510 SEC  DAMPING   0.544                           42
NO. OF POINTS   3002  DURATION   41.822 SEC                          43
UNITS ARE SEC AND G/10                                                22
RMS ACCLN OF COMPLETE RECORD   1.1934 G/10                            42
ACCELEROGRAM IS BAND-PASS FILTERED BETWEEN   0.070  AND  25.000  CYC/SEC
  2091  INSTRUMENT AND BASELINE CORRECTED DATA
AT EQUALLY-SPACED INTERVALS OF   0.02   SEC.
PEAK ACCELERATION   -1148.06055  CMS/SEC/SEC AT   7.7400 SEC
PEAK VELOCITY        -113.23398  CMS/SEC     AT   3.0400 SEC
PEAK DISPLACEMENT      37.66193  CMS         AT   7.7800 SEC
INITIAL VELOCITY        1.22996  CMS/SEC        INITIAL DISP.       0.42512 CMS
SAN FERNANDO EARTHQUAKE   FEB 9, 1971 - 0600 PST

IIC041  71.001.0   PACOIMA DAM, CAL.   COMP S16E

       1        1        3       41       71        1        0        5      279       34
      20        6      118       23       48       34       24        0      118       23
      42        2        9     1971      600        0      164     3002       23       17
       0        0        0        0        0        0        0        0        0        0
       0        0        0        0        0        0        0        0        0        0
    3002     3004     2091        2       10       10        1        0       48       48
      10       10        2     1046        5      419        0        0        0        0
       0        0        0        0        0        0        0        0        0        0
       0        0        0        0        0        0        0        0        0        0
       0        0        0        0        0        0        0        0        0        0
 0.05100  0.54400 41.82199  1.19340  0.10000  0.0      0.0      0.0      0.0      0.0
 0.0      0.0      0.0      0.0      0.0      0.0      0.0      0.0      0.0      0.0
 0.0      0.0      0.0      0.0      0.0      0.0      0.0      0.0      0.0      0.0
 0.0      0.0      0.0      0.0      0.0      0.0      0.0      0.0      0.0      0.0
 0.0      0.0      0.0      0.0      0.0      0.0      0.0      0.0      0.0      0.0
 1.00000  0.01020  0.01000 41.82199 123.19958  1.00000  1.00000 27.00000  2.00000 41.79999
 0.02000  0.07000  0.02000  0.0      7.74000 148.06055  3.04000 -113.23398  7.78000 37.66193
 1.22996  0.07000 25.00000  0.20000  0.20000  0.42512  0.0      0.0      0.0      0.0
 0.0      0.0      0.0      0.0      0.0      0.0      0.0      0.0      0.0      0.0
 0.0      0.0      0.0      0.0      0.0      0.0      0.0      0.0      0.0      0.0
    -78      -260     -122      259      -72     -208      306     -258     -341      371
   -295      -341      362     -249     -183      369      311     -144      -71      146
    -36        40      527       28     -715      183     1029      719      119     -254
   -594      -433       16      432      330       23       24     -149      -60      225
    409       -40     -814     -224      233      104      931      797     -425     -943
```

Appendix B - Integer Parameters (Interim)

	Parameter Description
1	Accelerogram channel number
2	Processing stage index of data
3	Station channel number
4	Number of channels in record (i.e., recorder)
5	Total number of channels at station (i.e., in recording system)
6	Original data sampling rate (samples per second if digital; -1 if analog)
7	Event identification code: 0 for mainshock, 1,2,3,.. for aftershocks, etc
8	Recorded medium code (index for film, tape, solid-state, etc.)
9	Code for network/agency operating network that recorded this record
10	Code for network/agency that owns the instrumentation at this station
11	Code for network/agency that processed this record
12	Station number assigned by Network/Agency
13	Unique station number assigned by COSMOS
14	Station type code (index for FF, Bldg, Bridge, Special array, other)
15	COSMOS data format version number for this file (3 digits)
16	Number of elements in this Integer header (e.g., 100)
17	Number elements in Real Header (e.g., 50 for Vol.1; 100 for Vol.2)
18	Accelerograph recorder type code
19	Sensor Type code
20	Units of raw Vol.1 data (index for g, cm/sec, etc)
21	Full-scale output of sensor (nominal; actual sens. n Real parameter 6)
22	Gain of this channel (1,2,4,8, etc)
23	Sample word length as originally recorded (number of bits)
24	Effective number of bits, if different
25	Orientation code for sensor for this channel
26	Orientation of sensor with respect to Reference direction
27	Number of raw acceleration points
28	Number of letters in earthquake name
29	Number of letters in station name
30	Number of letters in earthquake title line
31	Azimuth of Reference North of a structure, if applicable
32	Azimuth of accelerograph connector, for a FF accelerograph
33	Number of Vol.1 acceleration points in record (same as param. 27 in cases of equally-spaced Vol.1 data)
	Record start time:
34	Hour (GMT)
35	Minute
36	Second

37 Fraction of second (integer, msec)
38 Julian day of year
39 Month
40 Day of month

41 Year (inferred if necessary, 4-digit)
42 Time quality indicator (0-10)
43 Time source indicator
44 Event number of this record (in recorder)
45 Recorder serial number
46 Number of recorders in recording system at station
47 Recorder System serial number (if appropriate)

Additional parameters only appear for Vol.2 and Vol.3 files:

48 Number of Vol.2 acceleration data points
49 Desampling factor from Vol.1 to Vol.2
50 Decimation factor, if any, in long-period filtering of acceleration

51 Decimation factor, if any, for long-period filtering of velocity
52 Decimation factor, if any, for long-period filtering of displacement
53 Number of velocity points
54 Number of displacement points
55 No. of periods for which response spectra are computed
56 No. of damping values for which response spectra computed (typically 5)
57 Low-cut filter type, Vol.2 (1=Ormsby, 2=Cos bell, 3=Butterworth, ..)
58 Order of low-cut filter (if Butterworth, etc)
59 High-cut filter type, Vol.2
60 Order of high-cut filter
61 Frequency domain/time domain filtering flag (1 if filter applied in time domain, 2 if applied in frequency domain)
62-100 --

Appendix C - Real-Valued Parameters (Interim)

Description

1 Natural period of transducer (seconds)
2 Damping of transducer (fraction of critical)
3 Length of record (in seconds, Vol.1)
4 RMS value of record (in g)
5 Units of Vol.1 acceleration (fractions of g)
6 Sensitivity of transducer (cm/g for film recorder; for acceleration sensors, mvolts/g; for other sensors, volts per motion unit)
7 Peak acceleration (Vol. 1) for this channel (in g)
8 Time of peak acceleration value (seconds after start)
9 Natural frequency of transducer (in Hz)

Record Resolution Parameters:
A) For digitized film records (i.e., integer parameter 8 = -1):
10 Digitizer y-step (acceleration) size, in microns (cm/10000)
11 Digitizer y-step, in milli-g
12 Digitizer x-step (time) size, in microns (cm/10000)
13 Actual average time step of digitized record, in milliseconds
14 Standard deviation of time step, in milliseconds
15 Minimum time step size, as digitized (milliseconds)
16 Maximum time step size, as digitized (milliseconds)

B) For digital records (i.e., integer parameter 8 > 1):
10 LSB, in millivolts or microvolts (i.e., mv or uv/count; see param. 12)
11 LSB, in milli g or micro g (i.e., mg or ug/count; see param. 12)
12 LSB units code (1=mv/mg; 2=microvolts/micro g)
13 Sample interval, delta t (in msec)
14-16 --

17 Full scale output (volts) of sensor
18 Pre-event memory (PEM) length for recorder (seconds)
19 Post-event time for recorder (seconds)
20 Latitude of station (North positive)
21 Longitude of station (West negative)
22 Elevation of station (meters)
Earthquake location parameters
23 Latitude of earthquake epicenter (North positive)
24 Longitude of earthquake epicenter (West negative)
25 Depth of hypocenter (km)
Earthquake magnitudes
26 ML

27 Ms
28 Mw
29 mb
30 Other magnitude

Parameters values for Vol.2 and Vol.3 files:

31 Scaling factor for converting acceleration from Vol.1 units to cm/sec/sec (e.g., 98.0665)
32 Time step of Vol. 2 acceleration data (sec)
33 Length of Vol.2 acceleration time series (secs)
34 Termination frequency of high-cut filter (Hz), if Ormsby
35 Roll-off width of high-cut filter (Hz), if Ormsby
36 Length of Vol. 2 output (secs), after resampling to dt given in param. 32
37 Roll-off corner frequency (3 dB point) of low-cut filter (Hz); for non-Ormsby filter
38 Roll-off width of low-cut filter (Hz), if Ormsby
39 Time of peak acceleration (Vol. 2), seconds after start
40 Peak acceleration value (Vol. 2), cm/sec/sec
41 Time of peak velocity (secs after start)
42 Peak velocity (cm/sec)
43 Time of peak displacement (secs after start)
44 Peak displacement (cm)
45 Initial velocity value (cm/sec)
46 Roll-off corner frequency (3 dB point) for high-cut filter (Hz); for non-Ormsby filter
47 Velocity time step (sec)
48 Displacement time step (sec)
49 Initial displacement (cm)

Duration measures:

50 Bracketed, seconds over 5%g
51 5-95% Duration
52 5-75% Duration
53 Other duration
54 Arias Intensity
55 CAV (m/s)
56-100 --

ON THE DEVELOPMENT OF "USER-FRIENDLY" INTERFACES FOR THE USE OF STRONG-MOTION DATA ON THE INTERNET

R.D. Borcherdt, U.S. Geological Survey
A. Shakal, California Division of Mines and Geology

ABSTRACT

Public earthquake safety must necessarily be based on measurements in and of the built environment to damaging earthquake ground motions. Development of procedures for data archival and dissemination, based on rapidly evolving modern computer technology, can significantly improve data accessibility and usability for purposes of improving construction of an earthquake resistant environment. An essential component of such procedures is a flexible data format structure that will facilitate data archival and dissemination to a wide variety of research and practicing communities focused on improving public earthquake safety. It must be a structure that provides a standard for archive and exchange of data with other data centers, yet a structure that will permit the data to be retrieved and analyzed in a variety of "user-friendly" forms on the Web. Examples illustrating possible future "user-friendly" interfaces for presentation and analysis of strong-motion data are presented. The examples presented are intended to suggest a direction for development of "user-friendly" interfaces to facilitate dissemination and use of strong-motion measurements of the built environment for purposes of public safety. Pursuit of this objective, taking advantage of advances in computer technology and the Internet is an important goal of COSMOS.

INTRODUCTION

Recent earthquakes especially those effecting the United States, Japan, and Turkey emphasize the urgent need to improve public safety through improved design, retrofit and construction practice. Public earthquake safety must necessarily be based on measurements in and of the built environment to damaging earthquake ground motions. Strong-motion recordings provide the essential quantitative in-situ measurements needed to improve design and construction practice. Consequently, development of improved capabilities to acquire, disseminate and interpret strong-motion recordings of the built environment is crucial for improvements in public safety.

Recent advances in computer technology and the Internet offer dramatic new opportunities to facilitate the use of strong motion recordings for purposes of improving public safety. Concepts for a "Virtual Data Center" are presented by Archuleta and others (this volume). An essential component of such a Data Center is a modern data format standard that will facilitate data archival and dissemination to a wide variety of research and practicing communities, as discussed by Shakal and Borcherdt (this volume). In addition, the standard needs to permit the rapid transfer of the data to "user-friendly" formats developed to facilitate its use for improvements in public safety.

Attributes for a format standard for use in the context of a Virtual Data Center focussed on improved public earthquake safety are discussed by Shakal and Borcherdt (this volume). The format structure must include formats presently being used by contributing strong-motion

agencies. It must include a general format standard appropriate for future data archival and exchange with other data centers, such as the IRIS DMC. Inclusion of a variety of "user-friendly" procedures for interactive data retrieval and interpretation via the Internet can significantly improve data accessibility by the practicing communities. Because strong-motion data is the basis for modern design and construction codes, examples are chosen to emphasize aspects considered important for facilitating the use of the data by the practicing community.

EXAMPLES OF "USER-FRIENDLY" INTERFACE ON INTERNET

An important aspect of the "Virtual Data Center" being developed for consideration by COSMOS is the concept that the actual data will be maintained in linked databases maintained by contributing agencies. This aspect is important for maintaining data quality, for accomplishing agency mission, providing appropriate agency credit, and maintaining agency responsibility for data quality. Presently data stored at the centers is stored in different formats. Consequently, an important aspect of facilitating the use of strong-motion data is the development of a format structure to accommodate these differences. It must provide a standard for exchange of data with other centers and for the dissemination of "processed" data to the practicing community. It also must permit the data to be presented in a variety of "user-friendly" forms to simplify and facilitate its use by a wide variety of communities concerned with public safety.

Modern software tools and Internet capabilities offer significant opportunities to improve capabilities to use and interpret strong motion data. Examples are provided to illustrate the nature of "user-friendly" environments that have been developed. If space permitted, a number of additional examples also could be shown. Examples are chosen to illustrate possible future "user-friendly" interfaces that might be implemented as part of the capabilities of the COSMOS Virtual Data center to facilitate use of the data for public safety.

A relatively recent data search and retrieval system for the Internet developed exclusively for a strong-motion network is that developed for the Kyoshin strong-motion network following the 1995 tragic earthquake affecting Kobe, Japan. This system provides a "user-friendly" environment for accessing both strong-motion data and associated geotechnical metadata describing site response and station information at each site. Linked strong-motion data and associated geotechnical metadata is suggested as an important capability for future incorporation into capabilities of the COSMOS Virtual Data Center.

The Home page for the Kyoshin Net suggests a straightforward procedure for retrieving data recorded on the strong-motion network and associated borehole data collected at each site (Figure 1). Presentation of the data in this "user-friendly" form has significantly improved data use and accessibility to a wide range of communities concerned with public safety in Japan.

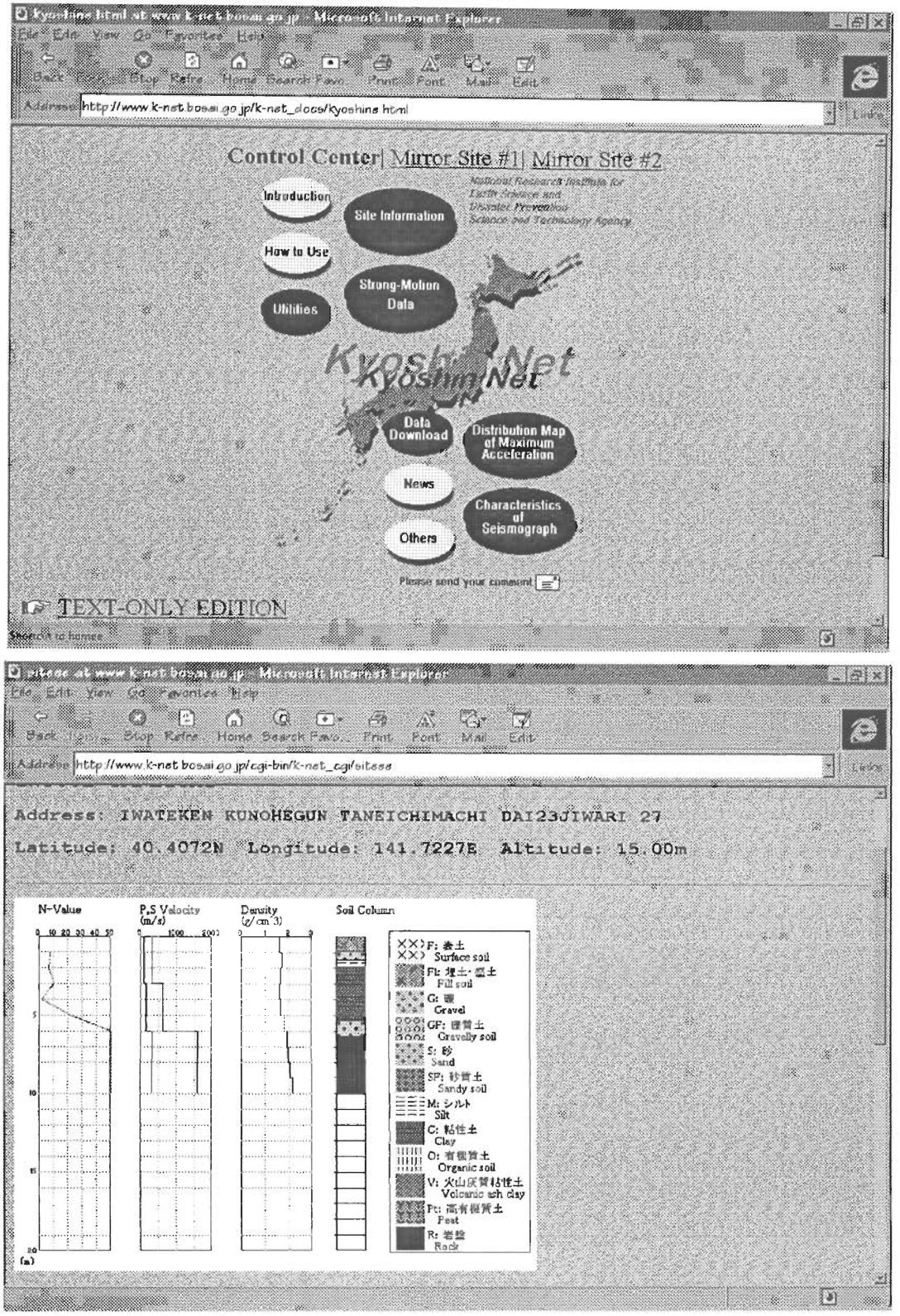

Figure 1. (a) Home page for Kyoshin strong-motion network (http://www.k-net.bosai.go.jp/k-net_docs/kyoshin.html), b) Geotechnical logs for a site in the Kyoshin net.

A principal objective of strong-motion networks is the measurement of the response of the built environment to damaging levels of ground motion. As a result, a major portion of databases maintained by conventional strong-motion programs in the United States is that recorded on buildings, bridges, hospitals, dams, and various other lifelines. As this information is the basis for site-specific design and corresponding design and retrofit codes, efforts to improve its communication to the engineering community are an especially important objective of the COSMOS. An especially useful "user-friendly" environment developed to interactively analyze and retrieve information on the response of the built environment is that developed with support of CDMG by Naeim (1997). The user-friendly database includes strong-motion response data and associated metadata for 20 buildings as recorded during the Northridge earthquake. The database is currently available via CD-ROM. It provides an excellent illustration of the nature of an interactive, "user-friendly" data analysis and retrieval capability for possible future inclusion in capabilities of the COSMOS Virtual Data Center.

Maps (Figure 2a) showing the location of cultural features as well as locations of well-instrumented buildings provide a simple and straightforward "user-friendly" format for selecting buildings of interest.

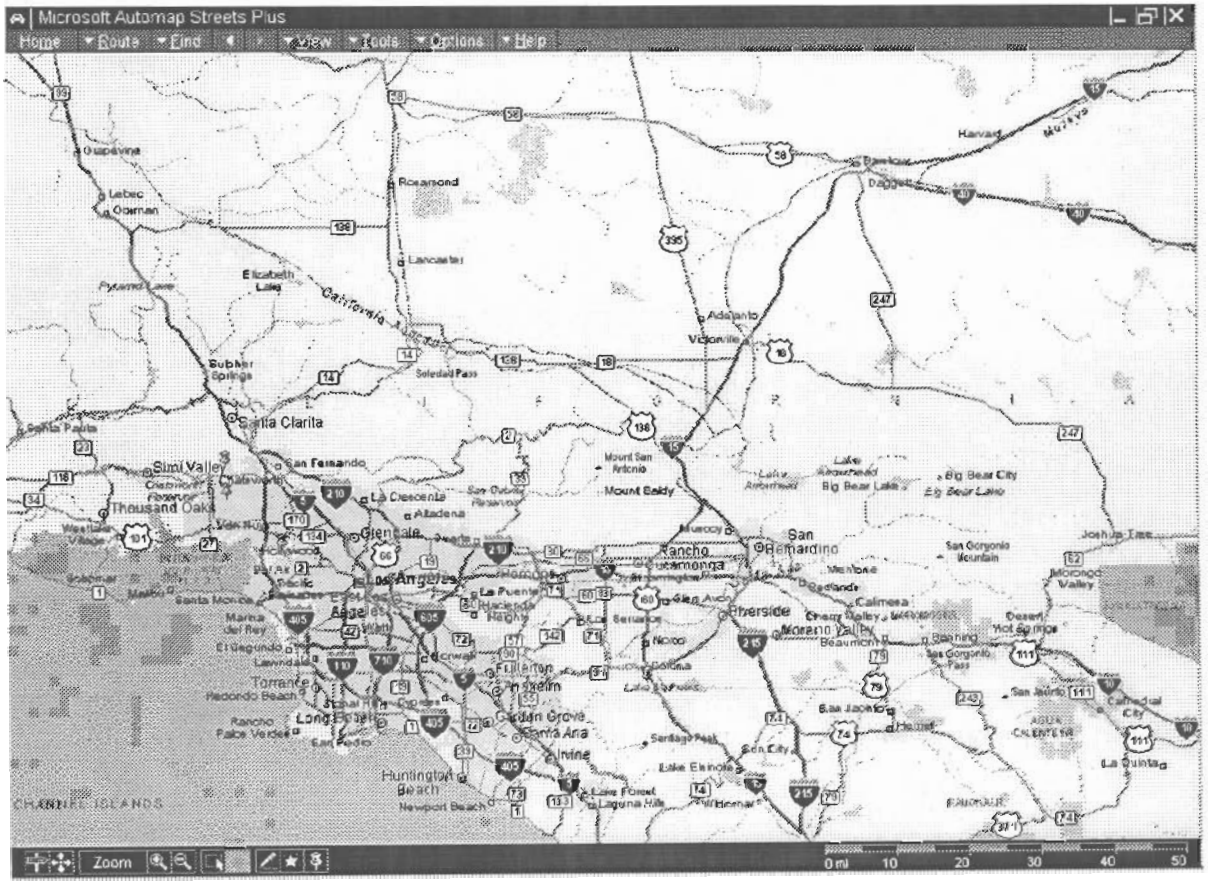

Figure 2a. Map showing locations of cultural features and well-instrument buildings included in the Northridge database (from Naeim, 1997).

A folder format developed for the recorded building data and associated metadata provides a convenient means of accessing the data (Figure 2b). The metadata accessible via folders includes information on the design and construction characteristics of the building, corresponding model building types, photos, and results of detailed damage evaluation following the Northridge earthquake, (see folders in Figure 2b). The metadata includes detailed and readily accessible tabular information about the recorded time histories (see Figure 3a) and an associated instrumentation array schematic (Figure 3b).

Time histories processed according to established "strong-motion" standards are illustrated in a convenient format showing acceleration, velocity and displacement (Figure 4a). These time series can be both easily retrieved in a tabular digital format or interactively analyzed via the CD ROM or in the future on the Internet. Capabilities illustrated here are readily transferable to borehole and ground motion measurements.

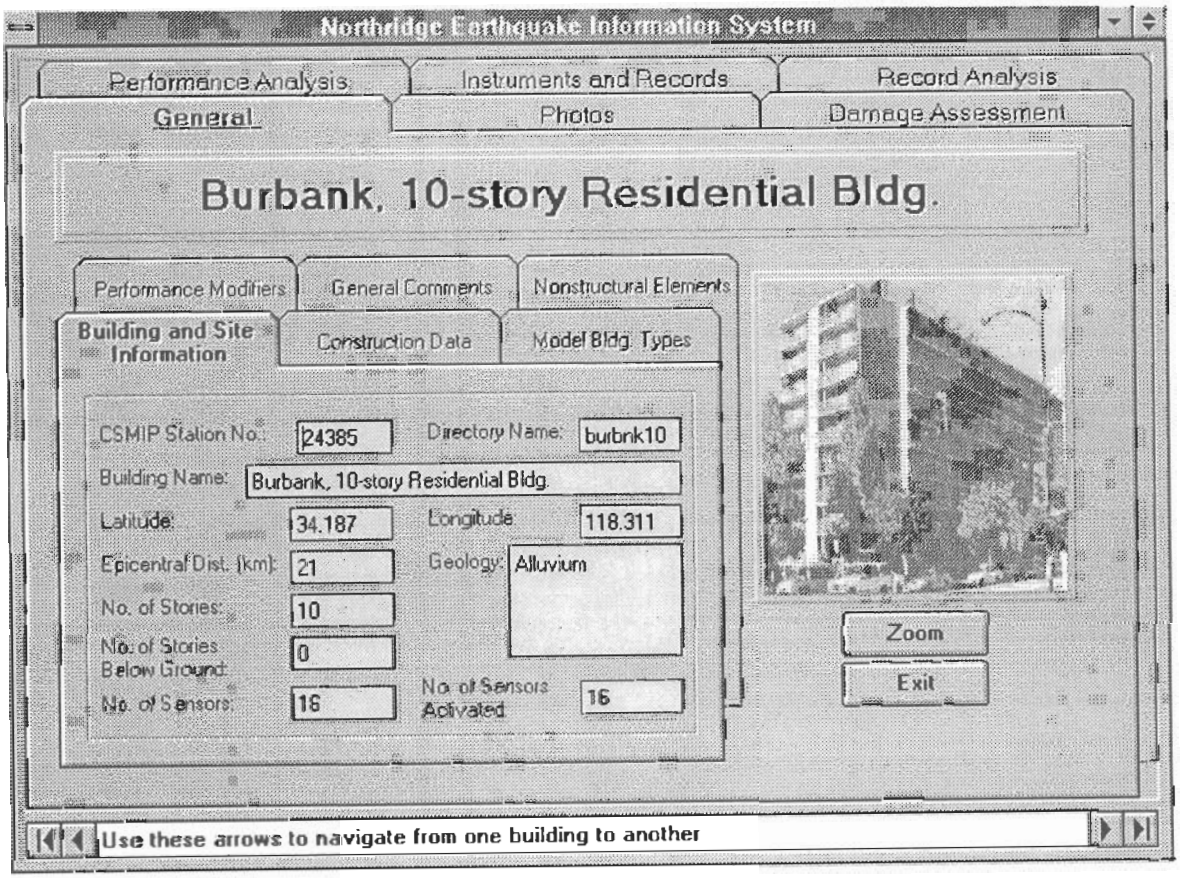

Figure 2b. A "User-Friendly" folder format for retrieval and interactive analysis of strong-motion data and associated metadata for buildings instrumented by the CDMG (from Naeim 1997).

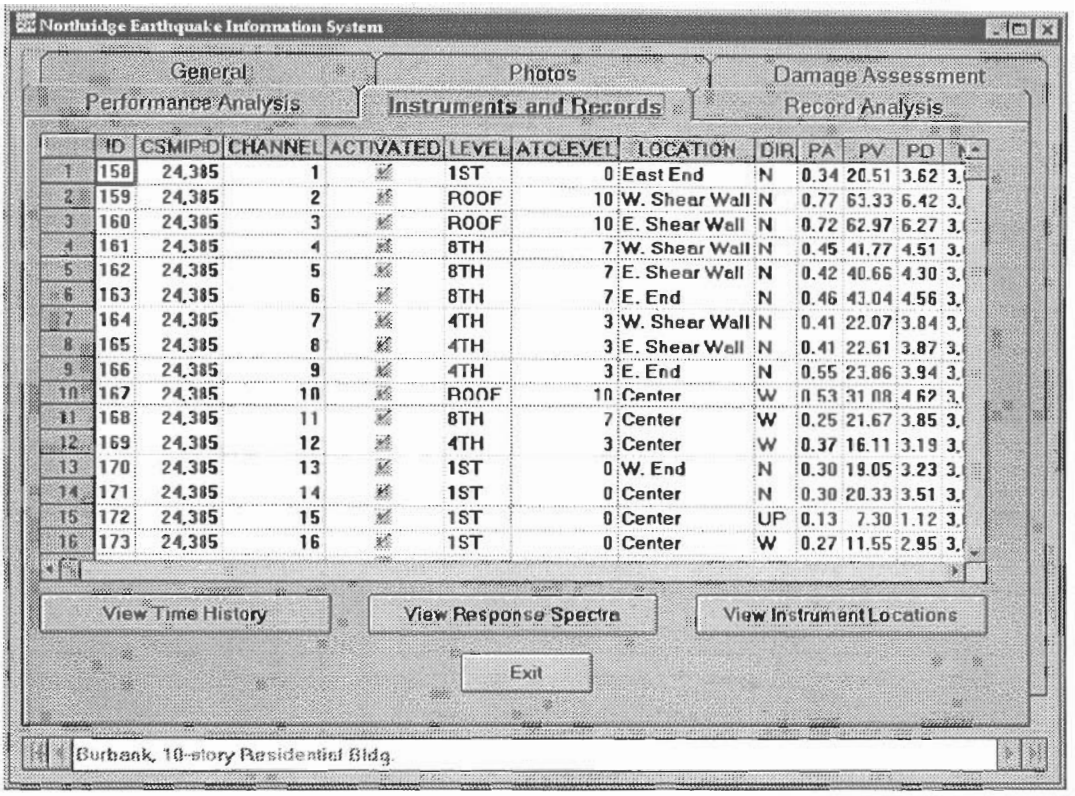

	ID	CSMIPID	CHANNEL	ACTIVATED	LEVEL	ATCLEVEL	LOCATION	DIR	PA	PV	PD	
1	158	24,385	1	☑	1ST	0	East End	N	0.34	20.51	3.62	3.
2	159	24,385	2	☑	ROOF	10	W. Shear Wall	N	0.77	63.33	6.42	3.
3	160	24,385	3	☑	ROOF	10	E. Shear Wall	N	0.72	62.97	6.27	3.
4	161	24,385	4	☑	8TH	7	W. Shear Wall	N	0.45	41.77	4.51	3.
5	162	24,385	5	☑	8TH	7	E. Shear Wall	N	0.42	40.66	4.30	3.
6	163	24,385	6	☑	8TH	7	E. End	N	0.46	43.04	4.56	3.
7	164	24,385	7	☑	4TH	3	W. Shear Wall	N	0.41	22.07	3.84	3.
8	165	24,385	8	☑	4TH	3	E. Shear Wall	N	0.41	22.61	3.87	3.
9	166	24,385	9	☑	4TH	3	E. End	N	0.55	23.86	3.94	3.
10	167	24,385	10	☑	ROOF	10	Center	W	0.53	31.08	4.62	3.
11	168	24,385	11	☑	8TH	7	Center	W	0.25	21.67	3.85	3.
12	169	24,385	12	☑	4TH	3	Center	W	0.37	16.11	3.19	3.
13	170	24,385	13	☑	1ST	0	W. End	N	0.30	19.05	3.23	3.
14	171	24,385	14	☑	1ST	0	Center	N	0.30	20.33	3.51	3.
15	172	24,385	15	☑	1ST	0	Center	UP	0.13	7.30	1.12	3.
16	173	24,385	16	☑	1ST	0	Center	W	0.27	11.55	2.95	3.

Figure 3a. Tabular header data for strong-motion building response measurements recorded on a well-instrumented building by the CSMIP during the Northridge earthquake (from Naeim 1997).

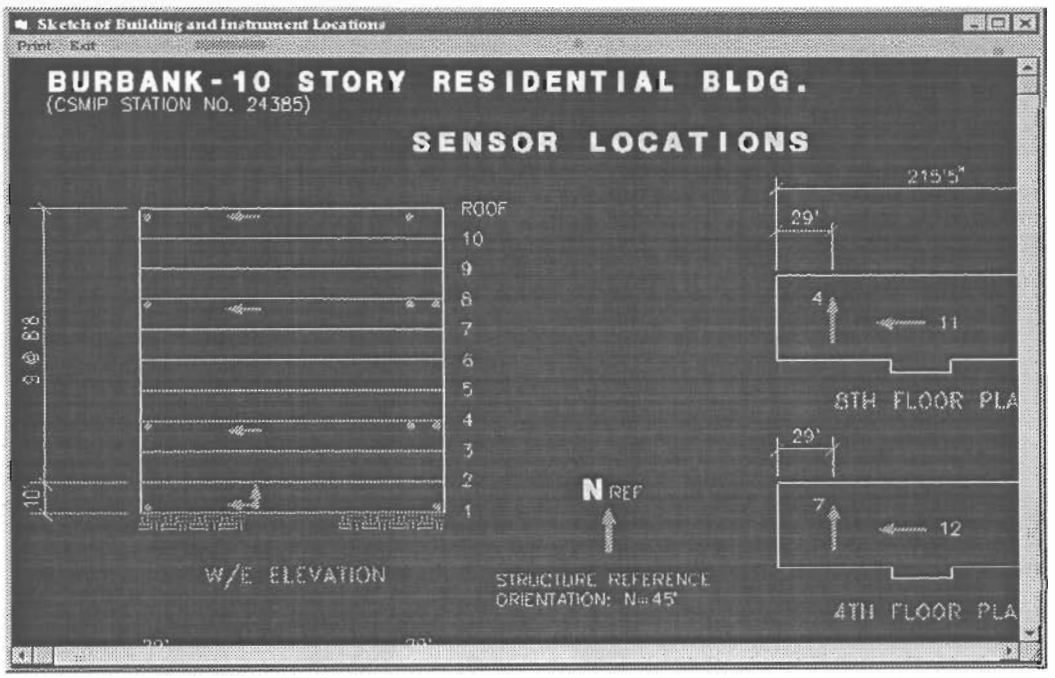

Figure 3b. Structural instrumentation array schematic for a "well-instrumented" structure maintained by the CSMIP (from Naeim 1997).

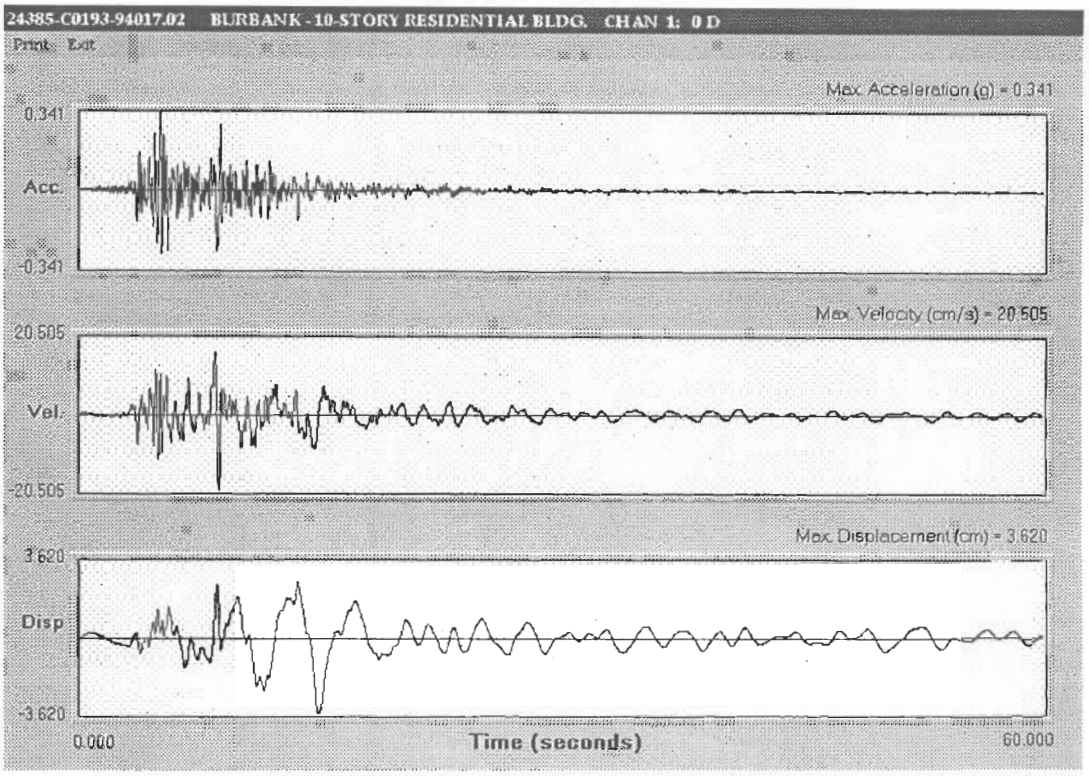

Figure 4a. Example of processed acceleration, velocity, and acceleration for strong-motion data recorded on a well-instrumented building by the CSMIP during the Northridge earthquake (from Naeim 1997).

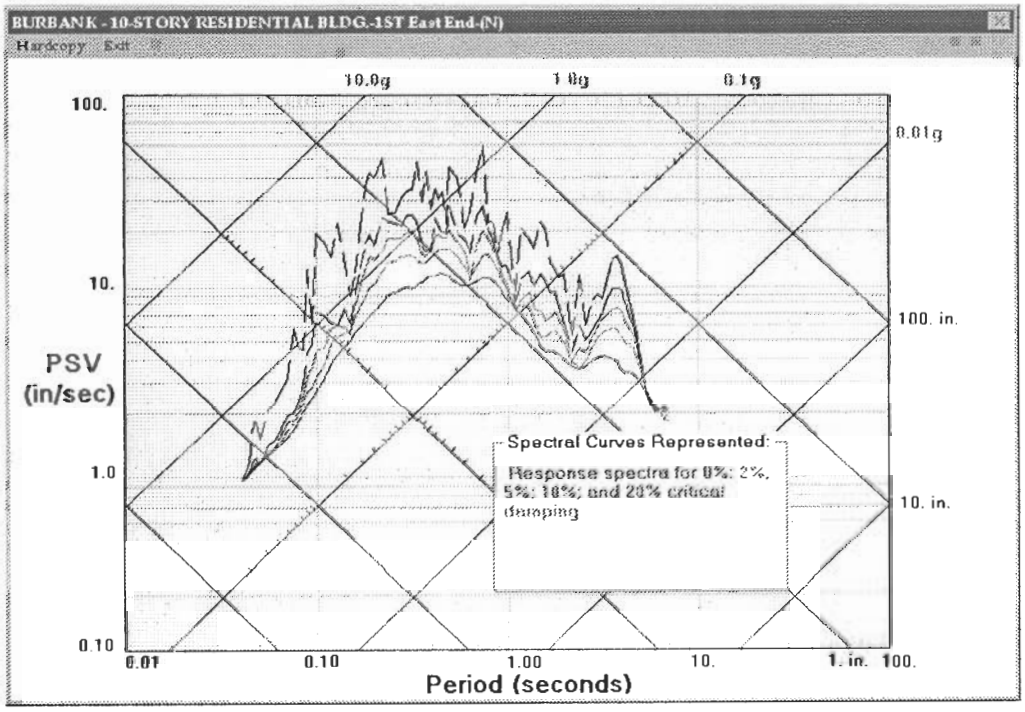

Figure 4b. Examples of pseudo-velocity response spectra inferred from strong-motion recordings obtained on a well-instrumented building by the CSMIP during the Northridge earthquake (from Naeim 1997).

Modern computer technology and the Internet provide an environment not only for rapid access to strong-motion data and associated Metadata, but also for rapid interactive analysis needed to interpret strong-motion recordings. An example illustrating building performance analysis is provided on the CD-ROM developed by Naeim (1997). The example (Figure 5) shows story shears inferred at the time of maximum base shear in the north-south direction. Such interactive capabilities can significantly enhance the usefulness of strong-motion data for the practicing engineering community.

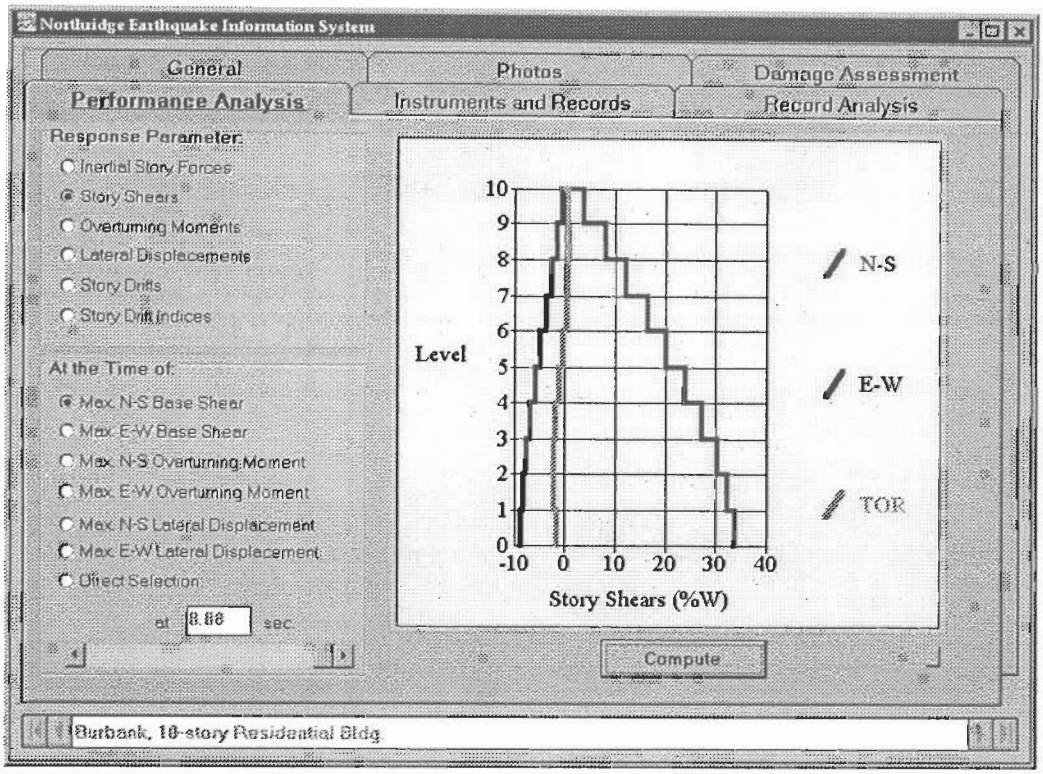

Figure 5. Results illustrating building response characteristics inferred interactively using capabilities developed by Naeim (1997). Structural response is inferred for a "well-instrumented" building (CSMIP) using standard analysis techniques prepared by Naeim (1997).

Another example illustrating interactive capabilities for analysis of strong-motion metadata is provided by the ROSRINE Web site. This site provides geotechnical borehole data recovered at strong-motion sites following the Northridge earthquake. The borehole seismic velocity logs are presented in tabular EXCEL spreadsheet format. This format permits interactive analysis of the tabular data on the Internet as well as rapid download for use on the users own computer. An EXCEL spreadsheet that summarizes the P and S velocity profiles for a strong-motion site is shown in Figures 6. Corresponding graphs of these data also available via the Internet are shown in Figure 7. User-friendly interactive analysis capabilities available on the Web can significantly simplify the problems associated with access and interpretation of strong-motion data by the engineering community.

Resolution of Site Response Issues
in Northridge Earthquake (ROSRINE) Project
P- & S-Wave Velocities Using Suspension Logging Method
Baldwin Hills
Data Collectd March 20, 1997

Depth (meters)	Vs (meters/sec)	Vp (meters/sec)
1.5	161.3	333.3
2.0	186.0	416.7
2.5	189.0	350.9
3.0	189.8	452.5
3.5	197.2	409.8
4.0	206.6	448.4
4.5	246.3	534.8
5.0	265.3	546.4
5.5	253.8	469.5
6.0	249.4	543.5
6.5	254.5	552.5
7.0	255.1	571.4
7.5	295.9	657.9
8.0	296.7	621.1
8.5	273.2	529.1
9.0	267.4	595.2
9.5	306.7	565.0
10.0	314.5	584.8
10.5	341.3	613.5
11.0	369.0	757.6
11.5	339.0	666.7
12.0	310.6	606.1
12.5	305.8	526.3
13.0	303.0	568.2
13.5	301.2	709.2
14.0	309.6	775.2
14.5	324.7	649.4
15.0	319.5	704.2
15.5	309.6	729.9
16.0	310.6	657.9
16.5	306.7	621.1
17.0	330.0	684.9
17.5	355.9	775.2
18.0	374.5	578.0
18.5	346.0	680.3
19.0	348.4	699.3
19.5	349.7	806.5
20.0	361.0	763.4
20.5	362.3	746.3
21.0	380.2	757.6
21.5	361.0	925.9
22.0	359.7	854.7
22.5	367.6	990.1
23.0	354.6	952.4
23.5	355.9	925.9

Figure 7. EXCEL format for P and S velocity profile data measured at a strong-motion site under the ROSRINE program (http://rccg03.usc.edu/rosrine). This format permits interactive analysis and retrieval of the data in EXCEL format via the Internet.

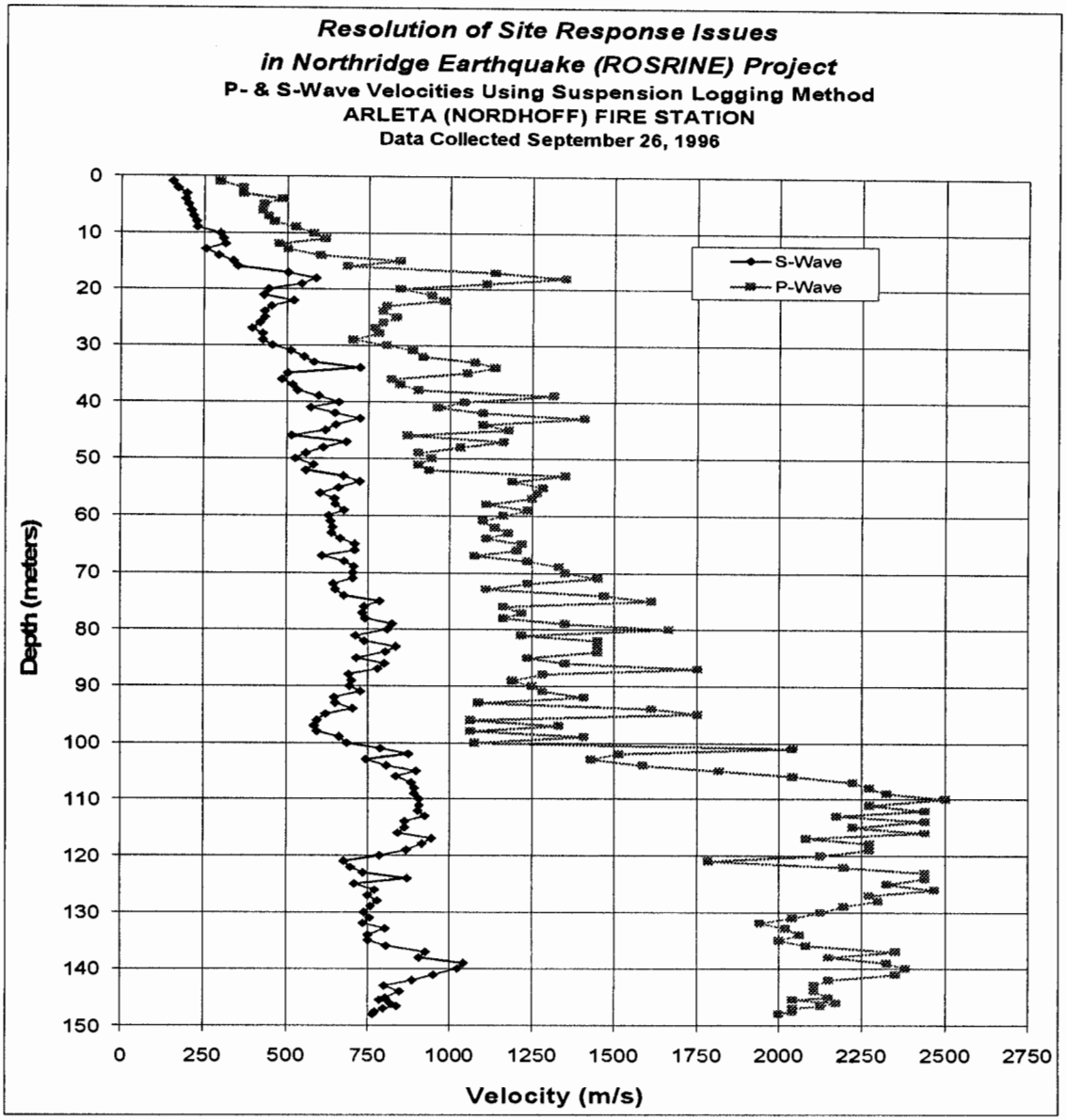

Figure 8. EXCEL chart format of P and S velocity profiles measured at a strong-motion site under the ROSRINE program (http://rccg03.usc.edu/rosrine).

ACKNOWLEDGEMENTS

Careful review comments by M. Huang are appreciated.

REFERENCES

Naeim, F., 1997, Response of Instrumented Buildings to the 1994 Northridge Earthquake -- An Interactive Information System, John A. Martin, Assoc., CD-ROM, also in SMIP96 Proceedings, CDMG.

A VIRTUAL STRONG-MOTION DATA CENTER FOR DATA DISSEMINATION THROUGH THE INTERNET

R. Archuleta[1], A. Tumarkin[1], G. Lindley[1]
A. Shakal[2] and R. Borcherdt[3]

Institute for Crustal Studies
University of California at Santa Barbara[1]

California Strong-Motion Instrumentation Program
California Division of Mines and Geology[2]

United States Geological Survey[3]

ABSTRACT

As a possible contribution to the COSMOS mission to expand the use and application of strong-motion data, a virtual, Web-based data center is being created. The database will include data from COSMOS cooperating networks, which currently includes the California Strong Motion Instrumentation Program, the U.S. Geological Survey, the Army Corps of Engineers, and the U.S. Bureau of Reclamation. If accepted by COSMOS, the database would be managed under COSMOS.

The database has been created, and methods of access through the World Wide Web are under development. Currently, the database includes 740 three-component accelerogram records. The database structure consists of twelve tables, allowing for data about the accelerogram records, earthquakes, recording sites, instruments, networks, and station owners to be stored. The database also allows for all items in the database to have a comment or scientific reference attached to them.

The database has been created using Microsoft SQLServer7 and is running on a 450 MHz PC. Two mirror sites are planned. The database access software is being written in the programming languages Java and Perl. These languages were chosen so that the software will be portable across database and operating system platforms. Multiple Web access methods are being developed to allow searching of the database from earthquake, station, or accelerogram record parameters. Users will be able to select data from lists of earthquakes or stations, to query the database through Web forms pages, or to select data from dynamically created maps.

INTRODUCTION

COSMOS has been created with the mission to expand and modernize the acquisition and application of strong-motion data to increase public earthquake safety. In order to increase the ease of use and accessibility of strong-motion data, a data center is being

created as a possible contribution to the COSMOS mission. The data center will include a strong-motion database that is accessible over the World-Wide Web, allowing the data to be downloaded over the Internet based on criteria supplied by the user. The Home Page is shown in Figure 1.

The features of the data center will include:

- True relational database with earthquake, station, instrument, network, and accelerogram parameters
- Data retrieved from agencies' existing FTP and Web sites
- Effective and efficient access for data users
- Effective feedback from users about the database, Web site, and the data itself
- Preservation of ownership and quality control for agencies collecting the data
- Appropriate credit for source networks

Users of the database will be able to access data based on a wide range of parameters, including peak ground acceleration, epicentral or hypocentral distance, earthquake or station name or location, site geology, housing structure, network name, station owner, or earthquake source parameters, such as magnitude, seismic moment, or focal mechanism. Multiple access methods will be made available to improve the effectiveness and efficiency for the database user.

In addition to ease of use, one of the advantages of the database will be the maintenance of the data by the agencies that collected the data. This will allow these agencies to maintain quality control over their data, to get appropriate credit for their work, helping to justify their missions, and it will give users an effective means of communication with these agencies.

This paper discusses the ongoing effort to meet these data center features. First, we discuss the details of the structure of the database. Then we describe the current and future data that is incorporated into the database. After that, we describe the hardware and software that is running the database. And finally, we discuss the methods of Web access that are currently being developed.

DESCRIPTION OF THE DATABASE

The database derives from an existing database produced at U.C. Santa Barbara, the Strong Motion DataBase. This database originally had four tables to hold information for the earthquakes, stations, accelerogram traces, and references or comments. In order to increase the functionality and store additional information, the new database has been expanded to twelve tables.

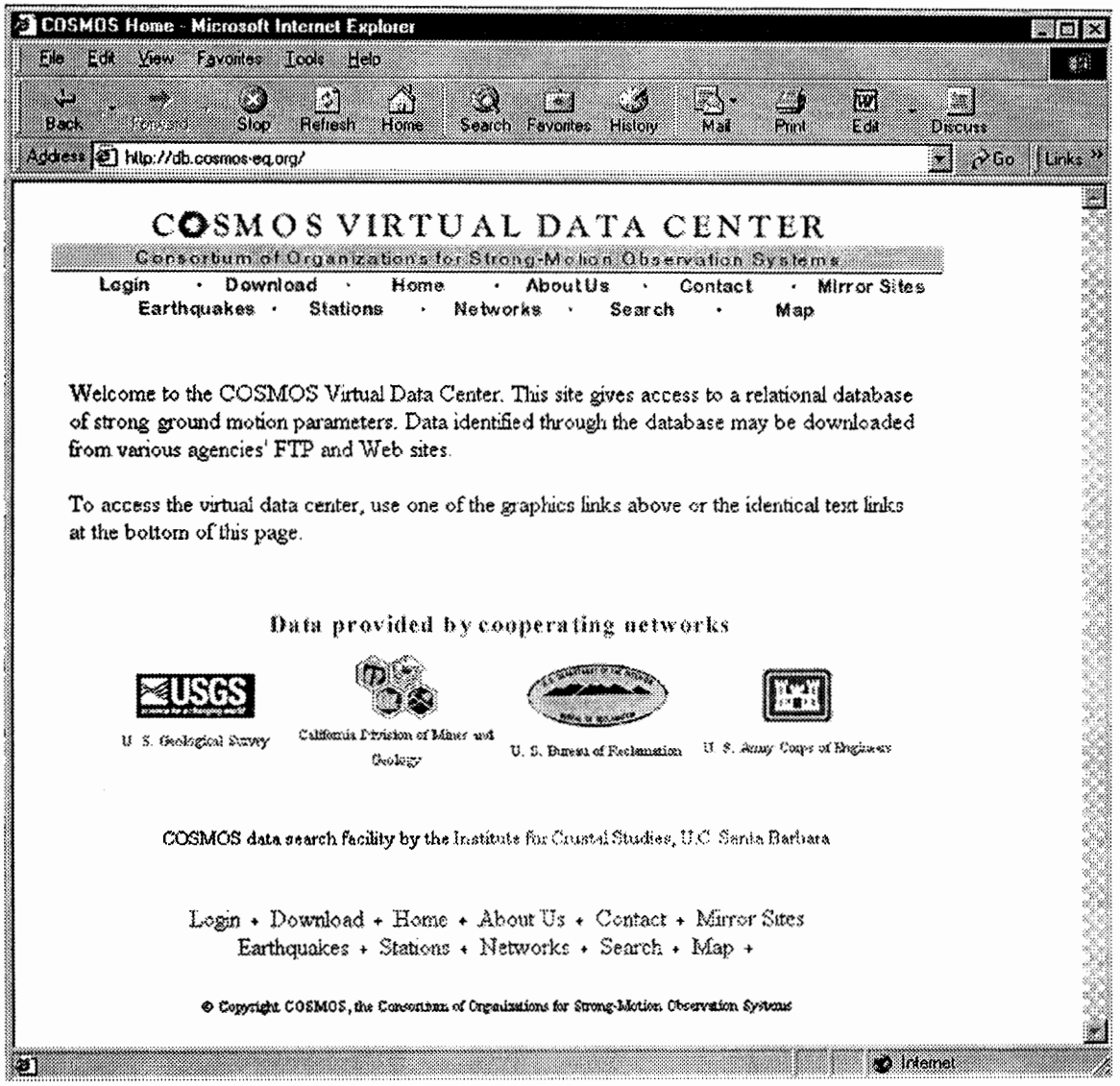

Figure 1. Proposed home page for the COSMOS Virtual Data Center.

By using twelve tables, the structure of the database more accurately matches the real-world structure of the data. The twelve tables are Station, Instrument, StationOwner, Network, Trace, Event, Region, Item, Download, WebUser, Comment, and CommentConnector. The relationships between the tables are shown in Figure 2. These tables can be placed into five groups: the station tables, the event tables, the trace or accelerogram table, the user tables, and the comment/reference tables.

The station tables consist of the Station, Instrument, StationOwner, and Network tables. The Station table is used to store characteristics of data recording locations. A station may be a single free-field instrument, or it may consist of multiple instruments such as might be found at an office building, a bridge overpass, or a dam. The Instrument table gives the location, type, and other parameters corresponding to the recording sensor. The StationOwner table contains information about the site's owner, including contact information for the user. The Network table identifies which network the data was derived from. These tables also include fields for Web addresses, where the user can find additional information about the stations, networks, and station owners.

The event tables consist of two tables, the Event and Region tables. The Event table contains information about the earthquakes, such as their location, magnitude, focal mechanism, and seismic moment. References for each of the parameters stored in the table can be included using the Comment and CommentConnector tables. The Region table increases the functionality of the database by allowing searches of the database that are limited to particular geographic regions.

The core of the database is the Trace table. This table contains the download addresses for the data, as well as information about the accelerogram traces such as the peak ground acceleration, epicentral distance, etc. The smallest "unit" of the database is a single accelerogram trace, allowing for maximum flexibility in use of the database. However, through the Instrument and Station tables, a user can easily select data from a particular location. For example, a user interested in data from the 1989 Loma Prieta, California earthquake might select all of the data recorded at Anderson Dam, or just the data from the downstream record, or just the vertical recording from the downstream record.

Comments, references, and additional Web or FTP addresses will be stored in the Comment and CommentConnector tables. These tables have been structured for maximum efficiency, allowing each element of the database to be commented or referenced multiple times if necessary. The same reference or comment can also apply to multiple elements within the database. This is important so that the user can track down the sources of information in the database. For example, to say that a particular earthquake had a surface magnitude of 6.9 is not very useful unless a reference is attached to it.

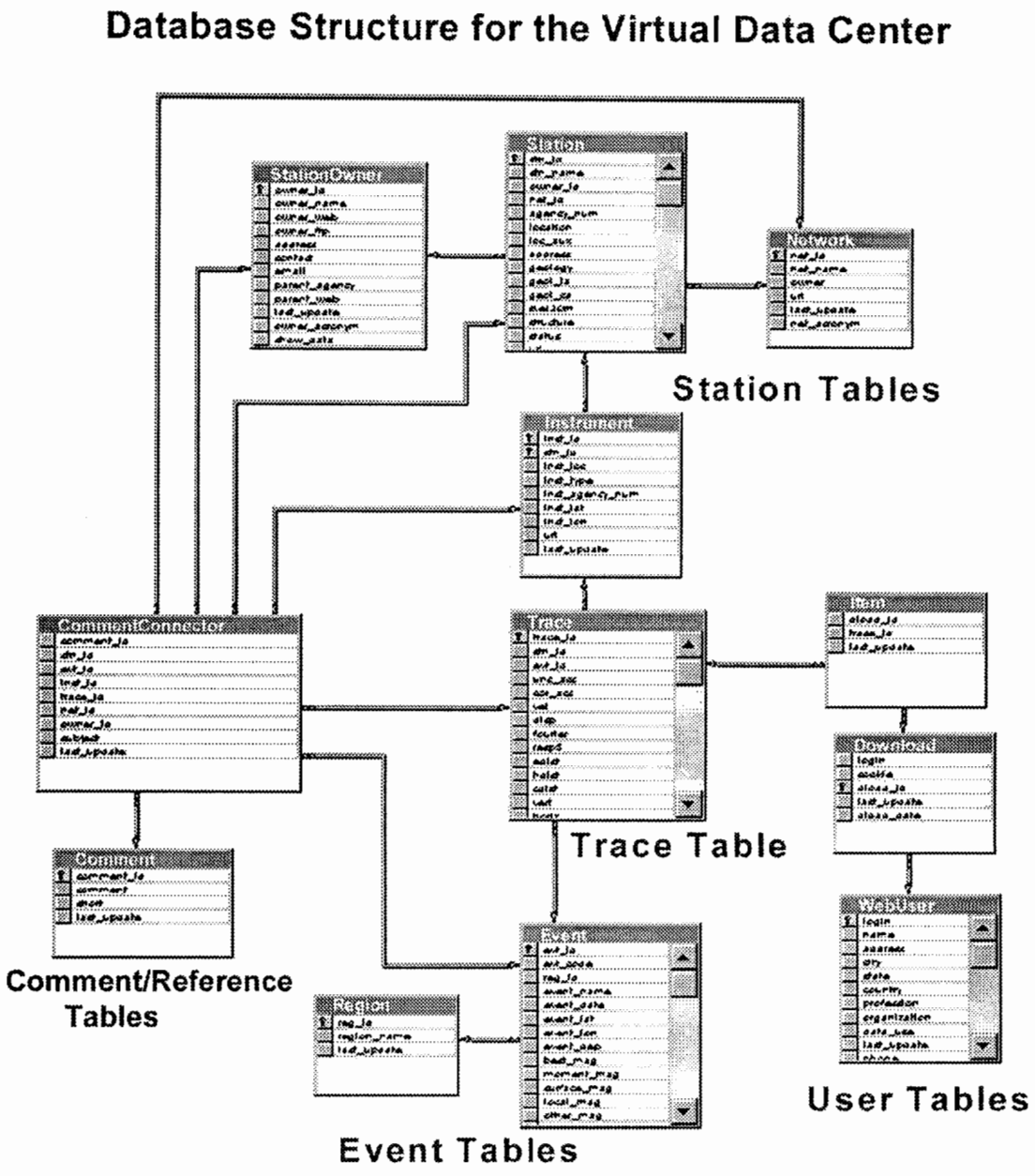

Figure 2. Basic structure of the database, showing the relationships between the various tables.

Finally, there are three tables that keep track of user information in the database: the WebUser, Download, and Item tables. Most of the information stored in these tables will be supplied on a voluntary basis, and will allow the agencies involved in the project to assess what types of uses the data is being put to. This will allow these agencies to more accurately justify their efforts and to adjust those efforts to meet the needs of the end-users. These tables will also allow the Web site to use a "shopping cart" type model, whereby the users will add data to their "cart" and download all of the data when they are through searching the database.

CURRENT AND FUTURE DATA

The database has already been populated with data from the USGS, CDMG, ACOE, and USBR networks, as well as the older Caltech "blue book" data. The database contains 740 3-component records recorded at 561 stations from 104 earthquakes. Ninety-two earthquakes are from California; five are from the Pacific Northwest; four are from the central and eastern United States; three are from Alaska, and one is from Mexico. The oldest event in the database is the 1933 Long Beach, California earthquake. The most recent is the 1996 Duval, Washington earthquake. The events in the database are summarized in Table 1.

Methods are being developed to add data from future earthquakes in a timely fashion. The cooperating agencies will use an automated method to add data to the database. In addition, as more networks become contributing COSMOS members, their data will be added to the database. The data in the database can be expected to grow rapidly.

HARDWARE/SOFTWARE

The hardware and software for the site were chosen for their ability to handle a moderate-sized database in an efficient and cost-effective manner. The database software is Microsoft SQLServer7. It is installed on a Microsoft Windows NT platform running a 450 MHz Intel chip. It is desirable, however, that the database be easily portable to other database software or to a different operating system. In order to meet this goal, the software that will drive the database on the Web site is being written in the languages Java and Perl. These languages are not highly dependent on a particular operating system or software manufacturer. The other option under consideration, Microsoft Active Server Pages, has not been chosen as it would limit future portability of the database.

In addition to the main server, which will operate, at least initially, from UC Santa Barbara, two mirror sites are planned, one to be operated by the US Geological Survey and the other to be operated by the California Division of Mines and Geology. This will reduce downtime of the database and will split the load among three different locations.

Table 1. Events in the Virtual Data Center

LONG BEACH CA	1933-03-11, 01:54:07
SOUTHERN CALIFORNIA	1933-10-02, 09:10:17
BAJA CALIFORNIA MEXICO	1934-12-30, 13:52:00
HELENA MONTANA	1935-10-31, 11:38:00
IMPERIAL VALLEY CA	1938-04-12, 19:29:00
IMPERIAL VALLEY CA	1938-06-06, 02:42:00
IMPERIAL VALLEY CA	1938-06-06, 12:35:00
EL CENTRO CA	1940-05-19, 04:36:40
EL CENTRO CA	1940-05-19, 04:41:02
EL CENTRO CA	1940-05-19, 04:42:13
SANTA BARBARA CA	1941-07-01, 07:50:54
TORRANCE-GARDENA CA	1941-11-14, 08:41:36
BORREGO VALLEY CA	1942-10-21, 16:22:13
WESTERN WASHINGTON	1949-04-13, 11:56:00
IMPERIAL VALLEY CA	1951-01-24, 07:17:02
KERN COUNTY CA	1952-07-21, 11:52:14
KERN COUNTY CA	1952-07-21, 12:05:00
KERN COUNTY CA	1952-07-21, 17:42:44
KERN COUNTY CA	1952-07-21, 19:41:22
SAN LUIS OBISPO CA	1952-11-22, 07:46:00
IMPERIAL VALLEY CA	1953-06-14, 04:17:29
WHEELER RIDGE CA	1954-01-12, 23:33:49
IMPERIAL COUNTY CA	1955-12-17, 05:17:21
IMPERIAL COUNTY CA	1955-12-17, 06:07:29
PORT HUENEME CA	1957-03-18, 18:56:00
SAN FRANCISCO CA	1957-03-22, 11:44:00
PUGET SOUND WA	1965-04-29, 07:28:00
SOUTHERN CALIFORNIA	1965-07-16, 07:46:00
PARKFIELD CA	1966-06-28, 04:26:00
BORREGO MOUNTAIN CA	1968-04-09, 02:28:59
LYTLE CREEK CA	1970-09-12, 14:30:52
SAN FERNANDO CA	1971-02-09, 14:00:41
SAN FERNANDO CA	1971-02-09, 14:01:33
SAN FERNANDO CA	1971-02-09, 14:01:50
SAN FERNANDO CA	1971-02-09, 14:02:24
SAN FERNANDO CA	1971-02-09, 14:03:25
SAN FERNANDO CA	1971-02-09, 14:04:34
SAN FERNANDO CA	1971-02-09, 14:05:50
CENTRAL CALIFORNIA	1971-03-08, 23:08:07
ADAK ALASKA	1971-05-02, 00:00:00
POINT MUGU CA	1973-02-21, 14:45:57
IMPERIAL VALLEY CA	1974-12-06, 12:13:08
ANCHORAGE ALASKA	1975-01-01, 00:00:00
IMPERIAL VALLEY CA	1975-01-23, 17:02:29
IMPERIAL VALLEY CA	1975-06-20, 05:48:24
HORSE CANYON CA	1975-08-02, 00:14:07
IMPERIAL VALLEY CA	1976-11-04, 05:48:20
IMPERIAL VALLEY CA	1977-10-20, 10:29:35
IMPERIAL VALLEY CA	1977-10-21, 13:24:24
IMPERIAL VALLEY CA	1977-10-30, 05:30:14
IMPERIAL VALLEY CA	1977-11-14, 00:11:35
IMPERIAL VALLEY CA	1977-11-14, 02:05:48
IMPERIAL VALLEY CA	1977-11-14, 05:36:55
IMPERIAL VALLEY CA	1977-11-14, 12:20:20
COYOTE DAM CA	1978-03-26, 00:27:00
SANTA BARBARA CA	1978-08-13, 22:54:53
SOUTHEASTERN ALASKA	1979-02-28, 00:00:00

COYOTE LAKE CA	1979-08-06, 17:05:22
IMPERIAL VALLEY CA	1979-10-15, 23:16:53
IMPERIAL VALLEY CA	1979-10-16, 06:58:32
LIVERMORE CA	1980-01-24, 19:00:09
LIVERMORE CA	1980-01-27, 02:33:35
ANZA CA	1980-02-25, 10:47:38
MAMMOTH LAKES CA	1980-05-25, 16:33:44
MAMMOTH LAKES CA	1980-05-25, 16:49:27
MAMMOTH LAKES CA	1980-05-25, 19:44:51
MAMMOTH LAKES CA	1980-05-25, 20:35:48
MAMMOTH LAKES CA	1980-05-26, 18:57:56
MAMMOTH LAKES CA	1980-05-27, 14:50:57
WESTMORLAND CA	1981-04-26, 12:09:28
NEW HAMPSHIRE USA	1982-01-19, 00:14:42
ANZA CA	1982-06-15, 23:49:21
ENOLA ARKANSAS	1982-06-26, 00:00:00
ENOLA ARKANSAS	1982-07-05, 00:00:00
COALINGA CA	1983-05-02, 23:42:38
COALINGA CA	1983-05-09, 02:49:11
COALINGA CA	1983-06-11, 03:09:52
COALINGA CA	1983-07-09, 07:40:51
COALINGA CA	1983-07-22, 02:39:54
COALINGA CA	1983-07-22, 03:43:01
COALINGA CA	1983-07-25, 22:31:39
COALINGA CA	1983-09-09, 09:16:13
MORGAN HILL CA	1984-04-24, 21:15:18
REDLANDS CA	1985-10-02, 23:44:12
NORTH PALM SPRINGS CA	1986-07-08, 09:20:44
WHITTIER NARROWS CA	1987-10-01, 14:42:20
WHITTIER CA	1987-10-04, 10:59:38
ELMORE RANCH CA	1987-11-24, 01:54:14
SUPERSTITION HILLS CA	1987-11-24, 13:15:56
LOMA PRIETA CA	1989-10-18, 00:04:15
UPLAND CA	1990-02-28, 23:43:36
SIERRA MADRE CA	1991-06-28, 14:43:54
JOSHUA TREE CA	1992-04-23, 04:50:00
CAPE MENDOCINO-PETROLIA CA	1992-04-25, 18:06:04
CAPE MENDOCINO-PETROLIA CA	1992-04-26, 07:41:00
CAPE MENDOCINO-PETROLIA CA	1992-04-26, 11:18:00
LANDERS CA	1992-06-28, 11:57:34
BIG BEAR CA	1992-06-28, 15:05:36
SCOTTS MILL OREGON	1993-03-25, 00:00:00
NORTHRIDGE CA	1994-01-17, 12:30:55
EUREKA CA	1994-09-01, 15:15:52
SOUTH LAKE TAHOE CA	1994-09-12, 12:23:42
PARKFIELD CA	1994-12-20, 10:27:47
DUVAL WA	1996-05-03, 00:00:00

Table 1. Events in the Virtual Data Center continued.

WEB SITE LAYOUT AND FUNCTIONALITY

Four basic methods of Web access are being developed for the database. These methods will allow the user to select data by viewing a list of earthquakes in the database, by viewing a list of stations in the database, by user input onto HTML forms pages, or through clickable maps showing earthquake and station locations. In addition to the dynamic database access pages, static Web pages will give basic information about the data center to the user including contact information and information about the mirror sites. See Figure 3 for a basic layout of the Web site.

Users will download data via a "shopping cart" model, which is commonly seen on Web sites today. As the user browses through the database, they will be given the opportunity to add the data they are interested in to a download bin. When the user is ready, they can select an option to download the data they have previously added to their bin. The downloaded data will be grouped by agency as a means of giving additional attribution to the contributing agencies.

Each page of the Web site will contain links to the database access methods, to the static pages of the Web site, and to the data download pages. A proposed home page showing these links can be seen in Figure 1.

To make the Web site as efficient as possible, the responses to database queries will be organized into a three-tiered structure. The three tiers will be station, instrument (3-component record), and trace. The user will have the option of selecting all of the data from a station (which may have multiple instruments), from a particular instrument, or selecting just a single accelerogram trace.

CONCLUSIONS

A relational, Web-accessible database of parameters related to strong-motion data is being developed for possible inclusion in a COSMOS virtual data center. The database will allow users to selectively acquire strong-motion data corresponding to the user's exact needs. The database will contain information about the accelerogram records and related information about the recording sites, networks, and earthquakes. The data itself will be downloaded from existing Web and FTP sites. The database will have the capacity to add references or comments to every element of the database. Multiple Web access methods will be made available as well as a means for the users to contact the agencies that recorded the data. The database will improve access to strong-motion data, and will provide an important way for the agencies that collected strong-motion data to gather information about the uses their data is being put to.

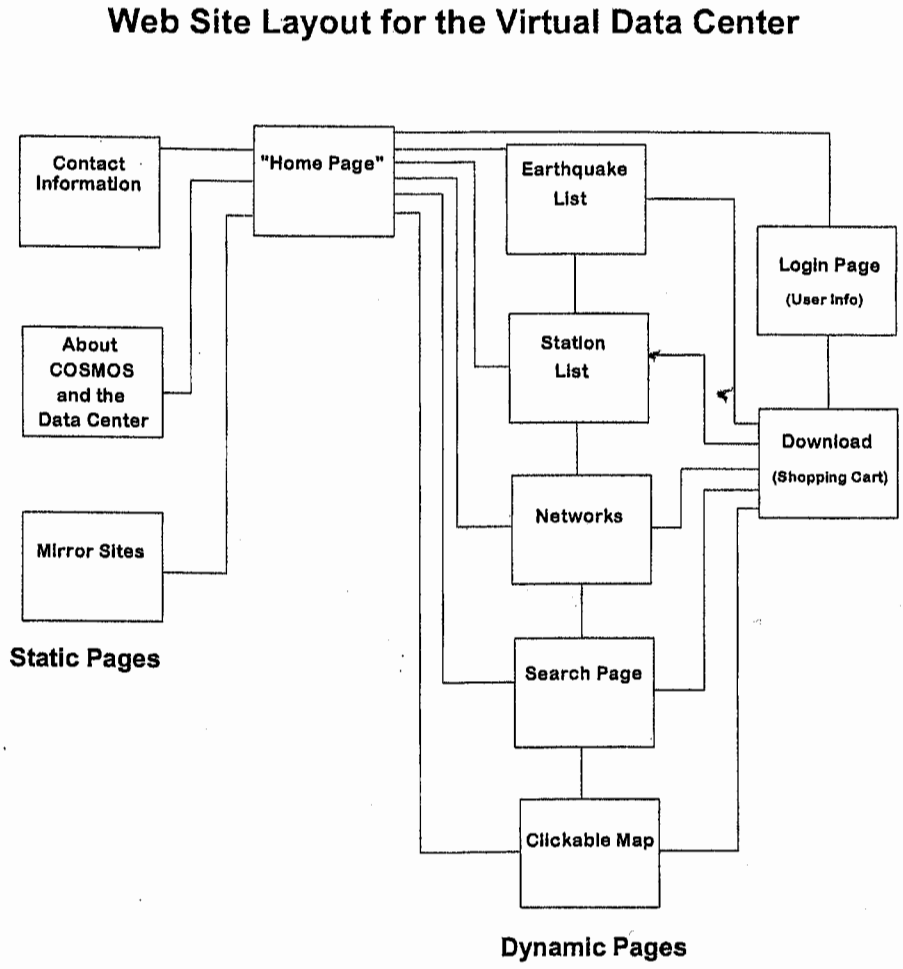

Figure 3. Layout of the Web site that will access the database.